On the Use of RCM Data and Gridded Climatologies for Regional Scale Glacier Mass Balance Modeling in High Mountain Topography; The Example of the Swiss Alps.

Dissertation

zur

Erlangung der Naturwissenschaftlichen Doktorwürde
(Dr. sc. nat.)

vorgelegt der

Mathematisch-naturwissenschaftlichen Fakultät

der

Universität Zürich

von

Horst Machguth
von
Würenlos AG

Promotionskommitee
Prof. Dr. Wilfried Haeberli (Vorsitz)
Dr. Frank Paul (Leitung der Dissertation)
Prof. Dr. Martin Hölzle

Zürich 2008

Summary

Mass balance modeling is an important tool in the investigation of the glacier-climate relationship. Mass balance computations using the energy balance approach have been successfully applied to individual glaciers but the application to entire mountain ranges, especially those with numerous glaciers, remains a challenge. Such an application would give information about process relevance as well the availability and quality of input data on a regional scale. Their biases must be taken into consideration but climate model data or gridded climatologies could be used as the input for such a regional application.

The present thesis focuses on the development and testing of a regional mass balance model based on an energy balance computation driven by Regional Climate Model (RCM) data. Prior to this regional application the performance and uncertainties of two differing complexity mass balance models have been assessed in a number of studies: (a) Snow distribution on two glaciers was measured by means of helicopter-borne Ground Penetrating Radar (GPR) to validate the mass balance computation. (b) A simple mass balance model was used in a long-term mass balance computation and compared to stake measurements. (c) To assess the influence of simplified parameterizations, the output of both models has been compared over the long-term. (d) Uncertainties in modeled mass balance were assessed in a parametric uncertainty analysis.

The simpler model was chosen to develop into a regional mass balance model because of its less intensive calculation requirements although its performance was similar to the more complex model. A coupling scheme was designed to bridge the gap in spatial resolution between the RCM (18 km) and the mass balance model (100 m). The regional mass balance model was run for a period of 24 years (1979–2003) for the Swiss Alps. The RCM data as well as model output were validated against different data sets to evaluate spatial and temporal model performance.

It was found that the gap in spatial resolution was not a drawback although the input parameters require individual coupling schemes. While the temporal variability of measured mass balance was well reproduced, spatial biases in the RCM data are reflected in the model output. Bias in precipitation was the main source of these errors. In a further model run a simple bias correction of input data was implemented. Precipitation was regarded as the unknown in the modeling process and adjusted until the modeled and measured mass balances agreed. Precipitation data were found to be particularly biased in two distinct areas of the Swiss Alps. Findings from other studies have confirmed these results.

Regional mass balance modeling is a valuable approach to assess process relevance on a regional scale and to learn about the quality of input data. Future studies should emphasize bias correction and make use of RCM ensembles. However, biases in precipitation data will remain the main challenge. Additional accumulation data, such as that obtained from helicopter-borne GPR, are required for the further improvement of regional mass balance modeling and high-mountain precipitation assessments.

Zusammenfassung

Massenbilanz Modellierungen sind eine wichtige Methode um die Gletscher-Klima Beziehung zu verstehen. Modelle basierend auf dem Energiebilanz-Ansatz wurden bereits erfolgreich angewandt auf einzelnen Gletschern. Die Anwendung auf Gebirgsketten mit zahlreichen Gletschern bleibt hingegen eine Herausforderung. Eine derartige Anwendung würde die Möglichkeit bieten Prozesse auf einer grösseren Skala hinsichtlich ihres Einflusses zu untersuchen. Daten von Klimamodellen oder Messwerte könnten als Input verwendet werden.

Die vorliegende Arbeit ist der Entwicklung eines regionalen Massenbilanz-Modells gewidmet. Das Modell wird angetrieben mit Daten eines regionalen Klima Modells (RCM). In vier vorbereitenden Studien wurden zwei Massenbilanz Modelle hinsichtlich ihrer Leistung und Unsicherheiten untersucht: (a) Die Schneeverteilung auf zwei Gletschern wurde mit helikoptergestütztem Radar gemessen um einen Modelllauf zu überprüfen. (b) Das einfache Massenbilanz-Modell wurde in einem langzeit-Modelllauf getestet. (c) Ein weiter langzeit-Modellauf wurde mit beiden Modellen parallel durchgeführt. Mittels eines Vergleichs der Resultate beider Modelle wurde der Einfluss vereinfachter Parametrisierungen untersucht. (d) In einer Unsicherheitsanalyse wurden Modellunsicherheiten berechnet.

Das regionale Massenbilanzmodell wurde auf dem einfacheren Massenbilanzmodel aufgebaut weil sich dieses als weniger rechenintensiv erwies und die Resultate von ähnlicher Güte sind wie diejenigen des komplexeren Models. Ein Schema wurde entworfen um den Unterschied in räumlicher Auflösung zwischen RCM (18 km) und Massenbilanz-Modell (100 m) zu überbrücken. Am Beispiel der Schweizer Alpen wurde das regionale Massenbilanz-Modell über 24 Jahre (1979–2003) laufen gelassen. Sowohl RCM-Daten als auch Modell-Resultate wurden anschliessend mit verschiedenen Messwerten verglichen.

Der Unterschied in räumlicher Auflösung erwies sich nicht als zentraler limitierender Faktor. Die zeitliche Variabilität der Messwerte wurde gut wiedergegeben. Räumliche Fehler der RCM Daten hingegen, spiegelten sich klar im Modellresultat wider, systematische Fehler in den Niederschlagsdaten sind die Hauptquelle von Modellfehlern. In einem weiteren Experiment wurde eine einfache Korrektur der RCM Fehler durchgeführt. Niederschlag wurde dann als die Unbekannte betrachtet und iterativ korrigiert bis modellierte und gemessene Massenbilanzen übereinstimmten. Die Niederschlagsdaten erwiesen sich in zwei Regionen als systematisch zu hoch oder zu niedrig. Andere Studien bestätigen dieses Resultat.

Massenbilanz Modellierungen auf einer regionalen Skala erlaubt die Betrachtung der Relevanz von Prozessen in einem grösseren Rahmen und erlaubt die Beurteilung der Güte von Input-Daten. Weiterführende Studien sollten vor allem auf Fehlerkorrekturen und die Verwendung mehrerer RCMs fokussieren. Systematische Fehler der Niederschlagsdaten werden die zentrale Herausforderung bleiben. Helikopter gestützter Radar böte die Möglichkeit Akkumulationsdaten zu gewinnen, die nötig sind für eine weitere Verbesserung regionaler Massenbilanz Modelle oder deren Anwendung zur Abschätzung von Niederschlag im Hochgebirge.

Contents

List of Figures

List of Tables

List of Abbreviations

AAR	Accumulation Area Ratio
AGCM	Atmospheric General Circulation Model
ALP-IMP	Multi-centennial climate variability in the Alps based on Instrumental data, Model simulations and Proxy data (EU research project)
AOGCM	Atmospheric Ocean General Circulation Model
ASRB	Alpine Solar Radiation Budget Network
AWS	Automatic Weather Station
BLFUW	Bundesministerium für Land- und Forstwirtschaft, Umwelt und Wasserwirtschaft (Austrian Ministry for Agriculture, Forestry, Environment and Water Resources Management)
DEM	Digital Elevation Model
ECMWF	European Centre for Medium-range Weather Forecasts
EL	Equilibrium Line
ELA	Equilibrium Line Altitude
ERA-40	ECMWF 45 years reanalysis
GCM	Global Circulation Model
GCOS	Global Climate Observing System
GPR	Ground Penetrating Radar
GPS	Global Positioning System
GTN-G	Global Terrestrial Network for Glaciers
GTOS	Global Terrestrial Observing System
IAHS	International Association of Hydrological Sciences
ICSI	International Commission on Snow and Ice
IDL	Interactive Data Language
IDW	Inverse Distance Weighting Interpolation
IMAU	Institute for Marine and Atmospheric research Utrecht
IPCC	Intergovernmental Panel on Climate Change
ISCCP	International Cloud Climatology Project
MIP	Model Inter-comparison Project
NetCDF	Network Common Data Format
NN	Nearest Neighbor Interpolation
PDF	Probability Density Function
PDDM	Positive Degree Day Model
PRISM	Parameter-elevation Regressions on Independent Slopes Model (Interpolation Scheme for Meteorological Data)
PRUDENCE	Prediction of Regional scenario and Uncertainties for Defining EuropeaN Climate change risks and Effects (EU Research Project)

RCM	Regional Climate Model
REMO	REgional MOdel (RCM from the Max-Planck Institute for Meteorology, Hamburg)
SD	Statistical Downscaling
SRTM	Shuttle Radar Topography Mission
TM	Landsat Thematic Mapper
TPS	Thin Plate Splines Interpolation
UNEP	United Nations Environment Programme
WGMS	World Glacier Monitoring Service

List of Symbols

Latin Letters

Symbol	Description	Units
A	Area	m^2
a	Ablation	m
B	Total mass balance	m^3
B_c	Cumulative Mass Balance	m
$\bar{B}$	Glacier Mass Balance	m
b	Specific Mass Balance	m
$\dot{b}$	Mass Balance Rate	$\mathrm{m\,s}^{-1}$
b_t	Mass Balance at the Glacier Tongue	m
C	Accumulation Due to Condensation	m
C_b	Background Turbulent Exchange Coefficient	
C_0	Coefficient Turbulent and Long-wave Energy Fluxes	$\mathrm{W\,m}^{-2}$
C_1	Coefficient Turbulent and Long-wave Energy Fluxes	$10\,\mathrm{W\,m}^{-2}\,\mathrm{K}^{-1}$
c	Accumulation	m
D	Reduction Factor Clear Sky Global Radiation	
d	Snow Depth	m
d^*	Characteristic Snow Depth	0.011 m w.e.
E	Mass Loss due to Evaporation	m
e_a	Relative Humidity	
F	Surface Energy Heat Flux	$\mathrm{W\,m}^{-2}$
g	Acceleration due to Gravity	$9.81\,\mathrm{m\,s}^{-2}$
G	Subsurface Heat Flux	$\mathrm{W\,m}^{-2}$
H	Altitude Above Sea Level	m
h_{max}	Characteristic Ice Thickness Near Equilibrium Line	m
K	Mass Loss due to Calving	m
L	Glacier Length	m
L_o	Original Glacier Length	m
L_{in}	Long-wave Ingoing Radiation	$\mathrm{W\,m}^{-2}$
L_{out}	Long-wave Emitted Radiation	$\mathrm{W\,m}^{-2}$
l_m	Latent Heat of Melt of Ice	$334'000\,\mathrm{J\,kg}^{-1}$ at 0 °C
l_s	Latent Heat of Sublimation of Ice	$2'835'000\,\mathrm{J\,kg}^{-1}$ at 0 °C
l_v	Latent Heat of Vaporization of Water	$2'501'000\,\mathrm{J\,kg}^{-1}$ at 0 °C
M	Melt	m
n	Cloudiness	
n_{corr}	Correction Factor Cloudiness	

n_{REMO}	Cloudiness (Obtained from the RCM REMO)	
P	Precipitation	$\mathrm{m\,s^{-1}}$
P_{solid}	Solid Precipitation	$\mathrm{m\,s^{-1}}$
P_{stored}	Liquid Precipitation Stored in the Snow Cover	$\mathrm{m\,s^{-1}}$
P_{corr}	Correction Factor Precipitation	
P_O	Original Precipitation in Iteration Procedure	$\mathrm{m\,s^{-1}}$
P_{scale}	Correction Array Precipitation	
p	Air Pressure	Pa
Q_h	Sensible Heat Flux	$\mathrm{W\,m^{-2}}$
Q_l	Latent Heat Flux	$\mathrm{W\,m^{-2}}$
Q_m	Energy Consumed Through Melting	$\mathrm{W\,m^{-2}}$
Q_R	Heat Flux from Rain	$\mathrm{W\,m^{-2}}$
R_A	Redistribution of Snow from Avalanches	$\mathrm{m\,s^{-1}}$
R_D	Redistribution of Snow from Wind Drift	$\mathrm{m\,s^{-1}}$
S_{in}	Short-wave Ingoing Radiation (Measured or Modeled)	$\mathrm{W\,m^{-2}}$
$S_{in,dif}$	Diffuse Part of Short-wave Ingoing Radiation	$\mathrm{W\,m^{-2}}$
$S_{in,dir}$	Direct Part of Short-wave Ingoing Radiation	$\mathrm{W\,m^{-2}}$
$S_{in_{meas}}$	Short-wave Ingoing Radiation (Measured)	$\mathrm{W\,m^{-2}}$
S_{in}^{REMO}	Short-wave Ingoing Radiation in the RCM REMO	$\mathrm{W\,m^{-2}}$
S_{out}	Short-wave Outgoing Radiation	$\mathrm{W\,m^{-2}}$
$S_{in,clr}$	Clear Sky Global Radiation	$\mathrm{W\,m^{-2}}$
$S_{in,clrdir}$	Direct Part of Clear Sky Global Radiation	$\mathrm{W\,m^{-2}}$
$S_{in,clrdif}$	Diffuse Part of Clear Sky Global Radiation	$\mathrm{W\,m^{-2}}$
s	Scaling Factor Snow Albedo Calculation	
T_a	Air Temperature in the Free Atmosphere	°C or K
T_{snow}	Air Temperature Threshold Snowfall	°C or K
T_{surf}	Surface Temperature	°C or K
t	Time	s
t_r	Response Time	s
t_{decor}	Time span of Temporal Autocorrelation	s
WET	Wet Day Frequency	
z_1	Thickness of Surface Layer	m

Greek Letters

Symbol	Description	Units
α	Surface Albedo	
α_f	Surface Albedo Firn	
α_i	Surface Albedo Ice	
α_{max}	Fresh Snow Albedo	0.82
α_{min}	Lower Threshold Snow Albedo	0.55
α_s	Surface Albedo Snow	
α_{surf}	Surface Albedo of Aged Snow	
α_u	Albedo of the Underlying Layer	
Γ_P	Vertical Gradient Precipitation	$\mathrm{m\,m^{-1}\,a^{-1}}$

$\hat{\Gamma}_P^*$	Precipitation Correction Array	
Γ_T	Lapse Rate Air Temperature in the Free Atmosphere	$\mathrm{K\,m^{-1}}$
ε	Emissivity	
ε_s	Systematic Uncertainty	
ε_r	Random Uncertainty	
σ	Stefan-Boltzmann constant	$5.67 \cdot 10^{-8}\mathrm{J\,K^{-4}\,m^{-2}\,s^{-1}}$
τ_{cl}	Attenuation from Clouds	
τ_a	Coefficient Snow Ageing	0.008
τ_l	Length of a Day	86'400 s
τ_f	Coefficient Snow Ageing	0.24
τ_r	Dynamic Response Time	s

Part I.

Background and Methods

1. Introduction

1.1. Motivation

Glaciers are phenomena of cold regions of the Earth – either the high latitudes or high mountains. As such, glaciers are often located in remote areas from a human perspective and documentations remained sparse for a long time in human history. With a growing population density, glaciers came into the focus of people's perception. In the 15th century their advances threatened pastures, forests and constructions (*Zumbühl*, 1980). From the onset of the 18th century a growing fascination for remote and unexplored areas moved glaciers into the focus of art so that they became as well a subject of scientific exploration and observation (*Haeberli and Zumbühl*, 2003; *Imbrie and Palmer-Imbrie*, 1986; *Vögele*, 1987).

The atmosphere of the Earth is currently undergoing changes that are unprecedented in human history (*McGuffie and Henderson-Sellers*, 2001), the most prominent feature of this being a distinct global warming (*IPCC*, 2007). Due to climatic change, glaciers are now attracting the interest of the scientific community for two main reasons:

- Glaciers are excellent climate indicators because they are sensitive to climatic change and they leave clear traces of past extent. Glaciers are of broad scientific interest because they witness current changes and traces from earlier glacier fluctuations are a valuable source of information on the climate history of the planet Earth.

- Glaciers and ice sheets are of social and economical importance. On the one hand there are concerns over the potential sea level rise due to melting ice. The disappearance of the Antarctic ice sheet would result in a sea level rise of approx. 60 m (Greenland ice sheet approx. 7 m) (*IPCC*, 2001). Further threats come from glacier avalanches and lake outbursts. On the other hand, glaciers are important for tourism (e.g. Alps, New Zealand) and their melt water is used for hydro-electric power and as water supply (e.g. in the tropical Andes, *Bradley et al.*, 2006).

Glaciers and ice caps not connected to either the Greenland- or the Antarctic ice sheet total an estimated number of 160'000 with an area of 680'000 km^2 (*Meier and Bahr*, 1996). Compared to the two ice sheets, their sea level equivalent is small (0.5 m, according to *IPCC*, 2001) but they would contribute most to the actual sea level rise (*Meier et al.*, 2007). Furthermore, their reaction to perturbations in climate is more direct and easier to interpret than for the two continental ice sheets. The key to glacier mass change is glacier mass balance which is the sum of all processes either adding mass to the glacier (accumulation) or removing mass (ablation). Mass balance modeling is therefore an important tool in understanding the glacier-climate relationship. Glacier mass balance studies vary from simple empirical approaches to more complex approaches based on energy balance considerations.

Whereas the first are regionally (on several glaciers or entire mountain ranges) and globally applied for impact assessment (e.g. *Haeberli and Hoelzle*, 1995; *Raper and Braithwaite*, 2006), the latter are run locally (at the point scale or on individual glaciers) (e.g. *Arnold et al.*, 1996; *Brock et al.*, 2000; *Gerbaux et al.*, 2005) to enhance process understanding (e.g. *Oerlemans*, 1992a,b; *Greuell*, 1992). Energy balance models on a regional scale would be desirable because they offer the advantages, over empirical approaches, of higher spatial and temporal resolution, more detailed output and higher flexibility in respect of their application in different areas (less tuning). Climate model data or gridded climatologies could be used as gridded input in such a regional application. However, biases are inherent to such data and their impact must be considered. Glacier energy balance modeling on a regional scale could, thus, be a valuable approach in assessing process relevance on a regional scale and to learn about the quality of the input data since this would be reflected in the model output. It is the goal of this thesis to address this issue by developing a regional mass balance model.

Precipitation is a key input parameter to mass balance models. However, precipitation is spatially highly variable, measurements are associated with large errors (*Sevruk*, 1985b, 1989) and the ability of climate models to reproduce precipitation is still rather limited (e.g. *Kotlarski et al.*, subm). In addition to precipitation, the redistribution of snow by wind and avalanches is also a controlling factor in glacier accumulation. The complexity of the latter becomes evident when looking at snow lines through summer as depicted in Figure 1.1: The snow line on Glärnischfirn shows only a rough correlation with altitude and several isolated patches of snow can also be seen. In consequence, accumulation is often used as a tuning factor in mass balance models while the ablation processes are treated in great detail. Scientists came up with the idea to use glaciers as precipitation gauges by deriving the unknown quantity (accumulation) from the known quantity (ablation). Pioneer work on this topic has been done by *Khodakov* (1975) and *Kotlyakov and Krenke* (1982). Glacier-derived precipitation estimates would be a valuable contribution to the sparse and uncertain precipitation measurements that currently exist for high Alpine regions. From this perspective, the idea of using glaciers as precipitation gauges would be well worth revisiting in the context of a regional application of glacier energy balance models.

Figure 1.1.: Glärnischfirn, a small mountain glacier in the Swiss Alps on 20 August 2002. Bare glacier ice and snow can be clearly distinguished.

1.2. Objectives

This thesis focuses on the understanding of the relationship between climate and mountain glaciers in the mid-latitudes. Using the Swiss Alps as an example, this study emphasizes the following two research questions. Regional scale mass balance modeling is the main subject of this thesis, precipitation assessment is a first application of the developed methodology:

Development of a regional mass balance model: The model should be designed based upon parameterizations from present day distributed energy balance models as cited in the previous section. Likewise, it should be operated at a similar spatial and temporal resolution. It is the aim of this thesis to apply the model regionally - that is to the Swiss Alps. The key question related to a regional application is the ability to acquire meteorological input data at the required spatial and temporal resolution. Climate modeling can provide the full set of required data at a denser spatial (10–20 km) and temporal resolution (hourly to daily) than meteorological data derived from meteorological observations (e.g. *Schwarb et al.*, 2001; *Schmidli et al.*, 2002; *Auer et al.*, 2007). However, the uncertainties in climate model data are large (e.g. *Kotlarski et al.*, 2005) and thus, an assessment of their influence on the model outcome will also be done in this study.

Assessment of precipitation distribution from glacier mass balance modeling: The applicability of the regional mass balance model to assess high mountain precipitation is evaluated. Precipitation is the main source of uncertainty in the model, it can be regarded as an unknown and iteratively adjusted to obtain the observed mass balances. However, the uncertainties stemming from precipitation must be significantly larger than the total of uncertainties from the remaining parameters. A parametric uncertainty analysis will be performed to address this issue.

The two main research questions can be further divided into the following detailed investigations which refer to the research papers and additional research chapters found in Part II of this thesis:

- application of helicopter-borne ground penetrating radar (GPR) to measure spatial patterns of accumulation; data from the GPR campaign are subsequently used to assess whether a horizontal accumulation gradient, estimated from a mass balance model run, actually exists
- pilot study to evaluate the performance of numerical mass balance models when applied either to groups of a few glaciers or over longer time spans
- comparison of energy fluxes and mass balance derived from two mass balance models of differing complexity
- realization of parametric uncertainty analysis to estimate uncertainties in mass balance in the form of probability density functions (PDF) of random and systematic uncertainties in input data.
- development of a regional mass balance model and an exploration of techniques to provide spatially distributed input grids at the correct resolution for the model
- application of this developed regional mass balance model to validate an existing precipitation climatology for the glacierized regions of Switzerland

In addition, measurements of mass balance distribution have been made and further data has been collected to provide data for model testing and calibration.

1.3. Outline of the Thesis

The thesis is divided into three parts: Part I includes the introduction, provides the background information related to the topic of the thesis and gives an overview of the state of the art glacier mass balance modeling. The applied methods are specified, emphasis is laid on the evolution of the applied mass balance models and on methods that are not described in detail in the research papers. Part II includes four research papers (three of them are published, one is about to be submitted), complemented by two additional chapters that contain unpublished research material. The research papers are embedded in the thesis as individual chapters. Except for the layout and the use of unified symbols, text and figures of the research papers are printed exactly as published or submitted. Furthermore, the respective lists of references have been integrated into the bibliography of the thesis. The order of appearance of the chapters in Part II reflects both the temporal and technical sequence of the fulfilled work. Finally, performed research and results are critically discussed in Part III and an outlook of related future research questions and the potential applications of the developed methodology is provided.

Throughout the text of the thesis a number of geographical regions or locations as well as individual glaciers are mentioned. The location of these geographical features is shown on a map in Figure 1.2.

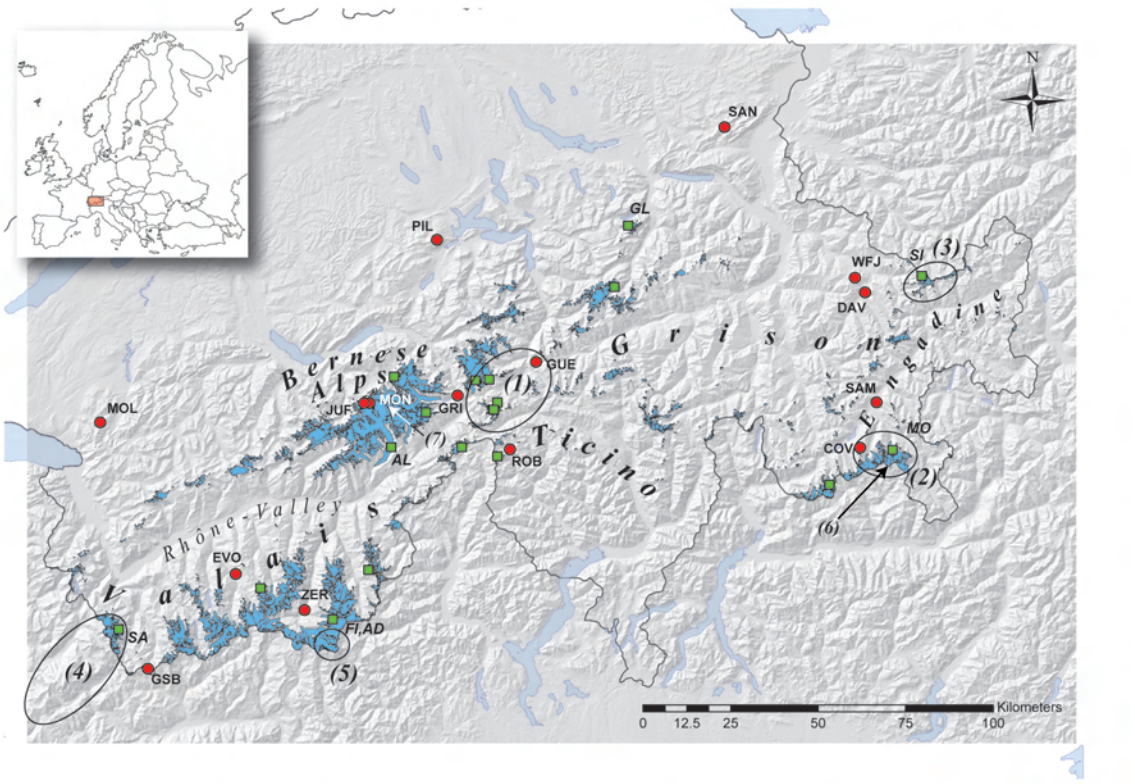

Figure 1.2.: An overview to the Swiss Alps, geographical regions and glaciers mentioned in the text. The border of Switzerland is shown in black and lakes in light blue. The black ovals refer to: (1) Gotthard Region; (2) Bernina Group; (3) Silvretta Group. (4) Mont Blanc Region; (5) Monte Rosa; (6) Piz Zupó; (7) Fieschersattel. Glacier outlines are in blue and glaciers who are either mentioned in the text or from which measurements were used are marked with green rectangles. Abbreviations (*in italic*) refer to the following glaciers: AL = Grosser Aletsch; FI,AD = Findel and Adler, SA = Glacier de Saleina, SI = Silvretta; GL = Glärnischfirn. Red dots show locations of 14 MeteoSwiss weather stations and one precipitation totalizator used in this thesis (altitude in m a.s.l.): COV = Corvatsch, 3315; DAV = Davos, 1590; EVO = Evolène, 1825; GRI = Grimsel-Hospiz, 1980; GSB = Grand-Saint-Bernard, 2472; GUE = Gütsch, 2287; JUF = Jungfraujoch, 3580; MOL = Molèson, 1972; MON = Mönchsgrat Totalizator, 3880; PIL = Pilatus, 2106; ROB = Robiei, 1898; SAM = Samedan, 1705; SAN = Säntis, 2490; WFJ = Weissfluhjoch, 2690 and ZER = Zermatt, 1638.

2. Background

2.1. Alpine Climate and Glacierization

2.1.1. General Characteristics of the Alpine Climate

The Alps form a 1000 km long and 100–250 km wide arc of mountains, stretching mainly from west to east, except for the western sector where they run from south to north (Figure 2.1). They reach elevations of up to 4800 m a.s.l. to the west, and are lower in the east. The elongated valleys running from east to west are a prominent feature of this mountain range. The Alps act as a natural barrier to atmospheric flow and form a boundary between two major climate systems: mid-latitude temperate and Mediterranean. The size and height of the Alps allow them both to modify and to trigger weather systems (*Schär et al.*, 1998). Typical modifications are, for example, rain shadows and foehn winds. In addition, lee cyclogenesis over the Gulf of Genova is induced by the presence of the Alps and is an important element of the precipitation regime in south-eastern Europe (*Schär et al.*, 1998).

Figure 2.1.: The European Alps as seen from space 11 December 2004 12:25 UTC. MODIS Rapid Response Project, NASA/GSFC (http://rapidfire.sci.gsfc.nasa.gov).

Vertical temperature gradients (atmospheric lapse rate) are a predominant feature of the Alpine climate (Figure 2.2). The lapse rate is more pronounced in summer than in winter where temperature inversion is a common feature below approx. 1500 m a.s.l. Temperatures at the southern foothills of the mountains are 2–4 °C higher compared to stations in the northern foreland (Figure 2.2). The latitudinal gradient over the Alps is greater than for other areas in Europe, causing the blocking of northern air currents from the Alps (e.g. *Schär et al.*, 1998; *Böhm et al.*, 2001; *Auer et al.*, 2007). At higher elevations the dependence of air temperature on latitude is less pronounced. In Switzerland, the 0 °C isotherm of mean annual air temperature is located at 2200–2300 m a.s.l.

It has been shown in several studies that mean temperatures at stations in high valleys, on passes and on summits are slightly lower than those in the free atmosphere (e.g. *Fliri*, 1975). This finding seems to contradict the so-called *Massenerhebungseffekt*, which refers to vegetational belts shifted upwards in the central Alps compared to the foreland. However, reduced snow cover and enhanced input of radiation are the reasons for the upward shift of, for instance, the tree line (*Barry*, 1992). Indeed, a *Massenerhebungseffekt* in the sense of higher temperatures compared to the free atmosphere cannot be observed in the Alps but is a phenomenon of dry high mountain plateaus, such as Tibet (*Flohn*, 1952). Although the general picture of mean summer and winter temperatures shows a rather strict dependency on a strong altitudinal and a weak latitudinal gradient, local circulation due to the complex topography becomes evident at individual stations or on a shorter time scale. The diurnal temperature range, for instance, decreases with altitude because valley stations are influenced by flow patterns and radiative cooling/warming at a local scale, whereas high mountain air temperature variability is dominated by synoptic air flow.

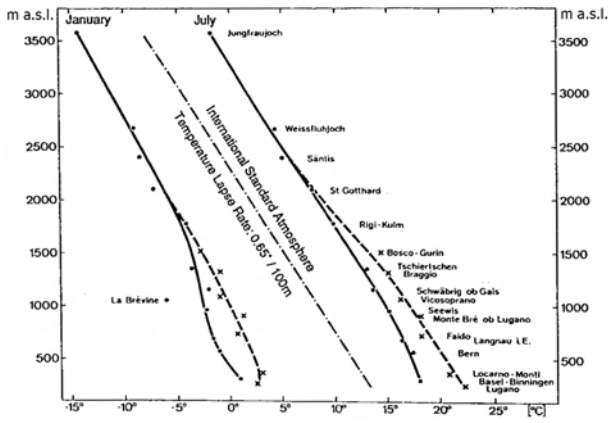

Figure 2.2.: Temperature lapse rates for mean temperatures in July and January in the Swiss Alps, obtained from synoptic weather stations. The dotted (solid) line is an approximation of the lapse rate for the stations south (north) of the main ridge, denoted with crosses (dots). Figure based upon *Schüepp et al.* (1978), reproduced in *Schär et al.* (1998).

The reduced snow cover mentioned previously in the central parts of the Alps is related to reduced precipitation. However, since spatial distribution of precipitation in the Alps is a main focus of this thesis, it is discussed separately in Section 2.1.2.

On a global scale, solar radiation is the driving force of atmospheric processes. In mountainous terrain, topography causes a complex spatial distribution of global radiation that gives rise to local circulation patterns (e.g. mountain wind systems, cf. *Barry* (1992)). Comparatively little is known about the more general features of global radiation distribution in the Alps. *Sauberer* (1955) compiled a larger set of observations for the eastern Alps and found that, in general, global radiation shows a positive trend with elevation, due to a reduction in the optical thickness of the atmosphere with elevation. The effect is most pronounced in winter and diminished during summer when convective clouds tend to form around the peaks. On a horizontal scale global radiation is reduced in the northern part of the Alps where the amount of clouds is greater than in the south (*Schär et al.*, 1998). Inner Alpine valleys are also at an advantage with respect to global radiation; the highest amounts in Switzerland are measured in the Valais and the adjacent southern valleys (*Swisstopo*, 2004).

2.1.2. High Mountain Precipitation

The Alps modify precipitation patterns on a local to regional scale and also induce weather systems on a regional to continental scale, which feed back to the precipitation distribution over the mountain range. Among the local effects is rain shadow, which results in reduced precipitation in the interior region of the mountains. However, in contrast to other mountainous areas (e.g. New Zealand Alps, Cascade Range) which have a distinct dry and humid side, the Alps receive high amounts of precipitation from both sides (e.g. *Efthymiadis et al.*, 2006). High precipitation amounts at their southern rim are partly related to lee cyclogenesis which is, in turn, due to the presence of the Alps (*Schär et al.*, 1998).

Horizontal and vertical variability of precipitation in the Alps was derived from a network of precipitation gauges which is among the densest worldwide (e.g. *Kirchhofer and Sevruk*, 2001; *Schwarb et al.*, 2001). Due to a number of effects (cf. *Sevruk*, 1985a) measured precipitation is in most cases systematically lower than real precipitation. The contribution from different sources of error to the total measurement error is a complex function of meteorological conditions, namely wind speed and type of precipitation, but is also related to the measurement device. In the case of rainfall, undercatch due to the deformation of the wind field around the gauge and wetting of the inner walls of the measurement device are of similar magnitude and mainly contribute to the total underestimation of 5–15% (*Sevruk*, 1985a). Snow crystals are lighter than rain droplets and thus, the undercatch of snowfall from wind field deformation around the precipitation gauges reaches values of 20–50% (*Sevruk*, 1985a,b). The proportion of snowfall from total precipitation and from wind speed increases with elevation and, along with it, the systematic underestimation in the measurements also increases (Figure 2.3). The local wind field as modified from obstacles in the vicinity of synoptic weather stations also has a distinct influence on undercatch. Sheltered stations experience lower wind speed and measure higher amounts of precipitation than exposed stations at similar altitudes (*Sevruk*, 1985b, 1989) (Figure 2.4).

Generally speaking, aridity is a function of distance to the northern and southern edge of the Alps, both of which receive about 2–2.5 m of precipitation annually. Only in the Gotthard area and in the Mont Blanc region do the northern and southern zones of high precipitation meet (*Frei and Schär*, 1998). Precipitation generally increases with altitude, but unlike air temperature, horizontal and vertical gradients are of similar orders of mag-

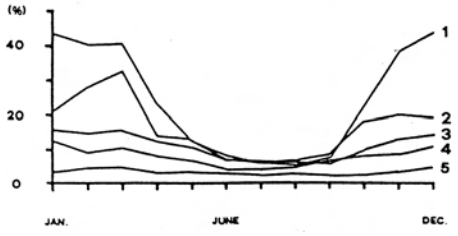

Figure 2.3.: Monthly correction estimates in percent for precipitation, measured at five synoptic weather stations. 1. San Bernhardino (1628 m a.s.l.); 2. Davos (1580 m a.s.l.); 3. Geneva (416 m a.s.l.); 4. Zürich (556 m a.s.l.); 5. Locarno (336 m a.s.l.). Figure from *Sevruk* (1985b).

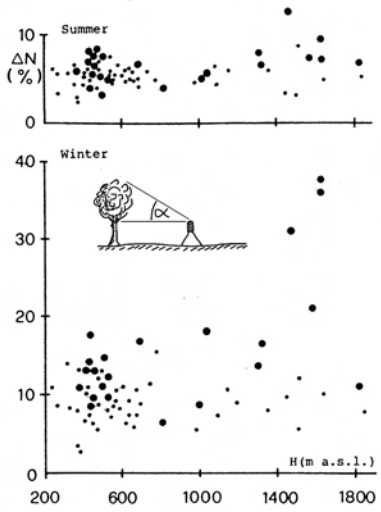

Figure 2.4.: The effect of altitude and local sheltering on correction estimates for measured precipitation. Large dots indicate exposed gauge sites ($\alpha < 10\,^\circ$) and small dots indicate sheltered sites ($\alpha \geq 10\,^\circ$) (α denotes the angle from the measurement device to obstacles nearby, as illustrated in the small inset drawing with the example of a tree close to the measurement device). Figure modified from *Sevruk* (1985b).

nitude and both are highly variable at a local level. Thus, it must be stressed that the vertical precipitation gradient (Γ_P) is, to some extent, a virtual parameter, since vertical and horizontal components of the precipitation distribution can never be fully distinguished (*Frei and Schär*, 1998; *Schwarb*, 2000). From an analysis of a large set of station records from the Swiss Alps, *Sevruk* (1997) found that Γ_P is generally higher in the northern areas (0.008–0.015 m m^{-1} a^{-1}) and lower south of the main divide (0.001–0.004 m m^{-1} a^{-1}). In the Ticino region, negative vertical gradients can also appear (*Sevruk*, 1997).

With respect to glacier mass balances, the elevation of maximum precipitation is of particular interest. It is estimated that precipitation decreases above roughly 3500 m a.s.l. However, reliable measurements to confirm this do not exist. A very rough estimate of precipitation in the highest areas of the Alps can be made from measured accumulation

rates in ice cores. For instance, *Schwerzmann et al.* (2006) found yearly accumulation rates of 1 to 3 m w.e. in an ice core obtained from Fieschersattel (3900 m a.s.l.) in the Bernese Alps. Similar accumulation rates could be observed in an ice core drilled in the eastern Swiss Alps, in the vicinity of Piz Zupó at 3900 m a.s.l. (pers. comm. Margit Schwikowski). *Suter* (2002) measured accumulation distribution in 1999/2000 in the highest parts (3900 – 4600 m a.s.l.) of Monte Rosa (southern Valaisian Alps). A complex spatial pattern was observed with values reaching from 0.3 m snow to almost 4 m snow. Lowest accumulation rates were measured at wind exposed saddles. The difference in accumulation by one order of magnitude within a few hundred meters of horizontal distance indicates the strong influence of wind and related snow redistribution in such high mountain areas.

2.1.3. Spatial and Temporal Variability of the Alpine Climate

A number of meteorological networks are maintained in the Alpine region, including the national weather services, weather observations for aviation, as well as highly specialized scientific observation programs. Together they form one of the densest networks of meteorological observations in mountainous terrain worldwide. Any attempt to assess temporal and spatial variability of the Alpine climate must first address the issue of collecting time series of measurements and related meta-data. Measurements have to be analyzed for inconsistencies, breaks and systematic errors which can stem from changes and modification in the measurement devices, changing measurement sites, or changes around the measurement site (e.g. urbanization). The process of detecting and removing systematic inconsistencies with respect to a norm period is called homogenization (e.g. *Böhm et al.*, 2001; *Begert et al.*, 2005). In recent years, a number of studies have been devoted to these issues. Climatologies for the Alps or subregions have been established and analyzed with respect to spatial and temporal variability. A selection of such studies is listed in Table 2.1.

Most studies focused on precipitation distribution over the Alps. They dealt with the uncertainties in different ways. For climatologies with low spatial resolution (e.g. *Schmidli et al.*, 2002) mean precipitation over the individual boxes of the chosen raster is usually calculated without explicit corrections for vertical gradients. For their high resolution precipitation maps *Kirchhofer and Sevruk* (2001) assumed a fixed Γ_P of $0.0008\,\mathrm{m\,a^{-1}\,m^{-1}}$ whereas (*Schwarb et al.*, 2001) used spatially variable Γ_P (mean $\Gamma_P = 0.0005\,\mathrm{m\,a^{-1}\,m^{-1}}$), as obtained through the PRISM interpolation scheme (*Daly et al.*, 1994). *Kirchhofer and Sevruk* (2001) presented a precipitation distribution that has been corrected for systematic measurement errors. *Schwarb et al.* (2001) depict raw values in their map and state that they should be corrected at 15–30% for areas above 1500 m a.s.l. In Figure 2.5 a section of the *Schwarb et al.* (2001) climatology is presented. Zones of higher precipitation at the northern edge of the Alps and south of the main ridge in the Ticino region can be seen. Both zones meet in the Gotthard area, whereas to the east and to the west they are separated by dryer inner-Alpine regions.

Climatologies dealing with temporal and spatial variability (e.g. *Schmidli et al.*, 2002; *Begert et al.*, 2005; *Auer et al.*, 2007) have been analyzed by their respective authors on temporal trends in the observed variables. According to *Böhm et al.* (2001) and *Auer et al.* (2007), observed increase in air temperature amounts to 1.1 K and 1.2 K, respectively, during the 20th century and exceeds the global mean as well as the mean of the northern hemisphere (*Begert et al.*, 2005). Mean precipitation for the Alps does not show a significant

Table 2.1.: Selection of different climatologies for the greater Alpine area, including homogenized time series for individual stations as well as gridded climatologies (for re-analysis data sets see Section 2.3.3). Most climatologies are based upon a longitude/latitude grid with varying grid size depending on distance from the poles. The approximate spatial resolution is given in km and valid for the greater Alpine region. The numbers in brackets refer to the following additional information: [1] Coarse Resolution Subregional (CRS) mean series have also been established; [2] shown is the longest time series available; [3] 20 year monthly means are also available; [4] homogenized time series for different stations. The number of available time series varies strongly with time and for the different parameters.

author	parameter	area	spatial res.	temporal res.	time frame
Frei and Schär (1998)	P	Alps	25 km	daily	1971–90
New et al. (2000)	T, P	worldwide	50 km	monthly	1901–96
Böhm et al. (2001)	T	Alps	97 stat. / 90 km [1]	monthly	1760–2000 [2]
Kirchhofer and Sevruk (2001)	P	Switzerland	1 km	30 yr-mean	1951–80
Kästner and Kriebel (2001)	n	Central Alps	15 km	monthly	1989-1996
Schwarb et al. (2001)	P	Alps	2 km	20 yr-mean [3]	1971–90
Schmidli et al. (2002)	P	Alps	25 km	monthly	1901–90
Skoda and Lorenz (2003)	P	Austria	6 km	30 yr-mean	1961–90
Meerkötter et al. (2004)	n	Europe	1 km	monthly	1989–2003
Begert et al. (2005)	T, P	Switzerland	12 stat.	monthly	1864–2003
Efthymiadis et al. (2006)	P	Alps	20 km	monthly	1800–2003
Auer et al. (2007)	T, P, p	Alps	90 km	monthly	1800–2000
Auer et al. (2007)	T, P, p, n, S, e_a	Alps	[1,4]	monthly	1760–2000 [2]

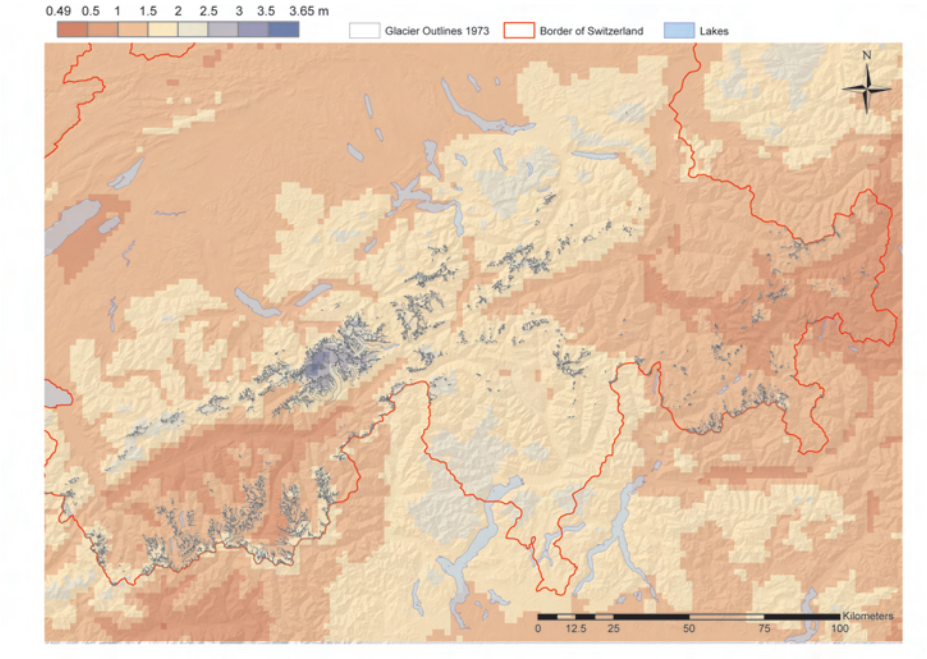

Figure 2.5.: Mean annual precipitation sum (1971–1990) for the Swiss Alps according to *Schwarb et al.* (2001).

increase or decrease. However, during the 20th century, an increase in winter precipitation by 20–30 % over the western Alps and a decrease in autumn precipitation south of the main ridge by 20–40 % was observed (*Schmidli et al.*, 2002).

A variety of cloud cover climatologies has been established from satellite data, including the two data sets listed in Table 2.1 (*Kästner and Kriebel*, 2001; *Meerkötter et al.*, 2004) as well as worldwide data sets, established in the course of the International Cloud Climatology Project ISCCP (e.g. *Rossow and Schiffer*, 1999). However, the latter are of rather course resolution of 280 km and 30 km. In general, the establishment of cloud maps from satellite data over non-vegetated, snow-covered or glacierized areas can result in errors that are in the order of 10–30% (*Kästner and Kriebel*, 2001). A direct comparison of the cloudiness map from *Swisstopo* (2004) based upon manual ground observations and *Kästner and Kriebel* (2001) reveals disagreement in the spatial distribution of cloud amount. While in the first data set cloudiness in the southern Valais is low (∼45% over the time period 1931–1970), mean cloud cover for the same area and the time span 1989–1996 amounts to 85–90% in the latter data set. Although time spans are different, a doubling in cloud amount is unlikely and the comparison indicates that a more detailed evaluation of cloud amount over high mountain areas derived from satellite data is required. Temporal analysis of the 14 years data set by *Meerkötter et al.* (2004) shows no trend in time.

With respect to radiative fluxes, no gridded climatologies are available. Monthly means of measured radiative fluxes are collected and stored by the Global Energy Balance Archive (GEBA) (cf. *Gilgen et al.*, 1997; *Gilgen and Ohmura*, 1999). Worldwide trends have been estimated from station records and it was found that global radiation decreased from 1940–

1980 at a global scale (global dimming, *Ohmura and Lang* (1989); *Gilgen et al.* (1998)) followed by recent global brightening (*Wild et al.*, 2005). *Philipona and Dürr* (2004) analyzed radiation measurements conducted in the Alpine region and concluded that the trend continued from 1981–2004, however at a reduced pace. *Philipona and Dürr* (2004) have also shown that for the respective time period the increase of long-wave downward radiation is significantly larger than the decrease in global radiation. The influence of long-term variability of global radiation on glacier mass balance was analyzed by *Ohmura et al.* (2007).

2.1.4. Alpine Glacierization and Precipitation

In the middle of the 1970s the total glacier area in the Alps amounted to approx. 2900 km^2 (*IAHS(ICSI)/UNEP/UNESCO*, 1989). From the end of the so-called Little Ice Age (around 1850) to the mid-1970s the Alpine glaciers had already lost roughly 1500 km^2 in area (*Zemp et al.*, 2006a). Another 22% of the area of the 1970s glaciation was lost by the year 2000 (*Paul et al.*, 2004). The glacierization of the Alps in the 1970s consisted of approx. 5000 glaciers but only about 1800 of these ice bodies were larger than 0.2 km^2 (*Haeberli and Hoelzle*, 1995). Nevertheless, they accounted for 88% of the surface area and 98% of the total volume. In the course of this study, small glacierets and ice patches $< 0.2\,km^2$ will not be further analyzed and where not mentioned otherwise, only glaciers $> 0.2\,km^2$ are considered. Most of the Alpine glaciers (90%) are small mountain glaciers of less than 5 km length and 10 km^2 area (*Haeberli and Hoelzle*, 1995). Larger valley glaciers (Grosser Aletsch Gletscher located in the Bernese Alps being the largest in the Alps with a length of 23 km and an area of 84 km^2 *Maisch et al.*, 1999) are rare but strongly contribute to total area and volume. The equilibrium line altitude (ELA) is on most glaciers (75%) above 2800 m a.s.l. Considering that at this altitude mean annual air temperature is approx. $-4\,°C$ it can be assumed that many Alpine glaciers are not strictly temperate but rather polythermal. On the other hand, only 3% of the Alpine glaciers start at above 4000 m a.s.l. and thus are very likely to possess a firn area that is at least partly cold (*Haeberli and Hoelzle*, 1995).

In the present thesis the Swiss glaciers are used as the test area for the regional mass balance model. They occupied an area of 1280 km^2 in 1973 and consisted of approximately 2000 individual glaciers (*Müller et al.*, 1976; *Paul et al.*, 2004). From 1973–2000 the Swiss glaciers experienced considerable shrinkage amounting to an area loss of 20% (*Paul et al.*, 2004; *Zemp et al.*, 2006a; *Paul*, 2007). In recent years many Alpine glaciers have been shifting towards a regime of downwasting instead of dynamical retreat (*Paul et al.*, 2007). Glaciers in the Alps are prone to downwasting because shear stress along the central flowlines are mostly low. Thus, flow speed is also low and the glaciers react more through vertical surface altitude adjustement than by distinct advance or retreat (*Haeberli and Hoelzle*, 1995). The loss in glacier surface and volume is attributed mainly to rising mean air temperatures and the related changes in the energy balance at the glacier surface.

The spatial distribution of glacier in the Swiss Alps clearly reflects precipitation patterns. Basically, glaciers tend to form where mountains are highest and thus temperatures are lowest so that snow can accumulate. In this way, precipitation also exercises a strong influence on glacier distribution. In the Swiss Alps topography strongly reflects temperature distribution because horizontal variability of air temperatures is small compared to vertical lapse rate (Section 2.1.1). Thus, glacier size is, in a first approximation, the combined result of topography and precipitation amounts because air temperature is assumed to depend on

altitude alone in this simple approximation. The equilibrium line altitude, on the other hand, is a good indication of the amount of precipitation. Equilibrium lines at 2550–2800 m a.s.l. are observed at the northern edge and the Gotthard area where precipitation is high. In the dryer central parts ELA are higher, culminating at 3200–3400 m a.s.l. in the south eastern part of the Valais (*Maisch et al.*, 1999). However, large local deviations from regional means in ELA occur where glaciers are fed mainly by avalanches or exposed on dome-shaped summits with high wind speeds and related erosion of snow. *Kotlyakov* (1973) and *Kuhn* (2003) noted that accumulation on glaciers is for the most part higher than local precipitation amounts. From measurements of precipitation and accumulation a relationship of these two quantities was established for different kinds of glaciers, extending from 3 for cirque glaciers to 1–1.4 for large valley glaciers (*Kotlyakov*, 1973). Such considerations are important in more detailed comparisons of precipitation patterns and glacier parameters, such as the ELA (cf. Section 2.4).

2.2. Glacier Mass Balance

The basic concept of mass balance distribution on a typical mountain glacier of the mid-latitudes is a straightforward one: Above a certain altitude which is referred to as the equilibrium line altitude (ELA), processes that add mass (accumulation) outweigh the processes that remove mass from the glacier (ablation). Below the ELA, ablation dominates and the glacier loses mass (Figure 2.6). The ELA is the mean altitude that separates the accumulation from the ablation area at the end of a mass balance year (the end of a mass balance year is reached when the accumulation season ends, i.e., the accumulation processes are again dominant, cf. stratigraphical and fixed date system, Section 2.2.1). When the ELAs have been determined over several mass balance years on a glacier, the ELA_0 can be estimated. The latter is the ELA for an average balanced year where surface accumulation equals ablation over the entire glacier. Over a longer time span, accumulated snow gradually converts into glacier ice and, passing the ELA_0, flows down-valley to the ablation zone.

While the ELA is more a theoretical concept that cannot be directly observed, other boundaries between different zones on a glacier can be seen: During summer, the snow-line separates snow-covered and snow-free parts of a glacier. The snowline moves up- and downward in the course of a year, it drops sharply after snowfall events and often describes a complex pattern (cf. Figures 1.1, 2.6). The equilibrium-line (EL) can be approximated from the firn-line which is the snow-line at its maximum elevation in the course of the ablation season. However, misinterpretations may result when the snowline is lowered by autumn snowfall events. Furthermore, superimposed ice is often formed at the bottom of the snow layer from refreezing meltwater percolating through the snow cover. Superimposed ice might look similar to glacier ice and thus, the EL is often somewhat lower than the visible firn-line (for an overview of the definitions of the different lines observed on a glacier and the related historical background, reference is given to *Braithwaite*, 2008).

The rate of accumulation or ablation processes at a point on a glacier is denoted with $\dot{b}$. The mass balance at a point and over a time interval t_1 to t_2 is obtained by integrating b:

$$b = \int_{t_1}^{t_2} \dot{b}\,\mathrm{d}t \tag{2.1}$$

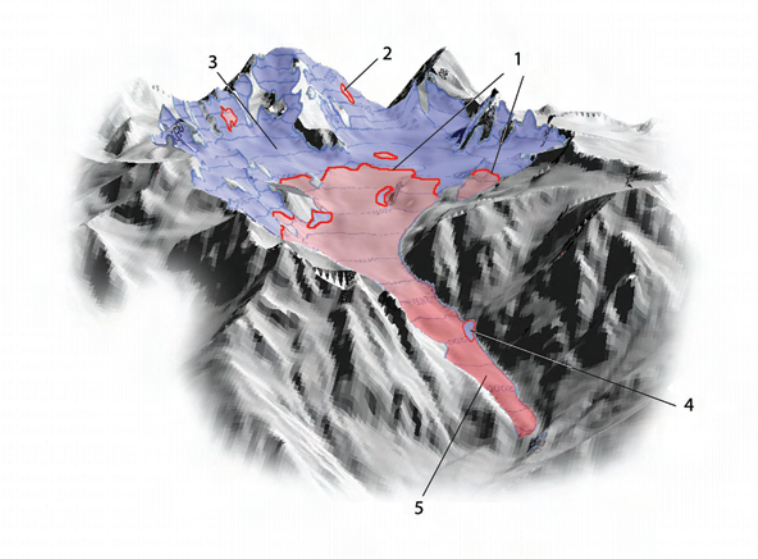

Figure 2.6.: A schematic picture of a mid-sized mountain glacier illustrating mass balance terms (glacier de Saleina, Swiss part of the Mont Blanc area). 1: equilibrium line (EL); 2: patch of negative mass balance above ELA due to avalanching; 3: accumulation area; 4: patch of positive mass balance below the ELA, fed from avalanches descending through the lateral valley; 5: ablation area.

where b is the sum of all accumulation (c) and ablation processes (a) as follows (e.g. *Kuhn*, 1981):

$$b = c - a = P_{solid} + P_{stored} + C + R_D + R_A - M + M_{stored} - E - K \tag{2.2}$$

P_{solid} denotes snowfall, P_{stored} is the part of liquid precipitation that is stored in the snow cover. C is accumulation due to condensation, R_D and R_A denote redistribution of snow from wind drift and avalanches, respectively. Both processes can add or remove mass. Evaporation is denoted with E and calving with K. On most mid-latitude glaciers melt (M) and solid precipitation (P_{solid}) are the dominant components of the mass balance. On cold and polythermal glaciers, M_{stored} – which is the part of M that does not leave the glacier but refreezes – is important. R_D influences the spatial distribution of accumulation on the entire glacier surface. R_A can be even more effective locally in snow redistribution, but is related to the occurrence of steep slopes (Figure 2.6). As a rule of thumb, the larger a glacier the more do R_D and R_A redistribute mass within the glacier perimeter, rather than removing or adding mass from outside to the glacier (*Kotlyakov*, 1973; *Kuhn*, 2003). Integration of b over a specific area A yields the total mass balance (B):

$$B = \int_A b \, \mathrm{d}t \, \mathrm{d}A \tag{2.3}$$

We are often interested in the total mass balance for the entire area of a glacier and the time span of one mass balance year, hence A is often equal to the total area of a glacier and t_1 to t_2 correspond to the beginning and end of a mass balance year (cf. Section 2.2.1). B has the unit m^3 and is divided by the glacier surface A to obtain the glacier mass balance

$\bar{B}$ which has unit m and allows for a direct comparison among different glaciers. Usually, all mass balance terms are given in m w.e. (meter water equivalent) instead of m or m^3 ice or snow.

Glacier dynamics come into play when mass balances over a longer time span are the subject of interest. When $\bar{B} = 0\,\text{m}$ w.e, integrated over a longer time interval, usually the response time of a glacier, the glacier is in steady-state. A change in climatic conditions will modify mass balance. To reach a new steady state again where $\bar{B} = 0\,\text{m}$ w.e, the glacier has to resize its ablation area by advance or melt-back and simultaneously adjust its geometry (e.g. glacier width, glacier surface elevation) till mass loss and mass gain are balanced again. After a certain time span (the reaction time), the glacier's dynamical response to the change in mass balance will set in. The response time (cf. *Jóhannesson et al.*, 1989) is the time a glacier requires to reach a new steady state. In reality, climatic conditions are under permanent change and glaciers are generally not in steady state. Nevertheless, the steady-state glacier is an important theoretical concept for understanding the glacier climate relationship (e.g. *Jóhannesson et al.*, 1989).

2.2.1. Measurement of Mass Balance

Different techniques are applied to measure glacier mass balance. The so-called 'direct glaciological method' and the 'geodetic method' are the most important ones and are explained below. Further methods exist. For instance, the hydrological methods are based upon discharge measurements that are brought into relation with precipitation and evaporation over a glacierized catchment. These latter methods are not discussed in further detail here.

In the direct glaciological method, point measurements of mass balance are performed directly on the glacier. Accumulation that occurs between two points in time (t_1 and t_2) is measured by probing the snow depth with snow probes, and by snow density readings, usually from snow pits (cf. Figure 2.7). Measuring accumulation in between t_1 and t_2 requires determination of the horizon within the snow pack that corresponds to t_1. Considerable uncertainty is often connected with the detection of this horizon (e.g. *Jansson*, 1999). Ablation is measured from stakes that are drilled into the glacier ice (Figure 2.7). At t_1 and t_2 the length of the stake that sticks out of the ice is noted and subtraction yields melt in between t_1 and t_2. Melt measurements from stakes are straightforward and can be performed at a large number of points on a glacier (see above and *Hoinkes*, 1970; *Østrem and Brugman*, 1991). However, accumulation is more difficult to quantify both for technical reasons (cf. *Østrem and Brugman*, 1991), and due to the high spatial and temporal variability of the snow cover (cf. Paper №1) that would require a dense sampling (e.g. *Holmlund and Jansson*, 1999; *Plattner et al.*, 2006).

Measurements of annual mass balance can be performed according to either the fixed date system or the stratigraphic system, which represent two different definitions of the so-called mass balance year. The latter system takes the real mass balance year into account which lasts from the end of the ablation season to the end of ablation season in the following year. The real mass balance year is not fixed to 365 days but varies depending on weather conditions. Furthermore, the mass balance year ends later on the tongue of a glacier than in the accumulation area where autumn snowfalls usually occur earlier (*Anonymous*, 1969). Consequently mass balance measurements are difficult to perform according to a strict

Figure 2.7.: Mass balance measurements on Findel glacier. Left: Stake measurement at the very terminus of the glacier (2600 m a.s.l.). Note the dark ice surface and the Matterhorn in the background. Right: digging a snow pit at about 3300 m a.s.l.

stratigraphic system. The fixed date system defines a mass balance year as starting on October 1 and ending on September 30 (*Anonymous*, 1969). Because the length of a mass balance year in the fixed date and the stratigraphic system can vary, measured mass balance for an individual year depends on the chosen system. However, over longer time spans, both systems yield identical balances.

The direct glaciological method has the advantage of providing information about processes at the point scale and if measurements are repeated regularly, a high temporal resolution can be achieved. The application of sonic rangers makes possible even continuous records of surface elevation changes at a point (e.g. *Klok and Oerlemans*, 2004). Regular measurements of annual mass balances for entire glaciers are usually performed with the direct glaciological method but measurements are limited to accessible areas; crevassed zones, steep regions and larger avalanche deposits cannot be measured using the direct glaciological method. The application to an entire glacier requires dense sampling (*Cogley*, 1999), the method is laborious and time-consuming and is thus mostly performed on smaller glaciers (a few km^2). As a consequence, larger glaciers are under-represented in the mass balance observation networks (*Zemp et al.*, subm). Determination of $\bar{B}$ for an entire glacier requires inter- and extrapolation from the point measurements, the main source of uncertainties inherent to the method. To find appropriate interpolation schemes is not a trivial task and misconceptions may result in systematic errors that accumulate throughout longer time series of mass balance measurements (e.g. *Andreassen*, 1999; *Krimmel*, 1999).

The determination of mass balance using the geodetic method involves the comparison of surface elevation at t_1 and t_2 over the surface of an entire glacier. Changes in surface elevations between t_1 and t_2 have to be translated into mass balance by multiplication with density. Mass balances further back in time are derived from the comparison of topographic

maps (e.g. *Østrem and Haakensen*, 1999; *Bauder et al.*, 2007) while more recent mass balances are often calculated from digital elevation models (DEM) derived from remote sensing data. Laser altimetry, for instance, has become popular for constructing DEMs of the glacier surface topography (e.g. *Favey et al.*, 1999; *Geist and Stötter*, 2007). The method is suitable for large glaciers or glacier ensembles. *Arendt et al.* (2002), for instance, have assessed mass balance for a large number of glaciers in Alaska from laser profiling which is similar to the geodetic method of mass balance measurement. Errors in constructed DEMs of the glacier surface at different points in time are usually independent and thus, the method is not prone to systematic errors accumulating through time. Geodetic mass balances are usually calculated over time intervals longer than one year because the signal to noise ratio improves when the DEMs being compared are further apart in time. *Haeberli* (2006) recommends time intervals of 10 years for regularly repeated surveys.

The geodetic method provides accurate estimates on $\bar{B}$ for entire glaciers. Usually some general assumptions on density are made, which is a potential source of error. Information at the point scale can only be obtained when the vertical flow field at the glacier surface is known. Initial attempts to combine geodetic mass balance and flow modeling to obtain mass balance distribution have been made by *Kääb and Funk* (1999); *Hubbard et al.* (2000) or *Bauder* (2001). However, the resulting point information has not yet achieved the accuracy of stake measurements.

The direct glaciological method has its strength where the geodetic method has its weaknesses and vice versa. Thus the combination of methods is the most sensible way to achieve accurate distributed mass balance over longer time spans (e.g. *Andreassen*, 1999; *IUGG (CCS) – UNEP – UNESCO*, 2005; *Haeberli*, 2006). In such a combined approach, systematic errors are minimized by deriving long-term cumulative mass balance from geodetic measurements while short-time variability and spatial distribution are measured with the direct glaciological method (e.g. *Østrem and Haakensen*, 1999; *Haeberli*, 2006).

Worldwide glacier observations including mass balance measurements are collected and published by the World Glacier Monitoring Service (WGMS) (*IUGG (CCS) – UNEP – UNESCO*, 2005; *WGMS*, 2007). The Global Terrestrial Network for Glaciers (GTN-G) is based upon a tiered observation strategy (*Haeberli et al.*, 2000, 2002; *Haeberli*, 2004). Tier 1 refers to coordinated observations across environmental gradients, as for instance, from southern Europe to the European arctics. At Tier 2 detailed process-oriented studies are performed (e.g. Storglaciären, Sweden). Annual mass balance measurements conducted with a reduced stake network in combination with regularly repeated geodetic mass balance surveys are classified as Tier 3. Tier 4 includes long-term observations of glacier length change while Tier 5 incorporates glacier inventories from remote sensing imagery (cf. *Haeberli*, 2006, for a more detailed description of the tiered observation strategy).

Two important components of the observation strategy are the linking of different levels of observation and the assessment of their meaning from theoretical considerations and modeling approaches. The combination of modeling approaches and measurements helps to assess feedback mechanisms, to evaluate the representativity of available measurements and to extrapolate from measured to unmeasured sites. For instance, it is often stated that the glacier mass balance is a direct measure of weather conditions. However, at closer inspection it becomes obvious that mass balance is one element in a chain of processes with inherent feedback mechanisms (Figure 2.8). Positive or negative mass balances over a longer time span will result in advance or retreat of a glacier. Nevertheless, a change in surface elevation

will feed back on mass balance (surface height feedback). *Raymond et al.* (2005) illustrate, based on the example of Glaciar Tyndall, Patagonia, how different feedback mechanisms impact mass balance and they give an estimate of the individual contributions. *Nemec et al.* (subm) modeled surface mass balance of Morteratsch glacier in southeastern Switzerland since 1865. Feedback from geometry changes was studied by performing runs with a variable and a fixed glacier geometry. It is recognized that mass balance modeling is an important component in glacier observation networks (cf. *Haeberli*, 2006 and Paper №2).

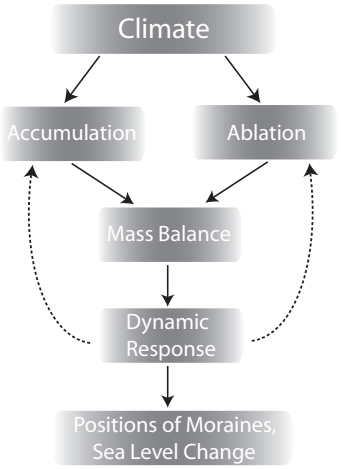

Figure 2.8.: The chain of processes describing the relationship of mountain glaciers and climate. Feedback mechanisms are indicated by dotted lines. (Figure modified from *Meier*, 1965 and *Kuhn*, 1981).

2.2.2. Surface Energy Balance

Ablation processes are a key element in the glacier-climate relationship (Figure 2.8). Thus a comprehensive understanding of the glaciers reaction to climate change also requires detailed investigations of the surface energy balance which governs the ablation processes. A large number of studies has been devoted to the energy balance at the glacier surface (e.g. *Sauberer and Dirmhirn*, 1952; *Hoinkes*, 1954; *Kraus*, 1973; *Kuhn*, 1981; *Greuell et al.*, 1997; *Oerlemans*, 2000; *Oerlemans and Grisogono*, 2002). The full energy balance is written as follows:

$$Q_m + G = S_{in} - S_{out} + L_{in} - L_{out} + Q_h + Q_l + Q_R \tag{2.4}$$

Q_m is the energy consumed through melting of snow, firn or ice whereas G denotes the loss or gain of heat in the snow, firn or ice pack. S_{in} and S_{out} are incoming and reflected short-wave radiation, L_{in} and L_{out} are incoming and emitted long-wave radiation. Sensible and latent heat fluxes are represented by Q_h and Q_l, respectively. Q_R denotes the heat flux from rain which is usually small. The different components of the glacier energy balance are illustrated schematically in Figure 2.9.

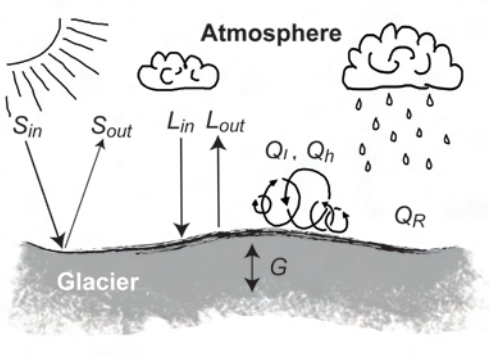

Figure 2.9.: A schematic illustration of the glacier surface energy balance.

To derive melt (M), Q_m has to be divided by l_m which is the latent heat of fusion of ice ($334\,kJ\,kg^{-1}$). $S_{in} - S_{out}$ is the short-wave radiation balance which can also be written as follows, indicating the influence of the surface albedo (α):

$$S_{in} - S_{out} = S_{in}(1 - \alpha) \tag{2.5}$$

S_{in}, which is also called global radiation, is the total of direct radiation ($S_{in,dir}$) and diffuse radiation ($S_{in,dif}$). Under clear sky conditions, $S_{in,dir}$ depends in the first order on solar zenith angle which is a function of daytime, day of the year and latitude (e.g. *Iqbal*, 1983) and is further modified by the atmosphere and in a complex manner by local topography, including inclination of the local surface, shading and reflections from surrounding terrain (*Garnier and Ohmura*, 1968). $S_{in,dif}$ depends mainly on atmospheric composition, reflections from surrounding terrain and the sky-view factor which is defined as the ratio of the sky portion seen from a specific point at the surface to that on an unobstructed horizontal surface. Cloudiness (n) has a decisive and complex influence on the short-wave radiation balance. Completely overcast skies reduce $S_{in,dir}$ to zero, high and thin clouds can result in even higher S_{in} than under clear sky conditions. Cloudiness is spatially and temporally highly variable and thus a major source of uncertainties in global radiation parameterizations (e.g. *Klok and Oerlemans*, 2002). Conversely, global radiation under clear sky conditions can be addressed quite precisely by solar radiation codes as described in *Iqbal* (1983); *Dubayah and Rich* (1995); *Wilson and Gallant* (2000) or *Corripio* (2003).

The short-wave radiation balance at the surface depends on the surface albedo (Eq. 2.5) which is the ratio of diffusely reflected to incident electromagnetic radiation, integrated over a specific range of the spectrum (here short-wave radiation). Glacier ice albedo ranges from 0.1 for very dirty ice to approx. 0.4 for clean ice. Snow albedo varies from approx. 0.5 for old and wet snow to 0.85 for fresh dry snow.

The emitted long-wave radiation is written as follows:

$$L_{out} = \varepsilon \sigma T_{surf}^4 \tag{2.6}$$

where ε is the emissivity, σ is the Stefan-Boltzmann constant ($5.67 \cdot 10^{-8} \mathrm{J\,K^{-4}\,m^{-2}\,s^{-1}}$) and T_{surf} is the surface temperature in Kelvin. Snow and ice act almost as ideal black bodies

($\varepsilon \approx 1$) in the long-wave spectrum and thus emit according to their temperature but also absorb virtually all of the received L_{in}. For a melting ice/snow surface with $T_{surf} = 0\,^{\circ}\mathrm{C}$ the value is fixed at $L_{out} = 316\,\mathrm{W\,m^{-2}}$. L_{in} is emitted from the atmosphere and thus a precise calculation requires a detailed description of the different layers in the atmosphere with their respective temperatures and emissivities (*Ohmura*, 2001). The latter depend on greenhouse gases, cloudiness, aerosols and water vapor content (e.g. *Konzelmann et al.*, 1994). Furthermore, surrounding terrain emits long-wave radiation. Its influence on the long-wave radiation balance depends on surface temperature and the terrain-view factor (= 1 - sky-view).

The sum of sensible and latent heat fluxes is called 'turbulent heat fluxes'. During summer, the air above the ice surface is usually warmer than the ice and sensible heat is transported through eddies along the resulting gradient toward the glacier. Latent heat fluxes are in the first order a function of the gradient in water vapor pressure over the ice surface. The efficiency of eddy conductivity and the related turbulent fluxes further depends on the surface roughness and on wind speed, which in the glacier boundary layer is dominated by the katabatic flow (*Oerlemans*, 2001). Both Q_h and Q_l can be determined from eddy correlation measurements. Detailed measurements of meteorological conditions (wind speed, humidity, air temperature at different heights above the surface) and other parameters (surface roughness length) are required to calculate turbulent fluxes from, for instance, the bulk approach or the Monin-Obukhov similarity theory (*Monin and Obukhov*, 1954). However, due to their high spatial and temporal variability, measured fluxes are of very limited representativity for entire glacier surfaces.

The influence of the individual components of the glacier energy balance on glacier mass balance varies depending on the climatic settings where a glacier is located. A short discussion on the weighting of the different components of glacier energy balance under the Alpine summer climate is given in the following. S_{in} reaches a daily mean of almost $400\,\mathrm{W\,m^{-2}}$ on sunny days in Summer. Assuming $\alpha = 0.25$ for a typical ice surface and $S_{in} = 250\,\mathrm{W\,m^{-2}}$ for an average daily mean during summer, the short-wave radiation balance amounts to $190\,\mathrm{W\,m^{-2}}$. L_{out} is fixed to $316\,\mathrm{W\,m^{-2}}$ for a melting ice surface of $0\,^{\circ}\mathrm{C}$. L_{in} attains daily means of up to $360\,\mathrm{W\,m^{-2}}$ on warm humid and cloudy days but is usually close to L_{out}, yielding a long-wave radiation balance close to zero. Q_h and Q_l are mostly positive (i.e. directed from the atmosphere toward the surface) and in the range of a few tens of $\mathrm{W\,m^{-2}}$. From this comparison it becomes obvious why it is often stated that the short-wave radiation balance contributes the major part of the energy available for melt. However, this statement is not very instructive for understanding the glacier climate relationship. A different picture emerges when the variability of the different fluxes is considered. *Ohmura* (2001) points out that L_{in}, Q_h and Q_l all strongly depend on air temperature. However, L_{out} is fixed to $316\,\mathrm{W\,m^{-2}}$ throughout the melt season and the short-wave radiation balance changes only slightly from year to year. Air temperature exhibits strong fluctuations; among all the meteorological properties that govern mass balance it has by far the most prominent altitudinal gradient and rising air temperatures are the most pronounced signal of ongoing climate change. Warmer air temperature also results in reduced amount of snowfall and, together with a more positive energy balance, in an earlier disappearance of the snow cover. The latter in turn leads to a lower surface albedo and a higher short-wave balance. Thus it becomes obvious that air temperature has a significant influence on the temporal and spatial (altitudinal) variability of the glacier surface energy balance.

2.2.3. Mass Balance Modeling

A wealth of different approaches to model glacier mass balance has been developed. In the following a short overview of the different approaches is given. For an in-depth discussion of different modeling techniques reference is given to *Oerlemans* (2001), *Greuell and Genthon* (2004) or *Hock* (2005).

More complex models are based upon energy balance considerations. In simplified energy balance models, only the dominant components are treated in detail while other components are parameterized or neglected. The surface temperature, for instance, is often fixed at 0 °C (e.g. *Arnold et al.*, 1996; *Paul et al.*, 2008). Complex energy balance models have frequently evolved from snow models (e.g. *Greuell and Konzelmann*, 1994; *Bartelt and Lehning*, 2002) and later been applied to the analysis of detailed aspects of the glacier mass balance such as the formation of superimposed ice (*Obleitner and Lehning*, 2004) or internal accumulation (*Reijmer and Hock*, 2008). Nonetheless, reasonable estimates of mass balance can also be obtained from more simple approaches. Positive degree day models (PDDM), for instance, are based upon empirical relationships of the sum of positive degree days to the melt rate and as such require only air temperature and precipitation as input. The reason for the good performance of these models is outlined in Section 2.2.2: The energy fluxes showing the greatest non-systematic temporal variability correlate strongly with air temperature. Nevertheless, PDDMs require tuning for each new site they are applied to (*Braithwaite*, 1995) and also at the same site for different time periods (*Huss et al.*, 2008a). It is generally stated that energy balance models are more suitable to the application in unmeasured areas since they do not depend as much on calibration as do PDDMs. However, the necessity for recalibration of PDDMs might stem from components in the energy balance that can not be successfully parametrized in energy balance models either. Temporal and spatial variability of the ice albedo, for instance, cannot yet be simulated reasonably but has to be obtained from observations (e.g. *Klok and Oerlemans*, 2004; *Paul et al.*, 2005). Energy balance models include ice albedo explicitly (cf. Eq. 2.5), whereas PDDMs account for varying ice albedo from glacier to glacier by recalibration of the degree day factor. Regardless of the model type applied to an unmeasured site, the unknown ice albedo poses a similar problem. Nevertheless, the advantage of an energy balance model is that once measurements are available, the values can be applied more directly.

In most mass balance models the governing equations are solved numerically, i.e., by performing calculations for short consecutive time steps where the outcome of the previous time step is used as input for the current one. PDDMs are usually run at daily time steps, whereas temporal resolution in complex energy balance models is often shorter than one hour. The following section focuses on the trade-off between detailed investigations requiring a large number of input data and more general mass balance estimates which can be derived from a reduced set of information.

Complex modeling approaches generally focus on process understanding while more general mass balance estimates are related to, for instance, projections of sea level rise. A number of studies that involve mass balance assessment for mountain glaciers and ice caps are plotted in Figure 2.10. The studies are arranged in six different classes of methods and are plotted against the investigated area. The availability of data for model input is a major limitation to the size of the test area. Statistical relationships or PDDM are applied for a large number of glaciers and require little meteorological input data. Energy balance mod-

els, in contrast, depend on numerous input variables. Consequently, they are usually run only for one glacier or individual points of the ice surface where detailed measurements are available. Information on glacier geometry is required for all studies involving mass balance assessment. However, the study by *Kotlyakov and Krenke* (1982) is based upon the ELA, and the parameterization scheme of *Haeberli and Hoelzle* (1995) on glacier length, area, maximum and minimum elevation. Degree day models which incorporate potential solar radiation (e.g. *Hock*, 1999) already depend on the availability of a DEM and detailed energy balance studies are not feasible without precise and high resolution terrain information.

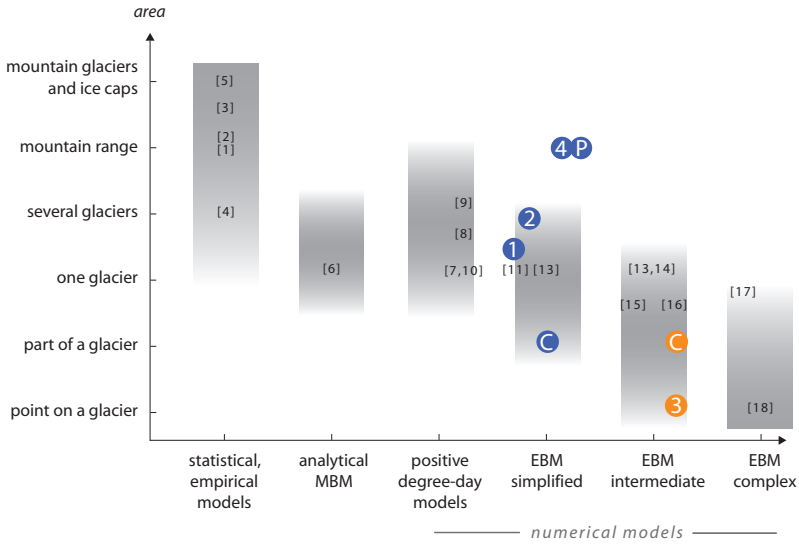

Figure 2.10.: Different approaches to assessing mass balance, and the area usually covered by these. A selection of studies involving glacier mass balance assessment or focusing on glacier mass balance modeling in particular is denoted by numbers in brackets: [1] *Haeberli and Hoelzle* (1995); [2] *Zemp et al.* (2006b); [3] *Kotlyakov and Krenke* (1982); [4] *Oerlemans and Reichert* (2000); [5] *Raper and Braithwaite* (2006); [6] *Oerlemans* (2001); [7] *Hock* (1999); [8] *Huss et al.* (2008a); [9] *Schneeberger et al.* (2003); [10] *Pellicciotti et al.* (2005); [11] *Oerlemans* (2001); [13] *Hock et al.* (2007); [14] *Hock and Holmgren* (2005); [15] *Arnold et al.* (1996); [16] *Klok and Oerlemans* (2002); [17] *Reijmer and Hock* (2008); [18] *Obleitner and Lehning* (2004). Dots indicate the study locations for this thesis. Numbers refer to the papers published in the course of this thesis, 'C' refers to the model comparison and 'P' to the precipitation assessment. Blue dots indicate application of the simple mass balance model and red dots the complex model.

Note that there is a third axis – the length of the investigated time span – that is not shown in Figure 2.10. The relationship to model complexity is similar, as described above for the size of the test area. However, difficulties in formulating appropriate parameterizations can also impose temporal restrictions. Complex energy balance models for instance, are usually restricted to the melt season. Although the physical base of the melt processes is well understood (Section 2.2.2), accumulation processes cannot yet be modeled at the desired spatial and temporal resolution. One of the main reasons is that the amount and the spatial pattern of precipitation, which have a major influence on accumulation, are not

known in sufficient detail. Measurements are sparse and uncertain at high elevation sites (Section 2.1.2) (e.g. *Sevruk*, 1985b, 1989). Redistribution of snow by wind and avalanches most likely results in deposition of snow on the smooth glacier surfaces (*Kotlyakov*, 1973) and modifies the spatial pattern of accumulation in a complex manner. Parameterizations of wind drift (e.g. *Liston and Sturm*, 1998; *Purves et al.*, 1998) have been developed but are not well tested in high mountain topography and are usually not incorporated in mass balance models. With regard to its high uncertainty compared to melt, glacier mass balance modelers have often chosen to either restrict their models to the melt season (e.g. *Arnold et al.*, 1996, 2006) or to tune accumulation by varying precipitation (e.g. *Gerbaux et al.*, 2005).

Mass balance models developed for the Greenland and Antarctic ice sheet are not depicted in Figure 2.10 although the range of applied approaches is similar. The mass balance of Greenland, for instance, has been modeled from degree day models (e.g. *Reeh*, 1991) as well as from rather complex energy balance approaches (e.g. *Bougamont et al.*, 2005). However, a direct comparison of mass balance studies conducted for mountain glaciers and ice sheets in Figure 2.10 is of limited validity: Mass balance models for glaciers and ice caps usually operate at a high spatial resolution and depend on the consideration of topographic effects. Computations at the scale of an ice sheet are performed at a low spatial resolution which does not allow for a precise treatment of small-scale effects. Nevertheless, particular attention must be paid to horizontal variability of meteorological input parameters (*van der Veen*, 2002). Mass balance models for glaciers and ice caps often neglect horizontal variability since vertical gradients are dominant on a small scale.

2.2.4. Uncertainty Assessment

In hydrological sciences there is lively discussion on the meaning of model results and uncertainties (e.g. *Beven and Binley*, 1992; *Konikow and Bredehoeft*, 1992; *Pappenberger and Beven*, 2006), while in glaciology only very little published material has been concerned with uncertainties. For instance, *van der Veen* (2002) argues that estimates of sea level rise from the Greenland ice sheet should be associated with a probability to eventuate, and calculates PDFs from Monte Carlo simulations. *Anslow et al.* (2008) conduct a simplified parametric uncertainty analysis in the course of a mass balance computation. The study of *Hebeler et al.* (2008) focused on parametric uncertainty and the influence of topographic error in ice sheet modeling.

Meaningful model evaluation requires not only the model result but also associated probability (*Tatang et al.*, 1997; *van der Veen*, 2002). Data from climate models is now used to drive mass balance computations (e.g., *Hock et al.*, 2007) and such data generally show larger deviations from measurements (e.g., *Kotlarski et al.*, 2005, subm; *Salzmann et al.*, 2007a), making an uncertainty assessment a fundamental requirement for the interpretation of the results. In view of the planned large-scale application of a mass balance model (cf. Section 1.2) uncertainty assessment is essential. The concept of uncertainty and related terms are introduced in the following, an uncertainty analysis for a mass balance model is presented in Paper №3.

Uncertainties may result, for example, from errors in measurements, from subjectivity in judgement, from a lack of information and knowledge or from the inability to precisely define either a measured value or to parameterize an observed or assumed relationship.

Traditionally, uncertainties are divided into the natural variability which refers to random fluctuations observed in nature, and knowledge uncertainty which follows from our imperfect knowledge and access to natural phenomena. The dividing line between the two components of uncertainty is blurry, since imperfect knowledge also imposes limited ability to define whether an observed fluctuation in nature is due to randomness or follows an unknown rule. The following section focuses on knowledge uncertainty.

Uncertainties in measured or computed values may stem from either systematic or random errors (cf. Figure 2.11). With respect to mass balance measurements, every individual stake reading is subject to random errors. Stake readings performed on the rough surface of a melting glacier during summer have inherent uncertainties. An important source of errors that are of a systematic nature is the interpolation from point values to the total glacier surface.

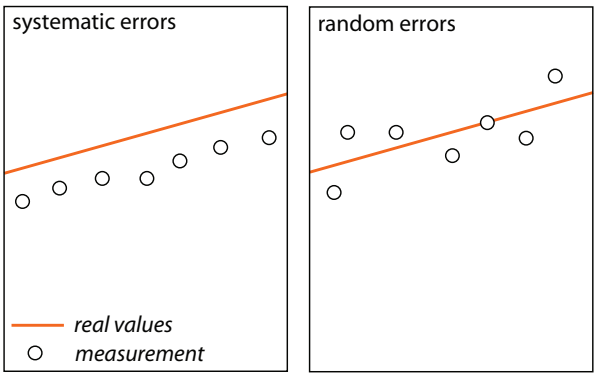

Figure 2.11.: Schematic illustration of systematic and random errors

Verification, which means the establishment of truth, is impossible for models of natural systems. This is because natural systems are never closed and model results are always non-unique (*Oreskes et al.*, 1994). Thus, uncertainties are an inherent component of the modeling process. According to *Konikow and Bredehoeft* (1992) three sources of uncertainties in modeling can be distinguished:

- uncertainties and inadequacies in the input parameters, reflecting our inability to describe properties, stresses and boundaries of the modeled object
- conceptional errors or theoretical misconceptions about the basic processes that are incorporated in a model
- numerical errors arising in the equation-solving algorithm

Regarding glacier mass balance modeling, the first two sources of uncertainties are generally dominant. Mass balance models are driven by meteorological data that are subject to uncertainties (e.g. precipitation, cf. Section 2.1.2) and the resulting mass balance is compared to measured values that are also uncertain.

Sensitivity testing is the simplest method to assess the impact of a parameter's uncertainty on the model outcome. However, only one parameter can be considered at a time

and the model response to combined uncertainties from different sources cannot be assessed. Uncertainty analysis, instead, aims at quantifying the overall uncertainty resulting from combined uncertainties in model input, parameters and parameterizations. Forward uncertainty propagation methods, for instance, are applied to consider and propagate different sources of uncertainties simultaneously through the model system. The outcome is a probability density function (PDF) associated to the model output which describes the probability of a certain outcome to eventuate. Forward uncertainty propagation methods are based upon prior analysis of the size and character of the various sources of uncertainty and they do not a priori include additional data for model evaluation. Thus, they are often accompanied by a separate comparison of model output to measured data.

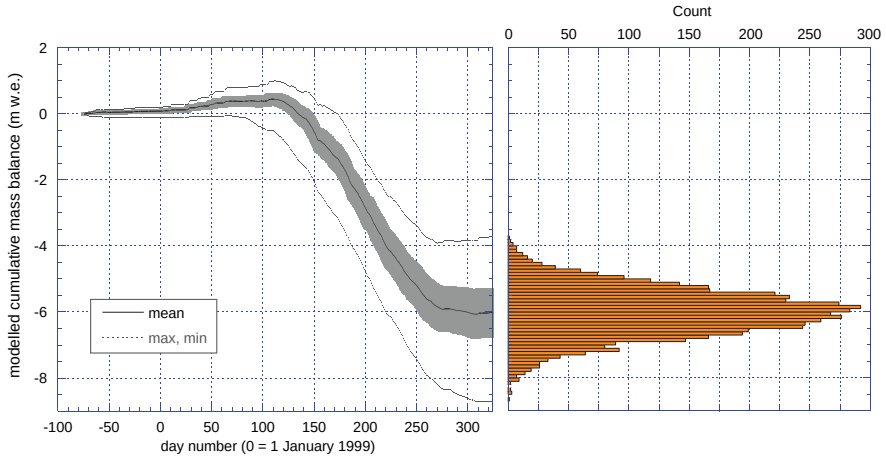

Figure 2.12.: Temporal evolution of modeled mass balance and related uncertainty in a mass balance calculation (left) and associated PDF of the final mass balance (right), computed from a Monte Carlo simulation with 5000 runs. The gray shading indicates ±1 standard deviation.

Among the different techniques of forward uncertainty propagation are analytical methods, Monte Carlo simulations, reliability methods and fuzzy methods, the latter two of which will not be further discussed here. Analytical solutions from the laws of error propagation are desirable. However, they become complex or impossible if the set of uncertain parameters is large and nonlinear effects are present. Monte Carlo simulations, although computationally expensive, are popular because they are relatively easy to apply and model complexity is a minor constraint in their application. In a Monte Carlo simulation a model run is performed many times while uncertain parameters are varied randomly within their estimated uncertainty ranges. Model outputs are stored to construct the PDF. Propagation of uncertainty through a model is illustrated in Figure 2.12, showing both the evolution of uncertainty over time and the PDF related to the final modeled mass balance (cf. Paper №3).

2.3. Climate Modeling and Regional Glacier Applications

Climate model data are widely used in impact modeling. Their use is particularly popular for estimating impact of climatic change. For large area applications such as the mass balance computations for the Swiss Alps performed in the course of this thesis, they offer some advantages: They provide information on meteorological properties that are not widely available (e.g. radiative fluxes) and their spatial and temporal resolution is high compared to meteorological observations. On the other hand, biases in climate model data have to be considered. In the following an overview of climate modeling and related downscaling approaches is given and the application of climate model data in impact modeling is discussed.

2.3.1. General Circulation Models (GCMs)

Climate models are tools employed to enhance understanding of the climate system and to aid prediction of future climates. Different types of climate models exist, such as simpler energy balance models, radiative convective models and statistical dynamical models (*McGuffie and Henderson-Sellers*, 2001). General Circulation models (GCM) aim at the calculation of the full three-dimensional character of the climate and are physically based upon conservation of energy, momentum, mass and the ideal gas law. In a GCM the atmosphere is split into columns that have a horizontal resolution of about 1 ° to 5 ° latitude/longitude ($\sim$ 200–550 km) and is vertically divided into about 20–30 levels. The vertical resolution is unevenly spaced with more layers close to the surface and fewer layers at higher levels (Figure 2.13). The numerical calculations are performed at a temporal resolution of typically 30 minutes. A distinction can be made between atmospheric GCMs (AGCMs) which model the atmosphere and impose sea surface temperatures, and coupled atmosphere-ocean GCMs (AOGCMs) that incorporate an ocean circulation and an atmospheric circulation model (Figure 2.13 shows a schematic illustration of an AOGCM). The approximation of the oceanic circulation is similar to the atmospheric model described above, however, spatial resolution must be higher in order to resolve oceanic circulation (*McGuffie and Henderson-Sellers*, 2001). Today most GCMs are AOGCMs which also incorporate, for instance, dynamic vegetation models, carbon cycle schemes and aerosol models and thus to a certain extent they take forcing and feedbacks from the different components of the climate system into account.

GCMs are the only tool that can provide quantitative estimates of future climate on a physically consistent basis *IPCC* (2001). To a certain degree they can cope with the nonlinear behavior of the climate system and thus have gained major importance in the course of scientific research on observed and future climate change *IPCC* (2001). Currently GCMs are applied for modeling large-scale synoptic circulation. Small-scale atmospheric processes are not directly accessible because of the coarse resolution and must therefore be parametrized or described from simplified equations. A higher spatial resolution would require computational resources not yet available and also makes model modifications necessary (i.e. certain simplified parameterizations must be replaced by physical relationships).

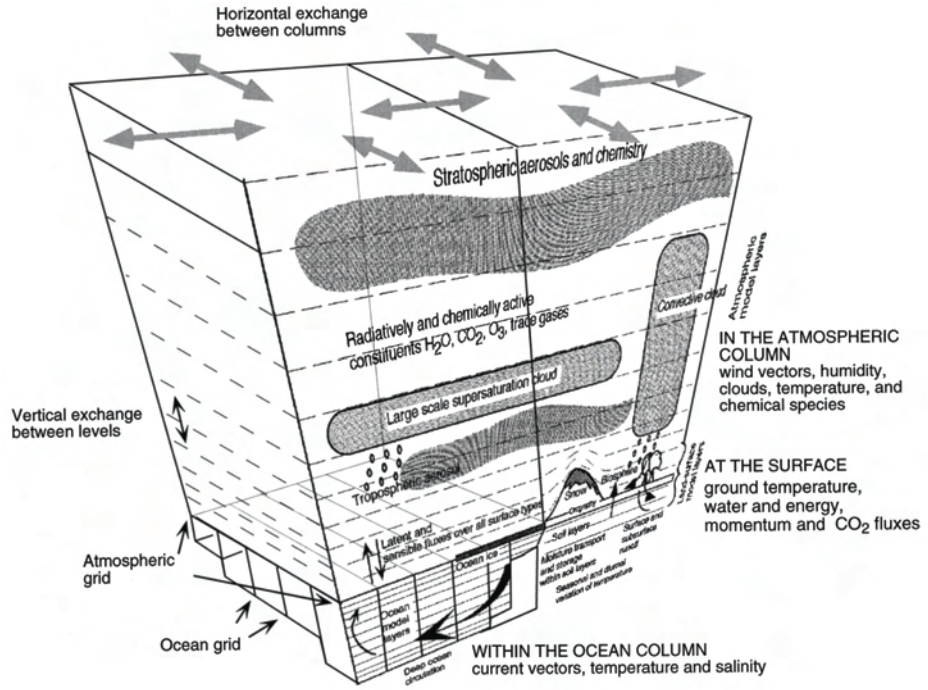

Figure 2.13.: Illustration of the basic characteristics and processes within a GCM. Figure from *McGuffie and Henderson-Sellers* (2001).

2.3.2. Downscaling Approaches

The spatial resolution of today's GCM is not yet high enough to resolve fine-scale structures of atmospheric processes, for example orographic processes which are of importance in complex mountain terrain such as the Alps. Climate modelers need tools for process studies on local to regional phenomena, e.g. orographic effects, land use and vegetation. For impact studies, more detailed scenarios are desirable to assess the impact of climate change on a regional and local scale. These requirements lead to the development of a variety of so-called downscaling techniques that can be categorized as follows:

- *Regional Climate Models (RCM):* The underlying strategy of regional climate modeling is to let GCMs provide the response of the global circulation to large-scale forcings, whereas nested regional climate models (RCMs) account for the effects of local forcing at sub-GCM grid scale (*Giorgi and Mearns*, 1999). The applied RCMs are physically based models that are in their structure similar to GCMs and often incorporate identical physical descriptions of the relevant processes. The spatial resolution of today's RCMs is in the order of 10–50 km. At their lateral boundaries RCMs are driven from the large-scale circulation obtained from either GCMs or re-analysis (cf. Sec 2.3.3). To bridge the gap in spatial resolution at the boundaries of the RCM domain, so-called "relaxation" methods are applied which involve a lateral buffer zone (*Giorgi and Mearns*, 1999). On the one hand, the selected RCM domain should be sufficiently small that the synoptic circulation does not depart far from that of the driving GCM.

On the other hand, the domain should also be large enough to allow development in the RCM of features having a finer scale than those resolved by the GCM (*McGregor*, 1997). The region of interest should be as far away as possible from the boundaries of the domain in order to be free from boundary effects, such as, for instance, spurious precipitation (*McGregor*, 1997).

It was shown in a number of studies that RCMs better represent observed spatial patterns of climate variables than their host GCMs (e.g. *Leung and Ghan*, 1999). They also perform better in representing the magnitude of observed events with respect to their statistical distribution. This concerns in particular extreme events that have a higher and more realistic probability of occuring in RCMs than in GCMs. Since extreme events are often local phenomena it is to be expected that they are better represented at higher resolution. Driving an RCM from re-analysis (so-called perfect boundary conditions, cf. Section 2.3.3) provides the possibility to compare the RCM output to measurements and is thus an important component in the process of model validation. Gridded climatologies as listed in Table 2.1 are of particular interest for model validation in a distributed manner (e.g. *Kotlarski et al.*, subm).

- *Statistical Downscaling (SD):* Many impact studies require climate change information of much finer scale than provided by GCMs or RCMs (*Wilby et al.*, 2004). Statistical downscaling is a method frequently used in impact modeling and is based on the assumption that the local climate is conditioned from the large-scale climate state on the one hand and regional/local factors (e.g. topography) on the other. SD requires, first, that a statistical relationship be found between one or more large-scale climate variables (predictor) and local variables (predictant). In a second step, large-scale information from GCMs, re-analysis or RCMs are fed into the statistical model to estimate local climate characteristics (*Fowler et al.*, 2007). Three main SD approaches can be distinguished: *Weather classification* means to establish a statistical relationship between a number of weather types and conditions at the test site. *Regression models* rely on linear or nonlinear regression between predictants and large-scale atmospheric forcing, whereas *weather generators* replicate the statistical attributes but not the individual events of a local climate variable and are most often used with precipitation, but with other climatic variables as well (*Kilsby et al.*, 2007).

  Statistical downscaling is usually performed for individual sites whereas GCM or RCM output is provided as a grid, imposing the question of which section of the climate model output is best suited for SD at the site of interest. Impact modelers often simply select the nearest grid box. However, *Frei et al.* (2003) suggest that the representative area for simulated climate variables is somewhere between one and four grid boxes and thus, SD requires a careful selection of one or more representative grid boxes (e.g. *Salzmann et al.*, 2007a).

- *Time Slice and Variable-Resolution GCMs:* The time slice method refers to running a GCM at enhanced spatial resolution for a limited period in time whereas variable resolution GCMs are of regionally enhanced resolution over a specific area of interest. These two downscaling approaches are not discussed in further detail here.

Downscaling makes sense when there is an added value compared to the original GCM or RCM data. It must be considered that advantages of additional information gained through

the downscaling process are possibly counterbalanced by enhanced uncertainty from inserting an additional element (the downscaling procedure) into the cascade of uncertainties (cf. *Mearns et al.*, 2003). Which downscaling approach is most appropriate depends on the research question. A short consideration of corresponding major advantages and limitations might provide a basis for decision. For local site-specific studies the combination of dynamical downscaling from RCMs and subsequent statistical downscaling should be considered a valuable approach as well (e.g. *Salzmann et al.*, 2007a).

The most important advantage of regional climate modeling is the possibility to generate physically consistent fields of several atmospheric variables for an entire region and for past, present and future climatic conditions (*Salzmann*, 2006; *Salzmann et al.*, 2007a). To a certain degree feedback in the climate system and nonlinear effects can be considered. An important limitation is that RCMs usually receive input at their boundaries from the host GCM but do not provide feedback. The lateral input can also be a limitation when biased. The current performance of RCMs (driven by perfect boundary conditions) is for a horizontal resolution of about 50 km for temperature within $\pm 2\,^{\circ}\mathrm{C}$ and for precipitation $\pm 50\%$. For many research questions RCM accuracy might not be sufficient and requires bias correction. In order to assess the variability in results of RCMs and to improve model performance so called model intercomparison projects (MIP) have been conducted. In an MIP a number of RCM are forced from ideally the same data set and their results are compared (e.g. *Gregory et al.*, 2005; *Meehl et al.*, 2007). For instance, within the PRUDENCE project (e.g. *Christensen et al.*, 2002) the results of ten RCMs that were driven from one GCM have been compared to each other as well as to observations, in order to derive an estimate of model performance and of the range of future predictions. In MIPs it has often been found that the mean of several models can perform better than the individual models (*Tebaldi and Knutti*, 2007). Thus it is generally recommended to use several RCMs at a time to assess variability around the mean of the model ensemble (*Salzmann et al.*, 2007b). The issue of applying model ensembles highlights the high computational expenses and high demand on expert knowledge which are major limitations to the application of regional climate modeling for impact assessment.

Statistical downscaling results in a high degree of accuracy since the statistical model is based upon measured data. In contrast to regional climate modeling the downscaling procedure can be tuned for small areas or individual points and is thus particularly useful in heterogeneous environments with steep environmental gradients (e.g. islands, mountains) (*Wilby et al.*, 2004). SD is based on the assumption that the statistical relationship found for today's conditions is also valid for future or past conditions (assumption of stationarity) (*Fowler et al.*, 2007). Clearly, this assumption is difficult to validate and thus must be considered a shortcoming. SD requires a careful selection of adequate predictors. However, it is difficult to assess whether good predictors under present conditions are still valid under a changing climate. Each statistical model is valid only for the range of values it has been calibrated to. Consequently, it is generally claimed that ranges of predictors for which the SD-model was calibrated should encompass the future climate conditions to which the model is then applied (e.g. *Schmidli et al.*, 2006; *Fowler et al.*, 2007). Furthermore, it must be noted the SD may exhibit low skills in producing extreme events (*Haylock et al.*, 2006) and no feedback to the forcing field can be provided (*Wilby et al.*, 2004).

2.3.3. Re-analysis

The two most widely known re-analysis data sets are ERA-40 (*Uppala et al.*, 2005) from ECMWF (covering the time span from 1958–2002) and the NCEP/NCAR re-analysis (*Kalnay et al.*, 1996) (1948 to present). Re-analysis data are of a comparable structure (gridded, three-dimensional, covering the entire globe) to GCM output. However, they are obtained from a methodology closely related to operational weather forecasting where a set of observations and a dynamical model are combined in a data assimilation scheme. Observations include a wide variety of data measured from synoptic weather stations, from satellites, from radiosonde ascents, from aircrafts, ships, buoys and others (cf. *Kalnay et al.*, 1996; *Uppala et al.*, 2005). Applied dynamical models for re-analysis are similar or identical to atmospheric models applied for operational weather forecast. Error estimation and error modeling are central to the concept of data assimilation. Any model is imperfect and starting conditions are incompletely known, inhibiting accurate forecasts beyond a limit of predictability (approx. 1–2 weeks for the forecast of the state of the global atmosphere). Through data assimilation techniques, uncertainties of modeled and observed data are balanced and the predictability error is controlled in order to achieve a best estimate of current conditions.

The main difference between GCMs and re-analysis data is that the first are used to model plausible states of the atmosphere whereas the latter aim to provide a best estimate of real conditions. Consequently, GCMs are validated against statistical properties of climatic conditions while re-analysis data are directly compared to measurements. Modern re-analysis data sets achieve accuracies of, for instance, air temperature prediction of approx. 1 °C. For time periods before the mid-seventies when satellite data were not available, performance is generally lower (*Uppala et al.*, 2005). Re-analysis data are also subject to downscaling by either RCMs or statistical downscaling. When an RCM is driven at the boundaries by data from re-analysis one speaks of perfect boundary conditions.

2.3.4. Application of Climate Model Results for Impact Modeling

Climate model data offer certain major advantages for impact modelers: They provide information on meteorological properties that are not widely available (e.g. radiative fluxes) or for remote areas. Temporal resolution, and in the case of RCM data spatial resolution as well, is high compared to most available climatologies established from measured data (cf. Section 2.1.3). Climate model data are consistent in the sense that they are free of inhomogeneities. On the other, hand climate model data are likely to be biased. In climate change impact assessment it must be recognized that there are a number of sources of uncertainties in the input data, RCM or GCM output which contribute to uncertainty in the final assessment (*Mearns et al.*, 2003).

A number of GCM simulations have been performed within *IPCC* (2001, 2007) to assess potential global climate change related to different emission scenarios. The applicability of GCM and RCM data for impact modeling has been compared based on the example of crop yield estimates by *Mearns et al.* (2001). In hydrological science, RCM model output has been integrated into a model chain to assess future runoff for large catchments such as the Rhine River (e.g. *Kleinn et al.*, 2005). With respect to glaciology, the applicability of high resolution RCM to model arctic permafrost distribution has been assessed by *Christensen*

and Kuhry (2000). GCMs and RCMs have been applied to assess present-day mass balance and the future evolution of the Greenland ice shield: *Lefebre et al.* (2005), for instance, validated a coupled atmosphere-snow RCM against measurements, whereas *Kilisholm et al.* (e.g. 2003) applied RCM data for climate change simulations on the Greenland ice sheet. *Kleinn et al.* (2005) noted that their simulation produced the largest model errors for high-altitude Alpine catchments. In high mountain areas with complex topography, small-scale effects are dominant that cannot yet be resolved by the comparable coarse resolution of RCMs but have to be addressed by downscaling techniques. The application of such approaches and high resolution RCM data for impact modeling on permafrost simulation in mountainous terrain has been explored by *Salzmann et al.* (2007a).

With regard to the use of GCM or RCM data for mass balance modeling in heterogeneous landscapes, two approaches can be distinguished. One is based on data from the nearest climate model grid box in combination with statistical downscaling (e.g. *Van de Wal and Wild*, 2001; *Schneeberger et al.*, 2003; *Radić and Hock*, 2006; *Stahl et al.*, 2008). The other one uses the meteorological fields from several grid boxes at the same time and the forcing of the mass balance model is more direct and physically based (e.g. *Bhatt et al.*, 2007; *Cook et al.*, 2003; *Ren et al.*, 2007; *Zhang et al.*, 2007). Nevertheless, until today no attempt was made to apply the climate model data as a coarse grid which is then downscaled to a finer resolution grid on which the mass balance calculation is performed. Given that such a coupling scheme between the RCM data and the mass balance model could be developed and tested, it would be possible to perform high resolution scenario calculations from RCM output for large areas.

2.4. Glaciers as Precipitation Gauges

Glaciers integrate meteorological processes on a variety of time scales (*Kuhn*, 1981). Daily melt rates are related to actual weather conditions, the surface snow cover and the EL experience a yearly cycle. Flow adjustment and geometry changes have a typical time frame of a few years to a few decades (cf. *Jóhannesson et al.*, 1989; *Haeberli and Hoelzle*, 1995). Consequently, glaciers could potentially be used as a way of measuring meteorological conditions integrated over different time frames (*Kuhn*, 1981). Mountain glaciers provide little or no feedback concerning the meteorological conditions (= the measured quantity) and thus fulfill a basic requirement for a measuring device. However, feedback mechanism from the dynamic response to accumulation and ablation processes have to be considered (Figure 2.8).

Glaciers could be used as natural precipitation gauges. The relationship between the level of glaciation and the amount of solid precipitation was already recognized by *Ahlmann* (1924). *Khodakov* (1975) and *Krenke* (1975) developed an approach for a quantitative assessment of precipitation from the level of glaciation, or more specifically, from observations of ELA on a large number of glaciers. Precipitation is not equal to accumulation but is modified in a complex manner by redistribution of snow by wind and avalanches (e.g. *Liston and Sturm*, 1998) and to a lesser extent by sublimation (e.g. *Strasser et al.*, 2008). *Krenke* (1975); *Kotlyakov and Krenke* (1982) recognized the influence of such processes and proposed correction factors to obtain precipitation from measured accumulation. *Kotlyakov and Krenke* (1982) applied a method for a spatial assessment of precipitation and water re-

sources in the mountain areas of Soviet Central Asia. In view of potential sources of errors from simplified parametrization, derived precipitation at individual glaciers was averaged over groups of glaciers to reduce errors. *Ohmura et al.* (1992) studied the climate at the ELA based upon a larger data set from glaciers throughout the world. *Kerschner et al.* (2000) applied the method of *Ohmura et al.* (1992) to calculate changes in precipitation during the Younger Dryas with respect to present conditions. They emphasize that meteorological properties derived from paleo-glacier extent could be valuable to evaluate climate model output and conclude with a simple qualitative comparison of their results to climate model runs for the Younger Dryas. *Beniston et al.* (1997) argued that climate models are difficult to evaluate in high mountain and remote areas where measurement networks are sparse and available data often related to considerable measurement errors. Instead they proposed to use observed properties of glaciers and permafrost to obtain meteorological quantities for the validation of climate model output. *Jóhannesson et al.* (2004) derived precipitation over two Icelandic ice caps from a combined approach of mass balance modeling and stake measurements. A degree day model was calibrated by means of horizontal and vertical precipitation gradients to match mass balance observations at a number of stakes spread over the two ice caps. A precipitation distribution was then derived from the precipitation gradients resulting from the tuning procedure.

Meteorological properties obtained from glacier extent could be valuable for climate model evaluation, not only with respect to paleo-climate (e.g. *Kerschner et al.*, 2000) where direct measurements are non-existent, but also to complement measurements of current conditions. Indeed, over mountainous terrain, climate models are generally been evaluated through the direct comparison to measurements or gridded data sets from observations (e.g. *Frei et al.*, 2003; *Schmidli et al.*, 2006; *Kotlarski et al.*, subm) and it is recognized that the data used for evaluation are associated with considerable uncertainty.

3. Applied Methods

3.1. Field Measurements on Findel and Adler Glacier

In the framework of this thesis field measurements with the direct glaciological method were performed to obtain original mass balance data for model validation. Helicopter-borne ground penetrating radar (GPR) was applied to measure snow thickness distribution. The results were analyzed with respect to a horizontal accumulation gradient, assumed from a mass balance model run. Specific mass balance obtained from the mass balance measurements are published in *WGMS* (2007) and listed in the Appendix. Methods and findings of the GPR campaign are described in Paper №1.

3.1.1. Stake Measurements

Mass balance observations were performed on Findel glacier (length 7.2 km, area 15.3 km^2) and the adjacent Adler glacier (length 3.1 km, area 2.0 km^2), situated in the south-eastern part of the Valaisian Alps (Figure 1.2). The two glaciers have been selected for detailed investigation because a preliminary assessment of mean mass balance for the 1971–1990 period indicated a distinct horizontal gradient in accumulation between the two glaciers. The preliminary mass balance calculation, performed with an early version of the simple mass balance model described in Section 3.2.1, resulted in a positive mass balance on Adler glacier (0.7 m w.e.) and a slightly negative value for Findel glacier (-0.25 m w.e.)(*Machguth*, 2003). The first value was considered unrealistic because the glacier showed no signs of advance and thus, the overestimation in mass balance is assumed to be related to a horizontal gradient in accumulation which is not incorporated in the model parameterizations. Direct measurements on the two glaciers are expected to either confirm or disprove the hypothesis of a strong horizontal gradient in accumulation. Furthermore, the Findel glacier catchment is favorable for mass balance investigations for further reasons:

- Most of the mass balance studies are conducted on smaller glaciers of a few square kilometers. Findel glacier is of a respectable size and thus, may represent mid-sized valley glaciers that are not well represented in the mass balance observation network (*Zemp et al.*, subm).
- The highest glacierized areas in the catchment of Findel and Adler glacier are located at 3800 to 4100 m a.s.l. and will thus remain accumulation area in the near future even if hot and dry summers like in 2003 should become the rule (cf. *Schär et al.*, 2004).
- High precision measurements of long-wave radiation balance and global radiation are available from the Alpine Solar Radiation Budget Network (ASRB) (e.g. *Marty et al.*, 2002; *Philipona et al.*, 2004) at nearby Gornergrat (3100 m a s.l., 4 km south-west

of the glacier tongue). Air temperature and several other climatological parameters are measured by MeteoSwiss at the same location. A further automatic weather station is operated by the PERMOS network for permafrost observation at Stockhorn (3400 m a.s.l.) which is only 1 km away from the glacier. These data could be used in a potential mass balance study.

- The glacier tongue can be reached quite easily by cable car and a one-hour walk.
- The glacier surfaces are mostly smooth, gently sloped and, to a large part extents can be accessed without rock or ice climbing.

The mass balance network on Findel and Adler glacier consists of a total of 14 stake locations and 4 regularly visited snow pit areas (Figure 3.1). The network is designed to provide data for model validation and is dimensioned to allow for one group of scientists to visit all stakes within one and a half days. The reduced number of stakes compared to full observational networks on glaciers of similar size (e.g. Pasterzenkees, Austria, 50 stakes) allows for a higher temporal coverage, and making it possible to apply the data for model validation over short time spans of individual months. The glacier was visited up to three times during each summer from 2005–2008 to obtain stake readings. Additional field campaigns of three to four full days were carried out in autumn and included the stake readings, the replacement of stakes and the measurement of the snow accumulation in snow pits that were dug in the snow pit areas.

On the tongue of Findel glacier stakes of 10 m length were drilled into the ice, in between the tongue up to the equilibrium line, and on Adler glacier 8 m and 6 m stakes were installed. In 2004 and 2005 wooden stakes were installed that had been assembled of 2 m pieces, connected to each other with a short chain and equipped with barbed hooks to prevent them from floating in water-filled holes (cf. *Machguth*, 2003). In the following years the stakes were made from 2 m plastic tubes (equipped with barbed hooks as well) because they are easier to assemble and unlike the wooden stakes, they endure more than one or two melt seasons and can thus be re-used. New stakes were always drilled before the old stake melted out. As a consequence, at most stake locations two stakes have often been in place in parallel, allowing for an assessment of the representativity of the point measurements.

3.1.2. Snow Pits

Snow pits were used within the regular mass balance measurements to measure either winter accumulation or annual mass balance in the accumulation area. In May 2005 a network of snow pits and snow depth soundings with avalanche poles was established to provide ground truth for a GPR campaign. Snow depth was measured from the actual snow surface down to the ice surface and where the snow cover outlasted the previous melting season, to the horizon of the previous autumn's snow surface. Both snow pits and snow probes were used to measure snow depth. Density of the snow cover and the internal layering was observed from the snow pits. The internal layering of the snow pack could result in misinterpretation of the snow depth measurements with snow probes. Consequently, they were mostly confined to the ablation area where the snow cover lies atop the solid ice surface, and on every test site a number of measurements were carried out to calculate a representative mean. Coordinates of snow pits and probes were captured with a hand-held GPS.

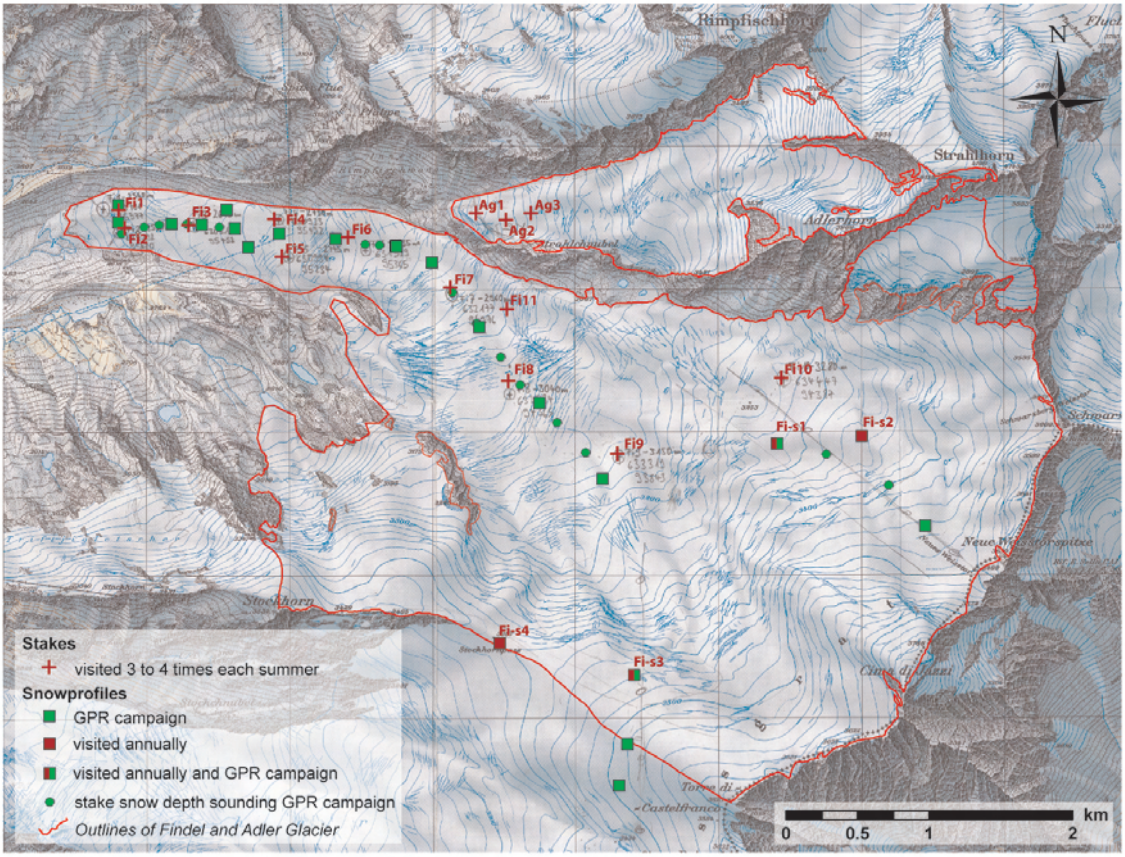

Figure 3.1.: The Measurement Network on Findel and Adler glacier. Flight tracks of the GPR campaign are depicted in Paper №1.

3.1.3. Snow Depth from GPR

In May 2005 snow distribution on Findel and Adler glacier was measured from helicopter-borne GPR. In contrast to this method, measurements of snow depth from snow pits and snow probes are time-consuming and limited to smooth glacier areas. However, a dense sampling network is essential to assess the high spatial variability of snow accumulation on an Alpine glacier and thus, helicopter-borne GPR was tested for its applicability and accuracy. GPR is a radio-echo sounding technique and a standard method in polar glaciology for determining past and present accumulation rates (e.g. *Foster et al.*, 1991; *Arcone*, 1996; *Rotschky et al.*, 2004). The method is especially rewarding in cold firn and ice because of the low absorption of electromagnetic energy and has been applied in cold Alpine firn as well (e.g. *Eisen et al.*, 2003). Liquid water results in strong absorption and sounding of ice

thickness on temperate glaciers requires low frequencies (<100 MHz) to penetrate down to the glacier bed. Higher frequencies (approx. 250 MHz–1 GHz) have limited penetration in temperate ice but they are suitable for measuring snow depth due to better spatial resolution. Such measurements performed with GPR systems operating directly from the surface allow for measurement along transects and are efficient on ice caps where snow scooters can be used (e.g. *Taurisano et al.*, 2007). On alpine glaciers measurements have to be conducted on foot, a method which is time-consuming, and with more pronounced topography and difficult access the spatial coverage is limited to smooth areas. To cope with the difficulties imposed by measurements in mountainous terrain and valley glaciers, airborne GPR is most suitable. Helicopter-borne radar provides the most reasonable platform. Although helicopter-borne radar has been applied to studies of sea and river ice (*Wadhams et al.*, 1987; *Arcone and Delaney*, 1987), snow on ground (*Marchand et al.*, 2003) or glacier thickness measurements (*Thorning and Hansen*, 1987; *Damm*, 2004), very few studies have made use of it to investigate the snow cover on glaciers (e.g. *Arcone*, 2002) and none of them had, at this point, been dedicated to the spatial accumulation distribution.

For the GPR campaign, a commercial Noggin Plus 500 radar (Sensors & Software Inc., Canada,) was operated at a center frequency of 500 MHz and 400 MHz bandwidth. The antenna was mounted on the helicopter runner. A GPS antenna was mounted at the nose of the helicopter and for each recorded trace the position of the helicopter was stored. The helicopter was supposed to fly a few meters above ground, resulting in a footprint size in the order of a few tens of m^2. The flight path was planned to follow the test sites where snow depth was measured from snow pits and snow probes.

Post-recording processing and radar-data analysis were carried out using ReflexWin (Sandmeier Scientific Software, Germany).

3.2. Mass Balance Modeling

The applied modeling strategy is based upon two distributed mass balance models of differing complexity: A simpler model (MB1), requiring a limited amount of input data was used as the working tool for regional mass balance modeling. The more complex model (MB2) was applied to improve process understanding; through model comparison, it served as a benchmark for MB1 to assess the influence of simplified parameterizations. The more complex model is less suitable for regional applications because it requires more input data at higher temporal resolution and computational expense. Prior to regional application, the two models had been validated against measurements on individual glaciers (MB1: Paper №1 and №2, Section 6 and MB2: Section 6 and Paper №3). Furthermore, mass balance and energy fluxes obtained from the two models have been compared (Section 6) and a parametric uncertainty analysis on the example of MB2 was carried out (Paper №3). The regional mass balance model (Paper №4) is based upon the experience gained through the above-mentioned studies and is accompanied by an extensive comparison of modeled and measured data on several glaciers. The general outlines of the two models, their evolution and model parameterizations that are not obvious from the papers, are described in the following two sections.

3.2.1. A Simplified Energy Balance Model

The glacier mass balance model MB1, presented in the following, is in simplified form, as compared to more sophisticated energy balance approaches. Nevertheless it includes one of the main features of energy balance models, a separate treatment of short-wave radiation and energy fluxes depending strongly on air temperature (turbulent and long-wave fluxes). In particular the calculation of the latter is much simplified, whereas the calculation of short-wave radiation is similar to more complex energy balance approaches (e.g., *Arnold et al.*, 1996). The model thus combines elements of energy balance models with features of more simple degree day models and therefore can be adopted easily to a higher or lower level of complexity, depending on the research question. Four different versions of the model have been applied in papers №1, №2 and №4. Table 3.1 gives an overview of which parameterizations were applied differently in the model versions. In the following, first the general outline of the model is presented and then more detailed explanations of the different model versions are given.

The model runs at daily steps, and the cumulative mass balance b_c on day $t+1$ is calculated for every time step and over every individual grid cell of the DEM according to *Oerlemans* (2001):

$$b_c(t+1) = b_c(t) + \begin{cases} \Delta t \cdot (-Q_m)/l_m + P_{solid} & \text{if } Q_m > 0 \\ P_{solid} & \text{if } Q_m \leq 0 \end{cases} \tag{3.1}$$

where t is the discrete time variable, Δt is the time step, l_m is the latent heat of fusion of ice ($334\,kJ\,kg^{-1}$) and P_{solid} is solid precipitation in meter water equivalent (m w.e.). The energy available for melt (Q_m) is calculated as follows:

$$Q_m = (1-\alpha)S_{in} + C_0 + C_1 T_a \tag{3.2}$$

where α is the albedo of the surface, S_{in} is the global radiation, T_a is the air temperature (in °C at 2 m above ground and outside the glacier boundary layer) and $C_0 + C_1 T_a$ is the sum of the longwave radiation balance and the turbulent exchange linearized around the melting point (*Oerlemans*, 2001). C_1 is set at $10\,\mathrm{W\,m^{-2}\,K^{-1}}$ according to the recommendation of *Oerlemans* (2001). C_0 was used as a tuning factor and was adjusted to fit measurements. For Paper №1 (model run conducted in *Machguth*, 2003) C_0 was set to $-10\,\mathrm{W\,m^{-2}}$ and for Paper №2 to $-25\,\mathrm{W\,m^{-2}}$. In the model comparison and Paper №4, the best fit of modeled and measured mass balances was achieved at $C_0 = -45\,\mathrm{W\,m^{-2}}$. The differences are mainly attributed to model improvements (e.g., modifications of the global radiation parameterization, see below). In MB1 the temperature of the ice surface (T_{surf}) is assumed to be always at the melting point (0 °C). Refreezing is not taken into account and any meltwater and rainfall is immediately removed from the glacier. Solid and liquid precipitation are distinguished from a threshold in air temperature (T_{snow}).

The originally one-dimensional model of *Oerlemans* (2001) was modified for distributed mass balance calculation in *Machguth* (2003). This early version, written in AML (Arc Macro Language) was transformed to IDL programming language and further modified in the course of the present thesis. Instead of calculating the temperature of every day of the year from a sine function (*Oerlemans*, 2001; *Machguth*, 2003), daily mean T_a are read from tables of measured meteorological data. The fixed threshold $T_{snow} = 1.5$ °C was modified

Table 3.1.: Overview to the different model versions of MB1. In the table "measured" refers to daily measurements.

	Machguth (2003) / Paper №1	Paper №2	model comparison	Paper №4 / precip. assessment
modeled glacier:	Findel, Adler	Claridenfirn	Morteratsch	Swiss Alps
programmed:	AML	IDL	IDL	IDL
input: T_a	sine curve	measured	measured	measured
input: $S_{in,clr}$	SRAD	*Iqbal* (1983); *Corripio* (2003)	*Iqbal* (1983); *Corripio* (2003)	*Iqbal* (1983); *Corripio* (2003)
input: P	every day, seasonally variable	measured	measured	measured
attenuation from clouds	fixed	Eq. 3.3, measured S_{in}	Eq. 3.3, measured S_{in}	Eq. 3.4, n from climate model
T_{snow} (°C)	1.5	1 to 2	1 to 2	1 to 2
C_1 ($\mathrm{W\,m^{-2}}$)	10	10	10	10
C_0 ($\mathrm{W\,m^{-2}}$)	-10	-25	-45	-45
α_s	0.72	0.7	0.72	0.72
α_f	—	0.4	0.45	0.45
α_i	0.27	0.3	0.34	0.27

to a linear transition from 100% snowfall at $T_a = 1\,°\mathrm{C}$ and 0% snowfall at $T_a = 2\,°\mathrm{C}$. This modification was introduced because applying a strict threshold temperature results in stepwise changes of snow cover thickness with altitude. Stepwise changes are more pronounced when time steps are larger. The originally applied SRAD code for the calculation of $S_{in,clr}$ (*Wilson and Gallant*, 2000) was replaced by a global radiation calculation from *Corripio* (2003), based upon *solar radiation model C* described in *Iqbal* (1983). Diffuse ($S_{in,clrdif}$) and direct portion ($S_{in,clrdir}$) of $S_{in,clr}$ are explicitly calculated from this code. However, for the calculation of the latter, skyview is not considered in MB1. Clouds exhibit a reducing effect on global radiation which was addressed in a more simplified manner in the original model, specifying a reduction factor (D) that was applied throughout the entire calculation (*Oerlemans*, 2001; *Machguth*, 2003). In the model version applied in Paper №2, a reduction factor for every individual day t is estimated from the ratio

$$D = \frac{S_{in}}{S_{in,clr}} \tag{3.3}$$

Measured mean global radiation on day t at a weather station is denoted with S_{in}, and $S_{in,clr}$ is modeled clear sky global radiation for day t on the DEM cell corresponding to the geographical location of the weather station. D is then applied to the entire array of $S_{in,clr}$. Making no difference between $S_{in,clrdif}$ and $S_{in,clrdir}$, this parameterization leads to an underestimation of S_{in} for shaded and steep, north orientated terrain. The same method was applied in the model version that was used for model comparison (Section 6). However, $S_{in,clrdif}$ served as a lower threshold. In Paper №4, spatially variable attenuation of clouds (τ_{cl}) for every individual day was derived from distributed cloudiness (n) according

to an empirical relationship established from observations on Pasterzenkees, Austrian Alps (*Greuell et al.*, 1997):

$$\tau_{cl} = 1.0 - 0.233n - 0.415n^2 \tag{3.4}$$

Again, $S_{in,clrdif}$ served as a lower threshold.

The earliest model version (*Machguth*, 2003) operated using two fixed values of surface albedo: α_s for snow surfaces and α_i for ice surfaces. To allow for model runs over long time spans a surface albedo value for firn surfaces (α_f) and a simple snow to firn to ice conversion parameterization was introduced with the model version applied in Paper №2. More detailed descriptions of the individual versions of MB1 are to be found in Papers №2 and №4.

3.2.2. A Detailed Energy Balance Model

Process understanding that can be gained from the model MB1 is somewhat limited. For this reason, an energy balance model of intermediate complexity (called MB2 in the following) was programmed to improve understanding of the relevant processes at the glacier surface and to serve as a benchmark for the model MB1.

The model is based upon the mass balance model described in *Klok and Oerlemans* (2002) and numerical calculation of mass balance is performed in steps of 1800 s or shorter. Similar to MB1, the model is driven by data from synoptic weather stations located outside the glacier boundary layer, which allows the model to be applied without data from an AWS operated on the glacier surface. The latter are available only for a few glaciers and mostly for short time intervals. *Klok and Oerlemans* (2002) developed and tested their model with the example of Morteratsch glacier, southeastern Switzerland (Figure 1.2). Furthermore, the original model or parts of it have already been used in other studies e.g. (e.g., *Klok and Oerlemans*, 2004; *Arnold et al.*, 2006).

According to *Klok and Oerlemans* (2002), the model is based upon the following equation describing the specific mass balance, $M(kg\,m^{-2})$:

$$M = \int \left(\frac{Q_m}{l_m} + P + \frac{Q_l}{l_s} \right) dt \tag{3.5}$$

Q_m is the melt energy and Q_l the energy involved in sublimation or riming, and l_s ($2.83 \cdot 10^6 J\,kg^{-1}$) is the latent heat of sublimation. When the surface is at the melting point and liquid water is present on the surface, the latent heat of evaporation ($l_v = l_s - l_m$) has to be considered instead of l_s. The surface energy heat flux (F) supplies energy for melting (Q_m) or for the glacier heat flux (G), which implies the warming or the cooling of the snow pack or of the subsurface ice and firn.

$$F = Q_m + G = S_{in} - S_{out} + L_{in} - L_{out} + Q_h + Q_l \tag{3.6}$$

S_{in} and S_{out} are incoming and reflected solar radiation; L_{in} and L_{out} are incoming and emitted long-wave radiation, respectively. Sensible and latent heat fluxes are represented by Q_h and Q_l. Melting can occur only when the surface temperature is at 0 °C and F is positive. If the latter is the case but the surface temperature is below zero, then $F = G$ and the snow pack or ice is heated.

The turbulent heat fluxes are calculated according to *Oerlemans and Grisogono* (2002). A three layer subsurface heat flux model is included for computing energy fluxes from and to the ice body. Refreezing of meltwater is not considered and energy supply from rain is neglected. Although T_{surf} is variable in MB2, the energy balance is not completely closed. Within one numerical time step, the energy balance is first calculated based upon T_{surf} from the previous time step and T_{surf} is then varied according to the calculated energy balance. The modification of the energy balance from changing T_{surf} throughout the time step is not considered. A closure of the energy balance would be possible through an iterative adjustment of T_{surf} for every time step. However, the shorter the numerical time steps the smaller the influence of the neglected feedback. Test runs with $\Delta T = 300\,\mathrm{s}$ and $\Delta T = 600\,\mathrm{s}$ resulted in negligible changes in mass balance (<0.05%) compared to the usually applied $\Delta T = 1800\,\mathrm{s}$ and thus, an iterative adjustement of T_{surf} was not included.

A detailed description of the applied parameterizations is given by *Klok and Oerlemans* (2002). All modifications to the original model are explained in the following.

The snow albedo (α_s) is calculated according to modified formulas from ECMWF that are based upon *Baker et al.* (1990); *Verseghy* (1991); *Douville et al.* (1995). For non-melting conditions the albedo of the snow surface at day t+1 (α_s^{t+1}) is calculated from a linear snow-aging function:

$$\alpha_s^{t+1} = \alpha_s^t - \tau_a \Delta t / \tau_l \tag{3.7}$$

where $\tau_a = 0.008$ and τ_l is the length of a day (86'400 s). Under melting conditions (assumed when the snow surface is at the melting point) an exponential function is applied:

$$\alpha_s^{t+1} = (\alpha_s^t - \alpha_{min}) exp(\tau_f \Delta t / \tau_l) + \alpha_{min} \tag{3.8}$$

where $\alpha_{min} = 0.55$, $\tau_f = 0.24$. For shallow snow depth α_s^{t+1} is adjusted to the actual surface albedo (α_{surf}^{t+1}) (modified after *Klok and Oerlemans* (2002)):

$$\alpha_{surf}^{t+1} = \alpha_s^{t+1} + (\alpha_u - \alpha_s^{t+1}) exp(-\frac{d}{d^*}) \tag{3.9}$$

The albedo of the underlying layer (either firn or ice) is denoted by α_u, d is the snow depth in m w.e. and d^* is the characteristic scale for snow depth (0.011 m w.e.) estimated from the depth scale arrived at by *Oerlemans and Knap* (1998) by multiplying it with the snow density ($350\,\mathrm{kg\,m^{-2}}$) (*Klok and Oerlemans*, 2002). For the calculation of the energy balance of day $t+1$, α_{surf}^{t+1} rather than α_s^{t+1} is applied.

The most important modification considers the surface albedo after a snowfall event. When snowfall occurs on day $t+1$ then α_s^{t+1} is reset to the albedo of fresh snow (α_{max}) prior to the shallow depth adjustment (Eq. 3.9) (*Klok and Oerlemans*, 2002). However, assuming that prior to a snowfall event the snow cover has undergone aging (Eq. 3.7 or Eq. 3.8) but is still quite thick (> 0.1 m w.e.), the snowfall event, even if it is small, will cause the undergone aging process to be "forgotten". In such a case the shallow depth adjustment is of little or no influence because only α_u is considered, whereas the surface albedo prior to the snowfall (α_{surf}^t) has no influence. To adjust for this effect, an additional shallow depth correction which considers α_{surf}^t was introduced in the case of snowfall events:

$$\alpha_s^{t+1} = \alpha_{max} + (\alpha_{surf}^t - \alpha_{max}) exp(-\frac{P_{solid}}{s\,d^*}) \tag{3.10}$$

where P_{solid} is the amount of snow fall in m w.e., $\alpha_{max} = 0.82$ and s was set to 0.5, yielding a good fit with observed snow albedo on the tongue of Morteratsch glacier (cf. *Oerlemans* (2000) and *Klok and Oerlemans* (2002)).

While in the original model (*Machguth*, 2003) a single threshold temperature (T_{snow}) of 1.5 °C is used to distinguish snowfall and rain, we apply a gradual transition between 1 °C and 2 °C, identical to MB1.

Direct and diffuse portion of clear sky global radiation is calculated identical to MB1, applying the solar radiation codes from *Corripio* (2003), based on *Iqbal* (1983). However, $S_{in,clrdif}$ was further modified by a sky view factor according to *Klok and Oerlemans* (2002).

3.3. Parametric Uncertainty Analysis

A parametric uncertainty analysis was conducted on the example of MB2 and published in Paper №3). In the framework of this study the robustness of the model was first tested in an 11-year model run. Monte Carlo simulations have been applied for the parametric uncertainty analysis considering both random and systematic uncertainties. Where appropriate, temporal autocorrelation in random uncertainties was considered. Monte Carlo simulations require a large number of repeated model runs. To allow for a computation within reasonable time limits, the originally 2-dimensional model was modified for a zero-dimensional calculation at a point. Resulting energy and mass balance of the point version of MB2 was compared to the original distributed model, yielding identical results. Twelve input and model parameters have been assigned uncertainties that were determined from the literature, based upon technical specifications and from data analysis. Simplified assumptions were made about the PDF of uncertainties of the individual model parameters, treating them all as normally distributed.

The chosen approach, the results and a discussion of their significance in mass balance modeling are shown in detail in Paper №3.

3.4. Coupling of a Mass Balance and a Climate Model

One goal of this thesis was to develop a regional mass balance model. With respect to its planned application to the entire Swiss Alps, the regional mass balance model was derived from the model MB1 in order to keep computation time within acceptable limits. The key issue was to choose appropriate spatially distributed meteorological input data and to develop a coupling scheme to drive the model from them. Several available gridded climatologies are listed in Table 2.1 but none of them provides all the required data at the requested temporal resolution of one day. From Sections 2.1.3 and 2.3 it becomes obvious that RCM output provides an alternative to driving the model, and a way to avoid a patchwork of data sets that are of differing spatial and temporal resolution and unknown interoperability. RCMs provide physically consistent fields of atmospheric parameters, for present day's as well as for future climatic conditions. Actually, the coupling of the mass balance model with RCM output would allow scenario calculations on mass balance to be performed under a future climate. However, there is a large gap in spatial resolution between RCMs (10–50 km) and the mass balance model (100 m) that has to be addressed with an appropriate coupling scheme. Existing coupling schemes for mountain areas rely on

manually selected individual grid cells whose data are downscaled to a point or a small area in space by statistical downscaling methods (e.g. *Salzmann et al.*, 2007a; *Paul and Kotlarski*, subm). The coupling of a coarse grid of input data to a finer grid on the impact model is not yet common in impact modeling (e.g. *Kleinn et al.*, 2005; *Früh et al.*, 2006). Furthermore, data from RCMs have certain biases, and the importance of the above-mentioned gridded climatologies or homogenized station data for a bias correction is recognized.

Beniston et al. (1997) argued that climate models are difficult to evaluate in high mountain and remote areas where measurements are sparse. Instead they proposed using observed properties of glaciers and permafrost to obtain meteorological quantities for the validation of climate model output. Studies like the one presented in Paper №4 might be able to provide feedback to climate modelers: Running a glacier mass balance model with climate model output is a test of whether the climate model is able to reproduce the spatial distribution of the parameters governing glacier mass balance. Although such a test might be of limited accuracy, it is definitely worth the effort because very few meteorological measurements are available for the altitude of glacier occurrence and, as in the case of precipitation, they also involve considerable uncertainties.

Paper №4 describes the applied coupling scheme, the resulting mass balance, and the evaluation procedure based on a larger set of stake measurements and meteorological data from weather stations. A bias correction has not been conducted in Paper №4. Instead, the emphasis was placed on a methodical description and evaluation of the chosen coupling scheme. Biases in the RCM data that are responsible for deviations in the mass balance from the measurements are discussed as well.

A modified version of the regional mass balance model, including a simple bias correction scheme and a precipitation calculation based on the *Schwarb et al.* (2001) precipitation climatology, has been applied for an initial precipitation assessment by means of mass balance modeling (cf. Section 9).

Part II.

Research Papers

4. Strong Spatial Variability of Snow Accumulation Observed with Helicopter-Borne GPR on two Adjacent Alpine Glaciers (Paper №1)[1]

Abstract This study compares high-resolution helicopter-borne radar measurements to extensive ground-based profiling of the snow cover on Findel- and Adler glacier, Switzerland. The results demonstrate that derived accumulation values of either method are well in accordance. The spatial distribution of radar based snow depth allows a clear distinction of three zones of different accumulation characteristics: (1) The lower part of Findelgletscher shows a clear altitudinal trend while (2) the upper part has no trend in altitude but high spatial fluctuations in snow depth. (3) Adler glacier's accumulation characteristics are similar to zone (2). However, despite their close vicinity, accumulation on (3) is reduced by 40% compared to (2). The observed strong spatial variability emphasises the need for spatially continuous measurements for studies involving accumulation on glaciers. Finally, reasons for observed variations (e.g. preferential snow deposition and snow redistribution) are discussed.

4.1. Introduction

Utilisation of radio-echo sounding techniques to determine past and present accumulation rates has become a standard method, especially in polar glaciology. On polar ice sheets and polythermal glaciers this method is rewarding because of the low absorption of electromagnetic energy in cold firn. On temperated glaciers, application is usually restricted to sounding of ice thicknesses with low frequencies ($< 100\,\mathrm{MHz}$). High-resolution measurements are mostly performed with so-called ground-penetrating radar systems (GPR) (*Richardson et al.*, 1997; *Kohler et al.*, 1997, among others), operating directly from the surface. They are thus relatively time consuming and the spatial coverage is limited to accessible areas. Application of high-resolution airborne radar, capable of mapping annual accumulation, is still rare and mostly limited to fixed-wing aircraft (e.g. *Kanagaratnam et al.*, 2004). To cope with the difficulties imposed by measurements in mountainous terrain and valley glaciers, airborne radar is most suitable. Apart from quasi-airborne measurements from an aerial tramway (*Yankielun et al.*, 2004), helicopter-borne radar provides the most reasonable platform and has been applied for studies of sea and river ice (*Wadhams*

[1] based on: Machguth, H., O. Eisen, M. Hoelzle and F. Paul (2006), Strong Spatial Variability of Snow Accumulation Observed with Helicopter-Borne GPR on two Adjacent Alpine Glaciers, *Geophysical Research Letters, 33,* L13503.

et al., 1987; *Arcone and Delaney*, 1987; *Melcher et al.*, 2002), snow on ground (*Marchand et al.*, 2003) or glacier thickness measurements (*Thorning and Hansen*, 1987; *Damm*, 2004). However, on mountain glaciers only few studies use helicopter-borne radar to investigate the properties of the snow cover and none was so far dedicated to the spatial accumulation distribution. For instance, *Arcone and Yankielun* (2000) focus on intraglacial features in the ablation zone of a glacier, whereas *Arcone* (2002) investigates processing techniques and autonomously derives physical properties of temperate firn.

TodaySs glacier mass-balance models are based on sophisticated formulations of the energy fluxes while accumulation processes are treated in a very simple way: precipitation varies only with altitude and any processes of snow redistribution are neglected (*Hock*, 2005). Using a similar model (described in *Machguth et al.* (2006b)) we have calculated the mass balance distribution for a glacierized catchment in southwestern Switzerland, including Findel glacier[2] (length 7.2 km, area 15.3 km^2) and its neighbour Adler glacier (3.1 km, 2.04 km^2) (Figure 4.1). The modelling for the 1971–1990 time period resulted in a very positive mass balance for Adler glacier of 0.7 m water equivalent (m w.e.) while its larger neighbour's mass balance was negative (-0.25 m we). In fact, the shrinkage of both glaciers indicates that a very positive mass balance is unrealistic. We assume that, in reality, accumulation on Adler- and Findel glacier differs strongly. The model's failure is most probably caused by treating precipitation as a function of altitude alone and by ignoring snow redistribution.

In this study we combine high-resolution helicopter-borne GPR measurements and extensive ground-based profiling of the snow cover to determine the spatial distribution of accumulation and to validate our assumption of a strong local variability in accumulation. In contrast to methods that require measurements at two points in time (e.g. mapping of elevation changes with laser altimetry, accumulation stakes without snowpits), GPR has the strong advantage that changes over time in surface elevation (e.g. melt, settlement of the underlying snow cover and glacier movement after the first measurement) do not affect the accuracy of the measurements. Furthermore, measuring only once requires less logistical efforts.

4.2. Methods

4.2.1. Radar system and data acquisition

A commercial Noggin Plus 500 radar (Sensors & Software Inc., Canada,) was operated with a shielded antenna (15 cm transmitter-receiver separation) at a centre frequency of 500 MHz and 400 MHz bandwidth. The helicopter–radar combination was developed by Airborne Scan, Visp, Switzerland. The antenna was mounted to the helicopter runner. Data acquisition was performed in a constant-time triggering mode, with a time increment of 0.1 s between traces. Helicopter speed was about 6 m s^{-1} on average, resulting in a mean trace increment of 0.6 m. Helicopter altitude above ground was between 2.5 and 30 m, being 11 m on average, resulting in a footprint size in the order of a few tens of m^2. 1876 samples were recorded per trace with a 0.2 ns sampling interval, resulting in a 375 ns time

[2] In this paper we refer to this glacier as "Findel glacier". According to the maps of the Swiss Federal Office for Topography (swisstopo) this is the official name of the glacier. However, in most glacier inventories the glacier is called Findelen glacier.

window. Four-fold pre-storage stacking of traces at a pulse repetition frequency of 25 kHz was applied. A GPS antenna was mounted at the nose of the helicopter. For each recorded trace the GPS-position was simultaneously stored. Real-time GPS results in a position accuracy of < 10 m.

The radar flight was accomplished on 9 May 2005, ground measurements for validation were conducted on 6 and 7 May 2005. During all four days air temperature at the glacier terminus was slightly below the freezing point. Below 2700 m a.s.l. the snow was wet and some water drained off at the snow-ice interface. Above 3200 m the entire snow pack was dry. In approximately 25 minutes of flight 10.0 km of radar profiles were collected, thereof 1.9 km on Adler glacier (Figure 4.1). On Findel glacier radar profiles reach from 2570 to 3560 m a.s.l., on Adler glacier they reach from 3240 to 3690 m a.s.l. Under the favourable weather conditions the sites of snow pits and -probes were visible from the helicopter allowing a consecutive visual determination of the flight direction. According to GPS data, the helicopter passed 26 snow pits and probes at a distance of < 5 m, four at 5–15 m and two at 15–30 m. Two snow probes and one snow pit were missed by 60–130 m because they could not be found again.

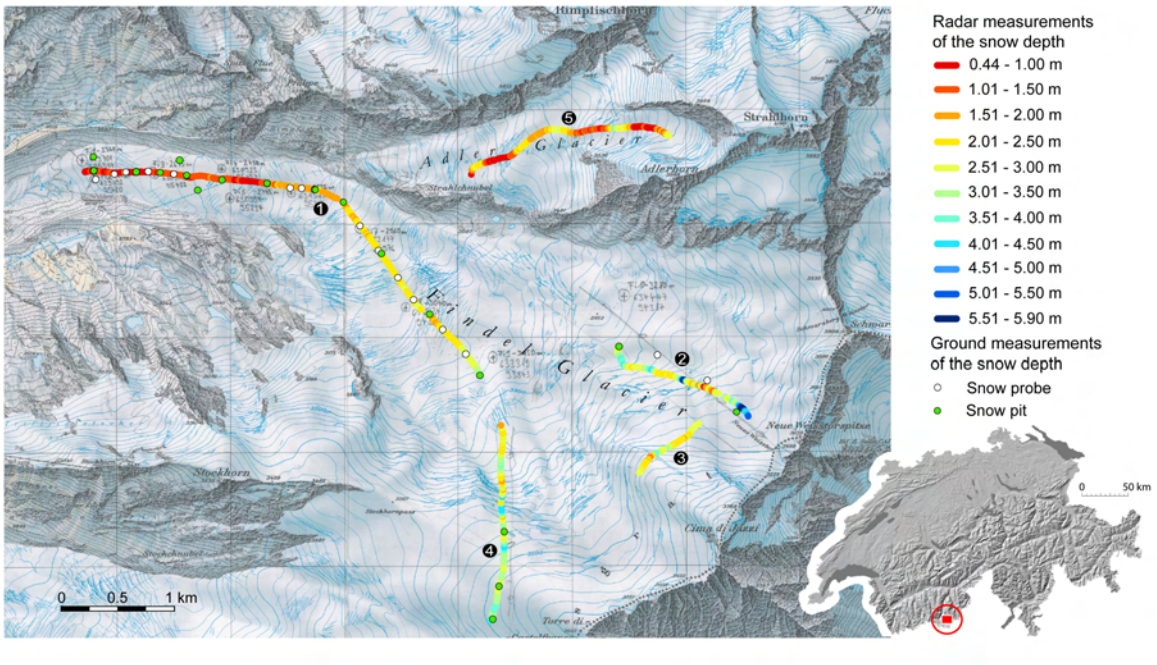

Figure 4.1.: Map of Findel and Adler glacier (red square in inset on Swiss map) with radar profiles (black numbered circles) and ground measurements. Color indicates radar-based snow depth. Reproduction of the background map with permission from swisstopo (BA067878).

4.2.2. Radar data processing

Post-recording processing and radar-data analyses were carried out with ReflexWin (Sandmeier Scientific Software, Germany). Processing steps include dewowing (high-pass filter), background removal, application of a gain function to mainly compensate for spherical spreading, and additional filtering. The varying helicopter altitude above ground required a static correction of each trace to the first break of the surface reflection (time-zero correction). Due to the relatively smooth surface topography and small layer thickness compared to the helicopter altitude no migration was necessary. Along most profiles one or more distinct reflections of different magnitude are visible (see sample radar profile Figure 4.2). Tracking of the uppermost strong continuous reflection horizon resulted in continuous profiles of last winters snow layer thickness (Figure 4.1). No interpretation was performed where no distinct reflection horizon was visible. Density measurements in the snow pits (see below) yielded a mean density of $400\,\mathrm{kg\,m^{-3}}$. Based on the linear and quadratic conversion formulas of *Tiuri et al.* (1984) and *Kovacs et al.* (1995), respectively, conversion of the radar data from time to depth domain was carried out with a mean wave speed in snow of 2.2 $10^8\,\mathrm{m\,s^{-1}}$. Using the same mean density of $400\,\mathrm{kg\,m^{-3}}$ the layer thickness is converted to water equivalent.

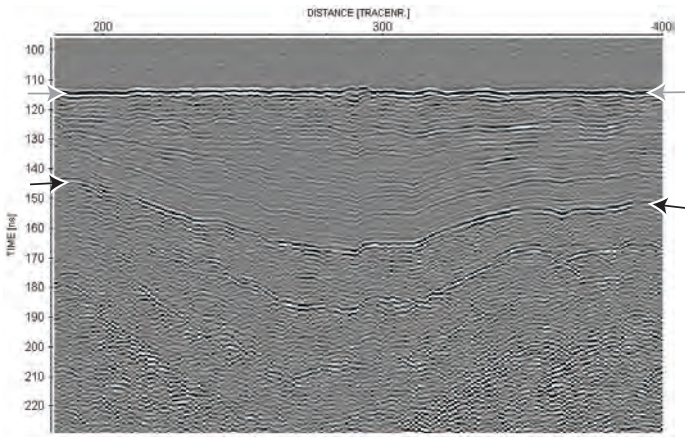

Figure 4.2.: A section of the radar profile 2 at 3460 m a.s.l. The horizontal axis corresponds to approximately 130 m. The varying snow depth, the internal layering of the snow pack as well as previous years' firn layers with some internal structures are clearly recognizable. Grey arrows indicate the air-snow interface and black arrows indicate the snow-firn interface.

4.2.3. Snowpits and -probes

Snow pits and snow probes were used to measure snow depth and density from the actual snow surface down to the ice surface. Where the snow cover outlasted the previous melting season (the remaining accumulation zone of 2004 is located above 3300 m a.s.l. on Findel glacier, for Adler glacier no data are available), snow pits were dug down to the horizon of the previous autumn's snow surface. According to data from the meteo station Gornergrat (located 5 km west of Findel glacier at 3100 m a.s.l.), the long melt season of 2004 ended

with heavy snow falls on 10 October. Consequently, the snow depth measured with radar, snow pits and -probes was accumulated within the time span of about 10 October 2004 to 7 May 2005. Coordinates of snow pits and -probes were captured with a hand-held GPS (position accuracy of 5–15 m). Within an altitudinal range from 2590 to 3510 m a.s.l. 20 snow pits have been sampled and snow depth and density as well as the internal layering of the snow pack was determined in all of them. This sample size was enhanced by 19 measurements of snow depth with snow probes. However, defining previous autumn's snow surface using snow probes is sometimes difficult (e.g. missinterpretations due to ice layers within the winter snow pack). Consequently, snow probes were restricted to the ablation area and for every test site the mean value of nine snow probes, sampled within a radius of 7 m, was calculated.

4.2.4. Data Merging

Field measurements were only used to validate the interpretation of the radar profiles, analyses were conducted separately. Neither GPS data nor a map were used for the interpretation of the radar profiles, thus the interpreter's knowledge about the field measurements could not influence his interpretation of the profiles. The data sets were joined within a GIS software (ArcGIS 9.1). The twenty closest radar traces to every ground measurement were selected and their mean value is used below for comparison with the corresponding ground measurement.

4.3. Results

The transition between winter snow and ice or winter snow and snow having outlasted the previous summer is in general clearly recognizable in the radar profiles. A total of 0.6 km radar profiles (6% of the total length) did not allow any tracking due to lacking or disturbed layering. Most of these zones are located within crevassed areas. Further analysis of the data is based on almost 15000 radar traces, representing the remaining 9.4 km of radar profiles. The thickness of the winter's snow layer varied in the ground measurements (radar measurements) from 0.32 (0.44) to 4.4 (5.9) m. The specific density measured in the snow pits is not correlated with altitude and varies from 360 to 470 $\mathrm{kg\,m^{-3}}$. The mean density is 400 $\mathrm{kg\,m^{-3}}$ with a standard deviation of 30 $\mathrm{kg\,m^{-3}}$. Figure 4.3 shows the agreement between radar profiles and all snow pits and -probes where the horizontal distance to the radar track is less than 30 m. The linear regression yields a correlation coefficient of $R^2 = 0.84$. Three data points must be considered outliers, as discussed below. Excluding these data points yields $R^2 = 0.96$.

According to the radar profiles three zones of different accumulation characteristics can be distinguished: the lower part (profile 1) and the upper part of Findel glacier (profiles 2, 3 and 4), as well as Adler glacier (profile 5). The lower part of Findel glacier shows a clear correlation between altitude and snow cover thickness ($R^2 = 0.81$) and the fluctuations in snow depth are small (Figure 4.4). On Adler glacier and the upper part of Findel glacier accumulation has no altitudinal trend ($R^2 \leq 0.01$). Fluctuations in snow depth are very large. The correlation coefficient calculated for the upper part of Findel glacier is based on all traces of the profiles 2, 3 and 4 but also represents well the characteristics of every individual profile: none shows any significant trend with altitude; and all show large fluctuations of

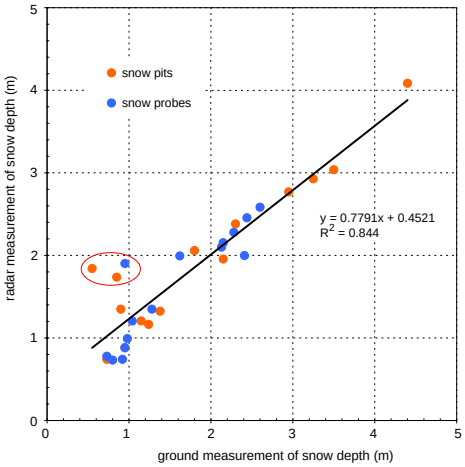

Figure 4.3.: Comparison of radar- and ground-based measurements of snow depth. The three outliers are marked with a red circle.

snow depth. At altitudes where radar profiles exist on both glaciers (3240 to 3560 m a.s.l.) the average accumulation is 2.98 m snow (5704 traces) on Findel and 1.80 m snow (2164 traces) on Adler glacier. The accumulation on Adler glacier is 0.5 m w.e. or 40% lower than on Findel glacier.

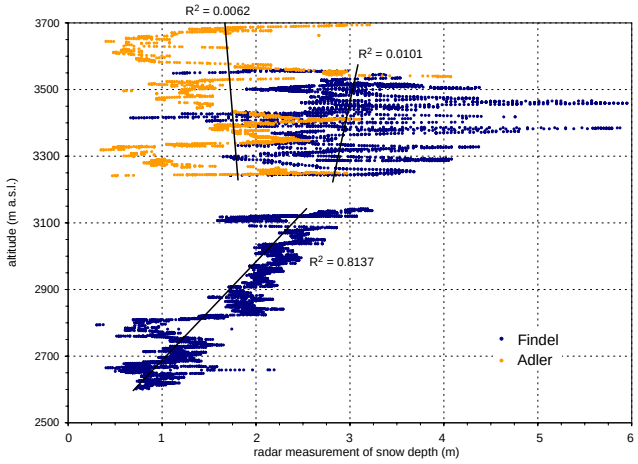

Figure 4.4.: Snow depth versus altitude for all profiles on Findel and Adler glacier.

4.4. Discussion

Our correlation between ground and radar measurements confirms the results of earlier studies with helicopter-borne radar in non glacierized landscapes, having achieved correlation coefficients of 0.82–0.97 (e.g. *Marchand et al.*, 2003). The three outliers mentioned above are presumably caused by misinterpretations in the field. Snow-probe measurements at those three sites, located within a diameter of 100 m at 2850 m a.s.l. are contradictory (0.5–1.7 m snow).[3] A massive ice layer at 0.5 m depth was recorded in the snow profile closest to them. We assume that this layer was interpretated as the ice surface. The layer is visible in the radar profile as a long, massive and smooth reflection horizon at a depth of 0.5 to 1 m. Normally, the snow-ice interface appears more uneven because of previous surface melt and is similar to the second, less distinct reflection horizon at about 1.8 m in that profile. The example shows that in situ measurements also present only partial truth. A correct interpretation of the internal layering of the snow pack is essential for both methods. Consequently, mutual comparison is important to combine their strengths. In the ablation area snow pits allow precise point measurements while the large footprint of helicopter-borne GPR has the advantage of averaging out the bumpiness of the ice surface. In the accumulation area, both methods have to deal with the difficulty to correctly identify last autumns snow horizon.

The overall pattern of accumulation distribution on Findel glacier corresponds well to the observations based on snow probes on other alpine glaciers (e.g. Vernagtferner in Austria, *Plattner et al.* (2006)). On the lower part of Findel glacier the correlation between altitude and snow depth can partly be explained by melt during long warm weather periods in March and April 2005. The large deviations in accumulation between Findel and Adler glacier are very unlikely to be caused by enhanced melt in March and April due to differing surface exposition: assuming that the entire difference in global radiation due to exposition (20 W m^{-2}) is available for melt and considering the high snow albedo of approximately 0.8 for this period, melt on Adler glacier is estimated to be 0.05 m w.e. higher than on Findel. We therefore assume that the large deviations in accumulation are primarily due to spatial variability of precipitation and redistribution of snow by wind. The area of investigation receives high amounts of precipitation under southern wind directions. Reduced wind speed leewards from ridges results in enhanced precipitation and additional snow deposition from wind transport (e.g. *Föhn and Meister*, 1983; *Gauer*, 2001). Findel glacier is located directly leewards of the main ridge and profits from this effect, whereas Adler glacier is farther away. In addition, strongly reduced accumulation is also observed in crevassed zones, probably caused by topography and microscale turbulences. Within this study we have only assessed the spatial and not the temporal variability of accumulation. However, taking into account the concurrent shrinkage of both glaciers, we assume that the observed deviations in accumulation for the winter 2004/05 are not exceptional.

[3] A figure showing the section discussed above as well as an other section of the radar profiles is provided in the online auxiliary material.

4.5. Conclusions and Outlook

The data of both methods used in this study are in very good agreement. The observed distribution of the snow cover confirms our assumption of strongly reduced accumulation on Adler glacier. Our results emphasize that the distribution of accumulation is not simply a function of altitude, confirming other studies (e.g. *Winstral et al.*, 2002). We suppose that the spatial variability of precipitation as well as the redistribution of snow are mainly governing the accumulation distribution. The observed variability of the mass balance for the accumulation period (0.5 m we) is one order of magnitude higher than the error of melt calculations for the entire ablation period with energy balance models (compare *Arnold et al.*, 1996; *Obleitner and Lehning*, 2004). The results underline that major improvements in glacier mass balance modeling can be achieved by focusing on the accumulation processes. Helicopter-borne GPR is recommended as a reliable tool for time-saving and accurate mapping of the snow cover. The method allows to enhance the sparse data base on accumulation distribution towards both spatial and temporal variability, providing a sound data basis for glacier monitoring (e.g. yearly repeated measurement of winter balance), for statistical analyses (e.g. digital elevation model attributes) or for validation and calibration of physical modeling. Field measurements remain essential for mutual validation and to determine snow density.

Acknowledgments Simon Allen, Sabine Baumann, Xavier Bodin, Esther Hegglin, Christian Huggel, Jeannette Nötzli, Theresa Tribaldos, Michi Zemp and Michael Ziefle have helped us on field work. Their large effort made this study possible and is gratefully acknowledged. We very much appreciate the cooperation with Airborne Scan and Air Zermatt. We would like to thank Michael Lehning and an anonymous reviewer for their valuable comments. H.M. was funded by the grant 21-105214/1 of the Schweizer Nationalfonds, O.E. was supported through an "Emmy Noether"-scholarship EI 672/1 of the Deutsche Forschungsgemeinschaft.

5. Distributed glacier mass balance modeling as an important component of modern multi-level glacier monitoring (Paper №2)[1]

Abstract Modern concepts of worldwide glacier monitoring include numerical models for (a) interconnecting the different levels of observations (local mass balance, representative length change, glacier inventories for global coverage) and (b) for extrapolations in space (coupling with climate models) and time (back and forth). In this context, one important new tool is distributed mass balance modeling in complex mountain topography. This approach builds on simplified energy balance models and can be applied for investigating the spatio-temporal representativity of the few mass balance measurements, for estimating balance values at the tongue of unmeasured glaciers in order to derive long-term average balance values from a great number of glaciers with known length change, and for assessing special effects such as the influence of Sahara dust falls on the albedo and mass balance or auto-correlation effects due to surface darkening of glaciers with strongly negative balances. Experience from first model runs in the Swiss Alps and from applications to the extreme conditions in summer 2003 provide evidence about the usefulness of this approach for glacier monitoring and analysis of glacier changes in high-mountain regions. The main difficulties concern the estimation of precipitation (strongly variable spatial pattern, snow redistribution by wind and avalanches) and the parameterization of local cloud cover. Field measurements remain essential to tie the models to real ground conditions.

5.1. Introduction

During the past few decades, rapidly increasing knowledge together with fast if not accelerating changes in nature have made glacier fluctuations to become a key element of early detection strategies related to atmospheric warming (*IPCC*, 2001). Monitoring and modeling approaches are thereby closely interconnected: data from monitoring can be used to calibrate or validate numerical models, and numerical model simulations help to understand information from monitoring programs and to design focused long-term observations.

The present contribution discusses distributed glacier mass balance models and their applicability for modern glacier monitoring. A brief introduction about the role of numerical models in modern and integrated multi-level glacier monitoring is followed by a detailed

[1] based on: Machguth, H., F. Paul, M. Hoelzle and W. Haeberli (2006), Distributed glacier mass balance modeling as an important component of modern multi-level glacier monitoring, *Annals of Glaciology, 43,* 335–343.

description of three case studies. They focus on the integrated use of field measurements and numerical modeling and should emphasize that modern glacier monitoring strategies have to apply both techniques in a complementary sense. The critical discussion of the results obtained lead to a discussion of future possibilities and still existing difficulties to be overcome.

5.2. Numerical model simulations in modern glacier monitoring strategies

Observational concepts for monitoring future glacier changes include the possibility of dramatic scenarios, i.e. the complete deglaciation of entire mountain ranges within a few decades. Advanced and future-oriented concepts have been developed (*Haeberli*, 2004; *Haeberli et al.*, 2000, 2002) within the framework of the Global Terrestrial Observing System (GTOS) as part of global climate-related observational programmes (GCOS). They follow a tiered strategy, which leads from (a) detailed process studies (extensive energy and mass balance, climate and flow measurements) via (b) regional measurements of mass balance (summary results from reduced stake networks and repeated mapping, laser altimetry on large glaciers), (c) the determination of glacier length changes (samples which are representative for variable glacier geometry and individual mountain ranges) to (d) periodically repeated glacier inventories compiled by means of satellite imagery and geo-informatics using digital terrain information (cf. *Haeberli and Hoelzle*, 1995).

This multi-level approach includes numerical models for (a) interconnecting the different levels of observations and (b) for extrapolations in space (coupling with climate models) and time (back and forth). The cumulative length change of glaciers, for instance, is the result of all mass-/ energy balance and flow effects combined and constitutes the key to a global inter-comparison of glacier mass losses at the decade and century time scale. Time series of balance and length measurements are now close to the estimated dynamic response times of individual glaciers (*Jóhannesson et al.*, 1989) and make it possible to derive long-term average mass balances from cumulative length changes of the network glaciers (*Haeberli and Hoelzle*, 1995; *Haeberli and Holzhauser*, 2003). Systematic analysis of corresponding data (*Hoelzle et al.*, 2003) shows that the reported mass balance series are indeed representative for large areas and long time periods. Past, current and potential future developments can be studied by dynamically fitting mass balance histories to present-day geometries and historical length change measurements of long-observed glaciers using time-dependent flow models (*Oerlemans*, 2001; *Oerlemans et al.*, 1998).

Application of such models leaves no doubt about the fact that many of the presently observed mass balance glaciers could vanish within a few decades. Indeed, surface lowering, thickness loss and the resulting reduction in driving stress and flow may increasingly replace processes of tongue retreat by processes of down-wasting or even collapse coupled with enhanced feed-backs from albedo and balance/altitude effects (*Paul et al.*, 2004). Assessing the regional representativeness of glacier mass balance measurements by comparison between long-term observational series of mass balance and glacier length change could face more and more difficulties. Distributed (spatial) mass balance modeling for glaciers in complex high-mountain topography is a possible way to not only solve this problem, but also to strikingly increase the time resolution of regional inter-comparison. As most glaciers with long-term

mass balance measurements were selected for easy access and logistical or political reasons, distributed mass balance models can help to assess the representativity of a specific glacier with respect to all glaciers in a larger region covering different sizes, aspects and topographic characteristics. Moreover, the inter-comparison is no longer limited to the typical response time of glaciers (decades), but can be assessed on annual or even shorter time periods (e.g. winter and summer balance). In this study we address these challenges by three case studies in the Swiss Alps which focus on the combined use of measurements and modeling utilizing modern geo-informatic techniques.

5.3. Case Studies

The location of the test sites for all three case studies is illustrated in Figure 5.1. All three case studies make use of mass balance models using the energy balance approach. For a comprehensive overview of energy balance modeling with respect to glacier melt refer to *Hock* (2005). Case study one and two are based on the same simple formulation of the energy fluxes, but for the first study the model has been extended by a parametrization scheme for avalanches. In case study three we apply a more complex formulation of the energy balance, but the model runs without considering avalanches.

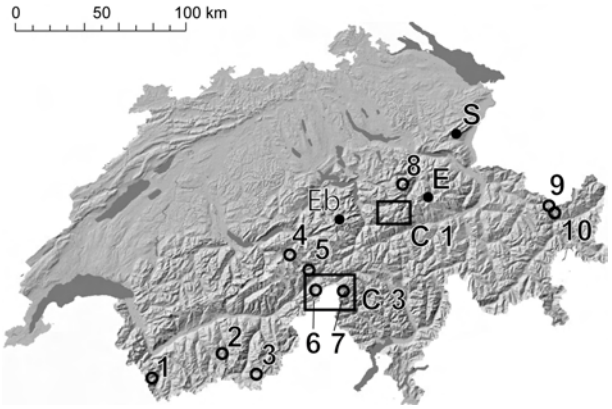

Figure 5.1.: Overview of the test site locations. C1: Test site for case study one, 1-10: Glaciers used in case study two (1: Saleina, 2: Moiry, 3: Findeln, 4: Oberer Grindelwald, 5: Oberaar, 6: Gries, 7: Basòdino, 8: Glärnisch, 9: Silvretta, 10: Tjatscha), C3: Test site for case study 3. Climate stations used in case study one are denoted by Eb: Engelberg, E: Elm and S: Säntis.

In the first case study we use index measurements of annual snow accumulation that are sampled at two sites (2700 m and 2900 m a.s.l.) on the glacier Claridenfirn since 1914. The data from Claridenfirn are of very good quality and were published by *Müller and Kappenberger* (1991), by *Glaciological Reports* (1992-2008) and in *IUGG (CCS) – UNEP – UNESCO* (2005). These isolated measurements lack a clear scientific concept and are difficult to integrate into modern glacier monitoring strategies (*Haeberli et al.*, 2000; *IUGG (CCS) – UNEP – UNESCO*, 2005). We here test there applicability for verification of a simple distributed mass balance model running over a 20 year period (1981–2002). The second case study derives mean specific glacier mass balance for the 1961–1990 period

on ten selected glaciers following an approach by *Jóhannesson et al.* (1989) and applied by *Haeberli and Hoelzle* (1995). In this case study we combine measured glacier length changes with modeled ablation at the glacier tongue using the same mass balance model as above. In the third case study we force a distributed mass balance model with the special meteorological conditions of the extreme summer of 2003 and compare the results to the measurements at the two mass balance glaciers Gries and Basòdino. The model also accounts for the specifically low 2003 glacier albedo as derived from satellite data and for the spatial variability of precipitation from the *Schwarb et al.* (2001) climatology.

5.3.1. Case study 1: Claridenfirn - modelling and observations

Model description

We use a simple mass balance model as described by *Oerlemans* (2001) that is based on the calculation of the energy balance. Our version of the model is enhanced by an accurate calculation of mean daily potential global radiation (which is the major source of energy available for glacier melt) using the DEM25 (a digital elevation model with 25m spatial resolution from swisstopo). Especially in the rough topography of the Alps, with glaciers of comparable low albedo and a long ablation period this approach has proven to perform well (*Brock et al.*, 2000). The model runs at daily steps and the cumulative mass balance b_{cum} on day $t+1$ is for every time step and every individual grid cell calculated as:

$$b_c(t+1) = b_c(t) + \Delta t\left[\min(0;\, -\frac{Q_m}{l_m}) + P_{solid}\right] \tag{5.1}$$

where t is the discrete time variable, Δt is the time step, l_m is latent heat of fusion of ice ($334\,\mathrm{kJ\,kg^{-1}}$), P_{solid} is solid precipitation in meter water equivalent (m we). Any melt water is immediately removed from the glacier and the energy available for melt (Q_m) is calculated as (see *Oerlemans*, 2001):

$$Q_m = D(1-\alpha)S_{in,clr} + C_0 + C_1 T_a \tag{5.2}$$

where D is a reduction factor for incoming short wave radiation which accounts for cloudiness or haze, α is the albedo of the surface, $S_{in,clr}$ is the clear sky short wave radiation, and $C_0 + C_1 T_a$ is the sum of the longwave radiation balance and the turbulent exchange linearized around the melting point (T_a in °C). As recommended by *Oerlemans* (2001), C_1 was set to $10\,\mathrm{W\,m^{-2}}$ and we used C_0 as a tuning factor (giving best fit at -25 $\mathrm{W\,m^{-2}}$). For every day D is calculated by dividing measured and calculated means of global radiation. The program operates with three different albedo values, for ice ($\alpha_i = 0.3$), for snow ($\alpha_s = 0.7$) and for firn ($\alpha_f = 0.4$). At the start of the calculation the albedo is set to α_i for the entire test site, and for any snow accumulation α_s is used. Accumulated snow is treated with the firn albedo ($\alpha = \alpha_f$) when its age exceeds 365 days and after 2 years its albedo is set to the value of ice ($\alpha = \alpha_i$). The mean daily potential global radiation $S_{in,clr}$ is calculated beforehand for all 365 Julian days from the SRAD code. This code takes into account the effects of slope, aspect and topographic shading as well as a standard atmospheric composition with a clear-sky transmissivity dependent on elevation for every individual gridcell of the respective DEM (*Wilson and Gallant*, 2000).

In order to improve the modeling of snow accumulation, snow redistribution by avalanches is included in the model. The parameterization scheme is based upon the multiple flow-direction algorithm developed by *Quinn et al.* (1991) and has been adapted for avalanches by S. Gruber. In the model, the percentage of removed snow is zero for cells with a slope of less than 30° and increases linearly to 100% for cells steeper than 60°. First, the transport fraction from each cell to its neighbours is determined. Then, an initial array of transported snow mass is iteratively propagated along its topographically-determined flow path. Finally, for cells with a slope of less than 30° a deposition function describes the amount of snow deposited and removed from the propagated mass. When all snow is deposited, the model iteration is stopped. Avalanches are computed for every day when snowfall at 3000 m a.s.l exceeds 0.02 m w.e., otherwise snowfall is distributed evenly.

Input data

Claridenfirn index measurements are used to verify a 20 year transient model run starting on 29 September 1981 and ending on 17 October 2002. The test site is 18 km by 14 km in size with Claridenfirn almost in its centre, and is represented by a rectangular section of the DEM25 (Figures 5.1 and 5.2). The highest correlation between mean measured winter accumulation on Claridenfirn and average winter precipitation at climate stations nearby exists for Elm at 960 m a.s.l. (*Müller and Kappenberger*, 1991). However, we calculate daily precipitation for Claridenfirn from the measurements in Elm (25 km to the west) and Engelberg (25 km to the east at 1020 m a.s.l.) to have a spatially more homogeneous coverage. Precipitation is distributed to the terrain by means of an elevational gradient that is calculated based on (*Müller and Kappenberger*, 1991) by matching the mean winter precipitation at Elm (1959–83) with the mean winter accumulation measured at the upper stake on the glacier over the same time period. A linear regression gives a correlation coefficient of 0.77 between measured and modeled winter accumulation at the upper stake, with an underestimation of 0.17 m w.e. by the model. However, matching the precipitation measurements with glacier accumulation is not satisfying. The accumulation on the glacier does not depend only on precipitation but is the result of a complex set of variables, including snowdrift or melt events after the autumn stake readings.

Daily means of global radiation (to obtain the daily correction factor d) and temperature (using a constant lapse rate of $0.00625\,\mathrm{K\,m^{-1}}$) are acquired from the Säantis climate station (2501 m a.s.l, 55 km to the northeast; Figure 5.1). Despite its long distance from the glacier, this high-mountain station was chosen to avoid extrapolations over large elevation intervals.

Results

The modeled 20 year mean mass balance distribution for the entire test site is presented in Figure 5.2. Large bands of avalanche deposits are visible on many glaciers beneath steep mountain slopes, indicating that their dominant source of nourishment is avalanche snow. In general the modeled mass balances are positive for most glaciers, which is in contrast to the observed glacier shrinkage in this time period. In view of the simplifications made in the model (wind redistribution of snow is not included, precipitation is only a function of altitude, cloudiness is a daily constant, and calibration has only been applied to the gradient of winter precipitation) the results are nevertheless promising.

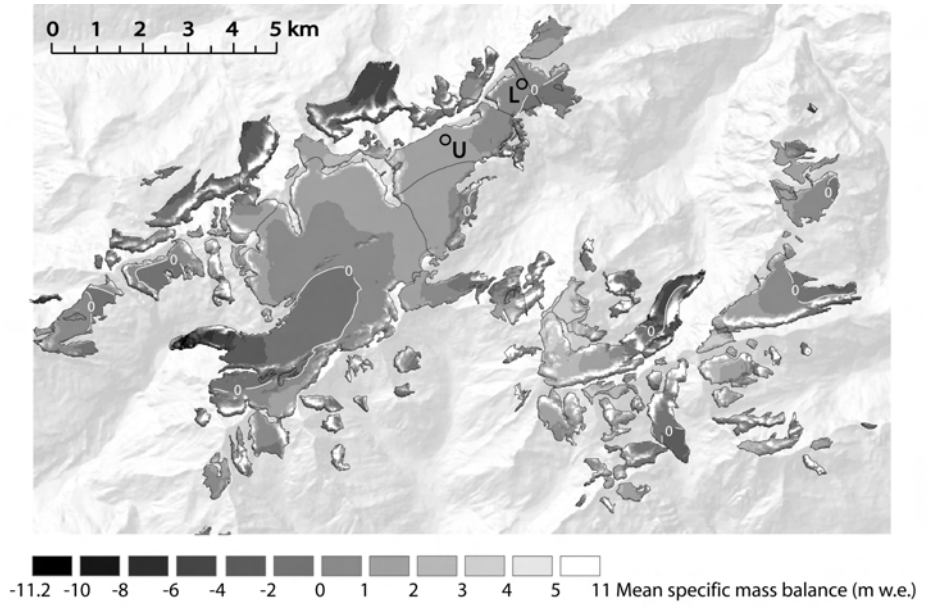

Figure 5.2.: Modeled mean distributed specific mass balance for all glaciers within the perimeter of the test site, calculated with the 20 year transient model run. Stake locations on Claridenfirn are indicated with circles (L = lower stake, U = upper stake). In the background a shaded relief of the DEM25 is shown. DEM25: reproduced by permission of swisstopo (BA057384).

To assess the accuracy of the 20 year transient continuous model run, we compare the measurements on Claridenfirn to the modeled values of the corresponding cells of the DEM25. The cumulative mass-balance curves at the positions of the two stakes are depicted in Figure 5.3a. The final values for both stakes are summarized in Table 5.1. A more detailed comparison of modeled and measured annual mass balances is depicted in the scatter plot given in Figure 5.3b. We obtain correlation coefficients of 0.77 for the lower and 0.86 for the upper stake. The mean yearly mass balance is underestimated by 0.09 m w.e. at the lower and overestimated by 0.08 m w.e. at the upper stake (Table 5.1). As stake measurements are performed at different dates with a varying time-span from year to year, the corresponding time periods are used for the modeled balances. In summary, we find that the simple mass-balance model performs well in the long-term calculation for the two stakes on Claridenfirn, but on the other hand the model run results in positive (up to 1.4 m w.e. on some glaciers) and consequently quite unrealistic mass balances for the neighboring glaciers. Hence, the parameterization of avalanches is an important improvement to the model. Nevertheless, the spatio-temporal distribution of precipitation, as well as the redistribution of snow by wind, are essential to obtain a more realistic mass-balance distribution over large areas and long time-spans. Measurements have shown that even adjacent glaciers have large differences in mean accumulation. In addition, the accumulation pattern of the measured glaciers has revealed a high spatial variability (cf. Paper №1).

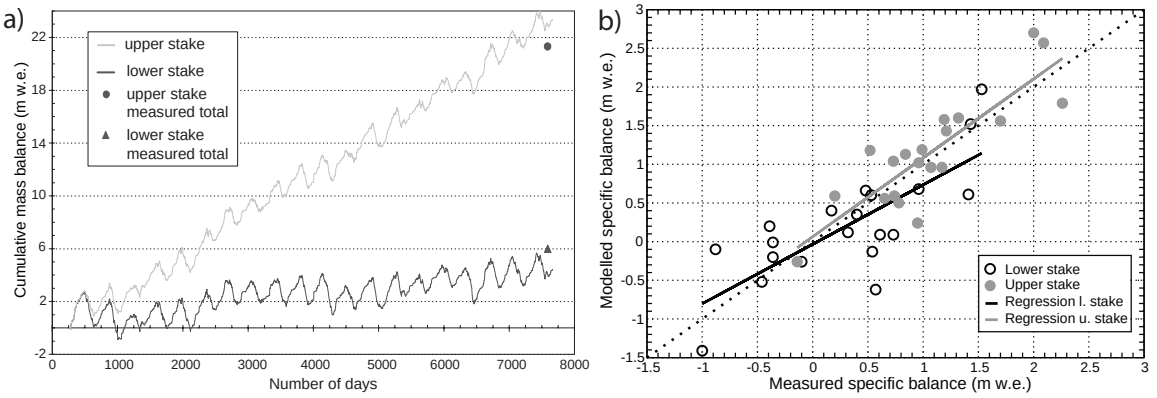

Figure 5.3.: *(a)* Cumulative mass balance for the upper and the lower stake, calculated in a 20 year transient model run from 1981 to 2002. The measured cumulative mass balance is also indicated. The stakes are located well above the equilibrium line and the measured mass gain does not represent the overall mean yearly mass loss of about -0.7 m w.e. that has been observed on Alpine glaciers during the same period. *(b)* Scatter plot of annual measured and modeled mass balance values with a linear regression trend line for the lower (2700 m a.s.l.) and upper (2900 m a.s.l.) stake.

Table 5.1.: Comparison of modeled and observed values at the two stake locations (2700 m a.s.l. and 2900 m a.s.l) on Claridenfirn. The calculation period ranges from from 29 of September 1981 till 17 of October 2002.

	lower stake		upper stake	
	modeled	observed	modeled	observed
cumulative balance (m w.e.)	4.3	6.1	23.0	21.3
mean mass balance (m w.e.)	0.22	0.31	1.15	1.07
mean winter balance (m w.e.)			2.11	2.28

5.3.2. Case Study 2: Glacier Mass Balance from Measured Length Changes and Modeled Tongue Ablation

Model description

Curves of cumulative glacier advance and retreat can be converted into time series of temporally averaged mass balance by applying a simple continuity model originally proposed by *Nye* (1960). This approach considers step changes after full dynamic response and new equilibrium of the glacier. Thereby, the mass balance disturbance (δb) leading to a corresponding glacier length change (δL) depends on the original length (L_o) and the annual mass balance (ablation) at the glacier terminus (b_t): $B = b_t \cdot L/L_o$. The dynamic response time (τ_r) is h_{max}/b_t (*Jóhannesson et al.*, 1989), where h_{max} is a characteristic ice thickness, usually taken at the equilibrium line where ice depths are near maximum. Assuming a linear adjustment of the mass balance B to zero during the dynamic response, the average mass balance $\bar{B}$ is roughly assumed to be as $B/2$. The so-obtained value is given in annual

ice thickness change (m we) averaged over the entire glacier surface, and can be directly compared with values measured in the field or modeled values as described in case study one. The main limitation is the resolution in time. Applying characteristic values for b_t and maximum thicknesses of 30 to several 100 meters, the response time is between 10 and 100 years (*Haeberli and Hoelzle*, 1995). The calculated mean specific mass balance values are, therefore, valid in the range of several decades up to a century (*Hoelzle et al.*, 2003).

For this case study the mean specific mass balances are calculated for ten selected glaciers of the Swiss glacier network according to their individual characteristic response times using the modeled values of b_t and db/dh (Table 5.2). They are compared to the modeled values of $\bar{B}$ as obtained with the same distributed mass balance model as used in case study one (*Machguth*, 2003). In contrast to the Claridenfirn model run, climatic means of temperature (1961–1990) and global radiation (1980–2000) from MeteoSwiss are used as an input. Seasonal precipitation- means (1971–1990) are obtained from *Schwarb et al.* (2001). The uncorrected precipitation values are raised by 30%, as recommended by the authors.

Table 5.2 shows that the calculated response times are in general longer than the 30 years, except for the Oberer Grindelwald glacier. The response times as calculated here use the b_t values determined by the mass balance model from the case study 1. These b_t values are much lower than the values calculated in earlier studies (*Haeberli and Hoelzle*, 1995), mainly because of shading effects at the tongue of the glaciers that are now considered. Therefore, the resulting response times are in general too long, compared to observations. The calculation of input parameters was not automatically carried out as in previous studies (*Haeberli and Hoelzle*, 1995; *Hoelzle and Haeberli*, 1995; *Hoelzle et al.*, 2003) but individually for each glacier (see input data in Table 5.2).

Results

Figure 5.4 shows a comparison between the modeled mean specific mass balances based on the length change data and the modeled mean specific mass balances based on the mass balance model described above (time period 1961–1990). Although the general agreement is quite good, there are two cases, where the correlation is low. The first case is the Tjatscha glacier, which has a complex topography with a cascade-like ice-fall near the tongue. This complex structure at the tongue produces a special length change behaviour with a delayed reaction of the tongue during an advance period. The second case is Silvretta glacier, which is difficult to model due to contradicting precipitation input data from *Schwarb et al.* (2001) and from *Skoda and Lorenz* (2003). We have to keep in mind that the simple model approach applied here has several limitations as well and that the data should be interpreted with care. Nevertheless the results show a new possibility for mass balance model validation in areas without direct measurements.

5.3.3. Case study 3: Distributed mass balance modeling for Gries and Basòdino glaciers in the extreme 2002/03 balance year

Model description and input data

In the third case study we apply a different distributed mass balance model which is of intermediate complexity with respect to the energy balance formulation and calculate the mass balance for Gries and Basòdino glaciers (for location see Figure 5.1 and Figure 5.5a)

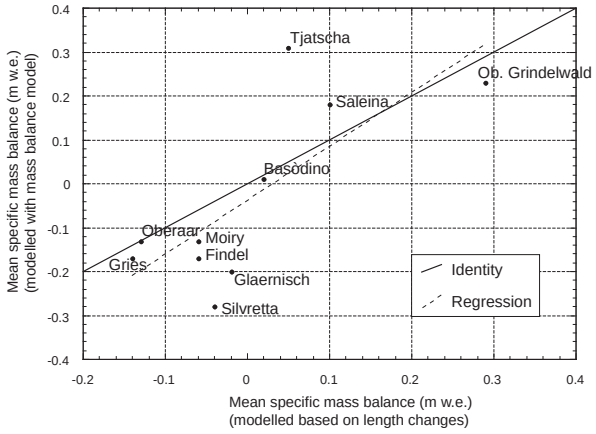

Figure 5.4.: Comparison between modeled specific mass balance, based on the mass balance model and modeled specific mass balance, based on measured cumulative length changes for the period of 1961–1990 for 10 glaciers from the Swiss glacier monitoring network.

Table 5.2.: Summary of input data (columns 2-9) used for the model and output data (columns 10-12) calculated by the model (see case study 2). max and min is maximum and minimum elevation, respectively, ELA is equilibrium line altitude, ΔL is length change from 1961–1990, L_0 is glacier length in 1961, gradient is mass balance gradient, b_t is mass balance at the tongue $\bar{B}$ is modeled mean mass balance for the 1961–1990 period, thick is glacier thickness, t_r is response time and $\bar{B}'$ modeled mass balance from length change data. Data sources: A: *Müller et al.* (1976), B: Topographic maps (1990), C: Mass balance model, D: *Glaciological Reports* (1992-2008), E: calculated.

Glacier	max	min	ELA	ΔL	L_0	gradient	b_t	$\bar{B}$	thick	t_r	$\bar{B}'$
Unit	m	m	m	m	km	m$(100\,\mathrm{m})^{-1}$	m w.e.	m w.e.	m	year	m w.e.
	A	B	C	D	D	C	C	C	E	E	E
	(2)	(3)	(4)	(5)	(6)	(7)	(8)	(9)	(10)	(11)	(12)
Basòdino	3220	2620	2860	54	1.6	0.65	-1.7	0.01	80	47	0.03
Findel	4200	2540	3240	-185	9.48	0.9	-6.2	-0.17	220	35	-0.06
Glaernisch	2920	2330	2590	-61	2.33	0.7	-1.8	-0.20	120	67	-0.02
Gries	3360	2450	2860	-564	6.77	0.7	-2.7	-0.17	200	74	-0.11
Moiry	3820	2450	3090	-150	5.78	0.63	-4.2	-0.13	200	48	-0.05
Ob. Grindelwald	3740	1500	2870	521	5.18	0.56	-7.9	0.23	180	23	0.29
Oberaar	3420	2320	2830	-343	5.0	0.7	-3.4	-0.13	200	59	-0.12
Saleina	3880	1800	2920	183	6.46	0.64	-7	0.18	250	36	0.10
Silvretta	3160	2450	2800	-115	3.46	0.88	-2.65	-0.28	150	57	-0.04
Tjatscha	3120	2540	2840	84	2.06	0.82	-2.35	0.31	120	51	0.05

for the extreme summer 2003 conditions (*Schär et al.*, 2004). Model results are compared with field measurements which are obtained by the direct glaciological method on both glaciers (*Glaciological Reports*, 1992-2008). This model too, is based on the general approach, that the most important variables for Alpine glacier mass balance are included with the highest possible precision (e.g. potential global radiation, albedo, precipitation pattern) while others are treated more general or are roughly parameterized (cf. *Oerlemans* (2001)). The model is combined from the formulations given by *Oerlemans* (1992a,b) and (*Klok and Oerlemans*, 2002) and adapted for a forcing by meteorological input data from a climate

station (temperature, precipitation, global radiation). Distribution of the input data to the terrain are performed by means of elevation dependent gradients (using the DEM25) and gridded data fields that are calculated beforehand (*Paul et al.*, 2008). This includes high-resolution fields of climatological (1971-1990 mean values) annual precipitation sums from *Schwarb et al.* (2001), as well as a map of glacier albedo obtained from Landsat Thematic Mapper (TM) scene acquired at 13 August 2003, utilizing a method developed by *Knap et al.* (1999a) and described in more detail in *Paul et al.* (2005).

The annual precipitation sum shows a local maximum near the used climate station Robiei (1900 m a.s.l.) with decreasing values toward higher elevations (Figure 5.5a). In order to retain the complex precipitation pattern observed throughout the region, we normalized the precipitation data by the value found at the location of Robiei. The daily precipitation at each cell is then obtained by multiplication of the measured precipitation at Robiei with the normalized grid and a final increasing of 20%, as proposed by *Frei and Schär* (1998) for elevations above 1500 m a.s.l. After a correction has been applied to the global radiation from SRAD, the cloud factor is obtained for the entire test site from the ratio of the measured to the potential global radiation at Robiei (Figure 5.5b).

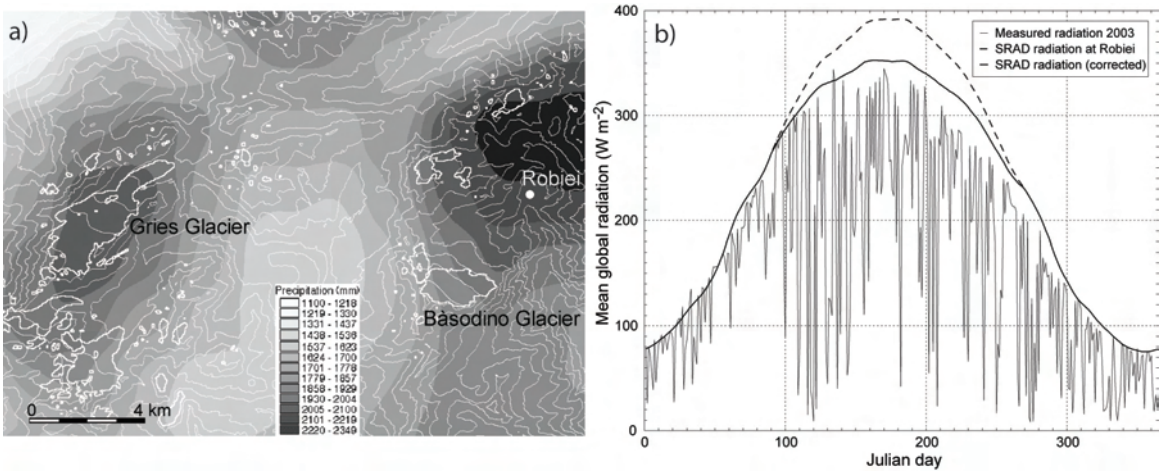

Figure 5.5.: *(a)* Annual precipitation sums for the test site from *Schwarb et al.* (2001) (1971–1990 mean values) resampled to 25 m cell size. Satellite derived glacier outlines from 2003 (thick, white) and 200 m elevation contours from the DEM25 (thin, light grey) are superimposed. The filled white circle (right, centre) marks the location of the Robiei climate station at 1900 m a.s.l. DEM25: reproduced by permission of swisstopo (BA057384). *(b)* Measured global radiation (daily means) at Robiei for 2003 together with modelled potential global radiation from SRAD at the same site before and after correction.

A snow albedo of 0.75 is used for freshly fallen snow (with an exponential ageing curve) and TM-derived glacier albedo is used if snow depth in the model becomes zero. As such, the model takes into account the extremely low glacier albedo values (below 0.2) observed at the end of the summer 2003 (*Paul et al.*, 2005). A constant value of 0.1 is added to all albedo values in order to account for effects of the non-Lambertian reflectance characteristics of ice and snow (*Greuell and de Ruyter de Wildt*, 1999). Some other variables required in the

model (e.g. pressure, humidity) use a fixed climatological mean value at a certain elevation and are extrapolated from the DEM25 for each pixel according to their gradients.

The model starts at Julian day 271 (1 October 2002) with zero snow depth at each cell and calculates cumulative mass balance for each cell at daily steps until day 635 (30 September 2003) is reached. Snow redistribution by wind and avalanches is not yet included in this model, but seems to be an important factor for the modeled mass balance of many smaller glaciers (see case study one). Mass balances and mass balance profiles at 50 m elevation bins are obtained by GIS-based modeling, i.e. intersecting the recent (2003) satellite derived glacier perimeter (*Paul et al.*, 2002) with the DEM25 and the obtained mass balance distribution.

Results and Validation

The modeled mass balance distribution for Gries and Basòdino glaciers are depicted in Figures 5.6a and 5.6b, respectively, with highlighted glacier areas and approximate position of the ablation stakes (numbered). While mass balance distribution on the glacier tongue is governed by the albedo pattern, the potential global radiation exerts a major influence in all other regions. In particular regions on steep slopes which are prone to heavy topographic shading exhibit positive balances, as avalanches are not included in this model. In consequence, these regions are actually not covered by glaciers (see Figure 6a and b). The modeled (measured) mean specific mass balances (in m w.e.) for Gries / Basòdino glaciers in the 2002/03 balance year are: -2.63 (-2.52) / - 2.08 (-2.04). These results are very promising with respect to the parameterizations made in the model and in view to the fact that no local tuning is applied.

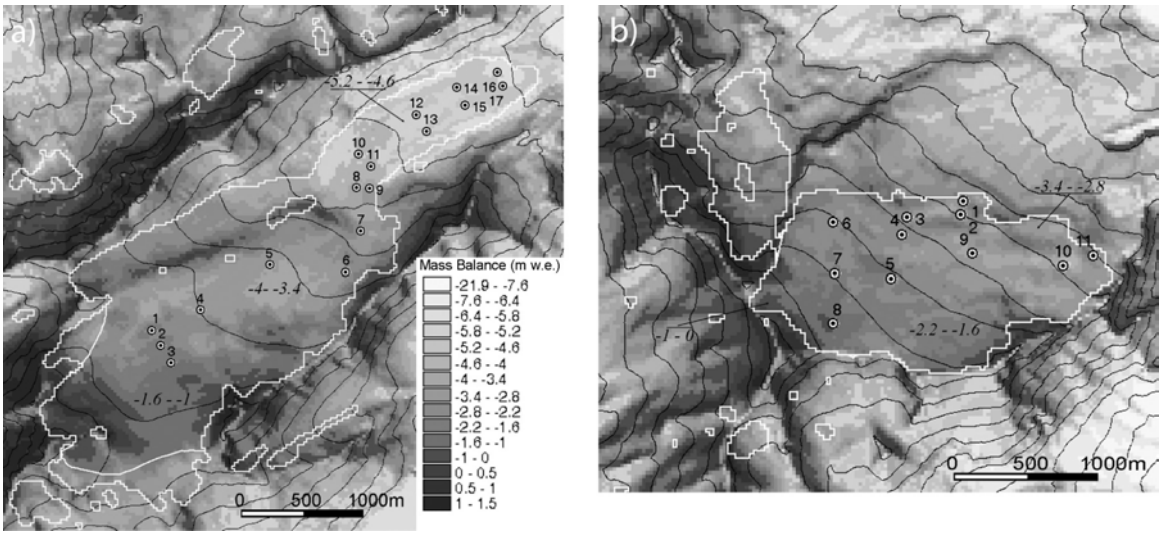

Figure 5.6.: Modeled mass balance distribution for the 2002/03 balance year with stake positions (numbered), 100 m elevation contours from the DEM25 (black) and high-lighted satellite derived glacier areas for the year 2003. DEM25: reproduced by permission of swisstopo (BA057384). a) For the region of Gries glacier, b) for the region around Basòdino glacier. The legend given in a) is also valid for b), the scale bar (thick white line) is 1 km.

A more detailed comparison of the modeled and measured values is presented in Figure 5.7a, showing the mass balance profiles of both glaciers. Apart from the overall good agreement of the two curves for both glaciers, some deviations are visible as well. They can be explained partly by the strong smoothing of the measured curves, which is due to the interpolation techniques applied. While the values for Gries glacier are determined by a regression function (Funk and others, 1997), the 100 m mean values for Basòdino glacier are obtained by manual interpolation (pers. comm. A. Bauder). As such, it is difficult to say which profile is more realistic. The interpolated curves might smooth out local topographic effects (that are clearly visible in the modeled curves) and even fail under extreme conditions (Paul and others, 2005). Assuming that the measured values are correct, the model overestimates ablation in the lower parts of Gries glacier and underestimates ablation for the upper parts. For Basòdino glacier it is vice versa.

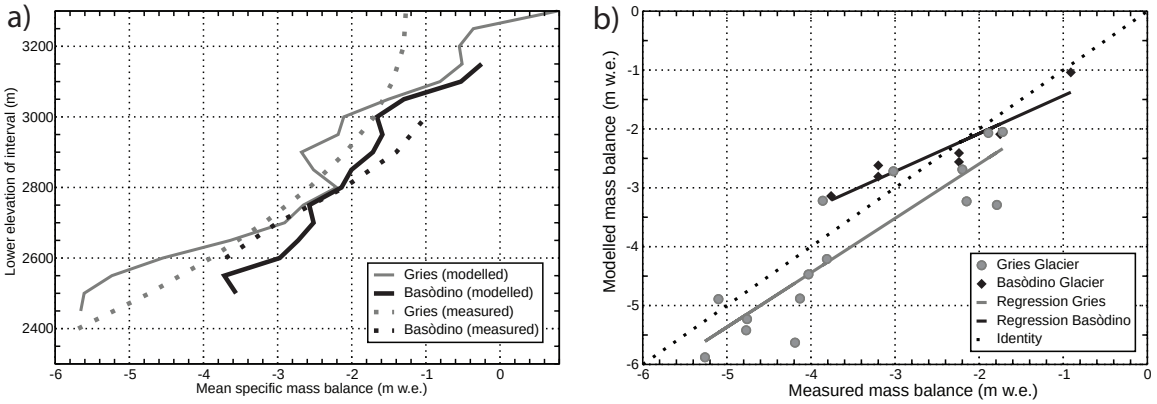

Figure 5.7.: (a) Modeled mass balance profiles sampled at 50 m elevation bins for both glaciers in comparison to measurements (regression curves) in the 2002/03 balance year. (b) Scatter plot of measured versus modeled mass balance values at the location of the stake positions (see Figures 5.6).

In order to circumvent any interpolation effects, we also compared the original stake readings with the modeled values at their locations (Figure 5.7a). The scatter plot displays a linear regression trend line which indicates a general overestimation of the ablation in the case of Gries glacier by the model and an under-/overestimation for the lower/upper parts of Basòdino glacier. However, considering the large number of local effects controlling the values at individual stakes (e.g. wind drift) and the general assumptions made in our model (e.g. clouds at Robiei = clouds at Gries glacier) the model results are satisfactory.

5.4. Discussion

In case study 1, the applied distributed mass-balance model is forced by precipitation that has been tuned with measured values of winter accumulation. Despite this tuning, a scatter of about $\pm$ 0.5 m remains for individual years at both stakes. Further improvement of the model results in individual years would primarily require the inclusion of several input parameters (e.g. cloudiness, precipitation). As the regression trend lines are very

close to identity (Figure 5.3b), the inter annual scatter averages out in long-term mean and cumulative values (yielding very small differences after 20 years). Nevertheless, case study 1 demonstrates that simple mass balance models can provide valuable long-term results if the most important processes are treated realistically. Case study 2 illustrates the possibilities of tuning with long-term length change values. Despite the simplicity of the approach, only small deviations of $\pm$ 0.2 m between long-term mean mass balance values from length-change measurements and those from a distributed mass-balance model have been obtained. Here we see a large potential of extending mass-balance series backwards in time, if the balance at the tongue is obtained from distributed modeling (accounting for local topographic effects) and glaciers with special characteristics (e.g. calving, debris cover) are excluded. Case study 3 illustrates that modeled profiles of mass balance vs elevation can reproduce the distribution patterns interpolated from measurements well if specific spatio-temporal characteristics (e.g. the low 2003 albedo values) are considered. However, the strong smoothing of the interpolated curves makes it difficult to assess which values are more accurate. For individual stakes, large deviations ($\pm$ 1 m) are found in this case, which could partly be explained by deficiencies of the applied model. Nevertheless, the measured values themselves can be influenced by spatial distribution of input parameters or small-scale topography, which is difficult to assess at the spatial scale of the DEM25.

5.5. Conclusions and Perspectives

The three case studies demonstrate the potential as well as the limitations of approaches combining point measurements with distributed mass balance modeling. Concerning future monitoring strategies, the following conclusions can be drawn:

1. The validation and calibration of distributed massbalance models is best done by using data from sites with extensive process-oriented measurements that include winter balance determined by an adequate number of snow pits in the accumulation area. Reduced stake networks (as on Griesgletscher) and isolated index stake measurements (as on Claridenfirn) are valuable for model verification but are of limited use for increased process understanding. The applied spatial interpolation techniques have to be reproducible.

2. Long-term average mass-balance values can be obtained for (numerous) unmeasured glaciers from cumulative length-change measurements as long as there is 'active retreat' as a dynamic response (instead of 'downwasting' or 'collapse') and the glacier is not affected by special conditions (calving, debris cover, flow instability). This approach can greatly increase the representativity of the few available mass-balance measurements and help to extend the series backwards in time.

3. Further improvements of distributed mass-balance models should focus first of all on the processes taking place during the accumulation season, in particular the snow redistribution by wind, and on the spatial and temporal variability of several input parameters. The introduction of an avalanche parameterization (case study 1) as well as the use of a gridded precipitation climatology and a TM-derived albedo map (case study 3) are small steps towards the consideration of the spatial variability.

Distributed mass balance models certainly have a much greater potential than purely statistical approaches. The following principal applications of such models can be envisaged as part of an integrated glacier monitoring strategy:

1. local extrapolation of stake measurements (for individual glaciers)
2. distributed modeling over larger regions (including gridded data sets)
3. interpolation and extrapolation of time series (forward / backward)
4. combination of process-based models with knowledge-based traditional methods (automated glacier length change measurements from satellite data)
5. coupling with high-resolution Regional Climate Models (RCMs).

Distributed mass balance modeling is an important tool in glacier monitoring and climate impact studies. It should become a standard component of corresponding long-term programs.

Acknowledgments We would like to thank A. Bauder (VAW/ ETH-Zurich) for providing us the mass balance data for Gries and Basòdino glaciers, S. Gruber for development and implementation of the avalanche model and M. Zemp for providing the length change data. All meteorological data are kindly provided by MeteoSwiss.

6. Comparison of two Mass Balance Models of Differing Complexity

Mass balance models should ideally deliver results that are in agreement with observations over a broad range of meteorological conditions, being different from the time frame where model tuning has been performed. Such an ability is essential when scenarios for future mass balances are calculated or when models are applied to unmeasured glaciers. The latter is a key element in the application of a mass balance model to the entire Swiss Alps which is one of the main goals of this thesis. The two mass balance models MB1 and MB2 have been compared for an extended time period (1995–2005) based on the example of Morteratsch glacier, southeastern Switzerland, where detailed measurements are available. The time frame of the model comparison encompasses the mass balance year 2000/01 with extensive winter accumulation, the strongly negative mass balance year of 1997/98 and the extremely hot summer of 2003 when the glaciers in the Alps experienced extraordinary mass losses (e.g., *Zemp et al.*, 2005; *Frauenfelder et al.*, 2005). Analyzing possible systematic deviations and their relation to such extreme events might help to assess whether the models will deliver stable results if, for instance, applied to project mass balances for a climate where summers as in 2003 are the rule (e.g. *Schär et al.*, 2004; *Beniston*, 2004). Furthermore, the application of the simplified mass balance model MB1 to calculate mass balance distribution for the entire Swiss Alps is desirable for several reasons (e.g., reasonable computational expenses, less input data required) and the model comparison should help to assess whether its performance is similar to the more complex model MB2. The two models as applied here are described in Sections 3.2.2 (MB1) and 3.2.1 (MB2).

In this chapter, modeled and measured cumulative mass balances at four points on Morteratsch glacier are compared first. Following this, the energy fluxes computed from the two mass balance models are compared at one selected point and the relationship between observed deviations in modeled mass balance and energy fluxes is explored. The spatial pattern of deviations in modeled mass balance is subsequently analyzed, and then the results are discussed.

6.1. General Approach and Model Tuning

The main characteristics and required input of MB1 and MB2 are listed in Table 6.1. The mass balance measurements on Morteratsch which are used for the model comparison are embedded in a long-term study of the glacier surface energy balance which was initiated by the IMAU, Utrecht, in 1995 (e.g. *Oerlemans*, 2000; *Oerlemans and Klok*, 2002). Since October 1995 an automatic weather station (AWS), a sonic ranger for continuous surface height measurements and three stakes have been in operation on the tongue of the glacier at approximately 2100 m a.s.l (cf. Figure 6.4 for a map of the glacier and location of the test sites). In 1999 mass balance measurements with stakes were started at two other

sites (approx. 2500 and 2700 m a.s.l.) and at a fourth site, close to the equilibrium line (2950 m a.s.l.) in the following year. For the model comparison the sonic ranger data and stake measurements from all four sites were used. Meteorological input data were acquired from the weather stations Corvatsch (3315 m a.s.l., located on a summit, 8 km west of of Morteratsch glacier) and Samedan (1705 m a.s.l., located on a wide and flat valley floor, 12 km north) at hourly and daily resolution for MB2 and MB1, respectively.

Both Models were first tuned to fit measured mass balance during 1998/99 mass balance year on the tongue of Morteratsch. However, only model-specific tuning parameters were used for tuning. Parameters that appear in both models were kept identical for a proper assessment of variations in energy and mass balance stemming from the differing parameterizations. Little tuning was required for MB2 since the model is based upon *Klok and Oerlemans* (2002) who developed and tested their model for Morteratsch glacier. The tuning procedure for both models is shown in the following in chronological order:

1. All parameters that exist in both the *Klok and Oerlemans* (2002) model and in MB2 were applied as adjusted in *Klok and Oerlemans* (2002). For those parameters that also appear in MB1 the same values were used.

2. The firn albedo (α_f) was set at 0.45 for both models. However, this value is of no influence to the tuning procedure since firn did not build up at the four test sites within the 1995–2005 time frame.

3. Model runs for the 1998/99 mass balance year were performed with MB2 and precipitation was tuned by a multiplication factor ($P_{corr} = 2.1$) to fit both the measured amount of accumulation and the date of the disappearance of the snow cover in May 1999. The same value for P_{corr} was then applied in MB1 since both models should have identical amounts of precipitation.

4. Best agreement of MB1 to measured snow depth, date of the disappearance of the snow cover and melt for the 1998/99 mass balance year was then achieved at $C_0 = -45\,\mathrm{W\,m^{-2}}$, $C_1 = 10\,\mathrm{W\,m^{-2}}$ and a fixed albedo for snow $\alpha_s = 0.72$.

6.2. Comparison of Modeled Mass Balances to Point Measurements

The two mass balance models MB1 and MB2 have been compared in model runs over the 1st October 1995 to 1st December 2005 time span and for four points on Morteratsch glacier. Cumulative modeled and measured mass balance for the four points and the mentioned time span are depicted in Figure 6.1. For 1st December 2005, modeled cumulative mass balance at point SR-1 (2100 m a.s.l.) calculated from MB1 (b_{MB1}) is -64.1 m ice while MB2 yields a slightly more negative cumulative mass balance ($b_{MB1} = -65.4$ m ice). According to the sonic ranger, measured mass balance at the same point (b_{SR}) is -66.0 m ice (Figure 6.1). Thus, b_{MB2} is somewhat closer to the measurements. However, both models perform well and the cumulative difference between b_{MB1} and b_{MB2} is in the order of only 2%. On three other points of Morteratsch glacier model results have been compared to stake measurements (Figure 6.1): At S-2 the agreement of the two models with the measurements is

Table 6.1.: Comparison of key elements of the mass balance models MB1 and MB2. Specifications for MB1 are given for the model version used in the model comparison. The numbers in brackets refer to the following: [1] *Corripio* (2003); [2] *Iqbal* (1983); [3] *Klok and Oerlemans* (2002); [4] *Oerlemans and Grisogono* (2002); [5] *Oerlemans* (1992b), [6] *Oerlemans* (2001)

	MB1	MB2
numerical model time step	86'400 s	$\leq$ 3600 s
meteorological input	T_a, S_{in}, P	T_a, S_{in}, P, e_a, p
source	weather station (WS) outside glacier boundary layer	
number of WS required	min. 1	min. 2
temp. res. meteo. input	86'400 s	$\leq$ 3600 s
interpolation T_a, P, e_a from source(s) to DEM	linear gradients with altitude	linear gradients with altitude
interpolation p from source(s) to DEM	-	barometric formula
terrain information	DEM	DEM, skyview
α_i	fixed value	fixed value
α_f	fixed value	fixed value
α_s	fixed value	$f(T_{surf}, t)$ (Sect. 3.2.2)
calculation $S_{in,clr}$	[1], [2]	[1], [2]
performed during	preprocessing	model run
clear sky atmospheric transmission coefficients	for standard atmospheric composition	$f(T_a, e_a, p)$ [1], [2]
diffuse global radiation	$S_{in,clrdif}$ as lower threshold	$f(n, skyview)$ [3], [5]
T_{surf}	0 °C	$f(G)$ [3]
turbulent heat fluxes	$f(T_a)$ (Sect. 3.2.1), [6]	$f(T_a, T_{surf}, n, e_a, p)$ [3], [4]
long-wave radiation balance	$f(T_a)$ (Sect. 3.2.1), [6]	$f(T_a, T_{surf}, n, e_a)$ [3]

similar (note that the second-last stake reading at S-2 is most probably erroneous, personal communication J. Oerlemans). At S-3 and S-4 the simple model MB1 performs even somewhat better, nevertheless, both models overestimate mass balance at the latter point by 3–4 m w.e. while measured cumulative mass balance amounts to only about -8 m w.e. on December 1st 2005.

The good agreement of cumulative mass balance obtained from the two models could have resulted from over- and underestimations in mass balance that balanced each other out, and thus do not yet provide proof that the model would deliver reliable results when applied for conditions that are systematically different from the mean of the 1995–2005 time period. The original idea was to search for systematic differences by comparing daily measured to daily modeled mass balances to explore whether systematic differences are related to particular conditions or seasonal phenomena. However, an attempt at such a comparison yielded no reasonable results, because there are several gaps in the measurements during summer, and for winter no comparison is feasible since the sonic ranger measures surface elevation which corresponds to snow height, but snow density is unknown. Thus it was decided to compare modeled and measured mass balances visually and to perform the comparison of daily mass balances using the two modeled curves.

In the case of MB2 a negative deviation from the sonic ranger measurements grows slowly with time and by the end of 2003 reaches 1 m ice or approx. 2% of b_{MB2} (Figure 6.1). The difference then diminishes comparably fast and finally, by the end of 2005, the sonic ranger measurments are more negative by approx. 0.6 m ice (1%). When comparing to the stake measurements instead of the sonic ranger the agreement is even better. For MB1 the pattern is similar but overestimations by the end of 2002 seem more pronounced (Figure 6.1). The similar tendency in MB1 and MB2 to overestimate mass balance after 2003 indicates that there might be a common source: for instance, α_i is an identical fixed value in both models and thus, a possible albedo lowering is not considered. *Oerlemans et al.* (subm) studied the evolution of the surface albedo at SR-1 and found that significant lowering took place since 2003. Furthermore, the mass balance height effect is neglected in both models since the DEM is treated as an invariate.

The cumulative difference of b_{MB1} and b_{MB2} amounts to 1.3 m ice (2%) on December 1, 2005. Figure 6.2 shows the differences in daily modeled mass balance (Δb) for each day from October 1, 1995 to December 1, 2005. The individual values of Δb exhibit a large scatter and thus, a 15-day running mean is depicted as well. In general, differences are close to zero during winter while the melt season is dominated by both negative and positive Δb. Mean modeled daily mass balance during the ablation season is approx. -0.04 m ice and thus maximum observed deviations of 0.06 m ice correspond to more than 100% of the mean. Maximum deviations of the 15-day running mean (0.015 m ice) correspond to roughly 40% of mean summer daily mass balance. Deviations in daily mass balance during the summer of 2003 are within the range of the other summers and do not reach the bounds of variability derived from all years.

The 15-day running mean of Δb as depicted in Figure 6.2 seems to describe a characteristic curve which looks similar for most of the summers. An initial weak positive peak in Δb (not present in all years) is followed by a drop to slightly negative values. In the second half of the melt season Δb reaches clearly positive values in most years and then drops again slightly below zero before winter begins.

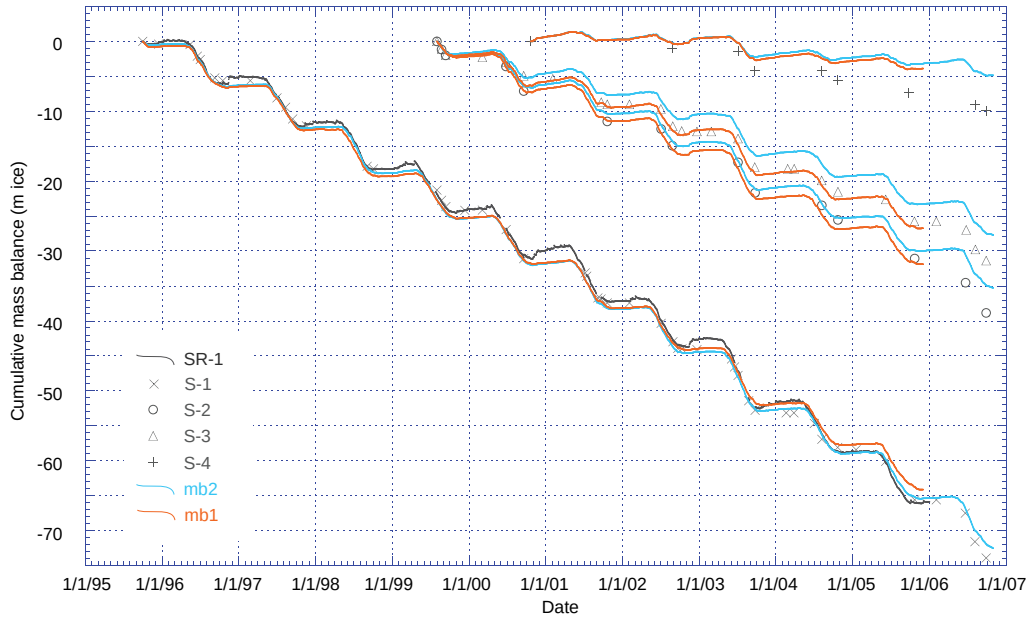

Figure 6.1.: Comparison of modeled mass balance and measured mass balance at four points on Morteratsch glacier (cf. Figure 6.4). 'SR' stands for sonic ranger, 'S' for stake measurements, 'MB1' for modeled values from the simple energy balance model and 'MB2' for the model of intermediate complexity. The elevation of the four points are: AWS: 2100 m a.s.l., 2: 2500 m a.s.l., 3: 2700 m a.s.l. and 4: 2950 m a.s.l. All data are given in meter ice except for the snow accumulation measured by the sonic ranger which is depicted in meter snow height.

6.3. Comparison of Modeled Energy Balance

In the following, an explanation is given of Δb as depicted in Figure 6.2 and described in Section 6.2 from the energy available for melt (Q_m) calculated by the two models. For MB1, Q_m is defined from Eq. 3.2, and for MB2 according to Eq. 3.6. Curves of mean modeled annual Q_m have been calculated for both models and are depicted in Figure 6.3a together with the difference in Q_m between the two models (ΔQ_m). The curve of mean Δb is shown in Figure 6.3b together with ΔQ_m and ΔS which is the difference in shortwave radiation balance of the two models. 15-day running means of ΔQ_m, ΔS and Δb, to eliminate noise and to make the signals better visible, are shown in both figures. From Figure 6.3a it becomes obvious that during winter, MB1 continuously exhibits a strongly negative Q_m, resulting from the assumption of $T_{surf} = 0\,^{\circ}\mathrm{C}$, which is obviously wrong. In spring, ΔQ_m diminishes continuously until it reaches slightly negative values over a short time span after day 145. However, during most of the melt season Q_m is larger by about 10–20 $\mathrm{W\,m^{-2}}$ in MB2. Only in autumn (day 270–310) Q_m calculated from MB1 is somewhat higher (approx. 10 $\mathrm{W\,m^{-2}}$). Later in the year, the energy balance of MB1 again decreases to unrealistic strongly negative values while MB2 exhibits a moderately negative Q_m, which is compensated by the subsurface energy flux (G) related to the cooling of the surface and the underlying layers.

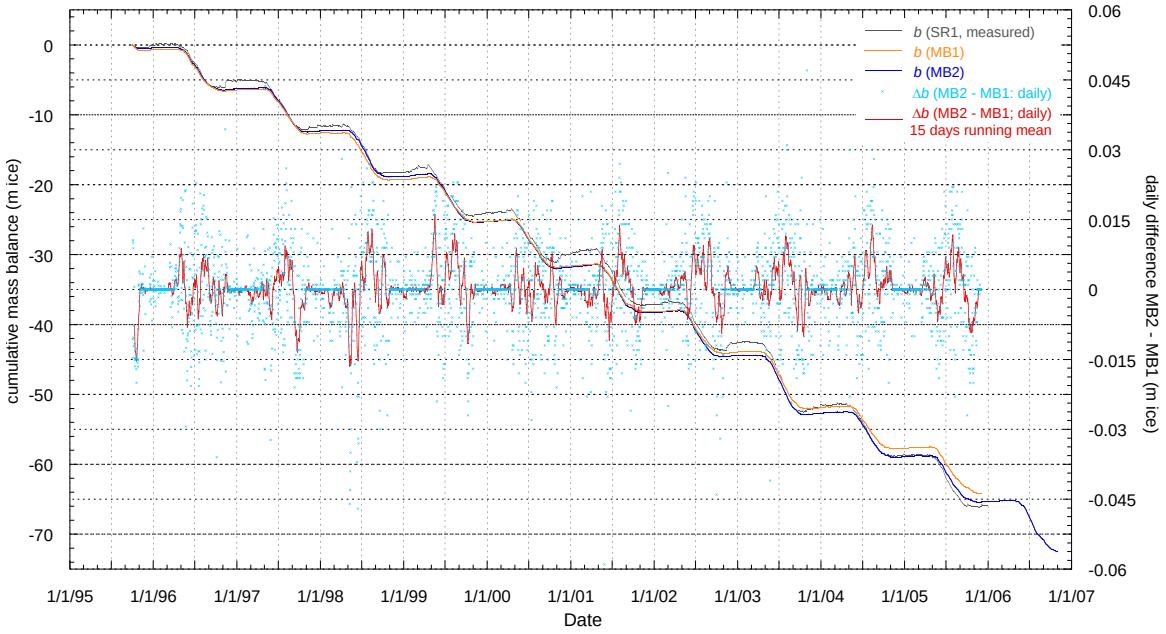

Figure 6.2.: Cumulative mass balance for the point AWS on Morteratsch glacier, modeled with MB1 (orange curve) and MB2 (blue curve). The difference in modeled mass balances from MB1 and MB2 is shown for every individual day with small blue crosses. To better show the general trend a 15 days running mean is depicted with the red line.

According to Figure 6.3b, Δb remains close to zero until approximately day 120 which is the start of an initial time period of underestimations in MB1 compared to MB2. In the following, from day 140 to 170, the reverse is the case. After day 170 melt is continuously greater in MB2 followed by a somewhat shorter and less pronounced period of reduced melt in MB2 compared to MB1. At day 310 the differences are again close to zero, where they remain throughout the winter. During winter, Δb remains close to zero despite a very positive ΔQ_m because negative Q_m is ignored in MB1 (Eq. 3.1). On the other hand, a clear correlation of ΔQ_m and Δb can be established over the entire melt period (approx. day 120–310). The correlation is somewhat less pronounced only in spring due to differences in surface albedo. Since there is obviously no correlation of ΔS and Δb, the deviations in mass balance between the two models can be attributed to the long-wave radiation balance and the turbulent fluxes.

6.4. Comparison of Modeled Mass Balance Distribution

Modeled distributed mean annual mass balance (October 1, 1995 to December 1, 2005) for the Morteratsch area, computed from MB1 and MB2, was compared in order to investigate whether characteristic spatial patterns in model differences can be established. Figure 6.4a shows mean annual mass balance distribution for Morteratsch glacier and some adjacent glaciers modeled with MB2. In Figure 6.4b spatial differences in mean distributed annual

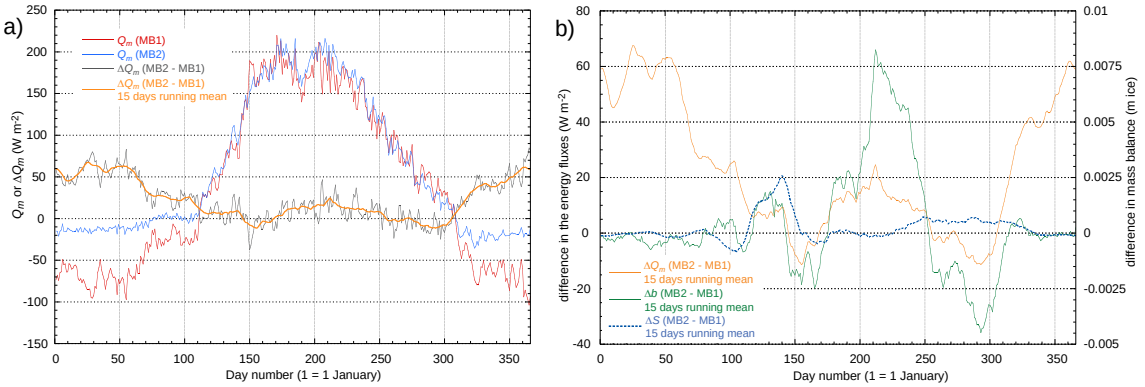

Figure 6.3.: a) Energy available for melt (Q_m) computed from MB2 and MB1 and difference in Q_m among the two models (ΔQ_m); b) ΔQ_m, ΔS in the context of mean difference in modeled mass balance Δb.

mass balances for the same perimeter are depicted. Differences among the two models rarely exceed 0.4 m w.e. Note that no systematic difference is visible between the ablation and accumulation areas. The greatest differences occur in west-to-south exposed steep zones below the ELA. In these areas melt in MB2 is reduced compared to MB1. On the lowest part of the tongue of Morteratsch, MB2 calculates more negative balances than MB1.

6.5. Discussion of the Model Comparisons

It is difficult to assess which of the two investigated models obtains a more realistic energy balance and related mass balance. For wintertime energy fluxes, the case is clear since in MB1 surface temperature is kept constant at 0 °C. However, there are indications that MB2 performs also slightly better during the melt season: modeled and measured melt rates are in good agreement (cf. Figure 6.1 and *Klok and Oerlemans*, 2002). In MB1, melt rates are somewhat too small during summer. Nevertheless, cumulative mass balances of the two models are very similar because underestimated melt in MB1 during summer is compensated by enhanced melt at the end of the melt season. In some years the melt season in MB1 ends quite abruptly, while according to the measurements, melt decreases more smoothly.

It can be concluded that the performance of the two models on Morteratsch is similar. Melt rates seem somewhat more realistic in MB2 which makes the model the better choice for detailed studies over short time spans. Nevertheless, there is no indication that one or the other of the two models performs less well under extreme conditions and thus, climate sensitivity seems to be similar. However, this statement is based on the presented analysis performed on only four points on one particular glacier and should therefore be confirmed by comparison to measurements on other glaciers. Furthermore, it must be emphasized that the accumulation area of Morteratsch glacier reaches up to almost 4000 m a.s.l. and thus it is possible that the glacier includes sections of cold ice and firn (cf. *Haeberli and Hoelzle*, 1995). Whether one of the four test sites is influenced by cold ice is difficult to assess but a large influence is unlikely for all four sites. On glaciers that are predominantly cold underneath the

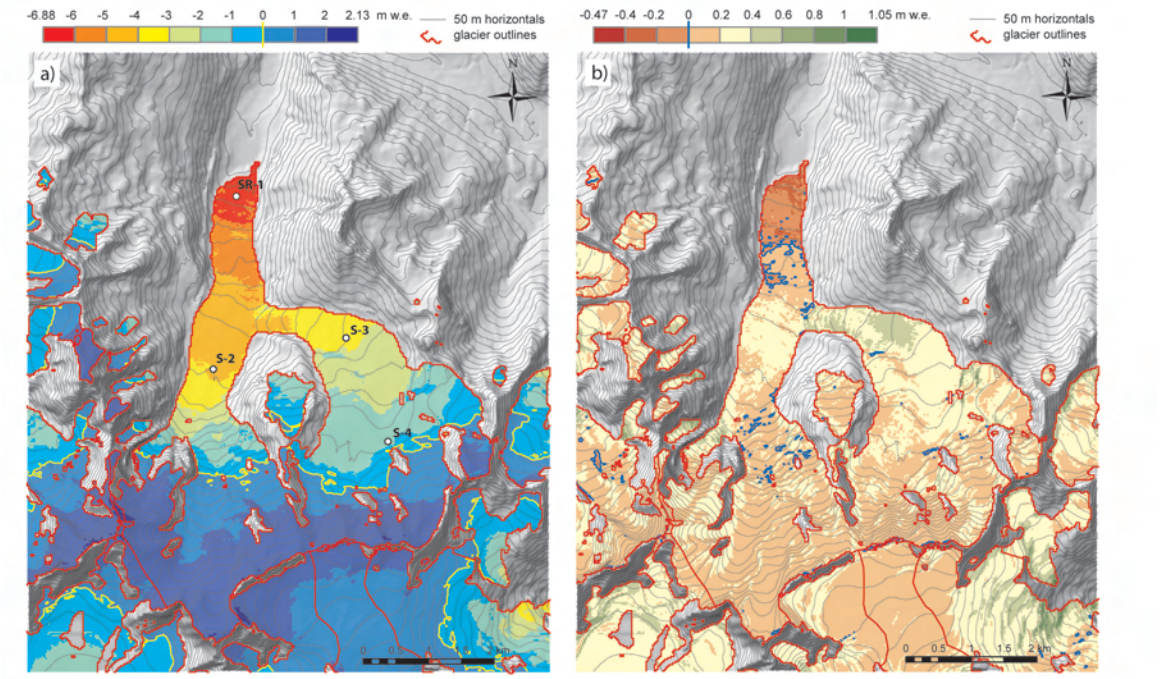

Figure 6.4.: a) Mean annual mass balance distribution for Morteratsch glacier and some adjacent glaciers modeled with MB2. b)Difference in mean annual B (MB2 - MB1) modeled over the Morteratsch area using the two mass balance models.

surface, warming and cooling of the ice or firn is important to mass balance computations. On one hand, the model MB2 includes a simple parameterization of subsurface energy fluxes and is thus able to consider the energy required to heat the surface layers of a glacier. Accumulation areas where cold firn is build up could be recognized from MB2. On the other hand, the distribution of cold ice in ablation areas is governed by glacier dynamics and cannot be simulated by a surface mass balance model alone. Furthermore, neither of the two models considers refreezing and formation of superimposed ice, which is important to the mass balance of polythermal glaciers. Simple parameterizations are available from the literature (e.g. *Bøggild*, 2007) and should be implemented in future model versions. To sum up, the results inspire confidence in the application of both models to extrapolate mass balance in time and space, as long as mostly temperate Alpine glaciers remain the subject of model application.

The running of a mass balance model for a point where it was tuned helps to assess model performance but is inappropriate to assess uncertainties inherent to the model. In the present model comparison, uncertainties are partly compensated for by the tuning procedure. However, uncertainties are likely to impact model results when the model is applied to sites it was not tuned for. For instance the models were not calibrated to match mass

balance at point S-4 which is located close to the ELA, where processes controlling mass balance are weighted differently than at point AWS. It is thus not surprising that a systematic shift from measured and modeled values occurs (Figure 6.1). An assessment of uncertainty in a mass balance model was carried out in Paper №3.

7. Exploring Uncertainty in Glacier Mass Balance Modeling with Monte Carlo Simulation (Paper №3)[1]

Abstract By means of Monte Carlo simulations we calculated uncertainty in modelled cumulative mass balance over 400 days at one particular point on the tongue of Morteratsch glacier, Switzerland, using a glacier energy balance model of intermediate complexity. Before uncertainty assessment, the model was tuned to observed mass balance for the investigated time period and its robustness was tested by comparing observed and modelled mass balance over 11 years, yielding very small deviations. Both systematic and random uncertainties are assigned to twelve input parameters and their respective values estimated from the literature or from available meteorological data sets. The calculated overall uncertainty in the model output is dominated by systematic errors and amounts to 0.7 m w.e. or approximately 10% of total melt over the investigated time span. In order to provide a first order estimate on variability in uncertainty depending on the quality of input data, we conducted a further experiment, calculating overall uncertainty for different levels of uncertainty in measured global radiation and air temperature. Our results show that the output of a well calibrated model is subject to considerable uncertainties, in particular when applied for extrapolation in time and space where systematic errors are likely to be an important issue.

7.1. Introduction

A wide range of approaches to the modelling of mass balance exist, ranging from simple temperature index correlations (e.g., *Braithwaite*, 1981; *Reeh*, 1991) through to complex physical models of energy balance and associated melt (e.g., *Brock et al.*, 2000; *Arnold et al.*, 2006). Typically, models are developed for the general case of modelling mass balance, but are calibrated and validated at a few point locations and therefore for a particular set of topographic and climatic conditions. Thus, for example, temperature index approaches require very little input data (positive degree days and a degree days factor) and could be applied in regions with sparse measurements (e.g., *Reeh*, 1991). However, they require calibration for each area in order to consider local charateristics (*Braithwaite*, 1995). By contrast, more complex physical models are assumed to require less tuning, and thus to be more suitable

[1] based on: Machguth, H., R. S. Purves, J. Oerlemans, M. Hoelzle and F. Paul (2008), Exploring Uncertainty in Glacier Mass Balance Modeling with Monte Carlo Simulation, *The Cryosphere, 2*, 191–204, http://www.the-cryosphere.net/2/191/2008/tc-2-191-2008.html

for extrapolating mass-balance in both space and time but at the expense of a higher demand for input data. Several studies exist where models of various complexities have been extrapolated over, for example individual glaciers or mountain ranges to produce seasonal values for mass balance (e.g. *Arnold et al.*, 1996), and a key question in the development of such methods is the uncertainty associated with them.

Any approach to quantifying uncertainty must firstly consider potential sources and techniques for the quantification of uncertainty. Mass balance models typically require both meteorological inputs and snow or ice parameterisations representing the point(s) at which the model is being run. Although many models have been developed using data measured at the same point as mass balance measurements, such an approach is not viable for extrapolating mass balance in space and time, where typical inputs to such a model have to be interpolated from point measurements or the projections of, for instance, general circulation models (GCM) or regional climate models (RCM). Equally, if we wish to explore mass balance in the past, point data are normally not available from the glacier of interest, and meteorological measurements from some long term data series, assumed to be correlated with the glacier location are generally used. In both cases, the meteorological inputs to the mass balance model must be extrapolated or interpolated in space, and perhaps interpolated in time, to derive values appropriate to the modelled mass balance.

Uncertainties in input parameters to mass balance models can thus be characterised as stemming from, in the case of measured data, errors and uncertainties in measured values, and in the case of modelled values, differences between modelled and measured values (which in turn stem from differences between the spatial extent over which these values can be considered to be representative). The methods used to extrapolate/ interpolate these data from the measurement location to the model location are other potential sources of uncertainty. Further uncertainties arise as a result of the abstraction of processes themselves within the mass balance model, and resulting generalisation of the real world system - for example, few mass balance models represent changes in snowpack form during melt (e.g. formation of ablation hollows or sun-cups during the ablation season) and the resulting increase in roughness length and change in turbulent energy fluxes. In considering uncertainties only in measured values of meteorological data there are two important sources of uncertainty to consider: random and systematic errors. Random errors are usually assumed to be related to the device making the measurement and its notional precision and are either temporally uncorrelated or only temporally correlated over short periods, whilst systematic errors are some constant offset or trend in measured values over long periods of time. Systematic errors are a well known problem in long term measurement series and can arise from, for example, incorrect calibration of an instrument or changes in a measurement site (e.g. *Böhm et al.*, 2001).

Despite our understanding of the likely sources of uncertainty in mass balance modelling, most papers in the literature limit their exploration of uncertainty to sensitivity studies which explore modelled responses to variation in individual parameters. While such approaches provide useful information and may be adequate for models calibrated and run at the same point in space, they are insufficient to understand the uncertainties in modelled mass balance extrapolated in time and space. For example, *van der Veen* (2002) argued that sensitivity studies were inadequate in modelling mass balance for polar ice sheets because they do not provide a probability for a certain result, but rather only the range of possible results for variation in a given input parameter. Furthermore, sensitivity studies do not

allow a full exploration of the parameter space and resulting non-linear effects as a result of combined uncertainties in multiple parameters. Parametric uncertainty analysis, in contrast to sensitivity tests, aims to evaluate the multi-dimensional response of a model to combined uncertainty in input parameters with a probability density function as an output (*Tatang et al.*, 1997; *van der Veen*, 2002).

In this paper we set out to estimate the uncertainty in mass balance calculations made with a glacier surface energy balance model of intermediate complexity (*Klok and Oerlemans*, 2002) applied to the Morteratsch valley glacier in the Swiss Alps. The paper has three key aims:

1. to estimate uncertainty for individual input parameters used in *Klok and Oerlemans*'s 2002 model;

2. to calculate a probability density function (PDF) for mass balance as a function of the uncertainties in input parameters at a point on the Morteratsch glacier; and

3. to assess the modelled uncertainties for studies extrapolating glacier mass balance forward in time and space.

In the first part of the paper we introduce the data and test area for the model, before describing the mass balance model. The basic model is compared to measurements over 11 years to validate that it can reproduce measured values. We then explore the size and form of random and systematic errors in the model's input parameters, before running Monte Carlo simulations to derive the overall uncertainty in modelled mass balance. In order to explore the likely implications of our uncertainty study for climate change projections, we then calculate PDFs for two key input parameters which are also outputs of most typical climate models: air temperature and global radiation.

7.2. Test Site and Time Frame

Morteratsch is a mid-sized valley glacier in the south-eastern Swiss Alps, extending from approximately 4000 m a.s.l. down to 2020 m a.s.l. and covering an area of about 16 km^2 (Figure 7.1). Mass balance measurements on Morteratsch are embedded in a relatively long term study of the glacier surface energy balance which was initiated by the IMAU, Utrecht, in 1995 (e.g. *Oerlemans*, 2000; *Oerlemans and Klok*, 2002). Since then an automatic weather station (AWS), a sonic ranger for continuous surface height measurements and three stakes have been operated on the tongue of the glacier at approximately 2100 m a.s.l. Mass balance measurements were initiated in 1999 at two other sites and in the following year at a fourth site. In this paper we make use of sonic ranger data and stake measurements from all four sites.

The present study focuses on the mass balance at the AWS over 400 days, starting from October 18, 1998 and ending on November 20, 1999. In the following, this time period is referred to as the "calculation period".

Data from four meteorological stations, operated by MeteoSwiss, are used in this study as input data for the model or for the assessment of uncertainties: Corvatsch (3315 m a.s.l., located on a summit, 8km west of the point AWS on Morteratsch glacier), Hospizio Bernina

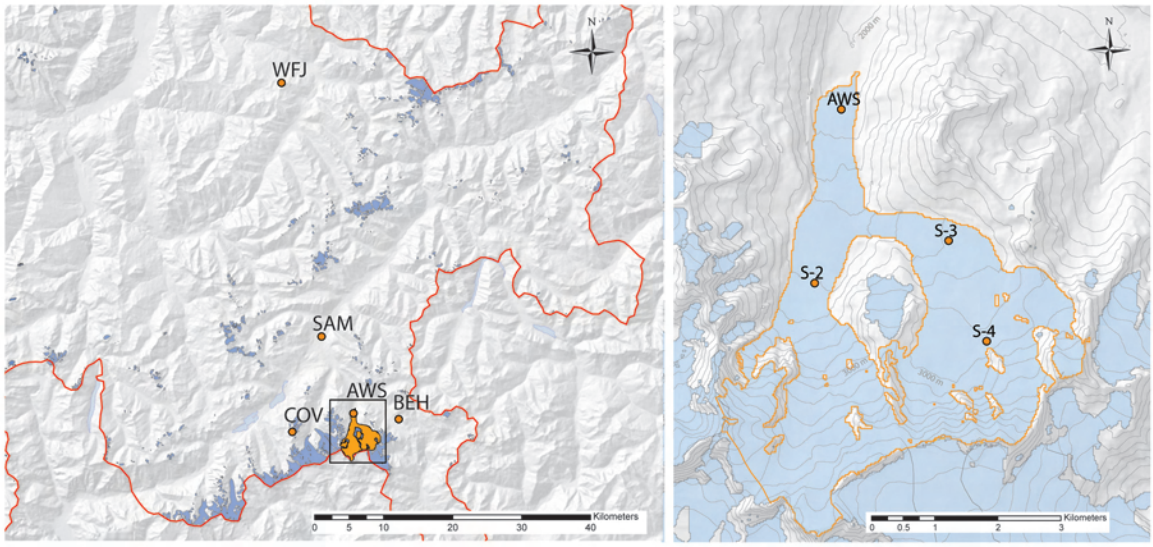

Figure 7.1.: Left: Location of Morteratsch glacier (orange) with the Automatic Weather Station (AWS) and the weather stations operated by MeteoSwiss that were used in this study: Corvatsch (COV), Hospizio Bernina (BEH), Samedan (SAM) and Weissfluhjoch (WFJ). The Border of Switzerland is marked in red and glaciers within Switzerland are depicted in blue. The area of the detail map of Morteratsch glacier is indicated with a rectangel. To the Right: Map of Morteratsch glacier (orange outlines) and the test sites used in this study. Contour lines every 100 m. Glacier outlines are from *Paul et al.* (2004). The digital elevation model (DHM25 level2) is reproduced by permission of swisstopo (BA081413).

(2307 m a.s.l., located at a pass, 7 km east), Samedan (1705 m a.s.l., located on a wide and flat valley floor, 12 km north) and Weissfluhjoch (2690 m a.s.l., located on a summit, 45 km north) (Figure 7.1). Hospizio Bernina is a manual weather station and only daily means are available - we acquired daily mean 2 m air temperatures (T_a). The other stations are automatic and we obtained from all three stations hourly means of T_a, relative humidity (e_a) and air pressure (p). In addition, global radiation ($S_{in_{meas}}$) and precipitation (P) were acquired from Corvatsch.

7.3. The Mass Balance Model

7.3.1. Description of the Model

In this study we investigate the numerical mass balance model developed by *Klok and Oerlemans* (2002). We selected this model because of the detailed and clear description of parameterizations, model output and validation procedure. Furthermore, the original model or parts of it have already been used in other studies e.g. (e.g., *Klok and Oerlemans*, 2004; *Arnold et al.*, 2006). The model is driven by data from synoptic weather stations located

outside of the glacier boundary layer. According to *Klok and Oerlemans* (2002), the model is based upon the following equation describing the specific mass balance, M ($\mathrm{kg\,m^{-2}}$):

$$M = \int \left(\frac{Q_M}{l_m} + P + \frac{Q_l}{l_s} \right) dt \tag{7.1}$$

Q_M is the melt energy involved in melting and Q_l the energy involved in sublimation or riming. l_m ($3.34 \cdot 10^5 \mathrm{J\,kg^{-1}}$) is the latent heat of melting, and l_s ($2.83 \cdot 10^6 \mathrm{J\,kg^{-1}}$) is the latent heat of sublimation. P represents the accumulation due to snowfall. The surface energy heat flux (F) supplies energy for melting (Q_M) or for the glacier heat flux (G), which implies the warming or the cooling of the snow or ice pack.

$$F = Q_M + G = S_{in} - S_{out} + L_{in} - L_{out} + Q_h + Q_l \tag{7.2}$$

S_{in} and S_{out} are incoming and reflected solar radiation; L_{in} and L_{out} are incoming and emitted longwave radiation. Sensible and latent heat fluxes are represented by Q_h and Q_l. Melting can occur only when the surface temperature is at 0 °C and F is positive. If the latter is the case but the surface temperature is below zero, then $F = G$ and the snow pack or ice is heated. The model is driven by data from synoptic weather stations located outside of the glacier boundary layer. Required input from meteorological measurements are: T_a, $S_{in_{meas}}$, P, e_a and p. Energy fluxes at the glacier surface are parameterized according to *Klok and Oerlemans* (2002). In their model parameterizations from *Oerlemans and Grisogono* (2002) are applied to calculate turbulent fluxes. Katabatic flow is parametrized therein and thus, measured wind speed is not required for input in the present model. While writing our program code we closely followed the explanations given by *Klok and Oerlemans* (2002). Some of the original parameterisations have been modified and are described here.

We calculated potential clear sky global radiation according to *Corripio* (2003) and *Iqbal* (1983). The snow albedo (α_s) is calculated according to *Klok and Oerlemans* (2002) and modified formulas from ECMWF, using snow-ageing functions for melting (exponential) and non-melting conditions (linear). Furthermore, in contrast to *Klok and Oerlemans* (2002), the new value of α_s after a snow fall event is not only a function of total snow depth and the underlying ice albedo (α_i), but also a function of α_s, the albedo of the old snow surface before the snow fall event.

Klok and Oerlemans (2002) calculate precipitation (P) from measurements at Samedan and two manual weather stations (Pontresina and Bernina-Curtinatsch) in combination with a multiplication factor. Here we simply use measured P from Corvatsch station in combination with a tuning factor (P_{corr}). While in the original model a single threshold temperature (T_{snow}) of 1.5 °C is used to distinguish snowfall and rain, we apply a gradual transition between 1 °C and 2 °C.

7.3.2. Testing of the Mass Balance Model

The original model is reported as having delivered results in good agreement with measurements on Morteratsch for both a two and a five year model run (*Klok and Oerlemans*, 2002, 2004). In order to calibrate our modified model, we first conducted a model run for the 400 days calculation period (Sect. 7.2). We adjusted P_{corr} over this period to achieve good agreement between modelled and observed date of the disappearence of the winter snow

cover at the AWS in spring 1999. Tuning was performed only at the AWS but the value we found for P_{corr} was applied uniformly at all points. Except for the new calculation of P_{corr}, we did not apply any other new tuning to the model.

The modelled cumulative mass balance after tuning ($P_{corr} = 2.1$) was -5.97 m w.e. According to *Klok and Oerlemans* (2002), measured melt at the AWS during the melt season of 1999 was -5.9 m w.e, which approximately equals to total observed mass balance for the full 400 days – according to the sonic ranger measurements, the 1998 melt period ended on October 18 and little accumulation (approx. 0.05 m w.e.) occurred between the end of the melt period in 1999 and November 20, 1999. Hence, the cumulative mass balance calculated for the tuning period agrees well with measurements. According to *Klok and Oerlemans* (2002) the snow cover at the AWS disapeared on May 18, 1999. After tuning of P_{corr} modelled melt out occurs on the same day.

Finally, to test the robustness of the calibrated model, an eleven year model run for four points on Morteratsch glacier was conducted and the results compared to measurements (Figure 7.2 and 7.3). For the point AWS, modelled cumulative mass balance is -72.5 meter ice (m ice) which agrees very well with a measured value of -74 m ice (Figure 7.2). The two curves are very similar, deviations during winter time are only apparent since the model results are shown in m ice and the sonic ranger measures surface elevation which corresponds to snow height in winter. The three other points with measurements available were also included in the comparison. The agreement for S-2 and S-3 is also good, however, the model systematically overestimates mass balance at S-4. The comparison of measured and modelled mass balance in a scatter plot (Figure 7.3) shows that for individual stake readings deviations occur. There is one clear outlier where measured melt at S-2 is strongly underestimated. The disagreement is likely due to an uncertain stake reading.

7.4. Uncertainty Assessment

7.4.1. The Uncertainty Model

Different approaches exist to determine the PDF of the output of a model. Analytical solutions are often desirable, however, they become complex or impossible if the set of uncertain parameters is large and nonlinear effects are present. Consequently, methods such as probabilistic collocation (e.g., *Tatang et al.*, 1997) or Monte Carlo simulations are commonly applied to approximate uncertainty. Although computationally expensive, Monte Carlo simulations are popular because they are relatively simple to apply even when working with complex models and large numbers of uncertain parameters. For instance, *van der Veen* (2002) used Monte Carlo simulations to assess uncertainty in the mass balance of the Greenland ice sheet.

In a Monte Carlo simulation a certain calculation (in our case a model run) is repeated many times and uncertain input parameters are varied within their uncertainty ranges. Model outputs are stored and a histogram is constructed to obtain the PDF for the desired output variable.

In the context of this paper the calculation being repeated is the modelling of the cumulative mass balance at a point AWS on Morteratsch glacier over the time span between October 18, 1998 and November 20, 1999, the period over which we tuned the parameter P_{corr}.

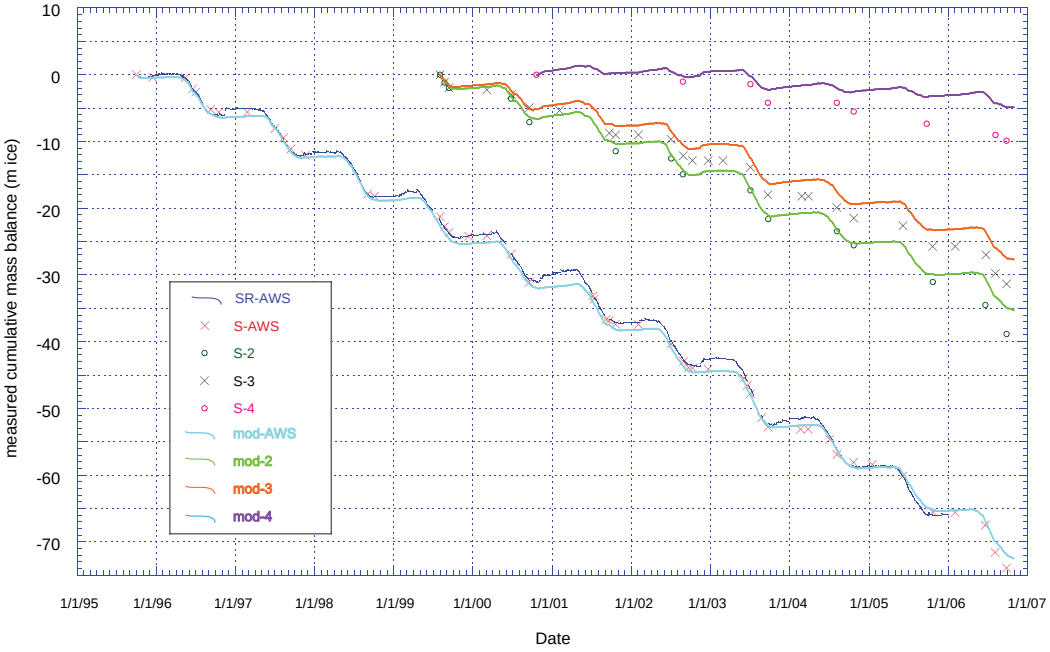

Figure 7.2.: Comparison of modelled mass balance and measured mass balance at four points on Morteratsch glacier. "SR" stands for sonic ranger, "S" for stake measurements and "mod" for modelled values. The elevation of the four points are: AWS: 2100 m a.s.l., 2: 2500 m a.s.l., 3: 2700 m a.s.l. and 4: 2950 m a.s.l. All data is given in meters ice except for the snow accumulation measured by the sonic ranger which is depicted in meters snow height.

For every uncertain parameter we estimated random and systematic uncertainty based on the literature and measured values of these parameters. An explanation of the uncertainties of individual parameters is given in Sect. 7.4.2 and the values chosen are listed in Table 7.1.

These uncertainties were then multiplied by normally distributed random numbers with a mean at 0 and a standard deviation of 1, resulting in systematic (ε_s) and random uncertainties (ε_r). The random numbers for the two classes of uncertainties as well as for the different parameters are independent of each other, implying the simplifying assumption that input parameter uncertainty is not correlated. Calculated ε_s and ε_r are then added to the measured values of the corresponding input parameters. The ε_s are calculated at the beginning of every run and remain constant throughout the run. The ε_r are treated as either fully random or temporally autocorrelated. In the first case, every second numerical time step (every hour) a new ε_r is calculated. In the case of temporal autocorrelation ε_r at time step t is correlated to ε_r at time steps $t+1, t+2, \ldots, t+(t_{decor}-1)$ and only at time step $t+t_{decor}$ is the uncertainty decorrelated from the original uncertainty at t. Where temporal autocorrelation was applied, a typical mean time span t_{decor} and a related standard deviation were defined. Based on the latter two values and another array of normal distributed random numbers, we calculated a series of consecutive time spans, of variable length with a mean length of t_{decor}. At the start of every time span a value for ε_r is calculated and finally linear interpolation was applied between two successive ε_r.

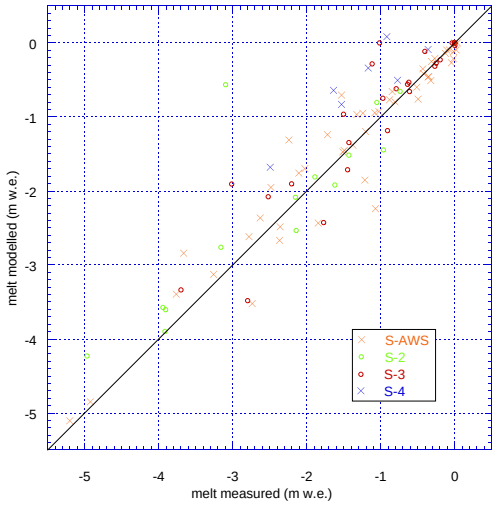

Figure 7.3.: Comparison of measured and modeled mass balance for all stake readings at the four test sites on Morteratsch glacier.

For some parameters the addition of ε_s and ε_r can result in impossible values (e.g. relative humidity of more than 100%). Physically defined limits were set where necessary (Table 7.1) and whenever such a limit was violated, the related parameter was set to its limiting value.

Table 7.1.: The selected uncertainties (ε_s, ε_r) and thresholds (min, max) and their respective units

parameter	symbol	ε_s	ε_r	unit	min	max	unit
measured air temperature	T_a	0.3	0.3	°C			
measured global radiation	$S_{in_{meas}}$	7.5	7.5	%	0		$\mathrm{W\,m^{-2}}$
measured precipitation	P	25	25	%	0		m
relative humidity	e_a	5	5	%	0	100	%
measured air pressure	p	100	100	pa			
temperature lapse rate	Γ_{Ta}	0.0002	0.001	$\mathrm{°C\,m^{-1}}$			
precipitation gradient	Γ_P	0.0001	0.0004	$\mathrm{m\,m^{-1}a^{-1}}$			
fixed albedo value for ice	α_i	0.05	-				
threshold temperature snowfall	T_{snow}	0.3	0.5	°C			
backg. turb. exch. coefficient	C_b	0.0005	-				
cloudiness	n	0.03	0.2		0	1	
thickness of the surface layer	z_1	0.055	-	m			

7.4.2. Parameters and Related Uncertainties

Twelve input parameters were assigned uncertainties: All five directly measured values (T_a, $S_{in_{meas}}$, P, e_a and p) as well as the parameters used in spatial interpolation, the lapse rate (Γ_{Ta}) and precipitation gradient (Γ_P). Furthermore, from the parameters selected by *Klok and Oerlemans* (2002) for sensitivity testing, we included ice albedo (α_i), T_{snow}, the

thickness of the surface layer (z_1), cloudiness (n) and the turbulent exchange coefficient (C_b). No uncertainties were assigned to the temperature of the lowermost layer in the three layer subsurface model since sensitivity testing of this parameter has previously shown it to have a neglible influence on mass balance (*Klok and Oerlemans*, 2002).

We aimed to give independent estimates of random and systematic uncertainties for each parameter. However, where both types of uncertainties are of similar magnitude or available data and literature did not allow for individual estimates of uncertainty, we made the assumption that $\varepsilon_s = \varepsilon_r$.

The present uncertainty analysis aims on showing a possible approach to assess uncertainty in mass balance modeling and on giving a first estimate. Not all potential sources of uncertainty could be considered. In particular, no uncertainty was assigned to the parameterization of the snow albedo and potential clear sky global radiation. Furthermore, uncertainties in precipitation are treated in a simplified manner.

Measured air temperature

Strasser et al. (2004) use a measurement error of 0.3 °C for unventilated thermometers of an AWS in their study. The ventilated thermometers from MeteoSwiss are believed to measure T_a very accurately. Nevertheless, we used 0.3 °C here for both stations because the microclimate at the respective stations (e.g. the Corvatsch Station is located on the roof of a house) may not be fully representative for nearby locations at the same altitude. Additionally, a systematic error of the same magnitude was introduced. The uncertainty assigned to T_a refers only to the uncertainty of the measurement at the synoptic weather stations. Total uncertainty in T_a at the point AWS is larger because uncertainty in the lapse rate (cf. Sec. 7.4.2) is multiplied with the difference in altitude and added to obtain total uncertainty in air temperature.

Measured global radiation

A detailed study on measurement errors in $S_{in_{meas}}$ published by Meteo Swiss concluded that after data corrections the remaining uncertainties are of the order of 5 to 10% (*Moesch and Zelenka*, 2004). We therefore assigned both systematic and random uncertainties of 7.5%.

Measured precipitation

Measuring precipitation, in particular snowfall, is related to large uncertainties reaching 50% or more (*Sevruk*, 1985a, 1989). In the present model, P is tuned by means of P_{corr}. Hence, we can not directly apply values on uncertainties in precipitation measurements from the literature. Tuning measured P to observed accumulation on the glacier introduces systematic errors since the observations on the glacier are also related to considerable uncertainties: only accumulation can be observed which is not identical to precipitation because the snow cover is subject to snow drifting, melt, riming and sublimation. Furthermore, spatial variability of snow accumulation is large (e.g., *Machguth et al.*, 2006a) and there are difficulties in determining the spatial and temporal variability of snow density. We therefore assigned systematic and random uncertainties of 25%. The latter is treated as fully random because precipitation intensity is spatially and temporally highly variable.

Measured relative humidity

It was difficult to find information on uncertainty in e_a that goes beyond technical specifications from typical measurement devices. A systematic and a random uncertainty of both 5% was assigned to e_a. The chosen values are a rough estimate to take into account uncertainties in the measurement itself, in the assumption that the values are representative and that they can be interpolated linearly inbetween the two stations. Consequently, the uncertainties at the two stations are assumed to be not correlated.

Measured air pressure

Air pressure has a very small influence on the model outcome and thus uncertainty in this parameter is not discussed in detail here. A systematic and a random uncertainty of 100 pa was assigned to p, uncertainties at the two stations are considered to be uncorrelated.

Lapse rate

To assess the variability of Γ_{Ta} we calculated mean lapse rates from measured T_a at the four selected meteorological stations in the vicinity of Morteratsch. The mean hourly Γ_{Ta} over the time span from 1995–2006 (app. 100'000 records for each station) is 0.0049 °C m^{-1} for Corvatsch-Samedan (13 km apart, 1607 m difference in altitude) and 0.0056 °C m^{-1} for Corvatsch-Weissfluhjoch (46 km apart, 625 m difference in altitude). The corresponding standard deviations are 0.0037 °C m^{-1} and 0.0022 °C m^{-1}, respectively. For Corvatsch-Hospizio Bernina (15 km apart, 1007 m difference in altitude), the mean daily lapse rate for the same time period amounts to 0.0062 °C m^{-1} with a standard deviation of 0.0022 °C m^{-1}. Taking into consideration the implication that a greater lapse rate will result in correspondingly higher values of T_a at the point AWS, it is at first glance surprising that running the model for the 400 days with data from Corvatsch and Weissfluhjoch results in a less negative mass balance (-5.19 m w.e.) than for Corvatsch and Samedan (-5.97 m w.e., see Sect. 7.2). Replacing Samedan with Weissfluhjoch also results in modifications of e_a and p. However, on closer inspection it becomes apparent that the main reason for reduced melt is the difference in summer lapse rates: from May 1 to September 30, mean hourly Γ_{Ta} (1995–2006) amounts to 0.0061 °C m^{-1} for Corvatsch-Samedan, 0.0058 °C m^{-1} for Corvatsch-Weissfluhjoch and mean daily Γ_{Ta} is 0.0074 °C m^{-1} for Corvatsch-Hospizio Bernina.

Although closer to the glacier than Weissfluhjoch, it is questionable as to whether Samedan better represents meteorological conditions at Morteratsch. Samedan is located on a wide valley floor with large diurnal and annual temperature fluctuations. Furthermore, linear regression of hourly T_a yields $R^2 = 0.61$ for Corvatsch-Samedan and $R^2 = 0.96$ for Corvatsch-Weissfluhjoch. On the other hand, Γ_{Ta} calculated from the latter pair of stations seems rather low, most probably because Weissfluhjoch is situated further to the north, in an area more open to colder air currents from the north and north-west, whereas the area around Morteratsch is more influenced from the south and south-west. These comparisons show that the calculation of Γ_{Ta} is very sensitive to the selection of the synoptic weather stations and that there is considerable uncertainty in its value. However, the small number of available station pairs makes it difficult to determine the magnitude and type of the uncertainty. As a rough estimate we assumed a normally distributed systematic uncertainty of 0.0002 °C m^{-1}.

Furthermore a temporally autocorrelated random uncertainty of $0.001\,^{\circ}\mathrm{C\,m^{-1}}$ is assigned to Γ_{Ta}. The assumption of temporal autocorrelation is essential here because otherwise strong hourly fluctuations and jumps in Γ_{Ta} would result. To determine the typical time span of temporal autocorrelation, we analyzed both twelve year time series of hourly Γ_{Ta} for their respective lag autocorrelation (Since Hospizio Bernina are not available on a hourly basis, this analysis could not be carried out for all three station pairs). Semivariograms of the temporal correlation of both time series are depicted for lags of between 1 and 24000 hours in Figure 7.4. In the case of Corvatsch-Samedan clear daily and seasonal variations are present whereas the time series Corvatsch-Weissfluhjoch decorrelates rapidly with little daily or seasonal variation. From these figures we conclude, that Γ_{Ta} decorrelate within roughly 24 hours. Once again, Figure 7.4 shows the dilemma of the two pairs of stations: The valley station shows strong diurnal and seasonal fluctuations which are not present when comparing two summit stations. Although these strong fluctuations are large compared to the conditions at the point AWS (e.g., *Oerlemans*, 2001), in particular during the melt season, the mean values of Γ_{Ta} calculated with data from the valley station may still be more representative for the glacier.

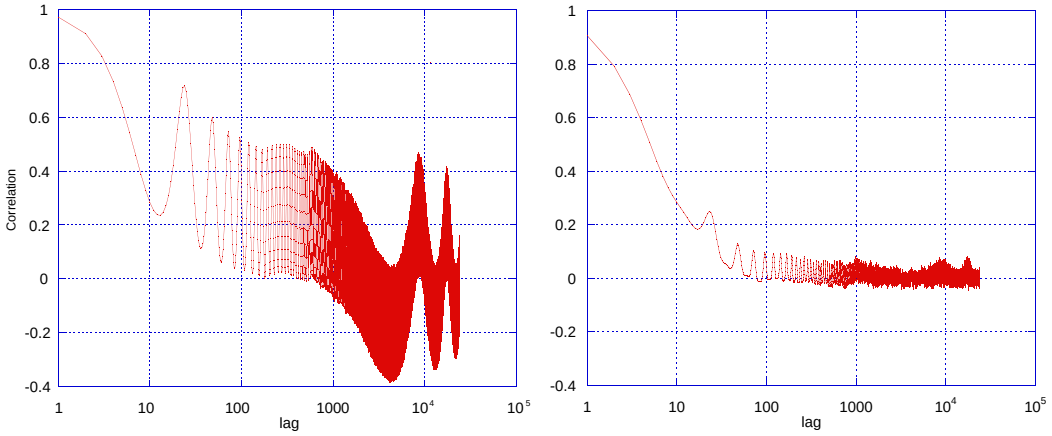

Figure 7.4.: Lag autocorrelation for two time series (1995–2006) of hourly lapse rates. To the left the lag autocorrelation for the lapse rates obtained from air temperature measured at Corvatsch and Samedan is depicted and to the right for Corvatsch-Weissfluhjoch.

Vertical precipitation gradient

According to *Schwarb* (2000), Γ_P is to a certain extent a virtual parameter because vertical and horizontal components of the precipitation distribution can never be fully distinguished. *Klok and Oerlemans* (2002) obtained $\Gamma_P = 0.0004\,\mathrm{m\,m^{-1}\,a^{-1}}$ from the same author who applied a comprehensive set of rain-gauge data to a complex interpolation scheme in order to derive spatially distributed Γ_P and P at approximately 2 km resolution. Based on the assumption that the methodology of *Schwarb* (2000) provides a reliable mean value for Γ_P in the Morteratsch area while temporal variability around that mean is large, we assigned a moderate systematic uncertainty ($0.0001\,\mathrm{m\,m^{-1}\,a^{-1}}$) and a large random uncer-

tainty ($0.0004\,\mathrm{m\,m^{-1}\,a^{-1}}$). Random uncertainties are not temporally correlated and the occurrence of negative Γ_P is allowed.

Ice albedo

In the present model α_i was fixed to 0.34 in order to have a good representation for the snow free part of Morteratsch glacier (*Klok and Oerlemans*, 2002). It is generally stated that the ice albedo is subject to significant small scale variability over short distances (e.g. *Knap et al.*, 1999b), thus a single mean value will result in either under- or overestimations for different parts of the glaciers ice surface (according to *Klok and Oerlemans* (2002), measured α_i at the AWS in summer 1999 was significantly lower than 0.34). In order to approximate the errors that result from assigning a fixed mean albedo to a glacier surface with an albedo distribution varying in both space and time (*Klok and Oerlemans*, 2004; *Paul et al.*, 2005), we assigned a normal distributed systematic uncertainty of 0.05. No random uncertainty was assigned here because α_i is not subject to significant random changes at an hourly time scale and the determination of a typical time span for a temporally autocorrelated random error seems rather difficult and uncertain.

Threshold temperature snowfall

Long term observations of air temperature and snow – rain transitions, compiled by *Rohrer* (1989) for a meteorological station in Davos (1590 m a.s.l., 45 km north of Morteratsch) show that the average of the transition range from rain to mixed precipitation to snow is somewhere between 0.75 °C and 1.5 °C with a standard deviation of roughly 0.3–0.5 °C. Furthermore, *Rohrer* (1989) shows that for the example of Davos, a change in both instrumentation and the measurement site resulted in significant change of the mean and the spread of the transition range. We applied a systematic error of 0.3 °C and a random error of 0.5 °C .

Thickness of the surface layer

The present mass balance model contains a three layer subsurface model to compute heat fluxes to and from the glacier. Since melt can only occur when the surface layer has reached the melting point, the chosen thickness of the surface layer (z_1) influences mass balance by controlling the time available for melt. *Klok and Oerlemans* (2002) varied z_1 by 0.11 m, here we assigned a normally distributed systematic uncertainty of 0.055, but since this parameter is initialised as a constant over an individual model run, it is not assigned a random uncertainty.

Cloudiness

In the present model cloudiness (n) plays an important role. It is derived from the ratio:

$$\tau_{cl} = \frac{S_{in_{meas}}}{S_{in,clr}} \tag{7.3}$$

τ_{cl} is used as a reduction factor to compute S_{in} and to derive n according to the following relationship, given by *Greuell et al.* (1997):

$$\tau_{cl} = 1.0 - 0.233n - 0.415n^2 \tag{7.4}$$

Consequently, errors in both $S_{in_{meas}}$ and in modeled clear sky global radiation ($S_{in,clr}$) affect cloudiness. If, for example, $S_{in_{meas}}$ is above the real value, this will result in an overestimation of τ_{cl}. However, n is derived from τ_{cl} and will be lowered. Finally, since L_{in} depends on cloudiness, it will also be lowered. Cloudiness during night time is interpolated from n before sunset and after sunrise. Consequently additional S_{in} is present only during daytime while L_{in} is affected 24 hours a day. Both effects, enhanced S_{in} and lowered L_{in} are of the same order of magnitude. An error in $S_{in_{meas}}$ will therefore shift the ratio of short- to longwave radiation balance but not have a large influence on their summed value.

In order to reduce this back-coupling effect and to account for uncertainties in the parameterisation of n, we first calculated τ_{cl}, applied it as a reduction factor, computed n and only afterwards modified n by adding an uncertainty. According to *Greuell et al.* (1997) eq. (7.3) performed very well in explaining the relationship between observed cloudiness (n_{obs}: eight classes, from 0 to 1 in steps of 1/8) and the mean observed τ_{cl} per class of n_{obs}. On the other hand, the mean τ_{cl} per class were computed from a larger set of individual values of τ_{cl} which showed a large variance. Thus we assigned normally distributed uncertainties, consisting of small systematic (0.03) and a larger random uncertainties (0.2). Since the observed variance of τ_{cl} for the individual classes of n might be due to differing effects of the various types of clouds, we introduced a temporal autocorrelation to n with a mean time span of 12 hours because cloud types typically persist for more than one hour.

Background turbulent exchange coefficient

The value for C_b was found by matching measured and modelled melt at AWS for the year 1999 (*Klok and Oerlemans*, 2002). Since the measurements are not error free (e.g., *Braithwaite et al.*, 1998), the tuning will result in a systematic over- or underestimation of C_b. Consequently, we have assigned a systematic uncertainty to this parameter and we selected the same value (0.0005) as used for the parameter sensitivity testing by *Klok and Oerlemans* (2002). As with surface layer thickness, this parameter is constant over an individual model run, and is thus not assigned a random uncertainty.

7.5. Results

7.5.1. Sensitivity Tests

Individual sensitivity studies were performed for every parameter listed in Table 7.1 to assess the combined influence of random and systematic uncertainties (Figure 7.5). For reasons of simplicity, sensitivity studies were also conducted by means of Monte Carlo simulations. Modelled mass balance is most sensitive to the prescribed uncertainties in P and Γ_{Ta}, followed by T_a and α_i. Uncertainties in $S_{in_{meas}}$ have a much smaller influence while the impact of the remaining parameters' uncertainties are less than half the most sensitive parameter.

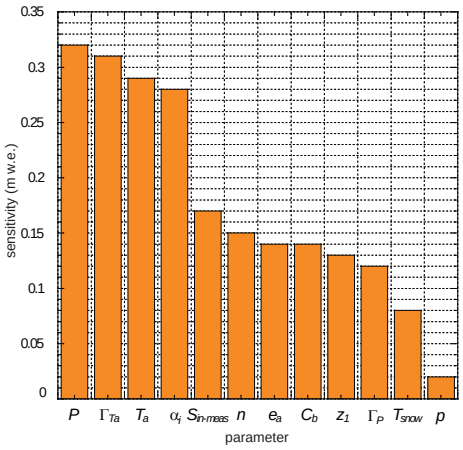

Figure 7.5.: Sensitivities to combined random and systematic uncertainties (according to Tab. 7.1) for the individual parameters. All values are given in m w.e.

7.5.2. Parametric Uncertainty Analysis

In order to assess the required number of runs for the Monte Carlo simulations, we plotted the evolution of the standard deviation, and standard deviation of standard deviation, of modelled mass balances over 5000 runs in a Monte Carlo simulation where all systematic and random uncertainties according to Table 7.1 were applied. Both parameters are depicted in Figure 7.6, indicating that fluctuations in standard deviations become small after roughly 1000 runs, suggesting that the chosen number of runs (5000) is likely to deliver stable results.

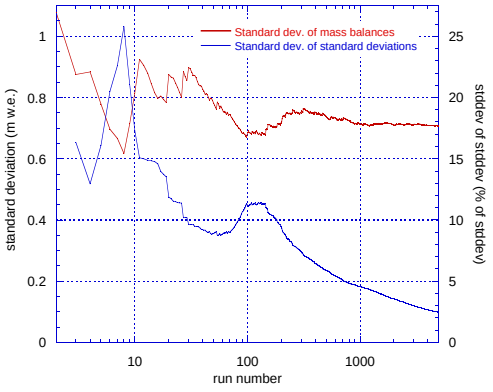

Figure 7.6.: Evolution of the standard deviation with increasing number of runs and related standard deviation of the standard deviations. Note the logarithmic scale on the X-axis, starting with run number two.

Figure 7.7 shows the PDF of the model outcome, resulting from a Monte Carlo simulation applying the full set of systematic and random uncertainties. The mean modelled mass balance is -6.02 m w.e., maximum and minimum values are -3.72 m w.e. and -8.69 m

w.e., respectively. The standard deviation is 0.71 m w.e. or roughly 10% of total cumulative melt. The PDF shows one distinctive peak at -6.3 m w.e. However, this peak could not be reproduced in further experiments with different initiation values for the random numbers. From the output of the same Monte Carlo simulation, we depicted the temporal evolution of mean mass balance over the calculation period, growth of the related standard deviation and most and least negative of all 5000 runs in Figure 7.8. In winter uncertainty grows with snow fall events, while during dry periods there is virtually no growth in uncertainty. With the onset of melt, uncertainty starts to grow continuously. Note that both the most and least negative of all runs can not be considered as obviously unrealistic: They show an accumulation and an ablation period. Winter accumulation is a few centimetres water equivalent in the most negative and almost one meter of water equivalent in the least negative. These values roughly mark the bounds of natural variability as observed on Morteratsch (cf. Figure 7.2). Furthermore, the dates of the disapearence of the snow cover were stored throughout the simulation and their PDF is shown in Figure 7.9. The mean date of melt out is day number 138 (according to *Klok and Oerlemans* (2002) the melt out happened one day earlier). The probability for snow cover disappearance is clearly not normally distributed but shows distinct peaks and troughs. Finally, the Monte Carlo simulations were repeated to estimate the contribution of random and systematic errors separately. Figure 7.10 shows PDFs accounting for all systematic or all random uncertainties. Corresponding standard deviations are 0.69 m w.e. and 0.14 m w.e., respectively. Obviously, overall uncertainty is dominated by the systematic uncertainty.

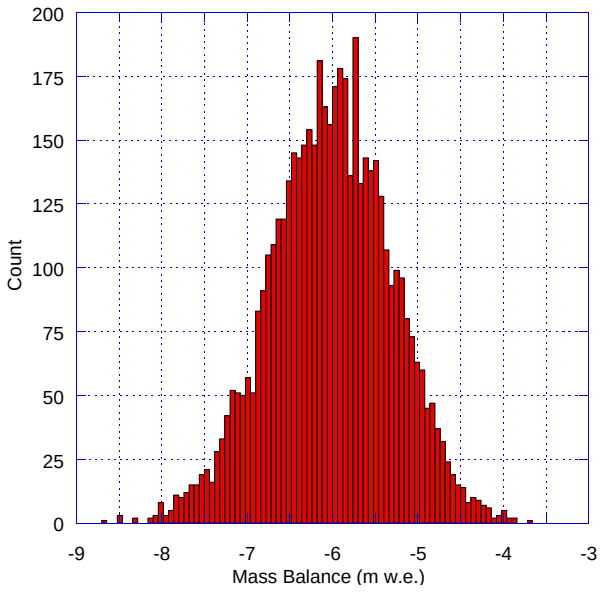

Figure 7.7.: Probability density function of the modeled cumulative mass balance (Oct. 18, 1998 - Nov. 20, 1999) at point AWS (2100 m a.s.l.) on Morteratsch glacier.

However, uncertainty will clearly vary according to the data set used for model input. In order to make this study applicable to a broader audience working with different data (e.g. data from climate models), a further experiment was conducted, evaluating model

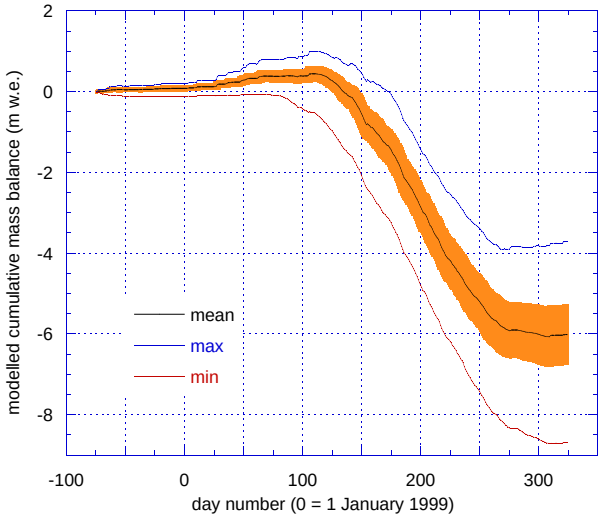

Figure 7.8.: Temporal evolution of the modeled cumulative mass balance (Oct. 18, 1998 - Nov. 20, 1999) at point AWS (2100 m a.s.l.) on Morteratsch glacier. The mean value is the mean of all 5000 runs in the full Monte Carlo simulation. Calculated uncertainty (±1 standard deviation) is depicted with the orange shading. The most and least negative of all runs are also shown.

response to different levels of uncertainty in $S_{in_{meas}}$ and T_a. Here, we varied uncertainty in T_a from 0 °C to 2 °C in steps of 0.5 °C and uncertainty in $S_{in_{meas}}$ from 0% to 20% in steps of 5%. The uncertainties in all other parameters were varied in the Monte Carlo simulation according to the values given in Table 7.1, except for uncertainties in Γ_{Ta} which were set to zero in order to have full control over the uncertainty in T_a. The number of runs was reduced to 1000 for every combination of uncertainties in the two parameters and resulting model uncertainties are listed in Table 7.2. Of course, it would be an interesting experiment to vary P similar to $S_{in_{meas}}$ and T_a since uncertainties in precipitation are particularely large. However, to our opinion a detailed assessment of its various sources of uncertainties is required and should be addressed in future studies.

Table 7.2.: Change in overall uncertainty (m w.e.) for different uncertainties in T_a and $S_{in_{meas}}$. Note that the means of the resulting PDFs are shifting with growing uncertainty, from -5.97 m w.e. at 0°C/0% to -6.47 m w.e. at 2°C/20%.

unc T_a \ unc $S_{in_{meas}}$	0%	5%	10%	15%	20%
0°C	0.56	0.57	0.61	0.68	0.79
0.5°C	0.72	0.73	0.76	0.82	0.92
1°C	1.09	1.10	1.12	1.16	1.23
1.5°C	1.51	1.52	1.54	1.57	1.62
2°C	1.96	1.97	1.99	2.01	2.05

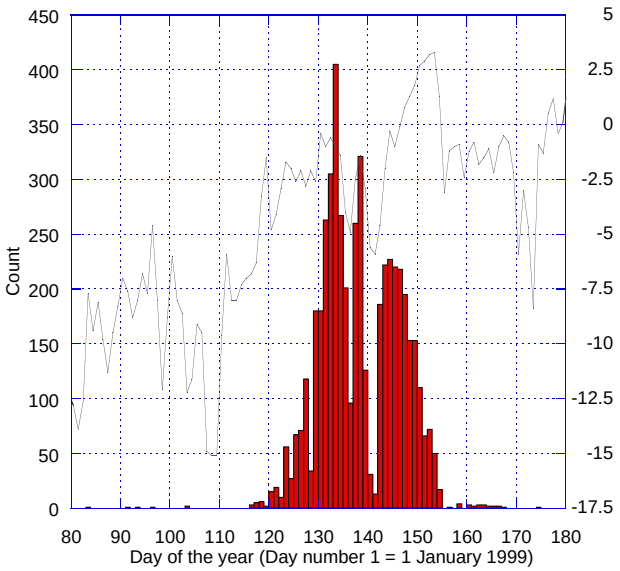

Figure 7.9.: Probability density function of the modeled date of melt out at the point AWS (2100 m a.s.l.) on Morteratsch glacier. Day no. 1 corresponds to 1. January 1999. Daily means of air temperature measured at Corvatsch are depicted with a grey line.

7.6. Discussion

7.6.1. Estimating parameter uncertainties

The first step in any sensitivity test, or a parametric uncertainty analysis, is the selection of parameters for sensitivity testing and estimation of their associated ranges. Most previous research on energy and mass-balance modelling has focussed only on sensitivity testing, with parameter ranges based on a variety of sources. In this work, we have recognised the importance of not only random uncertainty, which can be considered akin to instrument precision and accuracy, but also systematic uncertainties which have generally been ignored. An important limitation is the difficulty in estimating values for both random and systematic uncertainties, and where appropriate, temporal autocorrelation of random uncertainties. However, we believe that an approach based on the selection of parameters through literature is an appropriate one, and that all of these sources of uncertainty must be modelled.

7.6.2. Sensitivity Tests

Sensitivity testing was conducted to estimate the contribution of individual parameters to overall model uncertainty. The model appears to be most sensitive to the prescribed uncertainties in P and Γ_{Ta}. However, since air temperature at the AWS is calculated from T_a at Corvatsch, Γ_{Ta} and the difference in altitude from Corvatsch and AWS, the latter has an amplifying effect on the impact of uncertainties in Γ_{Ta}. Nevertheless, the discussion in Sect. 7.4.2 indicates that the lapse rate can vary significantly depending on which station pair is chosen. Air temperature is generally considered a well known parameter, however the sensitivity to the prescribed uncertainties in T_a, which might be considered conservative, is

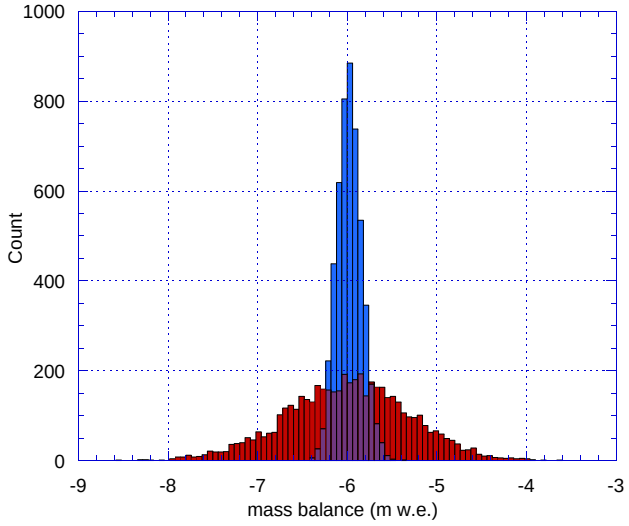

Figure 7.10.: Probability density function of modeled cumulative mass balance (Oct. 18, 1998 - Nov. 20, 1999) at point AWS (2100 m a.s.l.) on Morteratsch glacier, calculated separately with only systematic (red bars) and only random uncertainties (blue bars).

among the largest. Consequently, the common assumption of neglible uncertainties in air temperature must be regarded as questionable because air temperature has a large influence on the glacier mass balance (*Ohmura*, 2001). Sensitivity to uncertainties in $S_{in_{meas}}$ are quite small although realistic levels of uncertainty have been applied. However, the impact of errors in $S_{in_{meas}}$ is partly compensated due to the coupling of shortwave and longwave radiation balance through the parameterisation of cloudiness.

Furthermore, it should be noted that the impact of the chosen uncertainties in the two investigated internal model parameters (C_b and z_1) is smaller than the influence of most of the uncertainties related to the meteorological data or ice albedo.

7.6.3. Parametric Uncertainty Analysis

Several striking results are apparent from the parametric uncertainty analysis. Firstly, the standard deviation in cumulative melt of 0.71 m w.e. seems at first glance to be contradicted by the very good agreement of modelled and observed melt shown in Figure 7.2. However, this good result was obtained by a model tuned to a particular location, over 400 days in the same location as to which it is applied. The uncertainty shown in Figure 7.7 indicates the impact that typical uncertainties in measurement could have on such a point measurement – and which are in this case accounted for, at least to some degree, by the tuning of the model to the point. Furthermore, Figure 7.2 also shows the corresponding drift of modelled melt from measured for sites at which the model was not tuned - these differences are much more similar to the uncertainty associated with our PDF, and also indicated by the increase in uncertainty over time as shown in Figure 7.8.

Secondly, whilst the PDF of cumulative mass balance is normally distributed, the PDF of the day of melt out has a distinct bimodal appearance (Figure 7.9). This is because

uncertainty has a much smaller influence on the average melt out day, since meteorological events which occur over relatively short periods have a strong influence on the timing of melt out – for example, an influx of cold air around day 140 reduces the probability of melt out to almost zero, irrespective of uncertainty. To illustrate this in more detail, daily mean T_a at Corvatsch is shown in Figure 7.9. Until day 110 air temperatures are low, and only in 6 runs has the snow cover already disappeared by then. Temperatures then rise sharply and reach a first peak at day 119 which also marks the onset of a rise in probability for melt out. However, since the snow cover is still quite thick in most runs and its temperature most likely below 0°C, the rise in probability for snow cover disappearance lags temperature. T_a stays high and the longer the period of warm temperatures last, the higher becomes the probability for melt out. A further rise in T_a results in a peak at day 133 where the snow cover disapears in more than 8% of all runs. The number of runs with melt out and T_a then show a distinct correlation with two sharp drops in probability of melt out, both caused by an influx of cold air. Around day 145 the probability for melt out starts to diminish regardless of the still increasing T_a. By this date temperatures have been favourable for snow melt for almost one month (since approx. day 119), the probability that snow cover persists is already low and thus T_a and the day of melt out decorrelate. This result points to the importance of choosing appropriate parameters for model validation – the day of melt out is much less sensitive to uncertainty than cumulative mass balance.

Thirdly, we observe that systematic uncertainties contribute much more to overall uncertainty than random uncertainties which tend to cancel one another out. Although this result is perhaps rather obvious, it indicates the importance of considering techniques for estimating and characterising systematic uncertainties, which are generally ignored despite their well known importance in, for example, the homogenisation of long term temperature series (*Böhm et al.*, 2001). There is no reason to assume that measurements or projections made today are not subject to systematic uncertainties – for example, consistent under or over estimation of albedo through a melt season (*Paul et al.*, 2005) – and these should be accounted for in uncertainty analysis.

We calculated uncertainty to be approximately 10% of total melt at one particular point on one glacier. However, for two main reasons, the results of this study should be transferred to other glaciers with caution. Firstly, as already discussed the uncertainties in the input parameters may differ strongly depending on the data sets used. Second, the uncertainty model contains simplifications which may not apply to other sites. The study focuses on a test site where the total melt is about one order of magnitude larger than accumulation. Consequently only a rough estimate of uncertainty in the latter was applied and thus, the uncertainty model can not yet be applied to an entire glacier surface. Although it would be of particular interest to assess the uncertainty of the mass balance calculation for an entire glacier instead of a single point, such an uncertainty assessment would require a more profound analysis and description of the uncertainties in accumulation modelling, and also consideration of appropriate methods for spatially autocorrelated uncertainty analysis.

7.6.4. Impact of variation in individual parameter uncertainty

Many projections in the future are based on relatively simple models, where one or two parameters are varied to explore the response of a system (for example, increases in air temperature). However, these projections are in themselves subject to the uncertainty found

in all input parameters. Thus, we have carried out Monte Carlo simulations on two sets of scenarios based on particularly important parameters – air temperature and measured global radiation. The results demonstrate that the growth in overall uncertainty is not a linear function of uncertainty in T_a or $S_{in_{meas}}$, but rather an exponential one. Uncertainty of more than 1 m w.e. is reached for 1°C of uncertainty in T_a which is still a rather conservative estimate, in particular where a mass balance model is applied to unmeasured glaciers or driven by data from climate models. Uncertainty in measured global radiation is of clearly lower impact for reasons discussed in Sect. 7.4.2. This approach allows the assessment of not only scenarios of future change, but the sensitivity of these scenarios to uncertainty to be estimated.

7.6.5. Implications

According to *Anderson and Woessner* (1992) an uncertainty analysis should be built into modelling strategies from the onset. Models are often validated by comparing their output to measurements. However, since both observations and model results may be uncertain, meaningful model validation requires not only the mean outputs but also their PDFs (*Tatang et al.*, 1997). A parametric uncertainty analysis can contribute to process understanding by helping to identify which comparisons to measured values are sensible. It is then possible to identify modelled values, for example in Figure 7.3, that show larger deviations from measurement than their level of uncertainty (obviously, uncertainties of the measurements have to be considered as well). For these values it is likely that the model failed due to conceptualisation problems and not due to errors in input parameters. Identifying these conceptualisation problems by explaining why the model has failed at particular points will lead to an improved mass balance model and potentially add to our understanding of process.

Monte Carlo simulations are also a valuable tool to assess whether output of a mass balance model is more sensitive to the choice of tuning parameters or to uncertainties stemming from model input and parameterizations.

Finally, particularly when we wish to extrapolate in space or time, a parametric uncertainty analysis becomes essential. Since, uncertainties in data values are likely to increase as we extrapolate further from our observations in space and time, it is important to realise that uncertainties are also unlikely to be constant in space or time and modellers should take care not to over interpret results which are simply the mean of PDFs with potentially large standard deviations.

7.7. Conclusions

In this work we have calculated the uncertainty in a glacier mass balance model, estimated at a point on the Morteratsch glacier in Switzerland over a period of 400 days, using uncertainty values for individual meteorological and model parameters. Despite good agreement of the tuned model with observed mass balance over a period of 11 years, we estimate uncertainty in cumulative mass balance of approximately 10%. The uncertainty is dominated by systematic uncertainties in parameters, which in most studies are not considered. Thus, we believe it is important in future work to consider methods of estimating and quantifying systematic uncertainties in typical parameters.

Our estimate of overall uncertainty is most likely a conservative one: Not all potential sources of uncertainty could be considered and precipitation was tuned without assigning uncertainty to the respective tuning parameter. However, to consider all the different aspects of uncertainty in precipitation or accumulation is not trivial. Detailed studies on this subject are required and would add to a more comprehensive understanding of uncertainties in mass balance modelling.

However, the main implication of this work is related to the extrapolation of model results in time and space. This paper shows, that for a well-tuned model with relatively low values for individual uncertainties, one can expect considerable uncertainty in modelled outputs. This in turn implies that, for a glacier where appropriate data are unavailable for tuning, and where the measured input data are less certain, one could expect increased uncertainties in cumulative mass balance. In future work we will explore how we can integrate parametric uncertainty analysis into models which extrapolate glacier mass balance in both space and time.

Acknowledgments We would like to thank Javier Corripio for making his code for global radiation calculation available to us. MeteoSwiss provided the meteorological data and Swisstopo the digital elevation model. The careful and constructive reviews of two anonymous reviewers as well as the interactive comment by Ruzica Dadic are greatly acknowledged. H. Machguth is funded by the grant 20-117761 of the Swiss National Science Foundation.

8. Calculating Distributed Glacier Mass Balance for the Swiss Alps from RCM Output: A Methodical Description and Interpretation of the Results (Paper №4)[1]

Abstract This study aims at giving a methodical description on the use of gridded output from a regional climate model (RCM) for the calculation of glacier mass balance distribution for the perimeter of the Swiss Alps. The mass balance model runs at daily steps and 100 m spatial resolution while the REMO RCM provides daily grids (approx. 18 km resolution) of dynamically downscaled reanalysis data. A combination of interpolation techniques and sub-grid parameterizations is applied to bridge the gap in spatial resolution and to obtain daily input fields of air temperature, global radiation and precipitation. Interpolation schemes are a key element and thus, we test different interpolators. For validation, computed mass balances are compared to stake measurements and time series (1979–2003) of observed mass balance. The meteorological input fields are compared to measurements at weather stations. The applied inverse distance weighting introduces systematic biases due to spatial autocorrelation whereas thin plate splines preserve the characteristics of the RCM output. While summer melt at point locations on several glaciers is well reproduced by the model, accumulation is mostly underestimated. These systematic shifts are correlated to biases of the meteorological input fields. Time series of mass balance obtained from the model run agree well with observed time series. We conclude that the gap in spatial resolution is not a major drawback, given that interpolators and sub-grid parameterizations are selected upon detailed considerations. Biases in RCM precipitation are a major source for the observed underestimations in mass balance and have to be corrected prior to operational use of the presented approach. High resolution scenario runs (i.e. from climate model ensembles) on future mass balance distribution could be a further application of the presented methodology.

8.1. Introduction

The possible disappearance of glaciers under future climatic conditions is a major concern and numerous studies have assessed expected glacier changes from a wide range of

[1] based on: Machguth, H., F. Paul, S. Kotlarski and M. Hoelzle (submitted), Calculating Distributed Glacier Mass Balance for the Swiss Alps from RCM Output: A Methodical Description and Interpretation of the Results, *Journal of Geophysical Research*.

approaches. As glacier mass balance is closely linked to annual meteorological conditions, mass balance is a key feature in understanding the glacier-climate relationship. Consequently, mass balance modeling has been subject to a wealth of studies, ranging from very detailed process orientated approaches with sophisticated models operating at the point scale, to distributed and less complex models applied to entire glaciers and/or samples of several glaciers [see *Oerlemans*, 2001 and *Greuell and Genthon*, 2004 for an overview]. Thereby, the level of model complexity largely depends on the research question and the available data to run the model.

With respect to climate change impact assessment, there is need to cover entire glacierized mountain ranges at a sufficient level of detail. Two major challenges have to be faced when modeling glacier mass balances in rugged high-mountain terrain: the small number of measurements (e.g. climate stations) in most glacierized regions in the world and the spatial extrapolation of the meteorological input parameters from these measurements at point locations. In principal, regional climate models (RCMs) are able to provide the three basic drivers of glacier mass balance, temperature (T_a), precipitation (P), and global radiation (S_{in}) over large regions by dynamical downscaling of general circulation model (GCM) or re-analysis data to about 10–50 km spatial resolution. Their most important advantage is the possibility to generate physically consistent fields of atmospheric variables for an entire region and for today's climatic conditions as well as for climate scenarios (*Salzmann et al.*, 2007a). However, their main drawback is the coarse spatial resolution. Distributed mass balance calculation in rugged high mountain topography is usually performed at 25–100 m spatial resolution to account for small scale variability (e.g. slope and aspect, shading). Furthermore, local meteorological phenomena at a scale of less than one to a few kilometers (e.g. orographic precipitation) are also relevant to mass balance distribution and are not resolved by the RCMs.

Indeed, the scale mismatch is a problem in many studies related to climate change impact assessment on regional to local scales. Previous studies that have utilized output from climate models for mass balance calculations were mostly focused on individual glaciers, acquiring data from the nearest climate model grid box in combination with a statistical downscaling (e.g. *Van de Wal and Wild*, 2001; *Schneeberger et al.*, 2003; *Radić and Hock*, 2006; *Stahl et al.*, 2008). Other studies used the meteorological fields from several grid boxes at the same time and performed mass balance computations directly at the spatial resolution of the RCM (e.g. *Bhatt et al.*, 2007; *Cook et al.*, 2003; *Ren et al.*, 2007; *Zhang et al.*, 2007). However, so far no attempt was made to downscale a whole field of RCM output to a higher resolution and to apply these data for mass balance computation.

In this study we give a methodical description of a coupling scheme between RCM data and a mass balance model which is designed to compute mass balance distribution over entire mountain ranges, i.e. at the regional scale. Output from the RCM REMO (e.g. *Jacob et al.*, 2001) is downscaled from about 18 km to 100 m and then used as an input for a 24 year transient run of a distributed glacier mass balance model for the entire Swiss Alps. More specifically, we describe different methods of spatial inter/extrapolation of the RCM data and illustrate different ways of validating the model input (i.e. the downscaled field of RCM data) as well as the model output (i.e. the mass balance distribution). The underlying principle is to apply the RCM data without bias corrections in order to identify their limits and allow for a comprehensive description of the methodical steps.

The paper is organized in the following way: Basic considerations on how to apply RCM data for mass balance calculation are raised in the following section. Afterwards the model domain and the applied data are presented. The technical description of mass balance calculation includes the mass balance model and the explanation of the downscaling scheme for the RCM data. The results are then presented, followed by a section "Interpretation" which focuses on a technical analysis of the results with respect to the chosen parameterizations of mass balance computation and the RCM downscaling scheme. In the section "Discussion", the results are discussed in the broader context of overall model performance and its applicability for operational use. Finally, conclusions are drawn and an outlook is given.

8.2. Basic Considerations of Applying RCM Data

In this study the mass balance of a large sample of individual glaciers is modeled explicitly, i.e. as their topography is represented in a 100 m resolution digital terrain model (DTM) and the numerical time steps of the computation are chosen to be one day. The size of the model domain (the Swiss Alps, 300×200 km) implies that meteorological fields have to be used instead of data from individual weather stations (e.g. *Klok and Oerlemans*, 2002) or selected grid boxes from climate model output (e.g. *Schneeberger et al.*, 2003). The spatial and temporal resolution of the required meteorological fields should be similar to the mass balance model.

Basically there are two possible sources of meteorological fields: gridded climatologies derived from measurements, or RCM output. Neither of them has a similar resolution to the mass balance model both temporally and spatially. It was decided to work with RCM data for the following reasons: RCMs are of high temporal resolution and provide spatio-temporal consistent fields whereas the available gridded climatologies (e.g. *Böhm et al.*, 2001; *Schwarb et al.*, 2001; *Meerkötter et al.*, 2004; *Auer et al.*, 2007) are of differing spatial and temporal resolution and extent. Furthermore, given that a coupling scheme between RCM data and the mass balance model can be found, this would allow to use data from RCM climate-scenario runs. However, RCM data are biased (e.g. *Kotlarski et al.*, subm). Although often used as a reference to RCM data, gridded climatologies are also not free of errors, in particular in high mountain regions where measurements are sparse. Indeed, it would be interesting to combine both data sources, for instance to correct biases in the RCM data. Nevertheless, here we focus on RCM output because we believe that the incorporation of gridded climatologies should be the objective of pursuing studies.

In the present study, the mass balance model is driven by the RCM output through an offline coupling scheme and there is no feedback to the RCM. The spatial resolution of the RCM output is increased to the resolution of the mass balance model (100 m) through a combination of interpolation techniques and sub-grid parameterizations. The RCM output is treated as a gridded field of virtual climate stations at the grid box elevations. In a first step, this coarse field which accounts for large scale variability of the meteorological conditions is smoothed by means of interpolation techniques. We applied different interpolators to specify their influence on modeled mass balance. In a second step, sub-grid scale variability is accounted for by means of sub-grid parameterizations. The applied parameterizations are different for each of the three variables (T_a, P and S_{in}) as their spatial variability is

different and because they do not depend on the same factors. For T_a and P altitudinal gradients have been applied as a simple sub-grid parameterization. Based on altitudinal gradients (Γ_{Ta} and Γ_P) and the RCM grid box elevations, the RCM values will be rescaled to a higher resolution DTM. While the dependency of T_a with altitude is rather strict, it is less pronounced for P: Precipitation gradients are spatially variable (*Sevruk*, 1997) and measurements of solid precipitation at the elevation of glaciers are highly uncertain (e.g. *Sevruk*, 1985b, 1997). For S_{in}, the modeling approach is two fold: the RCM provides the cloud cover over a larger region while a radiation code (e.g. *Corripio*, 2003) based on the 100 m resolution DTM gives the spatial variability of the potential radiation for each day of the year. This approach allows to consider topographic influences on global radiation accurately while maintaining the overall reduction due to clouds (*Paul et al.*, 2008).

The applied downscaling procedure includes simplified parameterizations. To test their performance and to allow for a better assessment of the modeled mass balance distribution, the downscaled fields of S_{in}, T_a and P (i.e. the model input) are compared to measurements. These downscaled fields are in the following indicated with a hat: $\hat{T}_a$, $\hat{P}$, $\hat{S}_{in}$. The same notation is also applied to $\hat{n}$ and $\widehat{DTM}_{REMO}$, being cloudiness (n) and the REMO topography interpolated from the native REMO resolution to 100 m.

8.3. Model Domain and Data

8.3.1. Spatial and Temporal Model Domain

The mass balance calculation is conducted for the entire Swiss Alps which cover an area of approximately 25000 km^2. Together with adjacent areas they are represented by a DTM of 3000×2000 cells at a spatial resolution of 100 m (Figure 8.1). The DTM is a composite of two DTMs, both resampled to 100 m horizontal resolution: the Swiss Alps (including all the modeled glaciers) are represented by the DTM25 level2 from Swisstopo (a DTM with 25 m resolution and glacier surfaces mostly from the mid nineties) and the surrounding terrain by the SRTM 90 m DTM, generated in the year 2000.

The present study is based upon the Swiss Glacier Inventory from 1973 (*Müller et al.*, 1976) which is the most complete data set with respect to glacier polygons currently available for the area of interest. The glacierized area in Switzerland amounted to 1280 km^2 in 1973 and consisted of approximately 2000 individual glaciers (*Müller et al.*, 1976; *Paul et al.*, 2004). Glaciers of respectable size (> 0.5 km^2) are located within a perimeter reaching from 45.9 °–47.0 °N and from 6.9 °–10.4 °E (Figure 8.1). The digital glacier polygons applied in this study are based upon the inventory from *Müller et al.* (1976) which was revised by *Maisch et al.* (1999) and *Wipf* (1999) and digitized in the framework of the new Swiss glacier inventory project (*Paul*, 2007). Every polygon has a unique index and for the mass balance computation, a rasterized glacier mask (100 m grid spacing) is created by assigning the indices to all the grid cells being located within the corresponding glacier polygon. Both the DTM and the glacier polygons are given in the conformal Swiss Grid projection.

The temporal model domain was chosen to be 25 September 1979 till 5 October 2003. In the following, this time span is referred to as the calculation period. Thus, the model runs are conducted over 24 mass balance years (a mass balance year is defined here as starting 1 October and ending 30 September).

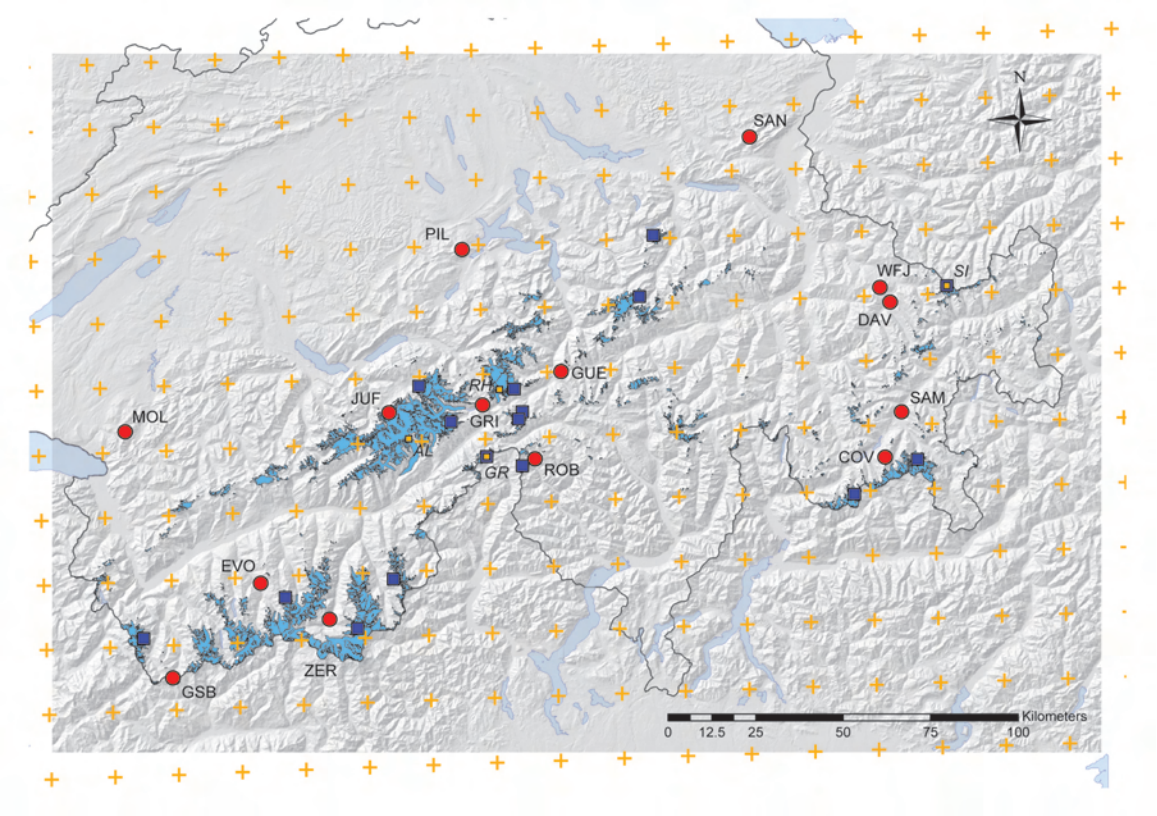

Figure 8.1.: Model domain with the full DTM. Glaciers are in light blue and glaciers with available stake measurements are marked with blue squares. Small orange squares mark glaciers where results of this study have been compared to data from *Huss et al.* (2008a), abbreviations (*in italic*) refer to: AL = Great Aletsch glacier; RH = Rhône glacier, GR = Gries glacier and SI = Silvretta glacier. Orange crosses denote the centers of the REMO grid boxes. Red dots show locations of the MeteoSwiss weather stations used for validation (altitude in m a.s.l.): COV = Corvatsch, 3315; DAV = Davos, 1590; EVO = Evolène, 1825; GRI = Grimsel-Hospiz, 1980; GSB = Grand-Saint-Bernard, 2472; GUE = Gütsch, 2287; JUF = Jungfraujoch, 3580; MOL = Molèson, 1972; PIL = Pilatus, 2106; ROB = Robiei, 1898; SAM = Samedan, 1705; SAN = Säntis, 2490; WFJ = Weissfluhjoch, 2690 and ZER = Zermatt, 1638. For orientation, the border of Switzerland is shown in black and lakes in light blue.

8.3.2. Input Data

The mass balance model is driven by the output of a regional climate model (RCM). For this purpose, we used version 5.5 of the hydrostatic RCM REMO (e.g., *Jacob et al.*, 2001), developed by the Max Planck Institute for Meteorology, Hamburg. REMO was selected because studies on the uncertainties in REMO exist (e.g., *Kotlarski et al.*, 2005), its performance in high-elevation areas of the European Alps has already been evaluated by *Kotlarski et al.* (subm) and first mass balance calculations using REMO output have been performed as well (*Paul and Kotlarski*, subm). In this study we use the output from a model run conducted over a larger portion of Central Europe (reaching from approximately 41 ° – 50 °N and from 1 °W – 17 °E) at a spatial resolution of 1/6 ° (approx. 18 km) on a rotated

spherical grid. The experiment covers the time span 1958 – 2003. At the lateral boundaries REMO is driven by ERA40 re-analysis data (*Uppala et al.*, 2005) (from 1 January 1958 to 31 July 2002) and by the operational analysis of the ECMWF (1 August 2002 to 31 December 2003). The internal model time step is 100 seconds and the model output is stored as hourly means. From the latter daily means and sums are computed and used in this study. For the mass balance computation, we use REMO output on 2 m air temperature (T_a), precipitation (P) and cloudiness (n).

8.3.3. Data for validation

The parameters $\hat{T}_a$, $\hat{P}$ (cf. Section 8.4.2), $\hat{S}_{in}$ (cf. Section 8.4.1) are compared to measurements. For the time period 1 January 1981 to 31 December 2003 we acquired daily means of measured S_{in}, P and T_a from 14 weather stations in the Swiss Alps (Figure 8.1). The stations are all operated by MeteoSwiss and are located at elevations from 1590 to 3580 m a.s.l. The sample size consists of summit stations, stations on passes and valley stations.

Modeled values of mass balance are compared to stake measurements on 16 different glaciers (Figure 8.1). Data have been acquired from *Müller and Kappenberger* (1991) (1 glacier) and *Glaciological Reports* (1992-2008) (3 glaciers). Data on measurements on Morteratsch have been provided by J. Oerlemans. Stake measurements from 11 other glaciers are from own measurements, conducted during the summer of 2002. Melt measurements on four glaciers during the summer 2003 are from *Zemp et al.* (2005).

The temporal variability of the modeled mass balance is compared to mean annual mass balances of 9 Alpine glaciers (two of them, Silvretta and Gries, being located in Switzerland) (*WGMS*, 2007) and to the results of *Huss et al.* (2008a) who applied a combined approach of geodetic mass balance measurements, stake measurements and mass balance modeling to obtain long term mass balance series for 4 Swiss glaciers: Silvretta, Great Aletsch, Gries and Rhone (cf. Figure 8.1).

8.4. Computation of the Mass Balance

8.4.1. The Mass Balance Model

The applied glacier mass balance model, presented in the following, is a simplified version of more sophisticated energy balance approaches. However, it still includes one of the main features of energy balance models, a separate treatment of shortwave radiation and energy fluxes depending strongly on air temperature (turbulent and longwave fluxes). In particular the calculation of the latter is strongly simplified whereas the calculation of shortwave radiation is similar to more complex energy balance approaches (e.g., *Arnold et al.*, 1996).

General outline

Apart from the DTM and the glacier outlines (Section 8.3.1), the model basically relies on the three meteorological parameters T_a, S_{in} and P. The model runs at daily steps, and the

cumulative mass balance b_c on day $t+1$ is calculated for every time-step and over each grid cell of the DTM according to *Oerlemans* (2001):

$$b_c(t+1) = b_c(t) + \begin{cases} \Delta t \cdot (-E)/l_m + P_{solid} & \text{if } Q_m > 0 \\ P_{solid} & \text{if } Q_m \leq 0 \end{cases} \tag{8.1}$$

where t is the discrete time variable, Δt is the time-step, l_m is the latent heat of fusion of ice ($334\,\mathrm{kJ\,kg^{-1}}$) and P_{solid} is solid precipitation in meter water equivalent (m w.e.). The energy available for melt (Q_m) is calculated as follows:

$$Q_m = (1-\alpha)S_{in} + C_0 + C_1 T_a \tag{8.2}$$

where α is the albedo of the surface, S_{in} is the global radiation, T_a is the air temperature (in °C at 2m above ground and outside the glacier boundary layer) and $C_0 + C_1 T_a$ is the sum of the longwave radiation balance and the turbulent exchange linearized around the melting point (*Oerlemans*, 2001). C_1 is set to $10\,\mathrm{Wm^{-2}\,K^{-1}}$ according to the recommendation of *Oerlemans* (2001). C_0 was used as a tuning factor and was adjusted to fit measurements on Morteratsch glacier for the mass balance year 1998/99 (*Klok and Oerlemans*, 2002), yielding best fit of observed and modeled mass balances at $-45\,\mathrm{Wm^{-2}}$. In Eq. (8.2) T_a actually stands for ΔT which equals to the difference between T_a and the glacier surface temperature (T_{surf}). In the present model, T_{surf} is fixed to the melting point (0 °C) and hence $\Delta T = T_a$. Consequently in winter the modeled energy balance is not zero but often very negative which is obviously wrong. However, according to Eq. (8.1), negative Q_m are of no influence to the mass balance.

Accumulation

In the present mass balance model the source of accumulation is solid precipitation, redistribution of snow by wind or avalanches is not considered. Refreezing is not taken into account and any melt water and rainfall is immediately removed from the glacier. A threshold temperature (T_{snow}) of 1.5 °C in combination with a transition range of 0.5 °C is used to distinguish snowfall and rain. The resulting gradual transition from snow to rain in-between 100% snow at $T_a = 1$ °C and 0% snow at $T_a = 2$ °C agrees fairly well with the long term observations on air temperature and snow – rain transition, compiled by *Rohrer* (1989) for the weather station in Davos (1590 m a.s.l., see Figure 8.1).

Incoming solar radiation

Global radiation (S_{in}) is calculated from potential clear sky global radiation ($S_{in,clr}$) and cloudiness (n). The latter is acquired from REMO output whereas $S_{in,clr}$ is computed through a radiation code (*Corripio*, 2003). Global radiation is directly available from REMO (S_{in}^{REMO}). However, the approach described in the following seems easier to apply since S_{in}^{REMO} is at 1/6 ° spatial resolution and does not consider slope and aspect. Furthermore, mean S_{in} obtained from our approach using only cloudiness from REMO and S_{in}^{REMO} yield similar deviations to measured mean S_{in} at the 14 selected weather stations (cf. Table 8.2).

$S_{in,clr}$ is computed according to *Corripio* (2003) and *Iqbal* (1983). $S_{in,clr}$ is the sum of diffuse ($S_{in,clrdif}$) and direct radiation ($S_{in,clrdir}$) which are both calculated separately. For

the latter all effects of surface topography including shading are considered. Daily means of both components of $S_{in,clr}$ are obtained from a calculation at a temporal resolution of 30 minutes. This calculation is only performed once in the pre-processing and the resulting 365 arrays of daily mean $S_{in,clrdif}$ and $S_{in,clrdir}$ for all days of the year are stored (In leap years the arrays of day number 365 are simply used twice). The outsourcing into a preprocessing procedure allows for a strong reduction of computation time. However, atmospheric transmission coefficients (such as for Rayleigh scattering, water vapor and other gases, aerosol extinction etc.) are applied in the pre-processing only for a standard atmospheric composition and can not be altered later. Only attenuation of clouds (τ_{cl}) is calculated for every individual time step in the actual model run according to a relationship established by *Greuell et al.* (1997) based on measured S_{in} and observed n on the Pasterze glacier in the Austrian Alps:

$$\tau_{cl} = 1.0 - 0.233n - 0.415n^2 \tag{8.3}$$

Cloudiness varies from 0 (cloud free) to 1 (complete overcast). τ_{cl} is then used to compute S_{in} from $S_{in,clr}$:

$$S_{in} = S_{in,clr}\tau_{cl} \tag{8.4}$$

where $S_{in,clr} = S_{in,clrdif} + S_{in,clrdir}$. A lower threshold is applied in order to avoid reduction of S_{in} to almost zero on grid cells that receive little or no direct radiation due to shading or exposition: Whenever for a particular grid cell S_{in}, calculated according to Eq. (8.4), falls below $S_{in,clrdif}$, then: $S_{in} = S_{in,clrdif}$.

Global radiation calculated according to the above described approach is in the following denoted as $\hat{S}_{in}$ since the calculation is based upon $\hat{n}$ which is interpolated from the REMO output (cf. Section 8.4.2).

Albedo parameterization

The ice surface is always treated as debris-free. Depending if the surface consists of snow, firn or ice, three different fixed values for the surface albedo are used in the model: $\alpha_s = 0.72$, $\alpha_f = 0.45$ or $\alpha_i = 0.27$. In the test runs for Morteratsch glacier $\alpha_s = 0.72$ was used and resulted in reasonable melt rates for the snow cover. The firn albedo is of rather small influence to the model result while α_i is decisive to the model output. During the test runs, $\alpha_i = 0.34$ was used according to *Klok and Oerlemans* (2002). However, this value seems rather high to represent a mean for all Swiss glaciers (e.g. *Paul et al.*, 2005) and we apply $\alpha_i = 0.27$ in this study. At the start of the calculation the albedo is set to α_i for the entire glacierized area, and for any snow accumulation α_s is used. Accumulated snow is assigned α_f when its age exceeds 1 year and after 2 years its albedo is again lowered to α_i. The idea behind this parameterization is an approximation of the albedo lowering related to the snow to ice conversion. Other aspects of the snow to ice transition are not addressed here. Although the model runs at daily steps, surface albedo is allowed to change somewhere in the middle of a time step if, for instance, the snow or firn cover remaining from the last time step was already very thin or after a small snow fall event.

Limitations of the mass balance model

Simplifications in the model make it impossible to calculate reasonable mass balance values for all types of glaciers. For instance, glaciers are regarded as debris free and thus mass balance of debris covered glaciers can not be modeled. For simplicity, model runs are performed for all glaciers of the Swiss Alps but most of the model output is provided only for a selection of glaciers where reasonable mass balance calculation is expected. These glaciers are selected manually based upon the following conditions: (a) no or little debris cover, (b) no or little influence of avalanches, (c) mass loss restricted to melting and (d) considerable size (area $> 1\,\mathrm{km}^2$). 94 glaciers were found to meet these conditions. The selected glaciers cover an area of $610\,\mathrm{km}^2$, or roughly 50% of the total glacierized area.

8.4.2. Downscaling of the REMO Output

The spatial resolution of the input data (REMO) and the DTM differs greatly and downscaling has to be applied to make the daily fields of REMO-output applicable to the mass balance calculation. In order to do so we treat the centers of the REMO grid cells as virtual weather stations. All data related to the grid cells are assigned to their respective centers. The downscaling procedure includes two steps: (1) The values in-between the virtual weather stations are interpolated to the DTM by means of interpolation techniques as described in the following paragraph. (2) Sub-grid parameterizations are applied.

The results of different interpolation schemes may vary and thus influence mass balance distribution. Consequently, we apply three widely used techniques: The Nearest Neighbor interpolation (NN), Inverse Distance Weighting (IDW) and Thin Plate Splines (TPS). The first was applied because it basically alters only the spatial resolution of the data while preserving the original values: NN results in areas of identical value and location, as well as near-identical shape of the original REMO grid boxes. However, these areas are composed of 100 m cells. The disadvantage of NN are step-changes at the boundaries of the areas representing the original $1/6\,^\circ$ grid boxes. On the contrary, IDW and TPS interpolate in-between the virtual weather stations by generating new values. IDW interpolates by predicting new values located inside the range of the original values while TPS may result in new values outside this range (*Burrough and McDonnell*, 2004). IDW as applied here is an exact interpolator; predicted values at the virtual weather stations are always identical to the original values. TPS is an exact interpolator but within smoothing limits (*Burrough and McDonnell*, 2004). Both interpolators achieve smooth surfaces and consequently, a prerequisite to their application is that the underlying (unknown) surface is smooth (*Burrough and McDonnell*, 2004). Meteorological quantities are not necessarily distributed smoothly in space. However, in our case the interpolation schemes are not used to reproduce an unknown "real" distribution since this is not possible from the RCM output alone. They are applied to generate smooth changes from one virtual weather station to the next because such a pattern is still more realistic than abrupt breaks from one RCM grid box to the next. The key question is which interpolator performs good in generating smooth surfaces while preserving characteristics of the REMO data, such as meteorological means and wet day frequency (*WET*).

Interpolations have been carried out with the GRIDDATA routine included in the IDL distribution (*RSI Research Systems Inc.*, 2004). To allow for a faster computation in GRID-

DATA the maximum number of nodes used for interpolation was reduced to 12 (IDW) and 24 (TPS). A lower threshold for interpolation with TPS resulted in interpolation artifacts. In the following, the term "interpolated" refers to the application of NN, IDW or TPS. For reasons of simplicity, only one interpolation technique is used in the course of a model run.

Downscaling of air temperature

Values of T_a strongly depend on the elevation of the respective REMO boxes (Figure 8.2a). Prior to the interpolation this dependence on altitude has to be removed. The values for T_a at the virtual weather stations are reduced to a standard altitude $H_0 = 0\,\text{m}$ a.s.l. by means of a fixed altitudinal gradient (atmospheric lapse rate) $\Gamma_{Ta} = -0.0065\,^{\circ}\text{C}\,\text{m}^{-1}$. The value of Γ_{Ta} was chosen according to the slope of the linear regression presented in Figure 8.2a.

$$T_a^{red} = T_a - DTM_{REMO} \cdot \Gamma_{Ta} \tag{8.5}$$

where T_a^{red} is the reduced air temperature, DTM_{REMO} is the REMO topography at native resolution. T_a^{red} is then interpolated to a 100 m array ($\hat{T}_a^{red}$). The influence of elevation is finally reintroduced, based on the 100 m DEM:

$$\hat{T}_a = DTM\,\Gamma_{Ta} + \hat{T}_a^{red} \tag{8.6}$$

where DTM is the 100 m DTM. Of course a reduction to a standard level is superfluous when using NN and for simplicity all interpolation techniques are treated identically.

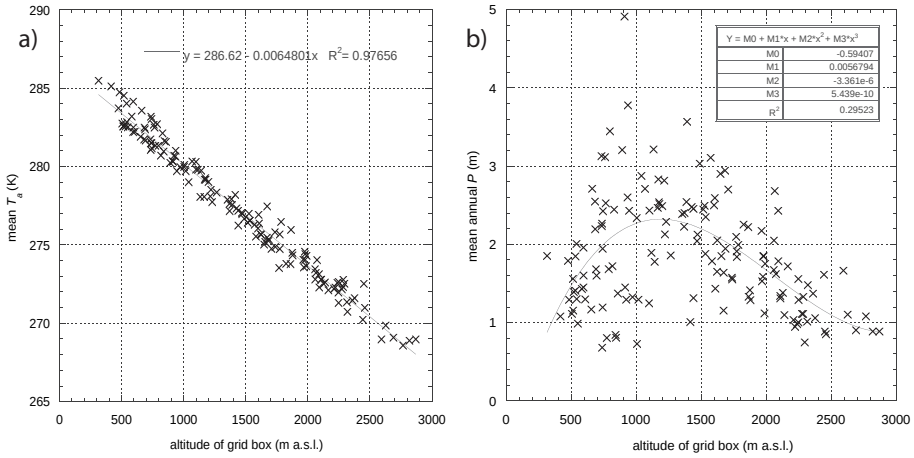

Figure 8.2.: Plot a): Mean T_a of the time period 1979–2003 for all REMO grid boxes of the Swiss Alps, plotted against grid box elevation. Plot b): Mean annual P of the time period 1979–2003 for all REMO grid boxes of the Swiss Alps, plotted against grid box elevation (number of grid boxes = 150).

Downscaling of precipitation

Precipitation is a critical parameter due to its high spatial and temporal variability and large uncertainties in the measurements. Furthermore, snow is redistributed by wind and

avalanches, leading to complex accumulation patterns on glaciers (e.g. *Machguth et al.*, 2006a; *Plattner et al.*, 2006). In this study we will not consider the latter effects (c.f. Section 8.4.1) but rather aim on parameterizing the general characteristics of precipitation distribution. Existing high resolution precipitation climatologies for the Alps (e.g. *Kirchhofer and Sevruk*, 2001; *Schwarb et al.*, 2001) show a distinct variability on the local scale with higher values on the ridges and dryer valleys. To derive such a pattern we apply a precipitation gradient (Γ_P) for sub-grid parameterization.

The selection of an appropriate value for Γ_P is difficult because Γ_P is spatially variable in the Alps (*Sevruk*, 1997; *Schwarb*, 2000) and values are uncertain due to the large errors in the measurements of P. *Sevruk* (1997) assessed the spatial variability of Γ_P in the Swiss Alps and rejected all measurements of P at sites above 2700 m a.s.l. because they were considered too uncertain. Furthermore, horizontal and vertical variability of P can not be completely distinguished (*Schwarb*, 2000). An attempt to derive Γ_P from the REMO data, similar to the temperature lapse rate, yields no applicable results: Between 400 and 1000 m a.s.l. P increases with elevation whereas above 1500 m a.s.l. the trend is negative (Figure 8.2b). This picture has three reasons: (1) The RCM systematically dislocates precipitation from ridges to the foreland, causing a moderate negative precipitation bias at high-elevation sites and a strong positive bias at medium altitudes (*Kotlarski et al.*, subm). (2) The REMO model domain contains the dry inner-alpine region with low precipitation at high altitudes. In the spatial mean, this contributes to the reversed precipitation-altitude gradient as derived from the RCM. (3) At the spatial resolution of REMO the variability of P on a horizontal scale is a major component of total variability among the grid boxes.

For Γ_P we finally applied the value used by *Kirchhofer and Sevruk* (2001) for their precipitation map of Switzerland ($\Gamma_P = 0.0008\,\mathrm{m\,a^{-1}\,m^{-1}}$). The idea of using locally variable Γ_P as provided by *Schwarb* (2000) or *Sevruk* (1997) was put aside for reasons of simplicity. Note that the application of Γ_P preserves mean P over each grid box, systematic biases in precipitation from REMO, discussed above under point (1) are not corrected for.

Since Γ_P is given in $\mathrm{m\,a^{-1}\,m^{-1}}$, but has to be applied to daily precipitation sums, it is converted to a dimensionless precipitation correction array ($\hat{\Gamma}^*_P$). This is done prior to the model run, based on DTM, the mean annual precipitation for the calculation period ($\hat{P}_{mean}$) and the REMO topography ($\widehat{DTM}_{REMO}$). The latter two variables are interpolated to a 100 m array from P and elevation at the virtual weather stations, respectively:

$$\hat{\Gamma}^*_P = \frac{\hat{P}_{mean} + ((DTM - \widehat{DTM}_{REMO}) \cdot \Gamma_P)}{\hat{P}_{mean}} \tag{8.7}$$

In the model run, precipitation distribution at a specific date is then calculated to $\hat{P} = \hat{P}_d \hat{\Gamma}^*_P$, where $\hat{P}_d$ is the precipitation sum of the current day interpolated from the virtual weather stations to a 100 m array. A reduction of P to a standard level prior to the interpolation could even exaggerate the systematic biases inherent to the REMO data and is thus not performed. Negative $\hat{P}$-values that may occur when using TPS are set to zero.

For illustration, the interpolation and downscaling scheme is applied to mean annual P (Figure 8.3a), resulting in mean annual $\hat{P}$ depicted in Figure 8.3b.

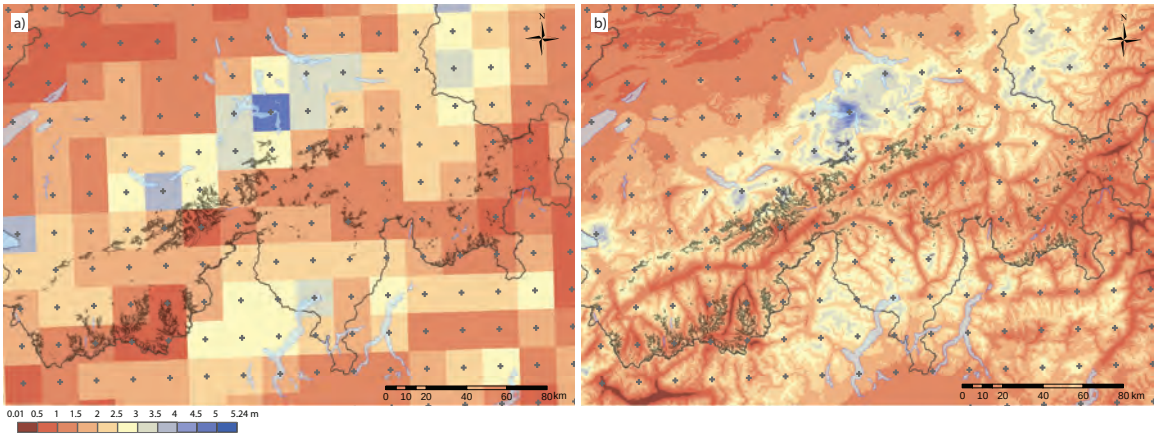

Figure 8.3.: Plot a: Mean annual P over the temporal and spatial model domain at the native REMO resolution. Plot b: Mean annual $\hat{P}$ after interpolation with IDW and application of the altitudinal gradient. For orientation, the border of Switzerland is shown in black, glacier outlines in gray and lakes in light blue. Note that the maximum value in plot a) is $4.9\,\mathrm{m\,a^{-1}}$ and no other grid box exceeds $3.8\,\mathrm{m\,a^{-1}}$ (cf. Figure 8.2b).

Downscaling of cloudiness

Mean cloudiness (1979–2003) for the individual REMO grid boxes reveals only a weak positive correlation with elevation (yielding $R^2 = 0.17$ in a linear regression). Consequently, cloudiness is interpolated directly from the virtual weather stations to a 100 m array ($\hat{n}$) and an altitudinal gradient is not applied. Attenuation of clouds is then calculated from interpolated cloudiness and applied to obtain $\hat{S}_{in}$ (cf. Section 8.4.1).

8.4.3. Implementation

A flow chart of the processing steps is given in Figure 8.4. The structure is optimized to keep computation time short because the calculation of solar radiation (Section 8.4.1) and the three daily interpolations of the REMO data (cf. Section 8.4.2) are time consuming.

The calculation of clear sky global radiation is conducted in the course of the preprocessing and on the full DTM in order to allow for the computation of shading. From the resulting arrays of $S_{in,clrdif}$ and $S_{in,clrdir}$ the values for the glacierized cells are extracted and converted into a simple one dimensional columnar format. Furthermore, the DTMs glacierized cells are also transferred into columnar format. These files are then used for input in the actual model run. Hence, the mass balance calculation and the related interpolations of the REMO data are performed only for the glacier surfaces of the Swiss Alps.

During the model run the measured data at the selected weather stations are consecutively compared to interpolated REMO data at the respective grid cells. In order to compare values of S_{in} being measured normal to a horizontal surface, the DTM is set to equal altitude over 3×3 matrices at the locations of the stations prior to the radiation calculation.

The individual stake measurements are compared to modeled mass balance at the corresponding grid cell whenever an observation date is encountered.

The final output includes the comparison of measured meteorological parameters to $\hat{T}_a$, $\hat{P}$ and $\hat{S}_{in}$, of measured and modeled mass balance at individual stakes as well as modeled

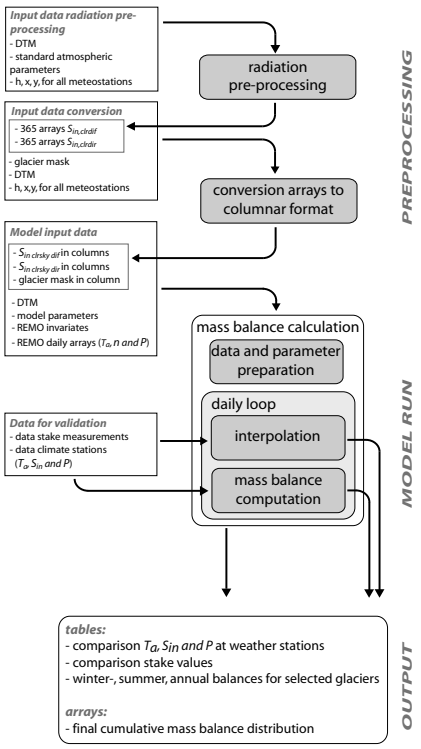

Figure 8.4.: Flow chart of the model structure and the main input and output components.

winter-, summer- and annual balances for the 94 selected glaciers and the 24 mass balance years. The final cumulative mass balance distribution is written to an array and division by the number of mass balance years (24) yields mean annual mass balance distribution.

8.5. Results

The presentation of modeled mass balances (Section 8.5.1) and the comparison of meteorological parameters (Section 8.5.2) are accompanied by a comparison of mean values for all three interpolation schemes. Figures and maps are based upon REMO data interpolated from IDW. The comparison of temporal variability (Section 8.5.2) and stake measurements (Section 8.5.2) is restricted to mass balances modeled from IDW.

8.5.1. Modelled Mass Balance Distribution

Two example maps of the resulting mean annual mass balance distribution over the modeled time period are given: The region around Great Aletsch glacier (Figure 8.5) and the south eastern part of Valais (Figure S1 in the auxiliary material). Glacier specific mean annual mass balances for all selected glaciers are depicted in Figure 8.6. In total, 23 glaciers have positive and 71 glaciers negative balances.

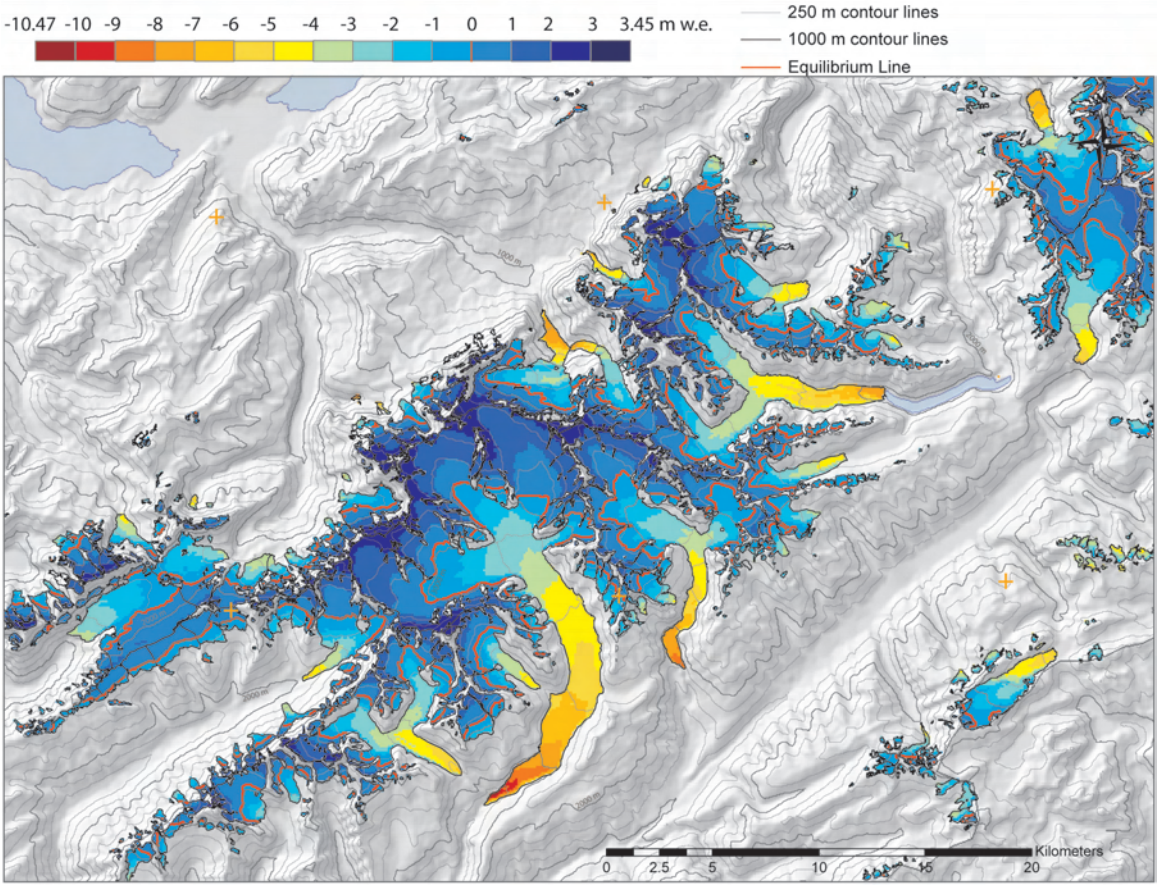

Figure 8.5.: Mean modeled annual mass balance distribution for all glaciers of the region around Great Aletsch glacier.

A visual assessment of Figures 8.5, S1 and 8.6 exhibits regional features: Positive balances are dominant at the entire northern edge of the Swiss Alps while strongly negative balances are dominating in the east. For the remaining regions mass balances are predominantly negative with adjacent glaciers showing often similar values. Mean mass balances around Zermatt reach from extremely negative (-2.87 m w.e.) to very positive (0.7 m w.e.) values. However, some spatial correlation can be found with predominantly negative values to the south and positive values to the east.

The modeled equilibrium line (EL) is mostly located on the glaciers, dividing them in accumulation and an ablation areas. The equilibrium line altitude (ELA) resulting from the model run is generally lower at the northern edge, reaching down to 2600–2700 m a.s.l. for some glaciers while around Zermatt ELAs culminate at 3200–3400 m a.s.l.

Mean modeled mass balance for all glacierized DTM-cells varies with the interpolator (see Table 8.1). NN and TPS yield similar results (-1.08 m w.e. and -1.21 m w.e., respectively) while IDW results in a less negative mean of -0.79 m w.e. The values do only shift slightly when the mean mass balance is obtained only from cells of the 94 selected glaciers: -1.11 m w.e. (NN), -1.21 m w.e. (TPS) and -0.76 m w.e. (IDW). Subtracting IDW from TPS yields a differential array of lower standard deviation than NN–IDW or NN–TPS (Table 8.1),

Table 8.1.: Comparison of mean mass balances computed with the three interpolation schemes and the related standard deviations.

	all glaciers	selected glaciers
NN - IDW	-0.27 ± 0.58	-0.35 ± 0.53
NN - TPS	0.14 ± 0.63	0.10 ± 0.60
IDW - TPS	0.41 ± 0.38	0.45 ± 0.37

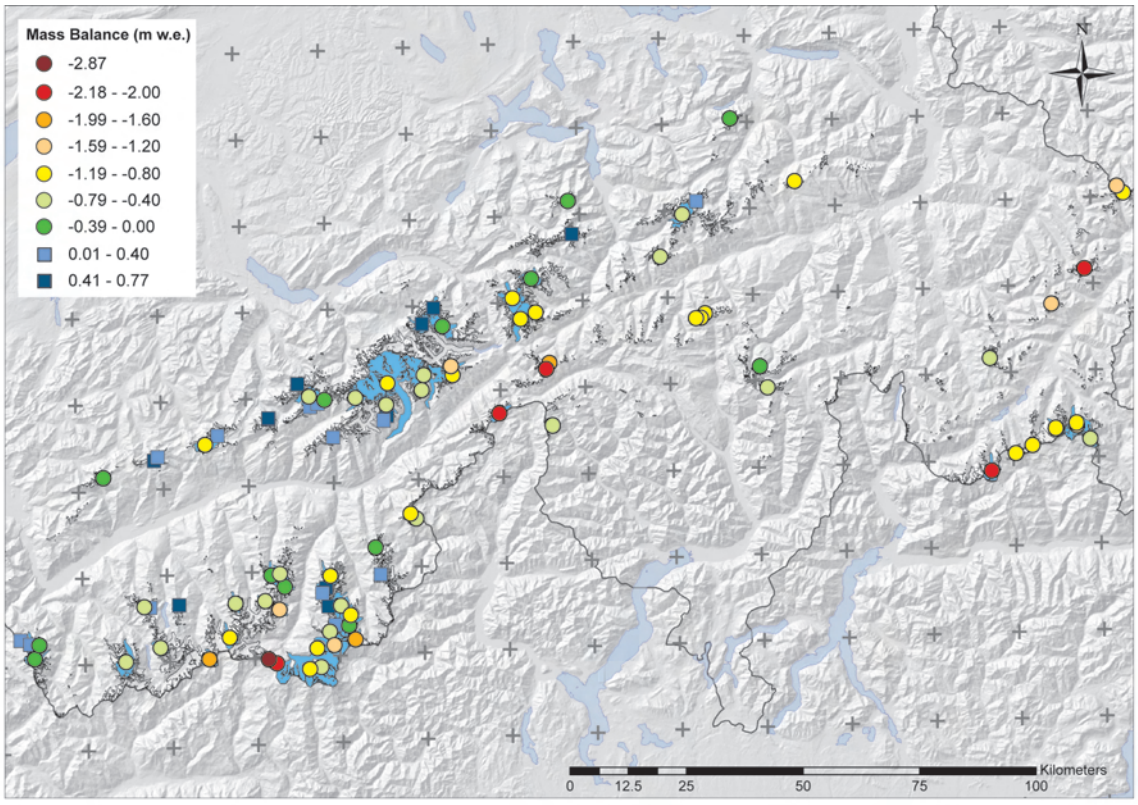

Figure 8.6.: Mean annual mass balances over the calculation period for the 94 selected glaciers. Circles denote negative and rectangles positive mean balances. Glaciers that have not been selected are depicted by hollow glacier outlines.

indicating that the spatial patterns of mass balance distribution are more similar between IDW and TPS than compared to NN. Since the former two interpolators generate smooth surfaces their lower standard deviation at pixel resolution was to be expected.

8.5.2. Validation

Modeled mass balance and annual variability

The data from *Huss et al.* (2008a) are compared to the modeled temporal variability of annual, winter and summer balance on the four glaciers investigated by *Huss et al.* (Figure 8.7a). Annually averaged balances for the 94 selected glaciers are compared to the data

from *Huss et al.* (2008a) as well as from *WGMS* (2007) in Figure 8.7b. Annual balances from Figure 8.7a are depicted as well to allow for a direct comparison. It becomes obvious that the curve built from the mean of the 94 glaciers agrees well to the *Huss et al.* and *WGMS* data whereas the curve built from the mean of the four glacier sample is systematically lower by approx. 0.25 to 0.75 m w.e. The temporal variability of both sample sizes are similar. Additionally, modeled annual, summer and winter balance are compared in a scatter plot (Figure S1a in the auxiliary material). A linear regression of the annually averaged balance for the 94 glaciers against the *WGMS* data yields $R^2 = 0.82$. The data from *Huss et al.* (2008a) agree somewhat better to the *WGMS* data ($R^2 = 0.89$) while the slope of both regressions is similar (1.12 and 1.09, respectively) (See Figure S1b in the auxiliary material for a visualization of the linear regressions).

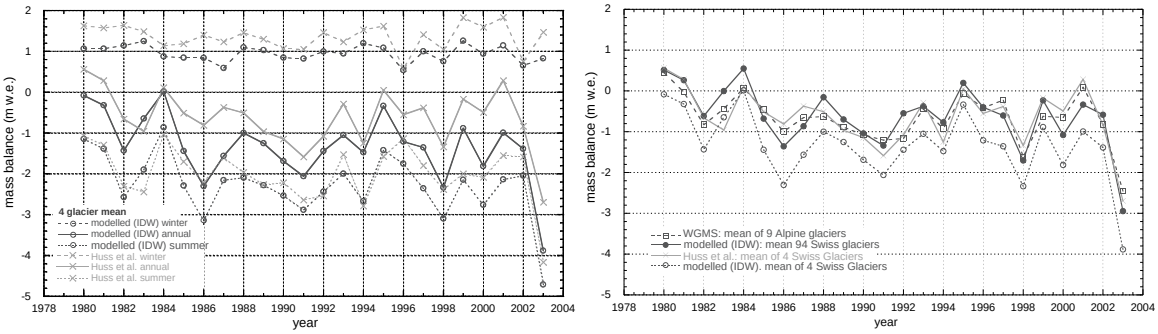

Figure 8.7.: a) Modeled winter, summer and annual balances over the calculation period compared to the values from *Huss et al.* (2008a). Values are the mean of the four glaciers: Grosser Aletsch, Gries, Rhône and Silvretta. b) Annual mean mass balances for the 94 selected glaciers compared to annual means from *Huss et al.* (2008a) and *WGMS* (2007). To allow for a direct comparison to a), modeled mean annual balance for the four glaciers sample size is depicted as well.

Stake Readings

Stake readings used for model validation have been divided into three subgroups and are depicted individually: (1) Stake measurements that are conducted during one summer and thus are mainly restricted to melt are compared to modeled values in Figure 8.8a. (2) On Claridenfirn both winter and annual balances are available and the data are compared in Figure 8.8b. (3) Data from stakes that are visited only once at the end of a balance year, representing the sum of accumulation and ablation processes are shown in Figure 8.8c. All modeled values are obtained from IDW.

Values in Figure 8.8a are close to identity with the exception of seven outliers where the model strongly underestimates summer melt. All measurements depicted in Figures 8.8b and c are systematically underestimated by the model. The shift toward modeled mass balances which are too negative is most pronounced for stake measurements from Silvretta and Gries glacier.

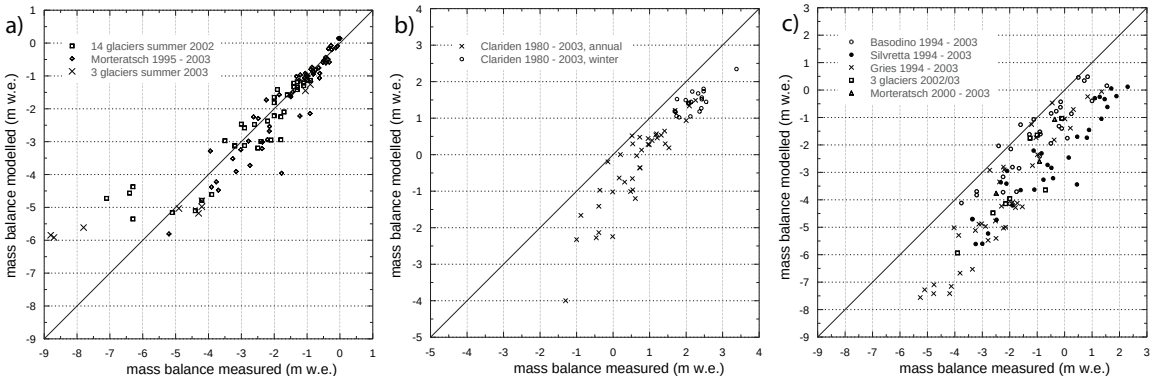

Figure 8.8.: Scatterplot of observed and modeled mass balances at stake locations. a) comparisons for stake readings of summer balances, dominated by melt processes. b) readings from Claridenfirn where winter and annual balances are available. c) stake readings that refer to a full balance year and thus incorporate both accumulation and ablation.

Modelled Meteorological Parameters

A comparison of measured T_a, P and S_{in} averaged over all 14 weather stations with $\hat{T}_a$, $\hat{P}$ and $\hat{S}_{in}$, averaged over the DTM cells corresponding to the location of the weather stations for all three interpolators is given in Table 8.2. Furthermore, $\hat{T}_a$, $\hat{P}$ and $\hat{S}_{in}$ averaged over the entire glacierized perimeter are shown as well. Wet day frequency (WET) averaged over the 14 stations and the corresponding grid cells, respectively, is also shown in the table and is here defined as the percentage of days with precipitation higher than 0.1 mm.

Table 8.2.: Comparison of modelled and measured meteorological parameters obtained from the three interpolation schemes. The wet-day frequency (WET) is given here as the percentage of days with $P > 0.1\,\text{mm}$ or $\hat{P} > 0.1\,\text{mm}$, respectively.

parameter	interpol.	weather stations		glac. perim.
		meas.	mod.	
T_a	NN		-0.81	-5.79
	IDW	0.67	-0.88	-5.73
	TPS		-0.74	-5.69
P	NN		0.0051	0.0050
	IDW	0.0041	0.0053	0.0057
	TPS		0.0045	0.0048
WET	NN		52%	-
	IDW	49%	63%	-
	TPS		51%	-
S_{in}	NN		168	139
	IDW	156	172	145
	TPS		165	138
S_{in}^{REMO}	NN	156	143	-

Mean measured values of all three parameters are generally overestimated but the amount of the overestimation depends on the chosen interpolation scheme. All three interpolators

show similar $\hat{T}_a$-values while for $\hat{P}$ and $\hat{S}_{in}$ only the values obtained from NN and TPS are similar and closer to the measurements than from IDW. Differences among the interpolation schemes are most pronounced for precipitation: when TPS is applied to calculate $\hat{P}$, precipitation over the glacier perimeter is reduced by 16% compared to IDW. Wet day frequency is also clearly higher when using IDW while both NN and TPS are in close agreement to the observations.

Mean measured T_a, P and S_{in} at the individual weather stations are compared to mean $\hat{T}_a$, $\hat{P}$ and $\hat{S}_{in}$ at the respective DTM cells in three scatter plots (Figures 8.9a, b and c). Mean values are calculated over the number of days with available data at the respective stations. Air temperature correlates best, a weak correlation can be established between P and $\hat{P}$ while no correlation exists for global radiation. T_a is underestimated by $\hat{T}_a$ while the other two parameters are overestimated at most stations.

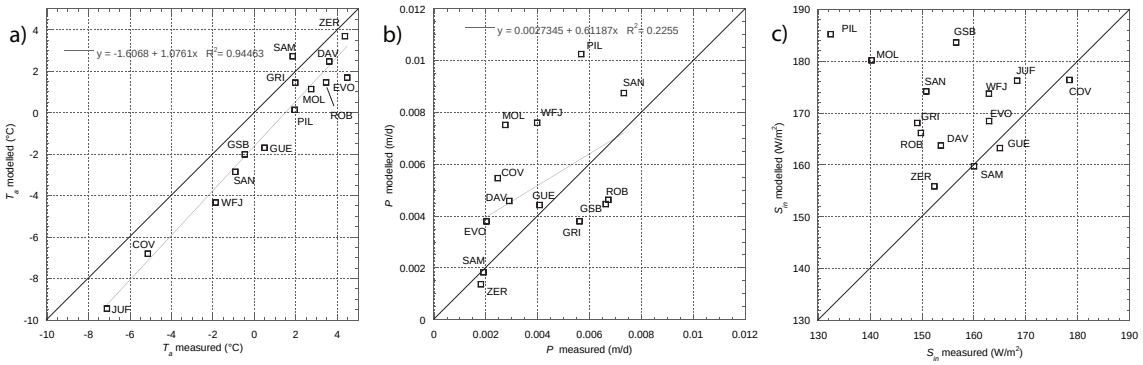

Figure 8.9.: Mean interpolated and downscaled values of T_a, P and S_{in} are plotted against observed means at the 14 selected weather stations of MeteoSwiss. For every individual station, mean values are calculated over the time span where measured data is available.

8.6. Interpretation

In the following, the modeled mass balance distribution is analyzed in relation to the comparison of stake measurements and the temporal variability of mass balance. Special emphasis is laid on effects of the different interpolators. Finally, the comparison of meteorological data is examined.

8.6.1. Calculated Mass Balance

An assessment of the quality of the modeled mass balance distribution is rather difficult because data are available only for a few glaciers. A rough assessment of the modeled mass balance distribution can be made by checking visually if the pattern of mass balances agrees with known features: The observed general pattern of low ELAs at the northern edge of the Alps and highest ELAs in the region north of Zermatt (e.g. *Maisch et al.*, 1999) is reproduced well. Furthermore, modeled ELAs are even present on most of the small

glaciers with a rather limited extent in altitude, which can be rated a success. On the other hand, the general retreat of all observed glaciers in Switzerland during the modeled time span (*Paul et al.*, 2004) indicates that modeled positive mass balances must be considered unrealistic. There are also areas where modeled mass balances are clearly too negative: for instance Gries glacier (the largest glacier in the south–eastern corner of Figure 8.5)

Figure 8.8a indicates that melt is modeled quite well for different types of glaciers spread over a large portion of the Swiss Alps. The seven outliers concern stake measurements on the terminus of Upper Grindelwald glacier, situated in a very narrow and deep gorge that can not be resolved by the 100 m DTM. Warm air currents and modification of the long-wave balance due to the surrounding rock walls are also possible reasons for the systematic underestimations of melt on that glaciers terminus. Since melt is modeled well, the systematic underestimation of annual and winter balances (Figure 8.8b and 8.8c) is attributed to an underestimation of accumulation. This assumption is confirmed by the systematic underestimation of winter balance on Claridenfirn (Figure 8.8b).

The assumption of a systematic underestimation in accumulation is supported by Figure 8.7a as well: Underestimations are persistent in winter balances. Although less pronounced, summer balances are also underestimated which might be caused by the albedo feedback mechanism related to reduced snow cover at the end of the winter and underestimations of summer snowfall. On the other hand, Figure 8.7b indicates that such underestimations might be a local effect which tends to average out when a larger sample is considered. Indeed, annual variability and the mean of modeled mass balances for the 94 glacier sample are very similar to the data from *WGMS* (2007) and *Huss et al.* (2008a) while the curve for the small sample is clearly shifted toward more negative values.

The mass balance model contains simplifications. Still, modeled and measured melt agree quite well for a large number of glaciers indicating that the simplifications (e.g. α_i is constant throughout the entire model domain) do not impact much on melt modeling, compared to the influence of RCM biases. Furthermore, glacier surfaces and outlines are fixed and an adaption of glacier geometry as a reaction to mass imbalance through retreat or advance, as well as related feedback-processes, can not take place. In Figure 8.7a differences in annual mass balance seem to be larger in more recent years. However, in 1999, 2000 and 2001, the differences are mainly due to underestimations of the winter balance which can not be attributed to changing glacier geometry. The impact of such simplifications is not investigated here and could become large when the model is applied to longer time spans (*Huss et al.*, 2008a). Parameterizations of changing glacier geometry should be introduced in future model versions. Maps of satellite derived surface albedo (e.g. *Knap et al.*, 1999b; *Paul et al.*, 2005) might be helpful to improve model performance for individual glaciers.

8.6.2. The Role of the Different Interpolators

The main reason for the less negative mass balances obtained from IDW are spatial autocorrelations of the location of glaciers and REMO parameters. The effect is most pronounced with P (Table 8.2).

As depicted schematically in Figure 8.10, positive and negative differences between the REMO topography interpolated with IDW ($\widehat{DTM}_{IDW}$) and NN ($\widehat{DTM}_{NN}$) (note that subscript $_{REMO}$ is omitted for simplicity) occur. Over the full spatial model domain, these differences average each other out and the mean altitude of $\widehat{DTM}_{IDW}$ and $\widehat{DTM}_{NN}$ varies

by only 2 m. However, glaciers are not equally distributed over the terrain but preferentially exist where both the real topography and the REMO grid boxes are highest. Hence, their occurrence is spatially autocorrelated to areas where the $\widehat{DTM}_{IDW}$ surface is located below $\widehat{DTM}_{NN}$ (Figure 8.10). When considering only the glacierized area, $\widehat{DTM}_{IDW}$ is by average 181 m lower than $\widehat{DTM}_{NN}$. As $\Delta_{DTM} = DTM - \widehat{DTM}_{REMO}$ is applied in Eq. (8.7) and because IDW results in a higher mean Δ_{DTM}, increased precipitation is obtained compared to NN.

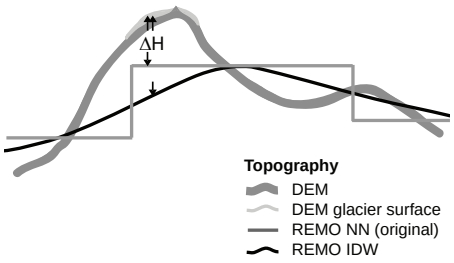

Figure 8.10.: A schematic illustration how the correlation between the spatial location of glaciers and the highest REMO grid boxes systematically influences ΔH.

No overestimation of $\hat{P}$ compared to NN results from TPS (Table 8.2) although the approach is the same as described above. In contrast to IDW, TPS gives interpolated values that may lie outside the range of original values and thus the peaks in the interpolated REMO topography lie above the elevation of the REMO grid cells, resulting in $\widehat{DTM}_{TPS} - \widehat{DTM}_{NN} = 25$ m for the glacier perimeter.

Furthermore, the different characteristics of NN, IDW and TPS also affect wet-day frequencies (WET). NN preserves the original WET of the REMO data and TPS is conservative with respect to the original value. IDW interpolates by building the distance weighted mean of all nodes within a search radius around the interpolant. When only one node within the search radius has significant precipitation the interpolant will be assigned a value above zero. The larger WET from IDW does not alter mean $\hat{P}$ but rather results in a smoother precipitation distribution with smaller $\hat{P}$ over a large perimeter instead of larger $\hat{P}$ on a smaller area. In the present model, enhanced WET is without influence to the results because α_s is a fixed value and surface albedo can switch even in the middle of a time step (cf. Section 8.4.1). However, more detailed mass balance models contain parameterizations of snow surface aging (e.g. *Klok and Oerlemans*, 2002) and frequent small snow falls will suppress the aging process.

Air temperature is reduced to a standard level prior to the interpolation and thus the correlation of glacier surfaces with areas of coldest air temperatures is removed.

The slightly higher $\hat{S}_{in}$ computed from IDW can only be due to different mean $\hat{n}$. Similar to the interpolation of the REMO topography, a spatial correlation of the glacier distribution and $\hat{n}$ causes the shift. However, the correlation is less pronounced here and the effect is small.

How can such effects be reduced or avoided? An interpolation scheme is required which preserves the mean over the entire interpolation area and over the area of every REMO grid box. The Nearest Neighbor interpolation meets these requirements. Despite its disadvantage

of creating breaks at the borders of the RCMs grid cells, NN is probably the interpolation scheme of choice if the aims is to calculate mean mass balances for entire mountain ranges. On the other hand, a study focusing on the mass balance distribution in detail requires the application of IDW, TPS or similar interpolation schemes to generate smooth surfaces. Hence, the effects as described above must be considered in detail and different interpolation schemes should be used in combination to avoid or minimize systematic distortions.

8.6.3. Comparison to Meteorological Data

The topography of the Alps is highly complex, resulting in many local climatic effects (e.g. *Schär et al.*, 1998). The REMO output at $1/6^\circ$ spatial resolution and also after downscaling is, of course, not able to reproduce such small scale effects. However, comparing the downscaled REMO output to measurements at point locations (Figure 8.9) is performed for two reasons:

1. If the sample of point measurements is large enough, local effects at the individual stations should average out and an estimate on general biases in the downscaled REMO output can be derived.

2. The variability of the observations around the mean value or around some general trend (e.g. temperature lapse rate) provides information on how large local variability is.

While general biases can be reduced in future studies by implementing bias corrections, climate models will most likely not be able to successfully reproduce small scale variability, at least for the next several years. Thus, estimates on small scale effects helps to determine a general level of uncertainty in mass balance modeling. This can be done, for instance, by means of a parametric uncertainty analysis (cf. *Machguth et al.*, 2008).

A comparison of modeled to measured precipitation might be of limited value, since measured P is not corrected for systematic under-catch. According to *Sevruk* (1985b), monthly correction values for precipitation measurements in the Swiss Alps reach +50% or more during winter and depend strongly on location and topography at the individual stations. Nevertheless, it seems that at least a weak correlation between $\hat{P}$ and measured P exists (Figure 8.9), although scatter is large and P is overestimated by REMO (Table 8.2). It is assumed that scatter and overestimation are combined effects of uncertainties in the measurements and systematic errors in the spatial precipitation distribution from REMO.

A correlation between measured S_{in} and $\hat{S}_{in}$ can not be established (Figure 8.9) and the latter exceed measurements by $16\,\mathrm{W\,m^{-2}}$ on average (IDW), for NN and TPS the positive differences are smaller (Table 8.2). The most apparent overestimations concern stations located at the northern edge of the Alps. In this region REMO strongly overestimates measured P (*Kotlarski et al.*, subm) while $\hat{n}$ is even lower than in the central parts of the Alps. This could be due to the large contribution of convective precipitation as generated by the RCM's convection scheme in this region. The associated sub-grid cloud systems do not contribute to the mean grid box cloud cover. Furthermore, n is a diagnostic quantity which is computed from the cloud cover in the individual model levels assuming certain overlap characteristics and can therefore be associated with a comparatively large uncertainty. Two other stations with strong overestimations (Grand-Saint-Bernard and Grimsel-Hospiz) are

located on passes where local clouds tend to form frequently. For the remaining stations, the correlation is better and the overestimation is less pronounced or even close to zero when $\hat{n}$ was obtained from NN or TPS.

The good correlation for air temperature can be expected since this parameter strongly depends on altitude. The shift of the regression line toward colder $\hat{T}_a$ is due to a systematic underestimation of winter temperatures by REMO. Summer temperatures, in contrary, are reproduced well (*Kotlarski et al.*, subm). Measured T_a over the Swiss Alps tend to decrease from west to east and more pronounced, from the south to the north (*Schär et al.*, 1998). It seems that horizontal gradients are reproduced to some degree by REMO: For instance, $\hat{T}_a$ is lower at Säntis (north-eastern Switzerland) than on Grand-Saint-Bernard (south-western Switzerland) although the stations are located at the same altitude. The same is the case for Davos and Zermatt, as well as for Molèson and Robbiei climate stations.

Kotlarski et al. (subm) have demonstrated that REMO is able to reproduce the temporal variability of annual means (T_a, P) well and consequently we refer to their study for a comparison of measured and modeled annual means.

8.7. Discussion

The good correlations of modeled and measured mass balances shown in Figure 8.7 confirm that REMO accurately reproduces the temporal variability of meteorological parameters (*Kotlarski et al.*, subm). However, the shift of mean modeled mass balance for the four glaciers compared to the data of *Huss et al.* (2008a) (Figure 8.7a) indicates systematic shifts of meteorological parameters at a local scale. Figures 8.7a and 8.8 indicate that the main source of such over- and underestimations lies in systematic errors in the accumulation calculation. This assumption is confirmed by *Kotlarski et al.* (subm) who state that REMO overestimates precipitation in the foreland and too little moisture reaches the main part of the Alps. Figure 8.6 shows that strongly negative mean balances mostly occur for glaciers in the interior parts of the Swiss Alps while the northernmost glaciers form a line of consistent positive or only slightly negative mass balances. Whereas the comparison to the measurements of winter or annual glacier mass balances indicates a general underestimation of accumulation, the comparison of precipitation at the 14 weather stations (Figure 8.9b), mostly indicates an overestimation of precipitation. The apparent discrepancy can be explained in various ways: (1) there are no measurements of winter and annual balance from the very northern edge of the Alps where REMO overestimates most, (2) compared are mean $\hat{P}$ obtained by IDW which gives higher values than NN or TPS (Table 8.2), (3) the precipitation measurements are not corrected for systematic undercatch, (4) winter precipitation is underestimated by REMO (*Kotlarski et al.*, subm) and (5), preferential deposition of snow on the smooth glacier surfaces as well as avalanche deposits resulting in enhanced accumulation on glaciers compared to the surroundings are not parameterized in the mass balance model.

To sum up, the REMO data allow for a good representation of the annual variability of mass balance. Systematic over- and underestimations in modeled mass balances are mainly caused by systematic errors in precipitation, by simplifications made in the parameterization of accumulation and by the applied interpolators. In our case TPS preserves the characteristics of the REMO data satisfactory while IDW results in enhanced precipitation, global

radiation and wet day frequency. The good reproduction of melt is achieved because REMO correctly reproduces the strong correlation of T_a and elevation. Furthermore, REMO provides summer temperatures in good agreement to measurements (*Kotlarski et al.*, subm) and seems to reproduce north–south and east–west gradients (cf. Section 8.6.3). Global radiation is generally regarded as the most important source of melt energy for glaciers in the Alps. The chosen approach of clear sky global radiation obtained from a radiation code and correction for cloudiness from REMO reproduces global radiation fairly well. Although Figure 8.9c shows strong overestimations by the model, the most apparent deviations do not impact on the model results: There are no glaciers located at the very northern edge of the Alps and local clouds on passes do mostly not affect the glaciers.

Our study confirms the assumption from *Kotlarski et al.* (subm) that errors in the REMO data are too large yet to allow for an operational assessment of mass balance distribution without correction of the systematic RCM biases. However, studies like the present one are able to provide feedback to climate modelers: Running a glacier mass balance model with RCM output is a test whether the RCM is able to reproduce the spatial distribution of the parameters governing glacier mass balance. Although such a test might have low confidence for individual glaciers, it is worthwhile to be conducted because very few meteorological measurements are available for the altitude of glacier occurrence and in the case of precipitation they are also related to large uncertainties.

8.8. Conclusions and Outlook

In this study we presented a method to apply RCM data for high resolution mass balance calculation over large glacier ensembles in complex alpine topography. In particular, we designed a useful method to convert meteorological output data, based on calculations of the RCM REMO, from a grid size of around 18 km to a cell size of 100 m, which is manageable with a local-scale distributed mass balance model. For calculation and validation purposes, a careful selection of the glaciers using exclusion criterion such as debris cover, or calving is an absolute prerequisite. Therefore, 94 glaciers, covering 50% of the total glacierized area, are used for calculation and 16 for validation. The main conclusion from this study is that the errors in the output of the RCM REMO are still too large to be used without any bias correction for the assessment of glacier mass balances in glacierized high-mountain environments. We believe, however, that the method could develop into a promising tool for future applications, especially in view of the fast improvements within the regional climate modeling community. The method could be applied to assess any possible impacts on the mass balances of large glacier samples due to a changing climate. In addition the following specific conclusions can be drawn:

- The temporal variability of mass balance could be represented quite well. This is confirmed by the high correlations between variability of winter, summer and annual balances, resulting from a 24 years model run with measurements and the results of an other study and from glacier monitoring.

- Modeled and measured ablation rates are in good agreement mainly because air temperature, as a dominating factor in melt modeling, is (a) strongly correlated with

elevation and (b) spatially well produced by the RCM REMO. This has resulted in an overall good agreement with measurements at local climate stations.

- In contrast to the well modeled ablation, measured accumulation is underestimated considerably. This is indicated by the systematic shifts of modeled mass balances in regions where measured annual and/or winter balances are available.

- Over- and under-estimates of the modeled mass balances are caused by a combined effect of a) systematic precipitation errors produced by the RCM REMO, b) the parametrization of accumulation (e.g. no refreezing considered) c) the application of different interpolations and d) the missing consideration of preferential snow deposition on smooth glacier surfaces.

Possible future improvements include:

- The application of multi-model approaches, using the output of several different GCM/RCMs, would allow a) a better assessment of possible ranges of the mass balance calculations and b) a better evaluation of the range of uncertainty associated with these models.

- The mass balance model contains several simplifications that could be replaced by more detailed parameterizations, such as the inclusion of parametrized long-wave radiation or turbulent fluxes.

- An in-depth analysis of the deviations between modeled and measured accumulation is required.

- The consideration of a variable glacier geometry.

- Remote sensing could be used as a future validation tool for the model results a) by the comparison of measured snow lines from satellites or aerial air photographs with the snow lines resulting from the transient model runs, b) by introduction of surface albedo derived from satellites and c) by the comparison of modeled and measured volume changes from satellites or aerial photographs

Acknowledgments We greatly acknowledge J. Oerlemans for providing the stake measurements from Morteratsch glacier, M. Huss for providing detailed mass balance data and J. Corripio for making the global radiation code available to us. We want to thank W. Haeberli and N. Salzmann for their helpful comments on a draft of the paper. MeteoSwiss provided the meteorological data. H. Machguth is supported by the Swiss Science Foundation (grant No. 20-117761). The Figures 8.1, 8.3, 8.5, S1 and 8.6 are based upon the DHM25Level2 and the Vector200 data set from swisstopo. Both data sets are reproduced by permission of swisstopo (BA081414)

Auxiliary Material

Introduction

In the paper "Calculating distributed glacier mass balance for the Swiss Alps from RCM output: A methodical description and interpretation of the results", a methodology to calculate high-resolution distributed glacier-mass balances using RCM output is described. The auxiliary data presented here contain two additional figures which provide more detailed information on the results presented in the paper. The auxiliary Figure S1 shows a detailed section of modeled mass balance distribution for the southwestern part of the Swiss Alps. The Figure is a complement to Figure 8.5 in the paper. In auxiliary Figure S2 the comparison of measured and modeled temporal variability of annual mass balances, shown in the paper in Figure 8.7, is shown in a scatter plot. Linear regressions are given as well and are discussed in the main text of the paper.

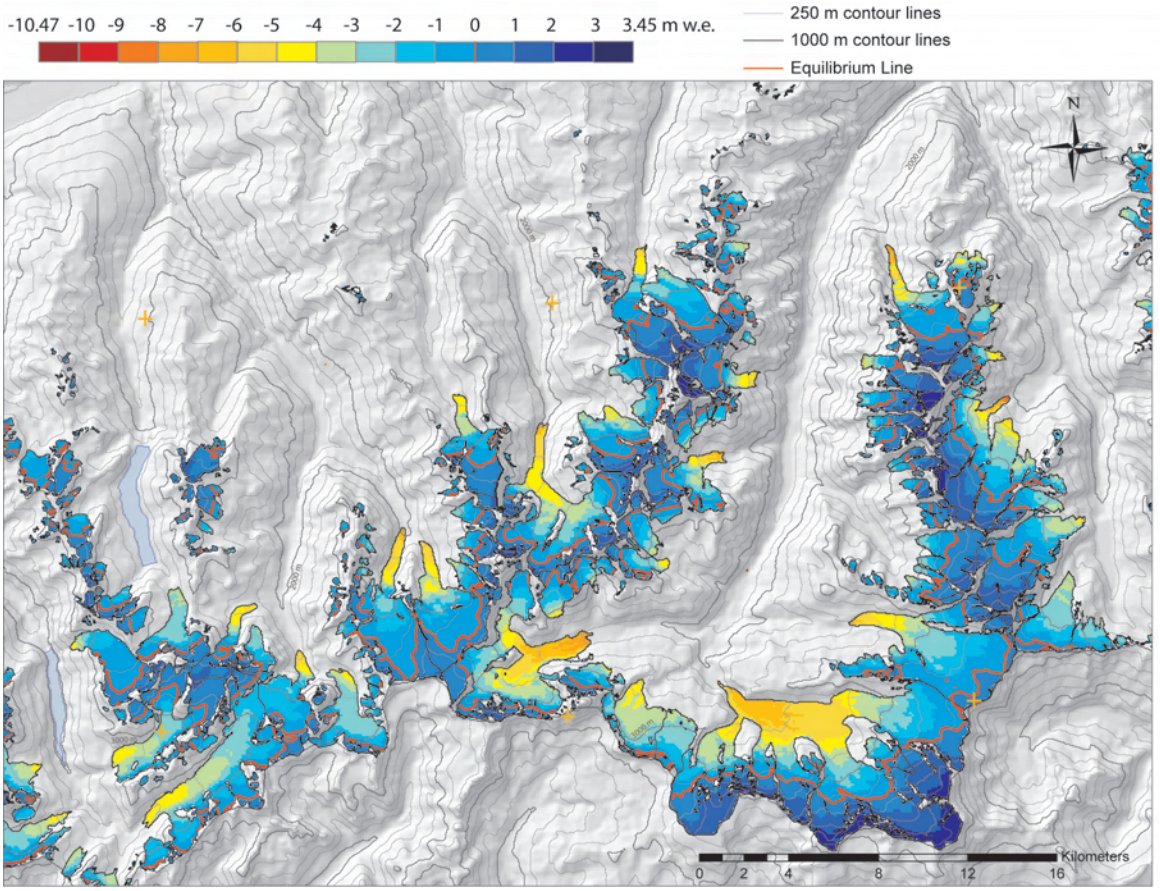

Figure 8.11.: (Figure S1) Mean modeled annual mass balance distribution for all glaciers of the southern Valais.

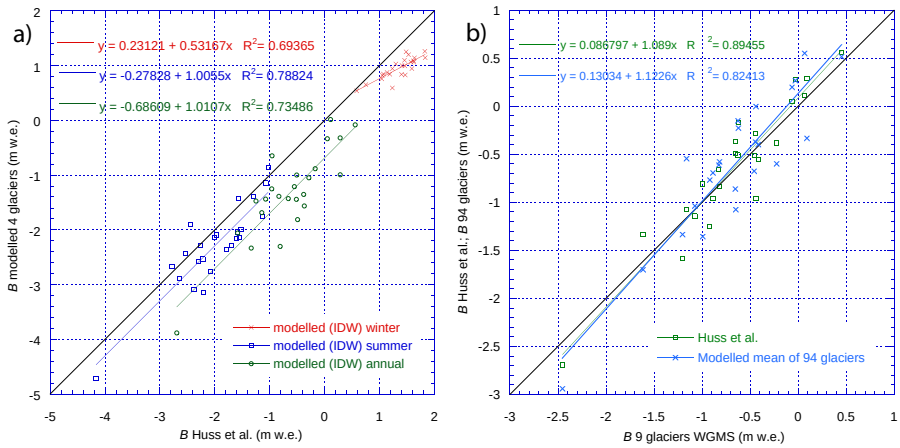

Figure 8.12.: (Figure S2) a) Modeled winter, summer and annual balances are plotted against values from *Huss et al.* (2008a). All data shown are averaged over the four glaciers: Grosser Aletsch, Gries, Rhône and Silvretta. b) Modeled mean annual balances for the 94 selected glaciers and mean annual mass balances for 4 glaciers (*Huss et al.*, 2008a) are compared to mean annual mass balances obtained from 9 Alpine glaciers (*WGMS*, 2007).

9. A First Simple Precipitation Assessment for the Swiss Alps from RCM Output and a Precipitation Climatology

The second goal of the present thesis is to apply distributed mass balance modeling to precipitation assessment in high mountain areas. The basic idea of such an approach would be to obtain measured mass balances, to consider precipitation the unknown in the modeling process, and to adjust precipitation in an iterative manner until modeled and measured mass balances are in agreement. A mass balance estimate over the 1985–2000 time span and for the Swiss Alps arrived at DEM subtraction was recently made available by *Paul and Haeberli* (2008); *Paul* (2008). The approach then requires a model that is capable of modeling mass balance distribution over an area that includes a large number of glaciers (here the Swiss Alps). Such a regional mass balance model was developed in Paper №4 and driven by data of the REMO RCM. However, uncorrected meteorological data from REMO were used in Paper №4 because the study focussed on the development of the method and the evaluation of the influence of biases. It was found that the accuracy of modeled mass balances of individual glaciers is rather low. Thus, a bias correction is performed to improve the reliability of the precipitation assessment based on the regional mass balance model and output of the RCM REMO. Since it was found in Paper №4 that precipitation biases in REMO are most likely the main source of error, the *Schwarb et al.* (2001) precipitation climatology (cf. Section 2.1.3) was applied to adjust the REMO data.

Biases in the data of the RCM REMO, the applied correction scheme and resulting improvements from the bias correction are shown in the first section. In the following section the mass balance data and the developed iterative precipitation adjustment scheme are described. Resulting modeled mass balances are then compared to the mass balance estimates from DEM subtraction. A level of significance in the observed differences in mass balance is established and an estimate of precipitation correction is made. In the concluding section the resulting precipitation adjustments are discussed in view of other studies, including two papers that also applied the *Schwarb et al.* (2001) data for mass balance assessment.

9.1. Applied Bias Correction

Biases in REMO output are discussed in-depth by *Kotlarski et al.* (2005); *Kotlarski* (2007); *Kotlarski et al.* (subm). An attempt to summarize biases in global radiation and air temperature with respect to both their temporal and spatial component was made in Figure 9.1. The curves of modeled and measured mean annual air temperature (Figure 9.1a) and global radiation are shown (Figure 9.1b), averaged over the 1985–2000 time span and 14 synoptic weather stations in the Swiss Alps. To allow for a rough estimate of spatial variability of

the biases, mean deviations (1985–2000) between measured and modeled air temperature as well as measured and modeled global radiation are shown individually for all 14 stations. Note that "modeled" refers to the data as applied for the mass balance computation, i.e., REMO data that have already been downscaled and interpolated as described in Paper №4. Reference is also made in Paper №4 to the locations of the 14 weather stations.

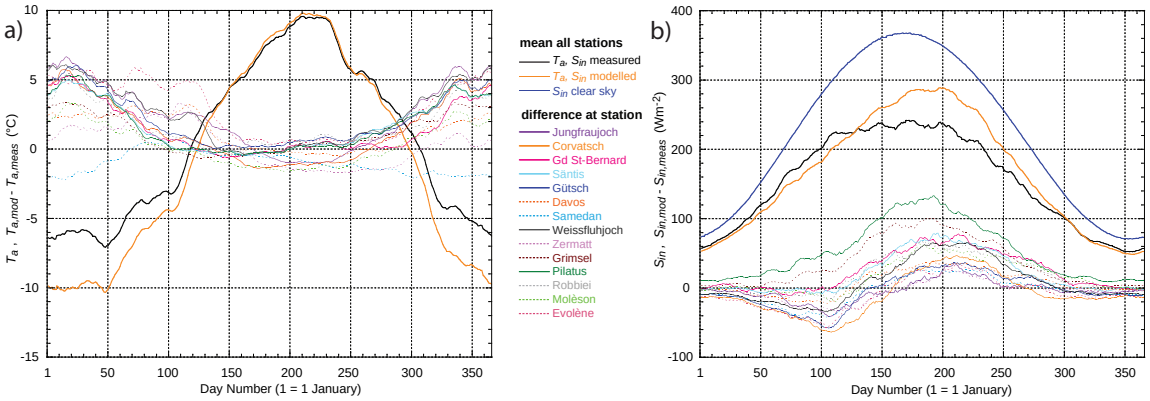

Figure 9.1.: Comparison of modeled and measured annual curves of air temperature and global radiation, averaged over 1981–2003. The bold lines depict the mean modeled and measured curves for all stations. The thin lines depict the differences (modeled - measured) at the individual stations. Dotted thin lines indicate stations located below 2000 m a.s.l. All curves, except for S_{in} *clear sky* are smoothed with a 15-day running mean for better readability.

Errors in T_a vary strongly with time while, at least during summer, spatial variability is already simulated satisfactorily from REMO and the chosen lapse rate (cf. *Kotlarski*, 2007; *Kotlarski et al.*, subm). Consequently, it was decided to perform a temporal correction of T_a by calculating the difference between mean measured and modeled T_a for every day of the year. The calculated offset in T_a is then added to the entire input arrays of air temperature depending on the day of the year. Conversely, S_{in} would require both a spatial and a temporal bias correction as indicated by the general overestimation during summer and the large variability between individual stations (Figure 9.1b). Errors in the calculated global radiation stem mainly from erroneous cloudiness values obtained from REMO. During summer, cloudiness is far too low which is due to the parameterization of convective clouds implemented in REMO (cf. Paper №4). Consequently, biases in S_{in} are corrected by adjusting n. In order to correct n, the mean curves of n in REMO (n_{REMO}) and for measured cloudiness (n_{meas}) are calculated from the two mean curves of measured and modeled global radiation ($S_{in,mod}$ and $S_{in,meas}$, respectively) according to Eq. (3.4). Equation (3.4) requires τ_{cl} which is obtained from either the ratio $S_{in,clr}/S_{in,mod}$ or $S_{in,clr}/S_{in,meas}$. (Cloud observations are not carried out at the 14 automatic synoptic weather stations and thus n_{meas} has to be calculated from $S_{in,meas}$.) From the resulting two curves n_{REMO} and n_{meas} a correction ratio n_{corr} is created for every day of the year which is then applied throughout the model run. This simple procedure imposes problems because n must always be in the range of 0 to 1. To avoid values outside this range, 1 is set as an upper threshold. In order to preserve values of $n = 1$ to be systematically lowered below 1 in case that $n_{corr} < 1$, n_{corr} is multiplied by $\sqrt{1 - n_{REMO}}$. Although a spatial correction of n would be necessary as

well, it has not been applied yet. A possible approach would require the implementation of observed cloud climatologies (e.g. *Meerkötter et al.*, 2004, see Table 2.1). The accuracy of these climatologies, however, is still rather poor for high mountain areas (Section 2.1.3).

The applied bias correction results in a much better agreement of measured and modeled air temperatures while the effect on global radiation is rather slight. The deficit in global radiation during spring is corrected well, while the overestimation during summer is only reduced by about $20\,\mathrm{W\,m^{-2}}$ and still amounts to approx. $35\,\mathrm{W\,m^{-2}}$. This is because the multiplication of n_{REMO} with n_{corr} does not affect values of n_{REMO} close to or equal 0 that appear very frequent in REMO during summer. If only inner Alpine stations and stations not located on passes with frequent local clouds are considered (excluding Säntis, Pilatus, Gd-St-Bernard and Grimsel) overestimation during summer amounts to $20\,\mathrm{W\,m^{-2}}$.

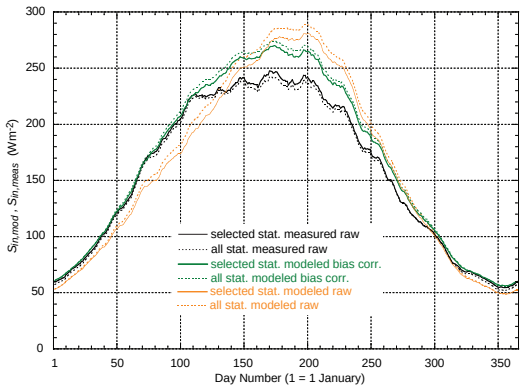

Figure 9.2.: Effect of the performed bias correction for global radiation. The uncorrected mean curves for all 14 stations and excluding Säntis, Pilatus, Gd-St-Bernard and Grimsel are shown. The corrected curves as well are averaged over both the full and the reduced sample size of synoptic weather stations.

In Paper №4 an assumed fixed precipitation gradient is applied to obtain sub grid-scale variability in precipitation. Instead of this rather rough simplification the precipitation climatology from *Schwarb et al.* (2001) is used which provides mean annual precipitation for the 1971–1990 time span at 2.5 minutes ($\sim 2\,\mathrm{km}$) spatial resolution (cf. Section 2.1.3). A spatial correction array (P_{scale}) which replaces the former precipitation gradient is calculated from the ratio of mean annual P (1971–1990) according to REMO and *Schwarb et al.* (2001). To do so, both data sets had been re-sampled beforehand to 100 m; *Schwarb et al.* (2001) by bilinear interpolation and REMO by inverse distance weighting. The correction array is then applied to daily precipitation arrays from REMO which have been interpolated to a 100 m grid. This methodology guarantees that the long-term mean precipitation agrees with *Schwarb et al.* (2001) while daily variability is acquired from REMO. Note that the *Schwarb et al.* (2001) data set is based on uncorrected precipitation measurements (cf. Section 2.1.3) and is also not corrected here prior to the application. Thus, precipitation is somewhat too low and it can be expected that mean modeled mass balances are below measured ones.

9.2. Iterative Precipitation Adjustment

Precipitation is varied in an iterative procedure until measured and modeled cumulative modeled mass balance ($\bar{B}_{meas}$ and $\bar{B}_{mod}$, respectively) agree. Data on cumulative mass balance for a large set of glaciers is available for the 1985–1999 time period from subtracting the DEM25 level1 from swisstopo and the SRTM90 DEM (*Farr et al.*, 2007) over Switzerland (*Paul and Haeberli*, 2008; *Paul*, 2008). The first DEM shows glacier size and surfaces for around the year 1985 while the latter provides glacier extent and surface for February 2000. The accuracy of mass balances obtained from DEM subtraction strongly depends on the quality of the input DEMs. Furthermore, an estimate of the density of the lost or gained volume is required which is a further potential source of error. The accuracy of the mass balance assessment is probably in the range of ± 20% (F. Paul, personal communication).

The model run must be performed for the time span corresponding to the DEM subtraction by *Paul and Haeberli* (2008). However, precipitation distribution can only be scaled to fit observed long-term average precipitation for 1971–1990 ($P_{meas71-90}$) according to *Schwarb et al.* (2001). A direct evaluation of the latter data set would be only possible if the condition $P_{REMO71-90}/P_{REMO85-00} = P_{meas71-90}/P_{meas85-00}$ is fulfilled. However, $P_{meas85-00}$ is unknown and thus a direct statement on $P_{meas71-90}$ is not possible. In a strict sense the precipitation assessment can test only whether the constructed precipitation ($P_{scale} \cdot P_{REMO85-00}$) is able to explain measured mass balance distribution and in which areas corrections have to be applied.

The model application is identical to Paper №4 except for the bias correction, the precipitation scaling based upon *Schwarb et al.* (2001) and the iterative precipitation adjustment, the latter being described in the following:

1. A manual selection of suitable glaciers is performed based upon the following conditions: (a) no debris cover, (b) little influence of avalanches, (c) mass loss restricted to melt, and (d) considerable size (area $> 2\,\mathrm{km}^2$). 94 glaciers were found to meet these conditions (glacier selection identical to Paper №4).

2. Observed total cumulative mass balances ($\bar{B}_{meas}$) for the selected glaciers and the full calculation period are obtained from *Paul and Haeberli* (2008).

3. A first model run with $P = P_O$ is conducted (P_O = original precipitation) to obtain the original glacier mass balances ($\bar{B}_O$). Subscript O stands for "original".

4. The mass balance deficit ($\Delta\bar{B}$) is calculated according to $\Delta\bar{B} = \bar{B}_O - \bar{B}_{meas}$.

5. For the following iteration, an assumption on the amount of the precipitation deficit is made: $\Delta P = -\Delta\bar{B}/2$.

6. ΔP, which is in m w.e., is converted to a dimensionless multiplication factor: $P_{corr}^{(O)} = (\Delta P + P_O)/P_O$,

7. Precipitation is adjusted to $P_1 = P_O \cdot P_{corr}^{(O)}$ and the mass balance calculation is repeated with P_1 to obtain $\bar{B}_1$.

8. From the resulting $\bar{B}_1$ a second correction factor ($P_{corr}^{(*)}$) is calculated following the procedure described under (4), (5) and (6), using $\bar{B}_1$ instead of $\bar{B}_O$.

9. $P_{corr}^{(*)}$ is multiplied with $P_{corr}^{(O)}$ to obtain $P_{corr}^{(1)}$ which is used for the second precipitation adjustment and mass balance calculation according to Point (7).

10. The iteration is repeated until $\bar{B}_{meas} = \bar{B}_{obs} \pm \varepsilon_B$ where m is the required number of iterations and $\varepsilon_B = 0.1$ m w.e. is a tolerance threshold defined prior to the precipitation adjustment.

9.3. Resulting Precipitation Adjustment and Related Uncertainties

Modeled mass balances (using uncorrected precipitation P_O) and measured mass balances are compared in a scatter plot (Figure 9.3) to identify statistical properties of their relationship. Differences between modeled and measured mass balance ($\Delta\bar{B} = \bar{B}_O - \bar{B}_{meas}$) for all selected glaciers are shown on a map (Figure 9.4) to assess whether values in $\Delta\bar{B}$ are spatially correlated or randomly distributed in space. In general $\bar{B}_O$ somewhat underestimates measured mass balance: Mean $\bar{B}_O$ averaged over all 100 m cells of the selected glaciers is -13.5 m w.e. $\pm$10.1 m w.e. whereas mean $\bar{B}_{meas} = -12.5$ m w.e. $\pm$3.9 m w.e., yielding mean $\Delta\bar{B}$ of -1 m w.e. From the standard deviations mentioned previously, and also Figure 9.3 it becomes obvious that the scatter in $\bar{B}_O$ of the individual glaciers is clearly larger than for $\bar{B}_{meas}$. However, if $\Delta\bar{B}$ is depicted on a map it becomes clear that differences in $\Delta\bar{B}$ primarily vary among the regions and are not randomly distributed in space (cf. Figure 9.4). In general, neighboring glaciers show similar $\Delta\bar{B}$ except for the region south of the Rhône valley where some scatter is present. The Aletsch area shows strongly positive $\Delta\bar{B}$ while all glaciers in the east have negative $\Delta\bar{B}$. In the remaining regions most glaciers show differences that are slightly negative and thus similar to the mean in $\Delta\bar{B}$.

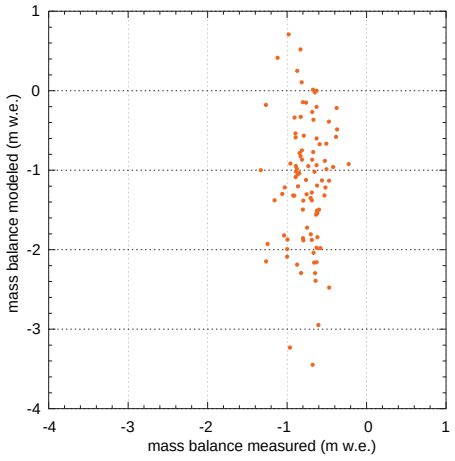

Figure 9.3.: Scatter plot showing the comparison of modeled and measured mean annual mass balances for the Swiss Alps (1985–2000).

The spatial pattern of $\Delta\bar{B}$ with its clear differences among the regions and slight local scatter is promising with respect to the precipitation adjustment. However, the process of

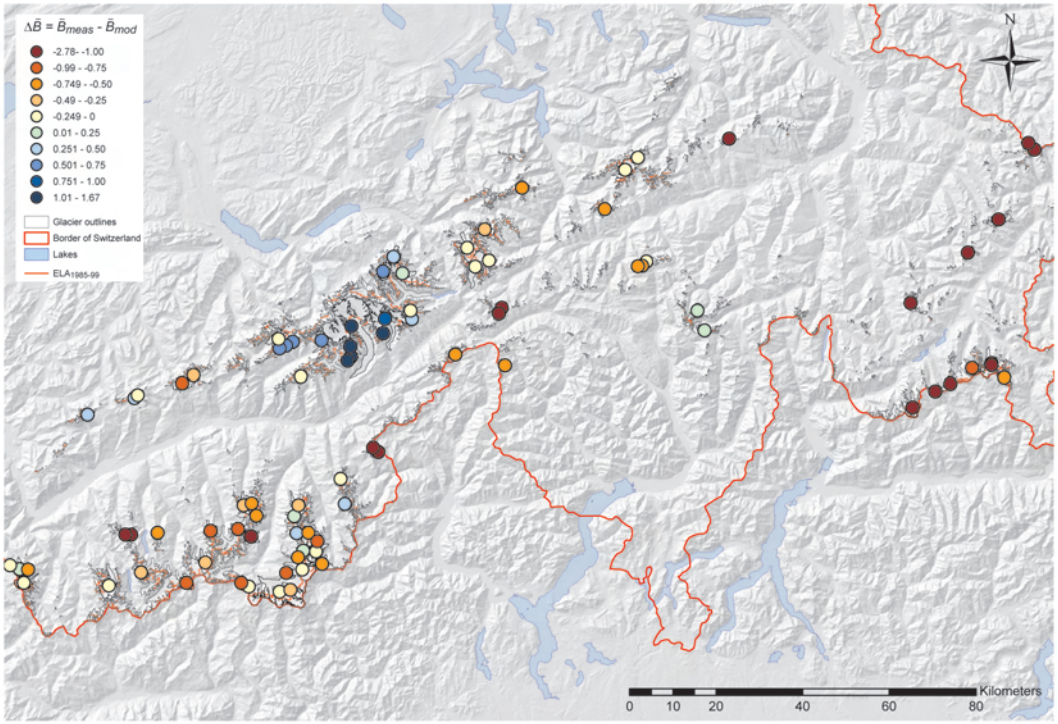

Figure 9.4.: Difference in mean annual mass balances for the 1985–2000 period ($\Delta\bar{B}$), resulting from subtraction of modeled and measured mean annual mass balance.

precipitation assessment from modeled mass balances includes a variety of sources of errors. In the first order this concerns the model simplifications (e.g. a fixed α_i) and uncertainties in the meteorological input data. The performed bias correction is very general and spatial biases are neglected. Furthermore, $\bar{B}_{meas}$ obtained from DEM subtraction is subject to respectable uncertainty. A study like the present one must be accompanied by a proper uncertainty analysis to establish a level of significance. Such an uncertainty analysis could be based upon Paper №3 and methods for distributed and spatially autocorrelated uncertainties as applied by *Hebeler et al.* (2008) but has not yet been conducted. Nevertheless. a rough estimate of uncertainty is possible from Paper №3 and simple theoretical considerations. According to Table 7.2, uncertainty in mass balance modeled from the model MB2 for the ablation zone of Morteratsch is around 1.2 m w.e. for uncertainties (S_{in}: 15–20%; T_a: 1°C) that roughly correspond to uncertainties in these two parameters during the summer months when obtained from REMO (cf. Figures 9.1 and 9.2). A test run of the uncertainty model for MB1 has shown that for similar uncertainties in input parameters output uncertainty is somewhat higher than for MB2 (however, uncertainties in the tuning parameters of MB1, C_0 and C_1, are difficult to determine). When precipitation is assessed from glacier mass balance modeling, precipitation is considered the unknown and only uncertainty in melt modeling determines whether a calculated precipitation adjustement is significant or not.

Absolute uncertainties (given in m w.e.) in melt modeling decrease with altitude as melt decreases as well. Thus the uncertainty of modeled melt for an entire glacier is lower than for the tongue. Based upon these considerations and the uncertainties in measured mass balance obtained from DEM subtraction (*Paul and Haeberli*, 2008), the assumption was made that $|\Delta\bar{B}| = \bar{B}_O - \bar{B}_{meas}$ is significant when above a threshold of 1 m w.e.

In the present model, accumulation equals solid precipitation and thus preferential deposition of snow on the glacier surfaces is not considered in the modeling process. *Kotlyakov and Krenke* (1982), for instance, provide correction estimates for different types of glaciers in order to calculate precipitation from measured snow accumulation. Snow concentration is minimal on large valley glaciers (not considering wind-exposed glaciers of cupola-like shape) but varies strongly for smaller glaciers depending on their specific shape, location and surroundings (*Kotlyakov and Krenke*, 1982). When preferential deposition of snow is neglected the precipitation assessment will result in higher values than occur in reality. However, glaciers where correction estimates are large (e.g. small cirque glaciers) have not been selected for the study. Assuming that snow accumulation on the selected glaciers is in general somewhat higher than solid precipitation, this would result in a slight reduction of underestimations in mass balances as well as enhanced overestimations. Furthermore, it must be emphasized that the given procedure of precipitation assessment for high mountain areas can only consider solid precipitation. Correction estimates are only valid for the solid fraction of precipitation which varies strongly with altitude. The fraction of solid precipitation is likely to be different for individual glaciers. During winter, all precipitation on the glaciers can be considered to fall as snow. However, during summer glaciers in dryer areas with high ELAs and accumulation areas at high altitudes will receive a larger portion of precipitation as snow than those glaciers at the northern border of the Alps where ELAs and accumulation areas are lower. Finally it must be noted that liquid precipitation can also add to accumulation through refreezing in the cold snow pack or in firn. This process can occur on all glaciers in spring when the snow cover is still cold and on polythermal or cold glaciers during summer as well.

From the considerations on model uncertainties and the fact that the given procedure for precipitation assessment does not consider snow redistribution and is only valid for solid precipitation, it becomes obvious that a quantitative map of precipitation corrections would suggest an accuracy that is not yet reached. Although the iterative precipitation adjustment would allow precipitation to be specified quantitatively, only a qualitative assessment of precipitation corrections is provided here. When considering the stated threshold of $|\Delta\bar{B}| =$ 1 m w.e., it can be concluded that P is overestimated in the Aletsch area. On the contrary, P is generally underestimated in the eastern part of the Swiss Alps, including the entire Bernina Group and all glaciers located further to the east (Figure 9.4). Recollecting that snow concentration on the glacier surfaces is not considered, underestimations could be somewhat reduced while overestimations might be even more pronounced. The differences between the regions, however, remain the same since there is no reason to assume that snow concentration is systematically different for the individual regions.

9.4. Interpretation

The overestimations of P for the Aletsch region probably stem from undesired side effects of the PRISM interpolation scheme (*Daly et al.*, 1994), applied in the *Schwarb et al.* (2001) climatology. The Aletsch area itself has only isolated precipitation gauges while the distance to the valleys north and south of the area with their denser measurement network is very large for Switzerland. This constellation might have resulted in an exaggerated influence of precipitation measurements performed at the northern edge of the Aletsch area where extraordinarily high values have been observed. For instance, at the Mönchsgrat precipitation totalizer (for location see Figure 1.2) annual precipitation amounts of up to 5.9 m have been measured (*meteoswiss*, 2008). The general underestimation in the east seems more difficult to explain, in particular since glaciers located in somewhat different climatological settings are affected: The Bernina group receives precipitation mainly from the south and south-west while the glaciers further to the east (Silvretta group) are also influenced from the north. Reasons for the generally low mass balances to the east could be errors in the process of regional mass balance modeling, such as overestimations of air temperature or global radiation in this area. However, the comparison to measured values at the two most relevant stations located in the eastern Swiss Alps – Weissfluhjoch at 2690 m a.s.l. and Corvatsch at 3315 m a.s.l. – contradicts this assumption. During summer, air temperature at the two stations is in close agreement with the measurements or is even underestimated, respectively. Overestimations in global radiation during the second half of the summer are similar to other regions.

With respect to potential errors in the *Schwarb et al.* (2001) precipitation climatology it should be noted that *Zemp et al.* (2006b), who calculated regional climatic ELAs for the glaciers of the Alps using the *Schwarb et al.* (2001) data set, have modeled climatic ELAs from the Bernina to the Silvretta Group that are also obviously too high. For the Aletsch region their ELAs are also too low. Furthermore, *Huss et al.* (2008a), who calculated long term mass balance for Silvretta glacier, had to raise precipitation to achieve good agreement with measured mass balance. For the area of Silvretta glacier precipitation data are available from the precipitation map of Austria (*Skoda and Lorenz*, 2003), indicating higher precipitation (approx. 2.5–3 m a^{-1} according to *Skoda and Lorenz*, 2003) than given by *Schwarb et al.* (2001) (approx. 1.6–2 m a^{-1}). Thus there is evidence that precipitation in the eastern Swiss Alps might be underestimated by *Schwarb et al.* (2001).

Further justification for confidence in the applied precipitation assessment is provided by the observation that deviations in modeled and measured mass balances are spatially correlated. Thus it is likely that there is a common source for the disagreement, rather than local processes on each individual glacier being responsible for the deviations. Only the glaciers of the southern Valais show a more pronounced local variability. Either precipitation in this area is locally more variable than elsewhere, or the scatter in modeled mass balance stems from local processes that are not yet considered or not modeled satisfactorily. It would be of particular interest to investigate the area in more detail. The study on Findel and Adler glacier, located in the southern Valais, has revealed that local variability of accumulation can be high in the area (cf. Paper №1).

The presented approach of precipitation assessment from numerical mass balance modeling is still in a rather experimental stage of development. As outlined above, uncertainties are regarded as too large to permit a reliable quantitative assessment of precipitation dis-

tribution. Less complex empirical relationships have been applied previously to obtain estimates of high mountain precipitation based upon glacier distribution or observed properties such as the ELA (e.g. *Kotlyakov and Krenke*, 1982; *Kerschner et al.*, 2000). *Kotlyakov and Krenke* (1982), for instance, applied their method to a quantitative assessment of precipitation in the mountains of Central Asia. Nevertheless, considerable uncertainties are inherent to such empirical approaches and to precipitation assessment as outlined in this chapter. The two concepts are regarded as complimentary, as discussed in more detail in Section 10.2.

Part III.

A Critical Review

10. Discussion and Conclusions

Mass balance assessment of a large set of glaciers and the use of glaciers as precipitation gauges have previously been addressed by more simple approaches (e.g. *Kotlyakov and Krenke*, 1982; *Haeberli and Hoelzle*, 1995; *Kerschner et al.*, 2000). Within this thesis both of these research questions have been revisited from the numerical and physically based mass balance modeling approach.

According to *Oerlemans* (2001) it is not possible to calculate the absolute mean mass balance from meteorological data alone. All mass balance models have to be calibrated because the accuracy of meteorological data is limited and glacier mass balance is very sensitive to meteorological conditions. Indeed, the investigations conducted within the course of this thesis confirmed this statement from the point of parametric uncertainty analysis. The aim of regional mass balance modeling thus cannot be to create a general mass balance model which delivers perfect output for all glaciers. Instead, the modeling process should focus on understanding where uncertainties occur and what influence they exercise on modeled mass balance. Deviations in measured and modeled mass balances can be analyzed and reasons for the disagreement ought to be found. Process understanding is established at a level different than from complex energy balance models. The latter are applied to study individual components of the energy balance at a point (e.g. *Greuell et al.*, 1997), or to assess spatial distribution of energy fluxes on a glacier (e.g. *Klok and Oerlemans*, 2002). Application of mass balance models to large areas including numerous glaciers is a tool for assessing the relevance of processes on a regional scale and for studying the relevance to mass balance of spatial variability in meteorological/climatological conditions. Finally it is also an instrument for learning about the input data. In high mountain areas, measurements of meteorological properties are sparse as well as uncertain, and thus biases in any established data set are difficult to determine. Glaciers serve to integrate meteorological conditions in these high mountain areas. As such, biases in the driving data of a mass balance model are reflected in modeled mass balances, and thus large-scale applications of mass balance models provide valuable information on model input.

10.1. A Review of the Approach

With regard to the two main goals of the thesis, a regional mass balance model based on a simple glacier energy balance model was first developed, tested and evaluated. In a second step, the model was applied to precipitation assessment for the glacierized areas of the Swiss Alps. The chosen modeling approach requires input data of high spatial and temporal resolution. Whereas previously applied empirical relationships were based mostly on climatological means, daily grids of meteorological data are required to drive the simple energy mass balance model. Throughout the modeling process, several scientific fields are involved:

- mass balance modeling and measurement are **glaciological** methods,
- the model is basically driven by RCM output obtained from **climate modelers**,
- data implementation requires downscaling techniques from **climate modeling** and **geostatistical** methods,
- glacier outlines have been established beforehand, using **remote sensing** methods,
- **meteorological** observations are used for validation and possible bias correction of the RCM data,
- evaluation of the model output must consider uncertainties in the input (**uncertainty modeling**),
- and finally, **climatological** data sets on precipitation should be evaluated and corrected by means of mass balance modeling.

Being situated at the interface of several disciplines, the chosen approach becomes rather complex, making collaboration with experts in the different fields essential.

It was decided to follow a stepwise approach toward the development of a regional mass balance model and its application to precipitation assessment. An initial study (Paper №1) focused on the adjacent glaciers Findel and Adler in southwestern Switzerland. The application of a simple energy balance model to the catchment under consideration had led to the assumption of a distinct horizontal gradient in accumulation (*Machguth*, 2003). Although the mass balance model was much simplified with respect to the input parameters (long-term mean conditions were approximated by sine curves of T_a and S_{in}, cf. *Machguth*, 2003), the assumed horizontal gradient in accumulation could be confirmed from the measurements. A long-term 20-year model run (Claridenfirn) and a mass balance study for the extraordinary year 2003 (Gries and Basodino glacier), published in Paper №2, led to model improvements and helped in the assessment of model performance in long-term runs and when precipitation was obtained from the *Schwarb et al.* (2001) climatology. Furthermore, a simple avalanching parameterization (*Gruber*, 2007) was applied in the Claridenfirn mass balance study. The avalanching parameterization resulted in an accumulation pattern which seemed visually more realistic than without such considerations. However, the parameterization was computationally expensive and modeled snow redistribution could not be validated. Furthermore, the influence on total glacier mass balances was marginal on most glaciers because modeled transport of avalanche snow from outside of the glacier perimeter onto the glacier surface was small. Thus, the avalanche parameterization was not applied in later model versions. Nevertheless, when tested and validated in-depth (e.g., from measurement of avalanche depositions from GPR or LiDAR, cf. *Dadic et al.*, subm), the parameterization should be re-integrated.

Some confidence in model performance in long-term runs or at the scale of glacierized catchment was obtained through the studies in Paper №1 and №2, and it was planned to further develop the simple energy balance model into a regional mass balance model. However, experience in modeling and process understanding from the simple model is limited. A second glacier energy balance model of intermediate complexity was programmed. The idea behind this two-model strategy was to gain process understanding from the more complex

model and to have a benchmark for the simple model. An 11-year long-term model run was performed with both models based on the example of Morteratsch glacier (cf. Section 6). Model calibration was performed using the example of one mass balance year, while the model output was compared to a large set of measurements for the full time span, including daily mass balance measurements from a sonic ranger. It could be shown that both models deliver similar results, even under the extraordinary conditions of the summer of 2003. Agreement with measurements is good at sites where the models were calibrated but considerable deviations occur where no calibration was performed.

The models applied in Papers №1, №2 and for model comparison (Section 6) were tuned to fit measurements by varying input and model parameters within their ranges of uncertainty and plausible values, respectively. Such a calibration to local conditions is not feasible in a regional application where a large number of glaciers is modeled at once. In such an application the key issue is to make an estimate of the level of overall uncertainty in a glacier energy balance model, stemming from the combined uncertainties in input parameters. Consequently, a parametric uncertainty analysis was conducted based on the example of the more complex model (Paper №3). With respect to regional mass balance modeling a distributed uncertainty assessment would be of primary interest. The study, however, had to be limited to a detailed uncertainty assessment at one point on a glacier to prevent investigations from becoming too complex. Calculated overall uncertainty turned out to be rather high and it was expected that deviations from measurements will become quite large in a regional mass balance model.

In the following a regional mass balance model was developed based upon the simple mass balance model. Different sources of input data were considered (cf. Table 2.1) and it was decided to drive the model by RCM data to avoid a patchwork of data from different sources with varying spatial and temporal resolutions. A validation procedure where different types of measurements are compared consecutively to modeled values was implemented and the model was tested extensively based on the example of the Swiss Alps (Paper №4). In this study, the focus was placed on technical aspects and the evaluation of the applied downscaling techniques. Finally, a simple bias correction was implemented and the regional mass balance model was applied to a precipitation assessment relevant to the Swiss Alps (cf. Section 9.1). From the experience gained through the parametric uncertainty analysis, and because the applied bias correction is very general, it was decided that the level of uncertainty is still too large to allow for a quantitative precipitation assessment and thus only a qualitative estimate was given.

10.2. A Review of Results

In the following, the results obtained for the two main goals of the thesis are discussed separately.

Regional Mass Balance Modeling A mass balance model which is capable of computing mass balance distribution for regions of several 10'000 km^2 at high spatial (100 m) and temporal (1 day) resolution was developed and applied to the Swiss Alps. Different interpolation schemes and downscaling techniques were tested. It was found that certain interpolation schemes can introduce biases to the meteorological data because glaciers generally exist where the mountains are highest. Comparison of measured and modeled mass

balances showed that the temporal variability of mean annual mass balances is modeled well but large systematic deviations from measurements occur locally. These findings indicate that the RCM reproduces inter-annual variability of meteorological conditions in a satisfactory way but is locally biased. Modeled mass balance for the summer months showed good agreement with measurements, whereas measured winter and annual balances are generally underestimated, i.e. more negative in the model than measured. From these observations it was concluded that underestimations in modeled mass balance are caused by a general underestimation of accumulation.

A major concern during model development was the large gap in spatial resolution between RCM and mass balance model. It could be shown that by applying appropriate interpolation and downscaling methods, it is possible to bridge the gap in spatial resolution. Furthermore, the grid spacing of the RCM is much denser than the network of available synoptic weather stations (cf. Figure 8.1). Nevertheless, the coarse RCM resolution still causes problems because certain processes in atmospheric circulation take place at a scale not resolved by the RCM. This became most evident for cloudiness in REMO which during summer is clearly too low over the Alps and the foreland. Cloudiness from synoptic circulation is modeled well by the RCM but convective cloud formation during summer, which usually takes place at a local scale, cannot be resolved and modeled at the RCM resolution. The subgrid-scale parameterizations included in the RCM to account for convective processes are obviously not yet able to prevent the general bias in summer cloudiness. The RCM bias is preserved through the interpolation and downscaling procedure and hence a bias correction is required. Such a bias correction was applied to the precipitation assessment. However, the improvements are limited and further efforts at bias correction are required. Furthermore, it is generally not recommended to work with only one RCM (e.g. *Mearns et al.*, 2003). Studies have shown that the mean of an RCM ensemble can perform better than individual RCMs. In the present thesis, the restriction to one RCM is justified in order to ease the model development process. In future research it must be tested whether the performance of the regional mass balance model could profit from being driven by data from RCM ensembles runs.

Related to the development of the regional mass balance model was the study of uncertainty in mass balance modeling. It was shown that uncertainty is in the range of 10% when data availability and quality is near the optimum (i.e., four synoptic weather stations located in the vicinity of the glacier). Furthermore, it was found that combined uncertainty in air temperature and lapse rate contribute largely to overall uncertainty. These findings contradict the often-stated assumption that air temperature is a well-known parameter with a horizontal correlation over long distances whose uncertainty can be neglected. Mass balance models are very sensitive to air temperature and consequently to uncertainties therein. Furthermore, the impact of uncertainties in the lapse rate is amplified with growing vertical distance from the point of measurement. From the uncertainty study it could also be concluded that uncertainties in mass balance modeling may reach 20% or more when data from climate models, themselves having considerable uncertainty, are applied.

Precipitation Assessment from Mass Balance Modeling A pilot study was performed on the adjacent Findel and Adler glaciers. The precipitation assessment from a mass balance model could be confirmed and the horizontal gradient in winter accumulation determined from the model run was in good agreement with the observations. Nevertheless, measurements were restricted to one particular winter season and further investigations to

assess temporal (inter-annual) variability of the snow cover and related gradients would be of interest. On the scale of the Findel glacier catchment, uncertainties in input parameters can be accounted for by local tuning. However, local tuning is no longer feasible when mass balance models are applied to large areas including numerous glaciers, as intended for precipitation assessment. In view of the simplifications made in the regional mass balance model, uncertainties in the input data and the findings from the uncertainty analysis, it was expected that uncertainties in the output of the regional mass balance model would become rather large.

A precipitation assessment for the Swiss Alps was nevertheless performed on the basis of the *Schwarb et al.* (2001) precipitation climatology. Measured and modeled mass balances were compared and where deviations exceeded a certain level of significance, it was assumed that the difference is likely to be at least partly caused by a bias in precipitation. It could be shown that the *Schwarb et al.* (2001) precipitation climatology is probably locally biased. Precipitation is likely to be overestimated in the Aletsch region and underestimated in the entire Engadine, eastern Switzerland. Although the mass balance calculation could not be performed for exactly the same time period as the *Schwarb et al.* (2001) precipitation climatology, these conclusions are in agreement with the results from other studies (*Zemp et al.*, 2006b; *Huss et al.*, 2008a). Nevertheless, numerous sources of uncertainties are inherent to the modeling approach while other issues, as for instance the ratio of solid and liquid precipitation and its variability among different glaciers have not yet been addressed. A quantitative precipitation assessment is not yet possible from the presented approach.

With regard to both regional mass balance modeling and its application for a precipitation assessment in high mountain areas, it must be emphasized that more data for validation is required. A small data base of mass balance measurements from stake readings and snow pits was established for the study presented in Paper №4. However, this data set must be added to by collecting more data. The availability of snow pit data is limited and these data are also not adequate to validate modeled accumulation since they provide only point information of a spatially highly variable snow cover. Helicopter borne GPR as applied in Paper №1 is a reliable method which potentially can be used to map snow thickness over several glaciers, steep areas as well as crevassed zones. Such data will allow for a comprehensive model validation and possibly for the implementation of snow redistribution schemes.

10.3. Precipitation Assessment from Mass Balance Modeling in the Context of Empirical Approaches

In the past glaciers have been used as precipitation gauges on the basis of empirical relationships (e.g. *Kotlyakov and Krenke*, 1982; *Kerschner et al.*, 2000). Considerable uncertainties are inherent to these empirical approaches and to precipitation assessment from numerical mass balance modeling. The first approach often depends only on a few input parameters and is thus particularly sensitive to errors therein. The empirical relationships themselves are a major source of uncertainty when, for instance, regression functions are fitted through a sample of measurements with considerable scatter. Furthermore, empirical relationships might be derived from measurements of a sample with properties that are not representative for the area where the empirical relationship is applied. On the other hand, numerical

energy balance models depend on a larger set of input parameters with their individual uncertainties, all contributing to overall uncertainty. Given that the sources of uncertainty are not identical, different modeling approaches complement each other. In the present case the application of the energy balance model and an empirical approach (*Zemp et al.*, 2006b) came to similar conclusions, inspiring additional confidence in the results.

The main difficulty and limitation in the application of glacier energy balance models to entire mountain ranges is the complexity of the approach. Detailed meteorological input is required, downscaling techniques have to be implemented, the approach is computationally expensive and quantifying uncertainties is a complex issue. Thus, the applicability depends on the availability of data, knowledge in several fields and computational resources. However, output is not limited to a quantity of interest (here precipitation) which is considered the main advantage and potential of the chosen approach. A wealth of additional information is given or can easily be obtained from the model output: mass balance distribution, ELA and ELA_0, mass balance gradients, mass balance rates, AAR and AAR_0, energy fluxes and much more. These data have a large potential to be analyzed and applied in the framework of further studies. Indeed, the model output can be tested from different angles and a direct comparison to different kinds of measurements is possible. For instance, in Paper №4 it could be concluded that the general underestimation of annual mass balance is likely to stem from underestimated accumulation, since the comparison of measured and modeled summer melt at a large number of stakes yielded good agreement. The model also allows individual processes to be analyzed with respect to their influence, spatial variability or uncertainty. Parameterizations can be changed (e.g. implementation of snow aging or maps of the ice albedo from satellite data) and the influence on the model output can be studied.

On the one hand, the high temporal resolution of the model allows for short-term model runs that are often not feasible from more simple approaches because the latter often require integration over certain time spans to yield robust results. On the other hand, the applicability of energy balance models for long-term calculations is hindered, mainly because of high computational expense and the need to implement glacier dynamics which is not a trivial matter when a two dimensional glacier geometry is to be considered. Simple parameterizations of changing glacier surface that could possibly be applied have been developed by *Plummer and Phillips* (2003) or *Huss et al.* (2008b). Finally, it should be noted that the use of regional mass balance models requires as input a DEM and glacier outlines, whereas most empirical studies rely on data from glacier inventories, such as length, area, maximum and minimum altitude (cf. *Haeberli and Hoelzle*, 1995). In the near future the availability of glacier outlines and DEMs will increase further (e.g. *Paul et al.*, 2009), thus facilitating numerical mass balance modeling in regions previously not investigated.

10.4. Conclusions

Based on the papers and additional research chapters presented in Part II and the previous discussion, the following conclusions are drawn:

1. The application of a numerical mass balance model to an entire mountain range is a feasible but rather complex approach at the interface of several disciplines.

2. The feasibility of regional mass balance modeling depends on the availability of RCM data for model input. To drive the model from climatologies established from measurements would be very difficult due to differing temporal and spatial resolutions of the available data sets. Furthermore, up to now reliable gridded climatologies for global radiation or cloudiness are not available.

3. A model run for the Swiss Alps showed that inter-annual variability of mass balance is modeled well while systematic local over- or underestimations due to biases in the RCM data became evident. Comparison to stake measurements indicate that summer balance is modeled well while winter accumulation is mostly underestimated.

4. Regional mass balance modeling driven by RCM output is hampered by biases in the input data. In particular, cloudiness from the RCM is strongly biased during summer. A simple bias correction has been carried out. The resulting correction of cloudiness is not yet satisfactory and further efforts are needed to find suitable bias correction schemes that potentially account for spatially variable biases.

5. It was found that the *Schwarb et al.* (2001) precipitation climatology is likely to be biased toward an overestimation of precipitation in the Aletsch region and an underestimation for eastern Switzerland. These regional correction estimates established from a mass balance computation for the entire Swiss Alps are confirmed by findings from other authors, using different approaches.

6. Regional mass balance modeling has a large potential for the validation of either climatologies or climate models in high mountain regions where measurements are sparse and uncertain. However, accumulation is not equal to precipitation and only solid precipitation can potentially contribute to accumulation. These issues need more detailed consideration than applied in this thesis.

7. Parametric uncertainty analysis indicated that uncertainty in the output is 10% for near optimum data quality and availability and 20% or more when climate model data is used for model input. Modelers should be aware that model output is only the mean of a PDF of potentially large spread. In particular, when geophysical models are applied to areas where measurements are rare, highly uncertain or unavailable, a parametric uncertainty analysis is an essential part of model application. Large-scale applications as performed in this study require techniques to consider spatial components of uncertainty as applied by *Hebeler et al.* (2008).

8. The present approach allows the influence of different processes on a regional scale to be considered. Additional information is provided by the model which allows for a detailed model validation from different sources of measurements and opens up multifarious possibilities for further studies. However, model improvements are essential. Some basic recommendation for further improvements are given in the following section.

10.5. Outlook

The approach proposed in this study is still in development. Numerous aspects are not considered yet or are still treated in a simplified manner. The regional mass balance model can be seen as a platform where further parameterizations can be implemented and tested. Main fields of potential improvement are listed in the following:

- collection of further mass balance data from stake measurements (own measurements and collection of available data);
- measurement of snow depth for a number of glaciers with helicopter-borne GPR (or LiDAR);
- use of data from RCM ensembles instead of only one RCM;
- improved bias correction;
- implementation of measured climatologies for bias correction or validation;
- consideration of spatial variability of uncertainties in an uncertainty analysis;
- parameterization of a variable glacier geometry from simple approaches or flow modeling;
- implementation of ice albedo maps from remote sensing data;
- modifications of parameterizations (e.g., refreezing of meltwater, variable snow albedo, snow redistribution)

The developed regional scale mass balance model is driven with data in NetCDF format which is widespread among climate modelers. Virtually any climate model data can be used to drive the model, opening up numerous possibilities for further model application. The model can be applied to unmeasured areas or in combination with climate scenarios calculated from RCMs as well as simulations of past climatic conditions (e.g., glacier readvance during the Younger Dryas). However, resulting mass balance distribution must be interpreted carefully because the high spatial and temporal model resolution implies an accuracy that cannot be achieved for regions or time periods where it is not possible to balance output against measurements. It is envisaged to first address the issues in model improvements listed above and to further test such a model in regions where larger data sets of measurements are available, such as the Alps or the Norwegian glaciers. Thus, further collection of mass balance measurements as listed above under the first two points is regarded as the base for future model development. A comprehensive validation of any regional mass balance model is only possible when data on the spatial distribution of accumulation are available for a larger set of glaciers. Helicopter-borne GPR as applied in Paper №1 has a great potential to provide such data. In addition, results from a precipitation assessment, performed with the given or an improved version of the regional mass balance model, could be validated against such data. Data on the spatial distribution of snow over larger areas would also allow horizontal and vertical gradients of snow accumulation in high mountain areas to be specified in a more favorable way.

Model performance also depends on the developments in regional climate modeling. The first experiments with RCMs at a spatial resolution below 5 km are underway. As an example, convection might be better resolved at such resolutions, reducing biases in cloudiness and precipitation. It will be interesting to follow whether these very high resolution model runs will improve model output.

Finally it should be noted that the Findel glacier measurements, although published in *WGMS* (2007), have not yet been applied in combination with one of the mass balance models developed in the course of this thesis. A potential study could deal with the application of mass balance models as a comprehensive tool for spatial interpolation of point measurements (stake readings and snow pits) to the entire glacier surface.

References

Ahlmann, H. W. (1924), Le niveau de glaciation comme fonction de l'accumulation d'humidité sous forme solide, *Geografiska Annaler*, *6*, 223–272.

Anderson, M., and W. Woessner (1992), The role of the postaudit in model validation, *Advances in Water Resources*, *15*, 167–173.

Andreassen, L. M. (1999), Comparing traditional mass balance measurements with long-term volume change extracted from topographical maps: A case study of Storbreen Glacier in Jotunheimen, Norway, for the period 1940–1997, *Geografiska Annaler*, *81A*, 467–476.

Anonymous (1969), Mass balance terms, *Journal of Glaciology*, *8*(52), 3–7.

Anslow, F. S., S. Hostetler, W. R. Bidlake, and P. U. Clark (2008), Distributed energy balance modeling of South Cascade Glacier, Washington and assessment of model uncertainty, *Journal of Geophysical Research*, *113*, F02,019, doi:10.1029/2007JF000850.

Arcone, S. (1996), High resolution of glacial ice stratigraphy: a ground-penetrating radar study of Pegasus Runway, McMurdo Station, *Geophysics*, *61*, 1653–1663.

Arcone, S. (2002), Airborne-radar stratigraphy and electrical structure of temperate firn: Bagley Ice Field, Alaska, U.S.A, *Journal of Glaciology*, *48*(161), 317–334.

Arcone, S., and A. Delaney (1987), Airborne river-ice thickness profiling with helicopter-borne UHF short-pulse radar, *Journal of Glaciology*, *33*(115), 330–340.

Arcone, S. A., and N. E. Yankielun (2000), 1.4 GHz radar penetration and evidence of drainage structures in temperate ice: Black Rapids Glacier, Alaska, U.S.A., *Journal of Glaciology*, *46*(154), 477–490.

Arendt, A., K. Echelmeyer, W. D. Harrison, G. Lingle, and V. Valentine (2002), Rapid wastage of Alaska glaciers and their contribution to rising sea level, *Science*, *297*(5580), 382–386.

Arnold, N., I. Willis, M. Sharp, K. Richards, and W. Lawson (1996), A distributed surface energy balance model for a small valley glacier: I. development and testing for Haut Glacier d'Arolla, Valais, Switzerland, *Journal of Glaciology*, *42*(140), 77–89.

Arnold, N., W. Rees, A. Hodson, and J. Kohler (2006), Topographic controls on the surface energy balance of a high arctic valley glacier, *Journal of Geophysical Research*, *111*, F02,011, doi:10.1029/2005JF000426.

Auer, I., et al. (2007), HISTALP – historical instrumental climatological surface time series of the Greater Alpine Region, *International Journal of Climatology*, *27*(1), 17–46.

Baker, D. G., D. L. Ruschy, and D. B. Wall (1990), The albedo decay of prairie snows, *Journal of Applied Meteorology*, *29*, 179–187.

Barry, R. G. (1992), *Mountain weather and climate*, Routledge physical environment series, 402 pp., Routledge, London and New York.

Bartelt, P., and M. Lehning (2002), A physical SNOWPACK model for the swiss avelanche warning part I: numerical model, *Cold Regions Science and Technology*, *35*(3), 123–145.

Bauder, A., M. Funk, and M. Huss (2007), Ice-volume changes of selected glaciers in the Swiss Alps since the end of the 19th century, *Annals of Glaciology*, *46*, 145–149.

Bauder, A. C. (2001), Bestimmung der Massenbilanz von Gletschern mit Fernerkundungsmethoden und Fliessmodellierungen. Eine Sensitivitätsstudie auf dem Unteraargletscher, Ph.D. thesis, VAW, ETH, Zurich, http://e-collection.ethbib.ethz.ch/view/eth:23940.

Begert, M., T. Schlegel, and W. Kirchhofer (2005), Homogeneous temperature and precipitation series of Switzerland from 1864 to 2000, *International Journal of Climatology*, *25*(1), 65–80.

Beniston, M. (2004), The 2003 heat wave in Europe: A shape of things to come? an analysis based on Swiss climatological data and model simulations, *Geophysical Research Letters*, *31*, L02,202, doi: 10.1029/2003GL018857.

Beniston, M., W. Haeberli, M. Hoelzle, and A. Taylor (1997), On the potential use of glacier and permafrost observations for verification of climate models, *Annals of Glaciology*, *25*, 400–406.

Beven, K., and A. Binley (1992), The future of distributed models: Model calibration and uncertainty prediction, *Hydrological Processes*, *6*(3), 279–298, doi: 10.1002/hyp.3360060305.

Bhatt, U. S., J. Zhang, C. S. Lingle, and L. M. Phillips (2007), Examining glacier mass balances with a hierarchical modeling approach, *Computing in Science & Engineering*, *9*(2), 60–67.

Bøggild, C. E. (2007), Simulation and parameterization of superimposed ice formation, *Hydrological Processes*, *21*(12), 1561–1566.

Böhm, R., I. Auer, M. Brunetti, M. Maugeri, T. Nanni, and W. Schöner (2001), Regional temperature variability in the European Alps: 1760-1998 from homogenized instrumental time series, *International Journal of Climatology*, *21*(14), 1779–1801, doi: 10.1002/joc.689.

Bougamont, M., J. L. Bamber, and W. Greuell (2005), Development and test of a surface mass balance model for the Greenland ice sheet, *Journal of Geophysical Research*, *110*, F04,018, doi:10.1029/2005JF000348.

Bradley, R. S., M. Vuille, H. F. Diaz, and W. Vergara (2006), Climate change: Threats to water supplies in the tropical Andes, *Science*, *312*(5781), 1755, doi: 10.1126/science.1128087.

Braithwaite, R. (2008), Temperature and precipitation climate at the equilibrium-line altitude of glaciers expressed by the degree-day factor for melting snow, *Journal of Glaciology*, *54*(186), 437–444.

Braithwaite, R. J. (1981), On glacier energy balance, ablation, and air temperature, *Journal of Glaciology*, *27*(97), 381–391.

Braithwaite, R. J. (1995), Positive degree-day factors for ablation on the Greenland ice sheet studied by energy-balance modelling, *Journal of Glaciology*, *41*(137), 153–160.

Braithwaite, R. J., T. Konzelmann, C. Marty, and O. Olesen (1998), Errors in daily ablation measurements in northern Greenland, 1993–94, and their implications for climate studies, *Journal of Glaciology*, *44*(148), 583–588.

Brock, B., I. Willis, M. Sharp, and N. Arnold (2000), Modelling seasonal and spatial variations in the surface energy balance of Haut Glacier d'Arolla, Switzerland, *Annals of Glaciology*, *31*, 53–62.

Burrough, P. A., and R. A. McDonnell (2004), *Principles of geographical information systems*, Spatial Information Systems and Geostatistics, Oxford University Press.

Christensen, J., T. Carter, and F. Giorgi (2002), PRUDENCE employs new methods to assess European climate change, *EOS*, *83*, 147.

Christensen, J. H., and P. Kuhry (2000), High-resolution regional climate model validation and permafrost simulation for the East European Russian Arctic, *Journal of Geophysical Research*, *105(D24)*, 29,647–29,658.

Cogley, J. G. (1999), Effective sample size for glacier mass balance, *Geografiska Annaler*, *81A*(4), 497–507.

Cook, K., X. Yang, C. M. Carter, and B. N. Belcher (2003), A modelling system for studying climate controls mountain glaciers with application to the Patagonian icefields, *Climatic Change*, *56*, 339–367.

Corripio, J. (2003), Vectorial algebra algorithms for calculating terrain parameters from DEMs and solar radiation modelling in mountainous terrain, *International Journal of Geographical Information Science*, *17*(1), 1–23, doi: 10.1080/713811744.

Dadic, R., R. Mott, M. Lehning, and P. Burlando (subm), Wind influence on snow depth distribution and accumulation over glaciers, *Geophysical Research Letters*.

Daly, C., R. Neilson, and D. Phillips (1994), Statistical-topographical model for mapping climatological precipitation over mountainous terrain, *Journal of applied Meteorology*, *33*(2), 140–158.

Damm, V. (2004), Ice thickness and bedrock map of Matusevisch Glacier drainage basin (Oates Coast), *Terra Antarctica*, *11*, 85–90.

Douville, H., J.-F. Royer, and J.-F. Mahfouf (1995), A new snow parametrization for the Météo-France climate model. Part I: Validation in stand-alone experiments. Part II: Validation in a 3D GCM experiment, *Climate Dynamics*, *12*(1), 21–52.

Dubayah, R., and P. M. Rich (1995), Topographic solar-radiation models for GIS, *International Journal of Geographical Information Science*, *9*(4), 495–419.

Efthymiadis, D., P. Jones, K. Briffa, I. Auer, R. Böhm, W. Schöner, C. Frei, and J. Schmidli (2006), Construction of a 10-min-gridded precipitation dataset for the Greater Alpine region 1800–2003, *Journal of Geophysical Research*, *111*, D01,105, dOI:10.1029/2005JD006120.

Eisen, O., U. Nixdorf, L. Keck, and D. Wagenbach (2003), Alpine ice cores and ground penetrating radar: Combined investigations for glaciological and climatic interpretations of a cold Alpine ice body, *Tellus*, *55B*, 1007–1017.

Farr, T., et al. (2007), The Shuttle radar topography mission, *Reviews of Geophysics*, *45*, RG2004, doi:10.1029/2005RG000183.

Favey, E., A. Geiger, G. Gudmundsson, and A. Wehr (1999), Evaluating the potential of an airborne laser-scanning system for measuring volume changes of glaciers, *Geografiska Annaler*, *81A*(4), 555–561.

Fliri, F. (1975), *Das Klima der Alpen im Raume von Tirol*, Univeritäts Verlag Wagner, Innsbruck.

Flohn, H. (1952), Hochgebirge und allgemeine Zirkulation, II. Die Gebirge als Wärmequellen, *Meteorology and Atmospheric Physics*, *5*(3), 265–279, doi: 10.1007/BF02247771.

Föhn, P. M. B., and R. Meister (1983), Distribution of snow drifts on ridge slopes: Measurements and theoretical approximations, *Annals of Glaciology*, *4*, 52–57.

Foster, R., C. Davis, T. Rand, and R. K. Moore (1991), Snow-stratification investigation on an Antarctic ice stream with an X-band radar system, *Journal of Glaciology*, *37*(127), 323–325.

Fountain, A. G., and A. Vecchia (1999), How many stakes are required to measure mass balance of a glacier?, *Geografiska Annaler*, *81A*(4), 563–573.

Fowler, H., S. Blenkinsop, and C. Tebaldi (2007), Linking climate change modelling to impact studies: recent advances in downscaling techniques for hydrological modelling, *International Journal of Climatology*, *27*(12), 1547–1578.

Frauenfelder, R., M. Zemp, W. Haeberli, and M. Hoelzle (2005), Worldwide glacier mass balance measurements: trends and first results of an extraordinary year in Central Europe, in *Ice and Climate News*, vol. 6, edited by C. Dick, pp. 9–10, CliC International Project Office.

Frei, C., and C. Schär (1998), A precipitation climatology of the Alps from high-resolution rain-gauge observations, *International Journal of Climatology*, *18*(8), 873–900.

Frei, C., J. H. Christensen, M. Déqué, D. Jacob, R. G. Jones, and P. L. Vidale (2003), Daily precipitation statistics in regional climate models: Evaluation and intercomparison for the European Alps, *Journal of Geophysical Research*, *108(D3)*, 4124, doi:10.1029/2002JD002287.

Früh, B., J. W. Schipper, A. Pfeiffer, and V. Wirth (2006), A pragmatic approach for downscaling precipitation in alpine-scale complex terrain, *Meteorologische Zeitschrift*, *15*(6), 631–646.

Garnier, B., and A. Ohmura (1968), A method of calculating the direct short-wave radiation income of slopes, *Journal of Applied Meteorology*, *7*(5), 796–800.

Gauer, P. (2001), Numerical modelling of blowing and drifting snow in Alpine terrain, *Journal of Glaciology*, *47*(156), 97–110.

Geist, T., and J. Stötter (2007), Documentation of glacier surface elevation change with multi-temporal airborne laser scanner data – case study: Hintereisferner and Kesselwandferner, Tyrol, Austria, *Zeitschrift für Gletscherkunde und Glazialgeologie*, *41*, 77–106.

Gerbaux, M., C. Genthon, P. Etchevers, C. Vincent, and J. Dedieu (2005), Surface mass balance of glaciers in the French alps: distributed modeling and sensitivity to climate change, *Journal of Glaciology*, *51*(175), 561–572.

Gilgen, H., and A. Ohmura (1999), The Global Energy Balance Archive (GEBA), *Bulletin of the American Meteorological Society*, *80*, 831–850.

Gilgen, H., M. Wild, and A. Ohmura (1997), *Global Energy Balance Archive (GEBA) Report 3: The GEBA Version 1995 Database*, *Zürcher Geographische Schriften*, vol. 74, 105 pp., Institute of Geography ETH, Zurich.

Gilgen, H., M. Wild, and A. Ohmura (1998), Means and trends of shortwave irradiance at the surface estimated from global energy balance archive data, *Journal of Climate*, *11*(8), 2042–2061.

Giorgi, F., and L. O. Mearns (1999), Introduction to special section: regional climate modeling revisited, *Journal of Geophysical Research*, *104*(D6), 6335–6352.

Glaciological Reports (1992-2008), *Die Gletscher der Schweizer Alpen/The Swiss Glaciers*, 105-124, Glaciological Comission (GC) of the Swiss Academy of Sciences (SAS) and Laboratory of Hydraulics and Glaciology at ETH Zürich (VAW/ETHZ).

Gregory, J. M., et al. (2005), A model intercomparison of changes in the Atlantic thermohaline circulation in response to increasing atmospheric CO2 concentration, *Geophysical Research Letters*, *32*, L12,703, doi:10.1029/2005GL023209.

Greuell, W. (1992), Hintereisferner, austria: mass balance reconstruction and numerical modelling of the historical length variations, *Journal of Glaciology*, *38*(129), 233–244.

Greuell, W., and M. de Ruyter de Wildt (1999), Anisotropic reflection by melting glacier ice: measurements and parametrizations in Landsat TM bands 2 and 4, *Remote Sensing of Environment*, *70*, 265–277.

Greuell, W., and C. Genthon (2004), Modelling land-ice surface mass balance, in *Mass balance of the cryosphere: observations and modelling of contemporary and future changes.*, edited by J. Bamber and A. Payne, pp. 117–168, Cambridge University Press.

Greuell, W., and T. Konzelmann (1994), Numerical modelling of the energy balance and the englacial temperature of the Greenland ice sheet. calculations for the ETH-Camp location (West Greenland, 1155 m a.s.l.), *Global and Planetary Change*, *9*(1–2), 91–114, doi:10.1016/0921-8181(94)90010-8.

Greuell, W., W. Knap, and P. Smeets (1997), Elevational changes in meteorological variables along a mid-latitude glacier during summer, *Journal of Geophysical Research*, *102*(D22), 25,941–25,954.

Gruber, S. (2007), MTD: a mass-conserving algorithm to parameterize gravitational transport and deposition processes using digital elevation models, *Water Resources Research*, *43*, W06,412, doi:10.1029/2006WR004868.

Haeberli, W. (2004), Glaciers and ice caps: historical background and strategies of worldwide monitoring, in *Mass balance of the cryosphere*, edited by J. Bamber and A. Payne, pp. 559–578, Cambridge University Press.

Haeberli, W. (2006), Integrated perception of glacier changes: A challenge of historical dimensions, in *Glacier Science and Environmental Change*, edited by P. G. Knight, pp. 423–430, Blackwell Publishing.

Haeberli, W., and M. Hoelzle (1995), Application of inventory data for estimating characteristics of and regional climate-change effects on mountain glaciers: a pilot study with the European Alps, *Annals of Glaciology*, *21*, 206–212.

Haeberli, W., and H. Holzhauser (2003), Alpine glacier mass changes during the past two millennia, *PAGES News*, *11*(1), 13–15.

Haeberli, W., and H. J. Zumbühl (2003), Schwankungen der Alpengletscher im Wandel von Klima und Perzeption, in *Welt der Alpen – Gebirge der Welt, Resourcen, Akteure, Perspektiven*, edited by F. Jeanneret, D. Wastl-Walter, U. Wiesmann, and M. Schwyn, Haupt Verlag, Bern – Stuttgart – Wien.

Haeberli, W., J. Cihlar, and R. G. Barry (2000), Glacier monitoring within the global climate observing system, *Annals of Glaciology*, *31*, 241–246.

Haeberli, W., M. Maisch, and F. Paul (2002), Mountain glaciers in global climate-related observation networks, *WMO Bull.*, *51*(1), 18–25.

Haylock, M. R., G. C. Cawley, C. Harpham, R. L. Wilby, and C. M. Goodess (2006), Downscaling heavy precipitation over the United Kingdom: a comparison of dynamical and statistical methods and their future scenarios, *International Journal of Climatology*, *26*(10), 1397–1415.

Hebeler, F., R. S. Purves, and S. S. R. Jamieson (2008), The impact of parametric uncertainty and topographic error in ice sheet modelling, *Journal of Glaciology*, *54*(188), 889–919.

Hock, R. (1999), A distributed temperature-index ice- and snowmelt model including potential direct solar radiation, *Journal of Glaciology*, *45*(149), 101–111.

Hock, R. (2005), Glacier melt: a review of processes and their modelling, *Progress in Physical Geography*, *29*(3), 362–391.

Hock, R., and B. Holmgren (2005), A distributed energy balance model for complex topography and its application to Storglaciären, Sweden, *Journal of Glaciology*, *51*(172), 25–36.

Hock, R., V. Radić, and M. de Woul (2007), Climate sensitivity of Storglaciären - an intercomparison of mass balance models using ERA-40 reanalysis and regional climate model data, *Annals of Glaciology*, *46*, 342–348.

Hoelzle, M., and W. Haeberli (1995), Simulating the effects of mean annual air-temperature changes on permafrost distribution and glacier size: an example from the Upper Engadin, Swiss Alps, *Annals of Glaciology*, *21*, 399–405.

Hoelzle, M., W. Haeberli, M. Dischl, and W. Peschke (2003), Secular glacier mass balances derived from cumulative glacier length changes, *Global and Planetary Change*, *36*, 295–306.

Hoinkes, H. (1954), Measurements of ablation and heat balance on Alpine glaciers, *Journal of Glaciology*, *2*(17), 497–501.

Hoinkes, H. (1970), Methoden und Möglichkeiten von Massenhaushaltsstudien auf Gletschern, *Zeitschrift für Gletscherkunde und Glazialgeologie*, *6*, 38–85.

Holmlund, P., and P. Jansson (1999), The Tarfala mass balance programme, *Geografiska Annaler*, *81A*(4), 621–631.

Hubbard, A., I. Willis, M. Sharp, D. Mair, P. Nienow, B. Hubbard, and H. Blatter (2000), Glacier mass-balance determination by remote sensing and high-resolution modelling, *Journal of Glaciology*, *46*(154), 491–498.

Huss, M., A. Bauder, M. Funk, and R. Hock (2008a), Determination of the seasonal mass balance of four Alpine glaciers since 1865, *Journal of Geophysical Research*, *113*(F01015), doi:10.1029/2007JF000803.

Huss, M., D. Farinotti, A. Bauder, and M. Funk (2008b), Modelling runoff from highly glacierized alpine drainage basins in a changing climate, *Hydrological Processes*, *22*(19), 3888, doi:10.1002/hyp.7055.

IAHS(ICSI)/UNEP/UNESCO (1989), *World glacier inventory – status 1988 (eds. Haeberli W. , H. Bösch, K. Østrem and G. Wallén)*, 458 pp., World Glacier Monitoring Service, Nairobi.

Imbrie, J., and K. Palmer-Imbrie (1986), *Ice ages: Solving the Mystery*, Cambridge, Massachusetts: Harvard University Press.

IPCC (2001), *Climate change 2001: the scientific basis. Contribution of working group I to the third assessment report of the intergovernmental panel on climate change. (eds. Houghton, J. T. , Y. Ding, D. J. Griggs, M. Noguer, P. J. van der Linden, X. Dai, K. Maskell and C. A. Johnson)*, Cambridge University Press, Cambridge, UK and NY, USA.

IPCC (2007), *Climate Change 2007: The physical science basis. Contribution of working group I to the fourth assessment report of the Intergovernmental Panel on Climate Change. (eds. Solomon, S., D. Qin, M. Manning, Z. Chen, M. Marquis, K.B. Averyt, M. Tignor and H.L. Miller)*, 996 pp., Cambridge University Press, Cambridge, United Kingdom and New York, NY, USA.

Iqbal, M. (1983), *An Introduction to Solar Radiation*, Academic Press, Toronto.

IUGG (CCS) – UNEP – UNESCO (2005), *Fluctuations of Glaciers 1995–2000*, vol. VIII, World Glacier Monitoring Service, Zurich.

Jacob, D., et al. (2001), A comprehensive model inter- comparison study investigating the water budget during the BALTEX-PIDCAP period, *Meteorology and Atmospheric Physics*, *77*(1–4), 19–43.

Jansson, P. (1999), Effect of uncertainties in measured variables on the calculated mass balance of Storglaciären, *Geografiska Annaler*, *81 A*, 633–642.

Jóhannesson, T., C. Raymond, and E. Waddington (1989), Time-scale for adjustment of glaciers to changes in mass balance, *Journal of Glaciology*, *35*(121), 355–369.

Jóhannesson, T., O. Sigurðsson, H. Björnsson, and F. Pálsson (2004), Use of glacier mass balance observations to derive spatial precipitation distribution in glaciated areas, International Conference on Mesoscale Meteorology and Climate Interaction, Reykjavik, http://andvari.vedur.is/∼tj/abstr/mmci2004eabstr.pdf.

Kääb, A., and M. Funk (1999), Modelling mass balance using photogrammetric and geophysical data: a pilot study at Griesgletscher, Swiss Alps, *Journal of Glaciology*, *45*(151), 575–583.

Kalnay, E., et al. (1996), The NCEP/NCAR 40-year reanalysis project, *Bulletin of the American Meteorological Society*, *77*(3), 437–471.

Kanagaratnam, P., S. Gogineni, V. Ramasami, and D. Braaten (2004), A wideband radar for high-resolution mapping of near-surface internal layers in glacial ice, *IEEE Transactions on Geoscience and Remote Sensing*, *42*(3), 483–490.

Kästner, M., and K. T. Kriebel (2001), Alpine cloud climatology using long-term NOAA-AVHRR satelite data, *Theoretical and Applied Climatology*, *68*(3–4), 175–195.

Kerschner, H., G. Kaser, and R. Sailer (2000), Alpine Younger Dryas glaciers as paleo-precipitation gauges, *Annals of Glaciology*, *31*, 80–84.

Khodakov, V. G. (1975), Glaciers as water resource indicators of the glacial areas of the USSR, in *Snow and Ice (Proc. Moscow Symp., August 1971)*, *IAHS Publ.*, vol. 104, pp. 22–29.

Kilisholm, S., J. H. Christensen, K. Dethloff, and A. Rinke (2003), Net accumulation of the Greenland ice sheet: High resolution modeling of climate changes, *Geophysical Research Letters*, *30*(9), 1485, doi:10.1029/2002GL015742.

Kilsby, C. G., P. D. Jones, A. Burton, A. C. Ford, H. J. Fowler, C. Harpham, P. James, A. Smith, and R. L. Wilby (2007), A daily weather generator for use in climate change studies, *Environmental Modelling & Software*, *22*(12), 1364–8152.

Kirchhofer, W., and B. Sevruk (2001), Mittlere jährliche korrigiert Niederschlagshöhe 1951-1980, in *Hydrological Atlas of Switzerland*, Landeshydrologie und Geologie, Bern, Switzerland, Plate 2.2.

Kleinn, J., C. Frei, J. Gurtz, D. Lüthi, P. L. Vidale, and C. Schär (2005), Hydrologic simulations in the Rhine basin driven by a regional climate model, *Journal of Geophysical Research*, *110*, D04,102, doi:10.1029/2004JD005143.

Klok, E. J., and J. Oerlemans (2002), Model study of the spatial distribution of the energy and mass balance of Morteratschgletscher, Switzerland, *Journal of Glaciology*, *48*(163), 505–518.

Klok, E. J., and J. Oerlemans (2004), Modelled climate sensitivity of the mass balance of Morteratschgletscher and its dependence on albedo parameterization, *International Journal of Climatology*, *24*(2), 231–245.

Knap, W., C. Reijmer, and J. Oerlemans (1999a), Narrowband to broadband conversion of Landsat TM glacier albedos, *International Journal of Remote Sensing*, *20*(10), 2091–2110.

Knap, W. H., B. W. Brock, J. Oerlemans, and I. C. Willis (1999b), Comparison of Landsat TM-derived and ground-based albedos of Haut Glacier d'Arolla, Switzerland, *International Journal of Remote Sensing*, *20*(17), 3293–3310, doi: 10.1080/014311699211345.

Kohler, J., J. Moore, M. Kennett, R. Engeset, and H. Elvehøy (1997), Using ground-penetrating radar to image previous years' summer surfaces for mass-balance measurements, *Annals of Glaciology*, *24*, 355–360.

Konikow, L., and J. Bredehoeft (1992), Ground-water models cannot be validated, *Advances in Water Resources*, *15*, 75–83.

Konzelmann, T., R. V. de Wal, W. Greuell, R. Bintanja, E. Henneken, and A. Abe-Ouchi (1994), Parameterization of global and longwave incoming radiation for the Greenland Ice Sheet, *Global and Planetary Change*, *9*(1–2), 143–164.

Kotlarski, S. (2007), A subgrid glacier parameterisation for use in regional climate modelling, Ph.D. thesis, University of Hamburg. Max Planck Institute for Meteorology, Reports on Earth System Science No. 42.

Kotlarski, S., A. Block, U. Böhm, D. Jacob, K. Keuler, R. Knoche, D. Rechid, and A. Walter (2005), Regional climate model simulations as input for hydrological applications: evaluation of uncertainties, *Advances in Geosciences*, *5*, 119–125.

Kotlarski, S., F. Paul, and D. Jacob (subm), Forcing a distributed glacier mass balance model with the regional climate model REMO, part I: RCM evaluation, *Journal of Climate*.

Kotlyakov, V. M. (1973), Snow accumulation on mountain glaciers, in *The Role of Snow and Ice in Hydrology. (Proc. Banff. Symp., September 1972)*, *IAHS Publication*, vol. 107, pp. 394–400, IAHS Press: Wallingford.

Kotlyakov, V. M., and A. N. Krenke (1982), Investigations of the hydrological conditions of alpine regions by glaciological methods, in *Symposium at Exeter 1982 – Hydrological aspects of alpine and high mountain areas*, *IAHS Publication*, vol. 138, pp. 31–42, IAHS Press: Wallingford.

Kovacs, A., A. Gow, and R. Morey (1995), The in-situ dielectric constant of polar firn revisited, *Cold Regions Science and Technology*, *23*(3), 245–256.

Kraus, H. (1973), Energy exchange at air-ice interface, in *The Role of Snow and Ice in Hydrology. (Proc. Banff. Symp., September 1972)*, *IAHS Publication*, vol. 107, pp. 128–164, IAHS Press: Wallingford.

Krenke, A. N. (1975), Climatic conditions of present-day glaciation in Soviet Central Asia, in *Snow and Ice (Proc. Moscow Symp., August 1971)*, *IAHS Publ.*, vol. 104, pp. 30–41.

Krimmel, R. M. (1999), Analysis of differences between direct and geodetic mass balance measurements at South Cascade Glacier, Washington, *Geografiska Annaler*, *81A*(4), 653–658.

Kuhn, M. (1981), Climate and glaciers, in *Sea level, ice and climatic change (Proceedings of the Canberra Symposium, December 1979)*, *IAHS Publ.*, vol. 131, pp. 3–20.

Kuhn, M. (2003), Redistribution of snow and glacier mass balance from a hydrometeorological model, *Journal of Hydrology*, *282*(1–4), 95–103, doi:10.1016/S0022-1694(03)00256-7.

Lefebre, F., X. Fettweis, H. Gallée, J.-P. V. Ypersele, P. Marbaix, W. Greuell, and P. Calanca (2005), Evaluation of a high-resolution regional climate simulation over Greenland, *Climate Dynamics*, *25*(1), 99–116.

Leung, L., and S. Ghan (1999), Pacific northwest sensitivity simulated by a regional climate model driven by a GCM. part I: Control simulations, *Journal of Climate*, *12*(7), 2010–2030.

Liston, G., and M. Sturm (1998), A snow-transport model for complex terrain, *Journal of Glaciology*, *44*(148), 498–516.

Machguth, H. (2003), Messung und Modellierung der Massenbilanzverteilung auf Gletschern der Schweizer Alpen, Master's thesis, University of Zurich, Department of Geography.

Machguth, H., O. Eisen, F. Paul, and M. Hoelzle (2006a), Strong spatial variability of snow accumulation observed with helicopter-borne GPR on two adjacent Alpine glaciers, *Geophysical Research Letters*, *33*, L13,503, doi:10.1029/2006GL026576.

Machguth, H., F. Paul, M. Hoelzle, and W. Haeberli (2006b), Distributed glacier mass-balance modelling as an important component of modern multi-level glacier monitoring, *Annals of Glaciology*, *43*, 335–343.

Machguth, H., R. S. Purves, J. Oerlemans, M. Hoelzle, and F. Paul (2008), Exploring uncertainty in glacier mass balance modelling with Monte Carlo simulation, *The Cryosphere*, *2*, 191–204, http://www.the-cryosphere.net/2/191/2008/tc-2-191-2008.html.

Maisch, M., A. Wipf, B. Denneler, J. Battaglia, and C. Benz (1999), *Die Gletscher der Schweizer Alpen. Gletscherhochstand 1850, Aktuelle Vergletscherung, Gletscherschwund-Szenarien. Schlussbericht NFP 31-Projekt Nr. 4031-033412,*, vdf-Hochschulverlag ETH Zürich.

Marchand, W. D., A. Killingtveit, P. Wilen, and P. Wikstrom (2003), Comparison of ground-based and airborne snow depth measurements with georadar systems, case study, *Nordic Hydrology*, *34*(5), 427–448.

Marty, C., R. Philipona, C. Fröhlich, and A. Ohmura (2002), Altitude dependence of surface radiation fluxes and cloud forcing in the Alps: Results from Alpine Surface Radiation Budget Network., *Theoretical and Applied Climatology*, *72*(3–4), 137–155.

McGregor, J. L. (1997), Regional climate modelling, *Meteorology and Atmospheric Physics*, *63*, 105–117.

McGuffie, K., and A. Henderson-Sellers (2001), Forty years of numerical climate modelling, *International Journal of Climatology*, *21*(9), 1067–1109, doi: 10.1002/joc.632.

Mearns, L., W. Easterling, C. Hays, and D. Marx (2001), Comparison of agricultural impacts of climate change calculated from high and low resolution climate model scenarios: part I. the uncertainty due to spatial scale, *Climatic Change*, *51*(2), 131–172.

Mearns, L. O., F. Giorgi, P. Whetton, D. Pabon, M. Hulme, and M. Lal (2003), Guidelines for use of climate scenarios developed from regional climate model experiments, *Tech. rep.*, Data Distribution Centre of the International Panel of Climate Change, http://www.ipcc-data.org/guidelines/dgm_no1_v1_10-2003.pdf.

Meehl, G., C. Covey, T. Delworth, M. Latif, B. McAvaney, J. Mitchell, R. Stouffer, and K. Taylor (2007), The WCRP CMIP3 multimodel dataset: A new era in climate change research, *Bulletin of the American Meteorological Society*, *88*(9), 1383–1394.

Meerkötter, R., C. König, P. Bissolli, G. Gesell, and H. Mannstein (2004), A 14-year European cloud climatology from NOAA/AVHRR data in comparison to surface observations, *Geophysical Research Letters*, *31*, L15,103, doi:10.1029/2004GL020098.

Meier, M., and D. Bahr (1996), Counting glaciers: Use of scaling methods to estimate the number and size distribution of the glaciers of the world, in *CRREL Special Reports 96-27*, pp. 89–94.

Meier, M. F. (1965), Glaciers and climate, in *The Quartenary of the United States*, edited by H. E. Wright and D. G. Frey, Princeton University Press, Princeton, New Jersey.

Meier, M. F., M. B. Dyurgerov, U. K. Rick, S. O'Neel, W. T. Pfeffer, R. S. Anderson, S. P. Anderson, and A. F. Glazovsky (2007), Glaciers dominate eustatic sea-level rise in the 21st century, *Science*, *317*, 1064–1067, dOI: 10.1126/science.1143906.

Melcher, N., et al. (2002), River discharge measurements by using helicopter-mounted radar, *Geophysical Research Letters*, *29*(22), doi:10.1029/2002GL015525.

meteoswiss (2008), http://www.meteoschweiz.admin.ch/web/en/research/good_to_know/records/switzerland.html, accessed 28 August 2008.

Moesch, M., and A. Zelenka (2004), Globalstrahlungsmessung 1981–2000 im ANETZ, *Arbeitsbericht 207*, MeteoSchweiz.

Monin, A. S., and A. M. Obukhov (1954), Basic laws of turbulent mixing in the ground layer of the atmosphere, *Trans. Geophys. Inst. Akad. Nauk. USSR*, *151*, 163–187.

Müller, F., T. Callfisch, and G. Müller (1976), *Firn und Eis der Schweizer Alpen, Gletscherinventar.*, vol. 57, 57a, ETH-Zürich.

Müller, H., and G. Kappenberger (1991), *Claridenfirn-Messungen 1914-1984*, *Zürcher Geographische Schriften*, vol. 40, ETH Zurich, Geographisches Institut.

Nemec, J., P. Huybrechts, O. Rybak, and J. Oerlemans (subm), Reconstruction of the surface mass balance of Morteratsch glacier since 1865, *Annals of Glaciology*.

New, M., M. Hulme, and P. Jones (2000), Representing twentieth-century space-time climate variability. Part II: development of 1901–96 monthly grids of terrestrial surface climate., *Journal of Climate*, *13*(13), 2217–2238.

Nye, J. (1960), The response of glaciers and ice-sheets to seasonal and climatic changes, *Proceedings of the Royal Society of London, Series A*, *256*(1287), 559–584.

Obleitner, F., and M. Lehning (2004), Measurements and simulation of snow and superimposed ice at the Kongsvegen glacier, Svalbard (Spitzbergen), *Journal of Geophysical Research*, *109D*(D04106), D04,106, doi:10.1029/2003JD003945.

Oerlemans, J. (1992a), A model for the surface balance of ice masses: part I. Alpine glaciers, *Zeitschrift für Gletscherkunde und Glazialgeologie*, *27/28*, 63–83.

Oerlemans, J. (1992b), Climate sensitivity of glaciers in southern Norway: application of an energy-balance model to Nigardsbreen, Hellstugubreen and Alfotbreen, *Annals of Glaciology*, *38*, 223–232.

Oerlemans, J. (2000), Analysis of a 3 year meteorological record from the ablation zone of Morteratschgletscher, Switzerland: energy and mass balance, *Journal of Glaciology*, *46*(155), 571–579.

Oerlemans, J. (2001), *Glaciers and Climate Change*, A.A. Balkema Publishers, Lisse.

Oerlemans, J., and B. Grisogono (2002), Glacier winds and parameterisation of the related surface heat fluxes, *Tellus*, *54A*, 440–452, doi:10.1034/j.1600-0870.2002.201398.x.

Oerlemans, J., and E. Klok (2002), Energy balance of a glacier surface: analysis of automatic weather station data from Morteratschgletscher, Switzerland, *Arctic, Antarctic, and Alpine Research*, *34*(4), 477–485.

Oerlemans, J., and W. H. Knap (1998), A 1 year record of global radiation and albedo in the ablation zone of Morteratschgletscher, Switzerland, *Journal of Glaciology*, *44*(147), 231–238.

Oerlemans, J., and B. Reichert (2000), Relating glacier mass balance to meteorological data by using a seasonal sensitivity characteristic, *Journal of Glaciology*, *46*(152), 1–6.

Oerlemans, J., R. Giessen, and M. van den Broeke (subm), Retreating alpine glaciers: increased melt rates due to accumulation of dust (Vadret da Morterastch, Switzerland), *Journal of Glaciology*.

Oerlemans, J., et al. (1998), Modelling the response of glaciers to climate warming, *Climate Dynamics*, *14*(4), 267–274, doi: 10.1007/s003820050222.

Ohmura, A. (2001), Physical basis for the temperature-based melt-index method, *Journal of Applied Meteorology*, *40*(4), 753–761.

Ohmura, A., and H. Lang (1989), Secular variation of global radiation in Europe, in *IRS'88: Current Problems in Atmospheric Radiation*, edited by J. Lenoble and J.-F. Geleyn, pp. 298–301, Deepak Publ., Hampton.

Ohmura, A., P. Kasser, and M. Funk (1992), Climate at the equilibrium line of glaciers, *Journal of Glaciology*, *38*(130), 397–411.

Ohmura, A., A. Bauder, H. Müller, and G. Kappenberger (2007), Long-term change of mass balance and the role of radiation, *Annals of Glaciology*, *46*, 367–374.

Oreskes, N., K. Shrader-Frechette, and K. Belitz (1994), Verification, validation, and confirmation of numerical models in the eart sciences, *Science*, *263*(5147), 641–646.

Østrem, G., and M. Brugman (1991), *Glacier mass-balance measurements: a manual for field and office work*, NHRI Science Report.

Østrem, G., and N. Haakensen (1999), Map comparison or traditional mass-balance measurements: Which method is better?, *Geografiska Annaler*, *81A*(4), 703–711, doi:10.1111/j.0435-3676.1999.00098.x.

Pappenberger, F., and K. J. Beven (2006), Ignorance is bliss: Or seven reasons not to use uncertainty analysis, *Water Resources Research*, *42*(5), W05,302, doi:10.1029/2005WR004820.

Paul, F. (2007), The new Swiss glacier inventory 2000 – application of remote sensing and GIS., Ph.D. thesis, University of Zurich, Zurich.

Paul, F. (2008), Calculation of glacier elevation changes with SRTM: Is there an elevation dependent bias?, *Journal of Glaciology*, *55*(188), 945–946.

Paul, F., and W. Haeberli (2008), Spatial variability of glacier elevation changes in the Swiss Alps obtained from two digital elevation models, *Geophysical Research Letters*, *35*, L21,502.

Paul, F., and S. Kotlarski (subm), Forcing a distributed mass balance model with the regional climate model REMO, part II: Downscaling strategy and first results, *Journal of Climate*.

Paul, F., A. Kääb, M. Maisch, T. Kellenberger, and W. Haeberli (2002), The new remote-sensing-derived Swiss glacier inventory. I. methods, *Annals of Glaciology*, *34*, 355–361.

Paul, F., A. Kääb, M. Maisch, T. W. Kellenberger, and W. Haeberli (2004), Rapid disintegration of Alpine glaciers observed with satellite data, *Geophysical Research Letters*, *31*, L21,402, doi:10.1029/2004GL020816.

Paul, F., H. Machguth, and A. Kääb (2005), On the impact of glacier albedo under conditions of extreme glacier melt: the summer of 2003 in the Alps, in *EARSeL eProceedings*, vol. 4, pp. 139–149.

Paul, F., A. Kääb, and W. Haeberli (2007), Recent glacier changes in the Alps observed from satellite: consequences for future monitoring strategies, *Global and Planetary Change*, *56*, 111–122.

Paul, F., H. Machguth, M. Hoelzle, N. Salzmann, and W. Haeberli (2008), Alpine-wide distributed glacier mass balance modelling: a tool for assessing future glacier change?, in *The Darkening Peaks: Glacial Retreat in Scientific and Social Context*, edited by B. Orlove, E. Wiegandt, and B. Luckman, pp. 111–125, University of California Press.

Paul, F., A. Kääb, H. Rott, A. Shepherd, T. Strozzi, and E. Volden (2009), GlobGlacier: Mapping the worlds glaciers and ice caps from space, in *EARSeL ePro-ceedings*.

Pellicciotti, F., B. Brock, U. Strasser, P. Burlando, M. Funk, and J. Corripio (2005), An enhanced temperature-index glacier melt model including the shortwave radiation balance: development and testing for Haut Glacier d'Arolla, Switzerland, *Journal of Glaciology*, *51*(175), 573–587.

Philipona, R., and B. Dürr (2004), Greenhouse forcing outweighs decreasing solar radiation driving rapid temperature rise over land, *Geophysical Research Letters*, *31*, L22,208, doi:10.1029/2004GL020937.

Philipona, R., B. Dürr, C. Marty, A. Ohmura, and M. Wild (2004), Radiative forcing measured at Earth's surface - corroborate the increasing greenhouse effect, *Geophysical Research Letters*, *31*, L03,202, doi:10.1029/2003GL018765.

Plattner, C., L. N. Braun, and A. Brenning (2006), Spatial variability of snow accumulation on Vernagtferner, Austrian Alps, in winter 2003/2004, *Zeitschrift für Gletscherkunde und Glazialgeologie*, *39*, 43–57.

Plummer, M. A., and F. M. Phillips (2003), A 2-D numerical model of snow/ice energy balance and ice flow for paleoclimatic interpretation of glacial geomorphic features, *Quaternary Science Reviews*, *22*(14), 1389–1406.

Purves, R., J. Barton, W. Mackaness, and D. Sugden (1998), The developmemt of a rule-based spatial model of wind transport and depostion of snow, *Annals of Glaciology*, *26*, 197–202.

Quinn, P., K. Beven, P. Chevallier, and O. Planchon (1991), The prediction of hillslope flow paths for distributed hydrological modeling using digital terrain models, *Hydrological Processes*, *5*(1), 59–80.

Radić, V., and R. Hock (2006), Modeling future glacier mass balance and volume changes using ERA-40 reanalysis and climate models: A sensitivity study at Storglaciaren, Sweden, *Journal of Geophysical Research*, *111*(F3), F03,003, doi:10.1029/2005JF000440.

Raper, S. C. B., and R. J. Braithwaite (2006), Low sea level rise projections from mountain glaciers and icecaps under global warming, *Nature*, *439*, 311–313, doi:10.1038/nature04448.

Raymond, C., T. A. Neumann, E. Rignot, K. Echelmeyer, A. Rivera, and G. Casassa (2005), Retreat of Glaciar Tyndall, Patagonia, over the last half-century, *Journal of Glaciology*, *51*(173), 239–247.

Reeh, N. (1991), Parametrizations of melt rate and surface temperature on the Greenland ice sheet, *Polarforschung*, *59*, 113–128.

Reijmer, C. H., and R. Hock (2008), Internal accumulation on Storglaciären, Sweden, in a multi-layer snow model coupled to a distributed energy- and mass-balance model, *Journal of Glaciology*, *54*(184), 61–72.

Ren, D., D. Karoly, and L. Leslie (2007), Temperate mountain glacier-melting rates for the period 2001-30: Estimates from three coupled GCM simulations for the greater Himalayas, *Journal of Applied Meteorology and Climatology*, *46*(6), 890–899.

Richardson, C., E. Aarholt, S.-E. Hamram, P. Holmlund, and E. Isaksson (1997), Spatial distribution of snow in western Dronning Maud Land, East Antarctica, mapped by a ground-based snow radar, *Journal of Geophysical Research*, *102*(B9), 20,343–20,353.

Rohrer, M. (1989), Determination of the transition air temperature from snow to rain and intensity of precipitation., in *WMO/IAHS/ETH International Workshop on Precipitation Measurements St. Moritz, 1989 Switzerland*, pp. 475–482, ETH Zurich, Switzerland.

Rossow, W. B., and R. A. Schiffer (1999), Advances in understanding clouds from ISCCP, *Bulletin of the American Meteorological Society*, *80*, 2261–2287.

Rotschky, G., O. Eisen, F. Wilhelms, U. Nixdorf, and H. Oerter (2004), Spatial distribution of surface mass balance on Amundsenisen plateau, Antarctica, derived from ice-penetrating radar studies, *Annals of Glaciology*, *39*, 265–270.

RSI Research Systems Inc. (2004), *IDL reference guide, July 2004 Edition*, RSI Research Systems Inc.

Salzmann, N. (2006), The use of results from regional climate models for local-scale permafrost modeling in complex high-mountain topography – posibilities, limitations and chalenges for the future, Phd-thesis, Department of Geography, University of Zurich, Switzerland.

Salzmann, N., C. Frei, P. Vidale, and M. Hoelzle (2007a), The application of regional climate model output for the simulation of high-mountain permafrost scenarios, *Global and Planetary Change*, *56*(1-2), 188–202, doi:10.1016/j.gloplacha.2006.07.006.

Salzmann, N., J. Nötzli, C. Hauck, S. Gruber, M. Hoelzle, and W. Haeberli (2007b), Ground surface temperature scenarios in complex high-mountain topography based on regional climate model results, *Journal of Geophysical Research*, *112*, F02S12, doi:10.1029/2006JF000527.

Sauberer, F. (1955), Zur Abschätzung der Globalstrahlung in verschiedenen Höhenstufen der Ostalpen, *Wetter und Leben*, *7*, 22–29.

Sauberer, F., and I. Dirmhirn (1952), Der Strahlungshaushalt horizontaler Gletscherflächen auf dem hohen Sonnblick, *Geografiska Annaler*, *34*, 261–290, http://www.jstor.org/stable/520156.

Schär, C., T. D. Davies, C. Frei, H. Wanner, M. Widmann, M. Wild, and H. C. Davies (1998), Current alpine climate, in *Views from the Alps. Regional perspectives on Climate Change*, edited by P. Cebon, U. Dahinden, H. C. Davies, D. Imboden, and C. C. Jaeger, pp. 21–72, The MIT Press, Cambridge, Massachusetts, USA.

Schär, C., P. L. Vidale, D. Lüthi, C. Frei, C. Häberli, M. A. Liniger, and C. Appenzeller (2004), The role of increasing temperature variability in European summer heatwaves, *Nature*, *427*(6972), 332–336, doi: 10.1038/nature02300.

Schmidli, J., C. Schmutz, C. Frei, H. Wanner, and C. Schär (2002), Mesoscale precipitation variability in the region of the european Alps during the 20th century, *International Journal of Climatology*, *22*(9), 1049–1074, doi:10.1002/joc.769.

Schmidli, J., C. Frei, and P. L. Vidale (2006), Downscaling from GCM precipitation: a benchmark for dynamical and statistical downscaling methods, *International Journal of Climatology*, *26*(5), 679–689, doi: 10.1002/joc.1287.

Schneeberger, C., H. Blatter, A. Abe-Ouchi, and M. Wild (2003), Modelling changes in the mass balance of glaciers of the northern hemisphere for a transient $2\times CO^2$ scenario, *Journal of Hydrology*, *282*(1–4), 145–163.

Schüepp, M., M. Bouét, M. Bider, and C. Urfer (1978), Regionale Klimabeschreibungen (1. Teil), in *Beiheft Annalen SMA*, SMA, Zürich.

Schwarb, M. (2000), *The alpine precipitation climate : evaluation of a high-resolution analysis scheme using comprehensive rain-gauge data*, ETH Dissertation No. 13911, ETH Zurich, Institute for Climate Research, http://e-collection.ethbib.ethz.ch/show?type=diss&nr=13911.

Schwarb, M., C. Daly, C. Frei, and C. Schär (2001), Mean annual precipitation throughout the European Alps 1971-1990, in *Hydrological Atlas of Switzerland*, Landeshydrologie und Geologie, Bern, Switzerland, Plate 2.6.

Schwerzmann, A., M. Funk, H. Blatter, M. Lüthi, M. Schwikowski, and A. Palmer (2006), Reconstruction of past accumulation rates in an alpine firn region: Fiescherhorn, Swiss Alps., *Journal of Geophysical Research*, *111*, F01,014, doi:10.1029/2005JF000283.

Sevruk, B. (1985a), Correction of precipitation measurements: Summary report., in *Proceedings Workshop on the Correction of Precipitation Measurements 1985 Zurich*, pp. 13–23.

Sevruk, B. (1985b), Correction of precipitation measurements: Swiss experience, in *Proceedings Workshop on the Correction of Precipitation Measurements 1985 Zurich*, pp. 187–193.

Sevruk, B. (1989), Reliability of precipitation measurements, in *WMO IAHS ETH, International Workshop on Precipitation Measurement, St. Moritz,1989 Switzerland*, pp. 13–19.

Sevruk, B. (1997), Regional dependency of precipitation–altitude relationship in the Swiss Alps, *Climatic Change*, *36*(3–4), 355–369.

Skoda, G., and P. Lorenz (2003), Mean annual precipitation, in *Hydrological Atlas of Austria*, Bundesministerium für Land- und Forstwirtschaft, Umwelt und Wasserwirtschaft (BMLFUW). Österreichischer Kunst- und Kulturverlag, Vienna.

Stahl, K., R. D. Moore, J. M. Shea, D. Hutchinson, and A. J. Cannon (2008), Coupled modelling of glacier and streamflow response to future climate scenarios, *Water Resources Research*, *44*, W02,422, doi:10.1029/2007WR005956.

Strasser, U., J. Corripio, F. Pellicoti, P. Burlando, B. Brock, and M. Funk (2004), Spatial and temporal variability of meteorological variables at Haut Glacier d'Arolla (Switzerland) during the ablation season 2001: measurements and simulations, *Journal of Geophysical Research*, *109*, D03,103, doi:10.1029/2003JD003973.

Strasser, U., M. Bernhardt, M. Weber, G. E. Liston, and W. Mauser (2008), Is snow sublimation important in the alpine water balance?, *The Cryosphere*, *2*, 53–66, www.the-cryosphere.net/2/53/2008/.

Suter, S. (2002), Cold firn and ice in the Monte Rosa and Mont Blanc areas: spatial occurrence, surface energy balance and climatic evidence, Ph.D. thesis, Versuchsanstalt für Wasserbau, Hydrologie und Glaziologie (VAW), ETH Zurich.

Swisstopo (2004), Atlas of Switzerland 2, DVD-ROM, Bundesamt für Landestopografie, Bern, Switzerland.

Tatang, M., W. Pan, R. Prinn, and G. McRae (1997), An efficient method for parametric uncertainty analysis of numerical geophysical models, *Journal of Geophysical Research*, *102*(D18), 21,925–21,932.

Taurisano, A., T. V. Schuler, J. O. Hagen, , T. Eiken, E. Loe, , K. Melvold, and J. Kohler (2007), The distribution of snow accumulation across the Austfonna ice cap, Svalbard: direct measurements and modelling, *Polar Research*, *26*, 7–13, doi: 10.1111/j.1751-8369.2007.00004.x.

Tebaldi, C., and R. Knutti (2007), The use of the multi-model ensemble in probabilistic climate projections, *Philosophical Transactions of the Royal Society A*, *365*, 2053–2075.

Thorning, L., and E. Hansen (1987), Electromagnetic reflection survey 1986 at the inland ice margin of Pakitsoq basin, central Greenland, *Rapport Grønlands Geologiske Undersøgelse*, *135*, 87–95.

Tiuri, M., A. Sihvola, E. Nyfors, , and M. Hallikainen (1984), The complex dielectric constant of snow at microwave frequencies, *IEEE Journal of Oceanic Engineering*, *9*(5), 377–382.

Uppala, S., et al. (2005), The ERA-40 re-analysis, *Quarterly Journal of the Royal Meteorological Society*, *131*(612), 2961–3012.

Van de Wal, R. S. M., and M. Wild (2001), Modelling the response of glaciers to climate change by applying volume-area scaling in combination with a high resolution GCM, *Climate Dynamics*, *18*(3–4), 359–366.

van der Veen, C. J. (2002), Polar ice sheets and global sea level: how well can we predict the future?, *Global and Planetary Change*, *32*(2-3), 165–194.

Verseghy, D. (1991), CLASS-A Canadian land surface scheme for GCMs. I. soil model, *International Journal of Climatology*, *11*(2), 111–133.

Vögele, A. (1987), Die Anfänge der Gletscherforschung und der Glazialtheorie, in *Sonderband Eiszeitforschung*, *Mitteilungen der Naturforschenden Gesellschaft Luzern*, vol. 29, pp. 11–50, Naturforschende Gesellschaft Luzern.

Wadhams, P., M. A. Lange, and S. F. Ackley (1987), The Ice Thickness Distribution Across the Atlantic Sector of the Antarctic Ocean in Midwinter, *Journal of Geophysical Research*, *92*(C13), 14,535–14,552.

WGMS (2007), *Glacier Mass Balance Bulletin No. 9 (2004–2005)*, ICSU(FAGS)/IUGG(IACS)/UNEP/UNESCO/WMO, World Glacier Monitoring Service, University of Zurich.

Wilby, R., S. P. Charles, E. Zorita, B. Timbal, P. Whetton, and L. Mearns (2004), Guidelines for use of climate scenarios developed from statistical downscaling methods, *Tech. rep.*, Data Distribution Centre of the International Panel of Climate Change, http://www.ipcc-data.org/guidelines/dgm_no2_v1_09_2004.pdf.

Wild, M., et al. (2005), From dimming to brightening: Decadal changes in solar radiation at the Earth's surface, *Science*, *308*(5723), 847–850.

Wilson, J. P., and J. C. Gallant (2000), *Terrain Analysis: Principles and Applications*, 479 pp., Wiley and Sons.

Winstral, A., K. Elder, and R. Davis (2002), Spatial snow modeling of wind-redistributed snow using terrain-based parameters, *Journal of Hydrometeorology*, *3*(5), 524–538.

Wipf, A. (1999), *Die Gletscher der Berner, Waadtländer und nördlichen Walliser Alpen. Eine regionale Studie über die Vergletscherung im Zeitraum "Vergangenheit" (Hochstand 1850), "Gegenwart" (Ausdehnung im Jahr 1973) und "Zukunft" (Gletscherschwund-Szenarien, 21. Jhdt.)*, *Physische Geographie*, vol. 40, Department of Geography, University of Zurich.

Yankielun, N., W. Rosenthal, and R. E. Davis (2004), Alpine snow depth measurements from aerial FMCW radar, *Cold Regions Science and Technology*, *40*(1-2), 123–134.

Zemp, M., R. Frauenfelder, W. Haeberli, and M. Hoelzle (2005), Worldwide glacier mass balance measurements: general trends and first results of the extraordinary year 2003 in central Europe, in *Materiali Gljaziologičeskix Issledovanij (Data of Glaciological Studies)*, vol. 99, pp. 3–12, Moscow, Russia.

Zemp, M., W. Haeberli, M. Hoelzle, and F. Paul (2006a), Alpine glaciers to disappear within decades?, *Geophysical Research Letters*, *33*(13), L13,504, doi:10.1029/2006GL026319.

Zemp, M., M. Hoelzle, and W. Haeberli (2006b), Distributed modelling of the regional climatic equilibrium line altitude of glaciers in the European Alps, *Global and Planetary Change*, *56*(1/2), 83–100, doi:10.1016/j.gloplacha.2006.07.002.

Zemp, M., M. Hoelzle, and W. Haeberli (subm), Six decades of glacier mass balance observations, a review of the worldwide monitoring network, *Annals of Glaciology*.

Zhang, J., U. Bhatt, and W. V. Tangborn (2007), Climate downscaling for estimating glacier mass balances in northwestern North America: Validation with a USGS benchmark glacier, *Geophysical Research Letters*, *34*(21), L21,505, doi:10.1029/2007GL031139.

Zumbühl, H. J. (1980), *Die Schwankungen der Grindelwaldgletscher in den historischen Bild- und Schriftquellen des 12. bis 19. Jahrhunderts – Ein Beitrag zur Gletschergeschichte und Erforschung des Alpenraumes*, *Denkschriften der Schweizerischen Naturforschenden Gesellschaft*, vol. 92, Birkhäuser, Basel/Boston/Stuttgart.

Acknowledgments

I would like to thank all those who supported and helped me in various ways during my PhD studies:

First of all I want to acknowledge the continuous and strong support from the side of my supervisors: Frank Paul, Martin Hölzle and Wilfried Haeberli gave me the opportunity to work on this thesis, they were always there when help was needed, they showed me their strong interest in my work and many ideas evolved from the numerous inspiring discussions with them. Thank you very much!

Johannes Oerlemans provided me the possibility to work in the glacier and climate research group at the IMAU, Utrecht University, the Netherlands. During the three months in Utrecht I gained valuable insight into new topics and different scientific approaches which hopefully broadened my scientific horizon. Thank you Hans and the people at IMAU for the good time in Utrecht, for many fruitful discussions and the possibility to work with the Morteratsch data.

During my PhD-studies I had the opportunity to collaborate with different scientists having their research topic outside of glacier mass balance modeling. Their input was a most valuable contribution to my work: Olaf Eisen thought me a lot about GPR and converted me to use LaTeX which made survival in science much easier for me. Ross Purves introduced me to the field of uncertainties and with him I could share many interesting discussions, about science and many other things. Sven Kotlarski, a climate modeler who also grazes in the field of glacier mass balance had the patience to explain numerous aspects of climate modeling to me and he performed the REMO run which was applied in this study.

During fieldwork on Findel and Adler Glacier I could count on numerous helping hands. Without you, the measurements would not have been possible: Andrey Abramov, Simon Allen, Sabine Baumann, Simone Bircher, Lorenz Böckli, Xavier Bodin, Ruzica Dadic, Stefan Gruber, Luzia Fischer, Regula Frauenfelder, Esther Frey, Holger Frey, Andi Hasler, Esther Hegglin, Martin Hoelzle, Hew Horgan, Christian Huggel, Simone Knecht, Sven Kotlarski, Jeannette Nötzli, Michel Obando, Kristina Roth, Nadine Salzmann, Marlene Scheel, Olga Stantsel, Bernd Steimann, Theresa Tribaldos, Matthias Ulmer, Reto Waldmeier, Michi Zemp and Michael Ziefle. I also want to say thank you to Gianni Mazzone, the Mountain Guides from Zermatt and the people from the Stockhorn Bahn for their support.

I very much enjoyed to work in the 3g group and want to say thank you to my colleagues who contributed to the good working atmosphere! There are also people behind the scene that gave me every-day support: The IT group at GIUZ, the secretaries as well as Susan Braun-Clarke and Ivan Woodhatch who did excellent proofreading of my PhD, thanks a lot!

My deepest gratitude is offered to my parents for their continuous support on my way.

Я чочу выражать мое самое большое благодарность Симон, за то что ты мне подержаешь так крепко, и за все наше замечательное совместное времия!

MeteoSwiss is acknowledged for providing access to their large data archive that formed an important base of all model runs. This PhD thesis was made possible thanks to the financial support of the Swiss Science Foundation (Grant 21–105214 and 20–117761).

Appendix A

Findel Glacier Measurements

The data from the Findel Glacier measurements are listed in a table on the following page. The applied naming convention for the stake loactions refers to the map of Findel and Adler Glacier (Fig. 3.1). On most of these stake locations not one but two stakes have been operated in parallel for most of the time to avoid complete melt-out and loss of data. Indeed, a complete melt-out never occurred during the four years of observation. At every stake location the newer one of the two stakes was always placed up-glacier to compensate for glacier flow. On the tongue of the glacier annual horizontal flow is within the uncertainty of the GPS (less than 5 m). The two stakes are thus placed not more than 10 m apart. In the Central part of the glacier, at Fi7 and Fi8, observed annual flow is roughly 50–70 m a year and the two stakes at these stake location are thus clearly separated. Nevertheless, at no stake location have the two stake readings ever diverged by more than 0.2 m w.e. Larger deviations only occurred when one of the two stakes was very close to melt-out. However, even then, the values were mostly similar. This observation underlines that stake readings are at least representative for their closer vicinity (cf. *Fountain and Vecchia*, 1999; *Cogley*, 1999).

The data given in the following table refer to the stake locations and not to the individual stakes at these locations. Where readings are available from two stakes the mean has been built. In cases where one of the two stake was less than 0.7 m in the ice (close to melt-out) the value from the other stake has been used. For more detailed data from individual stakes, please contact the author.

Table .1.: Measurements on Findel and Adler Glacier. All values are given in m w.e. and show measured mass balance at the respective points over the time span starting from the previous value given in the table and ending at the actual value. Vertical bars (|) denote the starting date of measurements at the respective points. Horizontal lines (—) indicate dates where no measurements have been performed, in most cases because the stake could not be located under the snow cover. A minus sign (-) denotes a snow pit location that was located in the ablation zone at the end of the respective mass balance year.

			2004	2005				2006			2007				2008	
point	Coord	alt	28.10.	7.5.	16.8.	25.8.	17.10.	3.8.	22.8.	11.10.	30.6.	5.8.	8.10.	19.11.	26.7.	12.10.
Fi1	629700 95580	2590	|	—	-5.2	-0.3	-1.6	-5.0	-1.0	-2.0	-2.6	-2.4	-2.3	-0.2	-3.5	-3.2
Fi2	629790 95420	2580	|	—	-5.4	-0.3	-1.8	-4.5	-0.9	-2.0	-2.2	-2.5	-2.5	—	-3.6	-3.2
Fi3	630320 95450	2660	|	—	-4.1	-0.2	-1.4	-4.0	-0.8	-1.4	-1.5	-2.1	-1.9	—	-3.2	-2.8
Fi4	630920 95490	2720	|	—	-3.6	—	-1.4	-3.4	-0.8	-1.4	-1.2	-1.9	-1.8	—	-2.7	-2.7
Fi5	630990 95230	2730	|	—	-3.8	—	-1.5	-3.8	-0.7	-1.5	-1.7	-2.1	-1.9	—	-3.2	-2.7
Fi6	631530 95370	2810	|	—	-3.0	—	-1.3	-2.8	-0.6	-1.2	-0.5	-1.8	-1.5	—	-1.9	-2.2
Fi7	632180 94980	2950	|	—	-1.5	—	—	-2.7	-0.4	-0.5	0	-1.4	-1.0	—	-1.0	-1.8
Fi8	632530 94370	3050	|	—	-0.9	—	-0.5	-2.1	-0.4	-0.5	—	-0.5	-1.1	—	-0.4	-1.8
Fi9	633320 93840	3140	|	—	—	—	—	—	-1.8	-0.3	—	—	-0.5	—	—	-1.4
Fi10	634450 94390	3270	|	—	—	—	0.2	—	—	-0.6	—	—	0.2	—	—	-0.3
Fi11	632415 94971	3000									|	-1.7	-1.3	—	-1.1	-1.8
Ag1	632320 95540	3040					|	—	-2.1	-0.5	—	-1.2	-0.9	—	-0.7	-1.8
Ag2	632532 95476	3090					|	—	-2.2	-0.4	—	-0.9	-1.0	—	-0.5	-1.6
Ag3	632712 95543	3130					|	—	-2.1	-0.5	—	-0.8	-1.0	—	-0.5	-1.8
Fi-s1	634415 93922	3290		1.4			0.3			-			0.2			
Fi-s2	635070 93920	3350								1.0			1.0			1.0
Fi-s3	633412 92300	3460		1.3			1.4			1.6						
Fi-s4	632450 92540	3390								-						

Appendix B

Curriculum Vitae

Name:	Horst Machguth
Date of Birth:	April 26, 1976
Citizenship:	Swiss (Würenlos, AG)

Education

1992–1996	Kantonsschule Baden (Switzerland), Matura Typus E
1997–2004	University of Zurich (Switzerland), Studies in Geography, Glaciology, Russian Literature, Geology and Mathematics
	Graduation: Diploma (MSc) in Geography
	Diploma-Thesis (in German): Messung und dreidimensionale Modellierung der Massenbilanzverteilung auf Gletschern der Schweizer Alpen
2004–2008	Research Assistant at the Institute of Geography, Glaciology and Geomorphodynamics Group, University of Zurich (Switzerland)

List of Publications Horst Machguth

Listed are publications that are either accepted or published (in chronological order):

Paul F., H. Machguth and A. Kääb (2005): On the impact of glacier albedo under conditions of extreme glacier melt: the summer of 2003 in the Alps. in: *EARSeL eProceedings*, Vol. 4, 139–149.

Machguth, H., O. Eisen, F. Paul and M. Hoelzle (2006): Strong spatial variability of snow accumulation observed with helicopter-borne GPR on two adjacent Alpine glaciers. *Geophysical Research Letters*, 33, L13503, doi:10.1029/2006GL026576.

Machguth, H., F. Paul, M. Hoelzle and W. Haeberli (2006): Distributed glacier mass-balance modelling as an important component of modern multi-level glacier monitoring. *Annals of Glaciology*, 43, 335–343.

Ceballos J. L., C. Euscategui, J. Ramirez, M. Cañon, C. Huggel, W. Haeberli and H. Machguth (2006): Fast shrinking of tropical glaciers in Colombia. *Annals of Glaciology*, 43, 194–201.

Paul F., H. Machguth, M. Hoelzle, N. Salzmann and W. Haeberli (2007): Alpine-wide distributed glacier mass balance modeling: a tool for assessing future glacier change? In *The Darkening Peaks: Glacial Retreat in Scientific and Social Context*, edited by B. Orlove, E. Wiegandt and B. Luckman, pp. 111–125, University of California Press.

Machguth, H., R. S. Purves, J. Oerlemans, M. Hoelzle, and F. Paul (2008): Exploring uncertainty in glacier mass balance modeling with Monte Carlo simulation, *The Cryosphere*, 2, 191–204, http://www.the-cryosphere.net/2/191/2008/tc-2-191-2008.html .

Machguth, H., F. Paul, M. Hoelzle and W. Haeberli (2008): Modeling mass balance distribution over glacierized mountain ranges: The example of Bernina Group in 1998/99. Glaciological Report, 123/124, 61–66.

Paul, F., H. Escher-Vetter and H. Machguth (2009): Comparison of mass balances for Vernagtferner obtained from direct measurements and distributed modeling. *Annals of Glaciology*, 50.